THE
PHYSICAL REVIEW

A journal of experimental and theoretical physics established by E. L. Nichols in 1893

SECOND SERIES, VOL. 72, NO. 8 OCTOBER 15, 1947

Theory of the Synchro-Cyclotron

D. BOHM AND L. L. FOLDY
Radiation Laboratory, Department of Physics, University of California, Berkeley, California
(Received May 31, 1947)

In the synchro-cyclotron (or frequency-modulated cyclotron) the higher energies available are obtained at the expense of a decrease in the ion current compared with that available from the conventional cyclotron. This decrease results from the fact that during only a small fraction of the frequency-modulation cycle is it possible for ions to be captured into phase stable orbits that do not return to the center during the first phase oscillation. By solving the phase equation, it is possible to obtain a general expression for this fraction, which is defined as the capture efficiency. At a constant dee voltage and varying rate of frequency modulation, the capture efficiency has a maximum at an equilibrium phase angle of 30° (corresponding to an energy gain per turn equal to half the maximum available). For larger equilibrium phase angles the efficiency decreases as a result of the smaller range of phase stability, while for smaller phase angles it decreases as a result of return of particles to the center. The maximum efficiency is proportional to the square root of the dee voltage or alternatively to the square root of the rate of frequency modulation, and depends on the charge and mass of the ions only through the ratio of charge to mass. Comparisons of the theoretical expectations with available experimental data show satisfactory agreement. Capture efficiencies for present designs of synchro-cyclotrons are of the order of 0.1 to 2 percent.

1. INTRODUCTION

IN the conventional cyclotron,[1] the maximum attainable energy is limited by the fact that the ions ultimately fall out of step with the applied electric field as a result of the decrease of angular velocity as the speed of light is approached.[2,3] V. Veksler[4] and E. M. McMillan[5] have independently proposed a new accelerator utilizing a cyclotron-like combination of electric and magnetic fields in such a way that a theoretically infinite number of accelerations may be accomplished. The theory of this accelerator has been studied in some detail by Dennison and Berlin,[6] by Saxon and Schwinger,[7] by Rabinovich,[8] and by the present authors[9] in a paper hereafter referred to as A. In all of these papers, the basic principles of the new accelerator are discussed, and the equations of orbital motion are solved, primarily with reference to applications to the acceleration of electrons in a machine which has come to be known as the synchrotron.

In the synchro-cyclotron (or frequency-modulated cyclotron) the same basic idea is applied to the acceleration of ions. One important new problem arises in this connection, however, which has not been treated in the previous papers. This new problem results from the manner in

[1] E. O. Lawrence and M. S. Livingston, Phys. Rev. **40**, 19 (1932).
[2] M. E. Rose, Phys. Rev. **53**, 392 (1937).
[3] R. R. Wilson, Phys. Rev. **53**, 408 (1937).
[4] V. Veksler, J. Phys. U.S.S.R. **9**, 153 (1945).
[5] E. M. McMillan, Phys. Rev. **68**, 143L (1945).
[6] D. M. Dennison and T. H. Berlin, Phys. Rev. **70**, 58 (1946).
[7] D. S. Saxon and J. Schwinger, Phys. Rev. **69**, 702A (1946).
[8] M. Rabinovich, J. Phys. U.S.S.R., **10**, 523, 531 (1946).
[9] D. Bohm and L. L. Foldy, Phys. Rev. **70**, 249 (1946).

which the ions are started. In the synchrotron the electrons are started at a large radius either by direct injection from an electron gun or by a preliminary operation of the device as a betatron. In the present design of the synchro-cyclotron it appears to be more practical to start the ions from rest at the center of the magnet as in the conventional cyclotron. However, in contrast to the conventional cyclotron, there is only a limited range of times in which ions starting in this way can enter into stable orbits which never return to the origin. This means, of course, that ions are accelerated intermittantly so that for a given dee voltage and gas pressure the average output is correspondingly reduced below that of a conventional cyclotron. We may define the *capture efficiency*, ϵ, as just the ratio of the time available during a frequency modulation cycle for starting particles into stable orbits which do not return to the center to the total time for repetition of the frequency modulation cycle. The calculation of ϵ is the principal object of this paper.

2. QUALITATIVE DISCUSSION OF FACTORS DETERMINING CAPTURE EFFICIENCY

In the synchro-cyclotron the decrease of frequency of ionic rotation accompanying the increase in energy of the ion is compensated by a corresponding decrease of frequency of the applied dee voltage with time. This decrease is achieved by a periodic modulation of the applied frequency by some means such as the use of a rotating condenser in the oscillator circuit. One may readily observe that there is always one way for a particle to be started into an indefinitely accelerating orbit under these circumstances. It is only necessary that the ion start at the instant when the applied frequency is equal to the ionic rotation frequency at the center of the machine and that the phase of the voltage at the time that it crosses the accelerating gap be such that the resulting energy gain per turn causes a decrease of the ionic rotation frequency which exactly matches the decrease of the applied frequency with time. Such a particle will gain energy steadily, never getting out of phase with the applied voltage.

However, just because the applied frequency is changing with time very few ions can start during the instant of time when their rotation frequency matches the applied frequency. Furthermore, the ions will not, in general, start with the ideal phase described above, which will hereafter be referred to as the equilibrium phase. The fundamental principle which makes the synchro-cyclotron feasible under these circumstances is the fact that ions in orbits whose frequency and phase do not differ too widely from that of the equilibrium orbit will execute stable oscillations of phase and frequency about the equilibrium values and so undergo an indefinite acceleration. This property of *phase stability* of the orbits has been discussed in the papers referred to above in considerable detail.

For any given starting phase of an ion there will, nevertheless, be a maximum discrepancy between ionic rotation frequency and applied frequency at the time of starting consistent with phase stable oscillations. Thus ions starting too late or too early will be subject to limitations on the maximum attainable energy similar to those applying in the ordinary cyclotron and will consequently be lost. Hence the property of phase stability is achieved at the expense of a reduction in the length of time available for starting particles into indefinitely accelerating orbits, so that the higher energies attainable with the synchro-cyclotron as compared with the conventional cyclotron are accompanied by a decrease in the output current.

Thus far, what has been said applies equally to the synchrotron and synchro-cyclotron. The additional complications in the synchro-cyclotron arise from the fact that ions start from rest at the center of the machine and consequently may return to the center during the course of a phase oscillation. The qualitative factors determining whether or not the ion returns to the origin can be seen quite easily with the aid of our picture of the motion as an oscillation of the actual orbit about an expanding equilibrium circle. If the expansion of the equilibrium circle is greater than the maximum inward swing of the radius of an ion in a phase stable orbit during the time when its phase becomes negative, the ion will not return to the center; otherwise it will. If it does not return to the center on the first phase oscillation, it will not do so on any subsequent oscillation because of the continual

expansion of the equilibrium radius. Hence, whether or not the ion is caught and indefinitely accelerated is determined entirely during the first phase oscillation. Normally the first phase oscillation will not carry the ion far from the origin so that the capture process is determined only by the character of the oscillations near the origin.

We shall show that the phase at which an ion starts is not subject to external control and that therefore the catching efficiency is determined, for either fixed applied dee voltage or fixed rate of frequency modulation, by the equilibrium phase. If the equilibrium phase is too great, then the catching efficiency is limited by the narrow range of phase stability. On the other hand, if the equilibrium phase is too small, the capture efficiency is limited by the fact that ions return to the center of the machine. There exists therefore an intermediate value of the equilibrium phase for which the capture efficiency is a maximum.

3. THE EQUILIBRIUM ORBIT

The first quantity that we shall need to know is the energy gain per turn required to keep an ion in the equilibrium orbit. In this orbit the fractional change of energy, $\Delta E/E_s$ corresponding to a given fractional change of rotation frequency, $\Delta\omega/\omega_s$ is given by (A–15) as

$$-K\Delta E/E_s=\Delta\omega/\omega_s,$$

where E is the total energy of the ion including its rest energy, ω is the frequency of rotation,

$$K=1+nc^2/v^2(1-n) \tag{1}$$

with c the velocity of light, v the velocity of the ion and

$$n=-r\partial H/H\partial r. \tag{2}$$

The subscript s denotes those values of the quantities that correspond to exact resonance with the applied frequency. $H(r)$ is the vertical component of the magnetic field in the median plane at a radius r. Now, since the change in frequency per turn is $(2\pi/\omega_s)d\omega_s/dt$, the required energy gain per turn is

$$\Delta E/E_s=-(2\pi/K\omega_s^2)d\omega_s/dt$$

and is also equal to $eV\sin\varphi_s$, where φ_s is the equilibrium phase and V is the maximum possible energy gain per turn. (See A for exact definitions.) Hence the equilibrium phase is given by

$$eV\sin\varphi_s/E_s=-(2\pi/K\omega_s^2)d\omega_s/dt. \tag{3}$$

Thus $eV\sin\varphi_s$ is the average energy gain per turn of an ion in a phase stable orbit, and $\rho=\sin\varphi_s$ represents the ratio of the average to the maximum possible energy gain per turn for such an ion.

Because the catching process is determined only by the motion near the origin, it is possible to express K with the aid of a power series for the magnetic field H, retaining terms only to the second order in r. With H satisfying Laplace's equation, there can be no linear term in the expansion so we may write

$$H=H_0(1-hr^2/2), \tag{4}$$

where H_0 is the field at the center. From this we obtain $n\simeq hr^2$, and since n is small near the center we have

$$K=1+nc^2/v_s^2=1+hc^2/\omega_s^2, \tag{5}$$

since $v_s=r\omega_s$.

This constancy of K occurs strictly only for parabolic fields, and in most cyclotrons deviations from the parabolic field occur even for moderately small values of the radius so that K has a higher order dependence on the radius. During the first phase oscillation, however, as has already been pointed out, these deviations are not generally important so that K may be regarded as constant during the catching process. In Appendix II, the phase equation is derived for the case that K is not constant, and limitations on the deviation of H from parabolic form for validity of our results are discussed.

4. PHASE OSCILLATIONS

The oscillatory motions resulting from deviations of an ion from the equilibrium orbit are discussed in detail in A; we shall merely quote here the results which are needed in the solution of the catching problem.

The equation of motion of the phase is given

by Eq. (A–17) as

$$\frac{d}{dt}\left(\frac{E_s}{\omega_s^2 K}\frac{d\varphi}{dt}\right)+\frac{eV}{2\pi}\sin\varphi=\frac{eV}{2\pi}\sin\varphi_s.$$

With the neglect of damping, a first order equation may be derived from the above by integration and is given by Eq. (A–18). However, the constant of integration there has been expressed in terms of φ_m, the maximum value of the phase during the phase oscillation. For our purpose it is more convenient to express it in terms of φ_0, the initial value of the phase φ, and $\dot{\varphi}_0$, the initial value of $\dot{\varphi}=d\varphi/dt$. We also approximate E_s by Mc^2 and approximate K by (5), thus obtaining

$$\dot{\varphi}^2=\dot{\varphi}_0^2+\frac{eV}{\pi Mc^2}(\omega_s^2+hc^2)\times[\cos\varphi-\cos\varphi_0+(\varphi-\varphi_0)\sin\varphi_s]. \quad (6)$$

It should be noted that according to the definition of the phase given in (A-7), $\dot{\varphi}$ is just the difference between the frequency of rotation and the applied frequency,

$$\dot{\varphi}=\omega-\omega_s. \quad (7)$$

5. RANGE OF PHASE STABILITY; PENDULUM MODEL

We shall be interested here primarily in the behavior of the large phase oscillations since these are the ones which may lead to loss of particles. In A it is shown that the equation of motion of the phase is exactly the same as that of a pendulum acted upon by a restoring torque due to gravity and also by a constant torque of such magnitude that the position of stable equilibrium of the pendulum is at $\varphi=\varphi_s$ instead of at $\varphi=0$. Such a pendulum will execute stable oscillations about $\varphi=\varphi_s$ unless it reaches the point of unstable equilibrium $\varphi=\pi-\varphi_s$, in which case it will go into accelerated circular motion. For any given starting phase φ_0 there will then be a maximum starting angular velocity, $\dot{\varphi}_0$ which will just bring the pendulum to the position $\varphi=\pi-\varphi_s$. For larger values of $\dot{\varphi}_0$ the motion is unstable. The maximum $\dot{\varphi}_0$ corresponding to phase stability can be obtained quantitatively from Eq. (6) by setting $\dot{\varphi}=0$ and $\varphi=\pi-\varphi_s$. This gives just the condition that φ reach its maximum amplitude at the point of unstable equilibrium. The result may be written

$$(\dot{\varphi}_0)^2_{\max}=\left(\frac{eV}{\pi Mc^2}\right)(\omega_s^2+hc^2)\times[\cos\varphi_0+\cos\varphi_s-(\pi-\varphi_s-\varphi_0)\sin\varphi_0] \quad (8)$$
$$=\frac{eV}{\pi Mc^2}(\omega_s^2+hc^2)F_1(\varphi_0,\varphi_s).$$

6. DETERMINATION OF CATCHING EFFICIENCY

With the results given above we are ready to calculate the catching efficiency with the neglect of return of ions to the center. According to the definition given in the introduction this is determined by the range of times in which ions can start in orbits which are phase stable and which do not return to the origin. Since the rate of decrease of applied frequency is practically constant over the first phase oscillation, this range of times is determined by the corresponding range of applied frequencies through the equation

$$\Delta t=\Delta\omega_s/|d\omega_s/dt|,$$

where $\Delta\omega_s$ is the range of $\omega-\omega_s$ with which an ion can start into an indefinitely accelerating orbit. If τ is the period of repetition of the cycle of frequency modulation, the efficiency is given by

$$\epsilon=\Delta t/\tau=\Delta\omega_s/\tau|d\omega_s/dt|. \quad (9)$$

The quantity $\tau|d\omega_s/dt|$ is independent of the rate of rotation of the condenser which modulates the frequency; hence for a given machine it is constant and the efficiency is proportional only to $\Delta\omega_s$.

The range of phase stability has already been calculated. According to Eq. (8) the maximum initial discrepancy between rotation and applied frequency consistent with stable motion is $\pm(\dot{\varphi}_0)_{\max}$. Consequently, since $\Delta\omega_s$ is the total range of $\omega-\omega_s$ during which capture in phase stable orbits is possible,

$$\Delta\omega_s=2(\dot{\varphi}_0)_{\max}=2\left[\frac{eV}{\pi Mc^2}(\omega_s^2+hc^2)F_1(\varphi_0,\varphi_s)\right]^{\frac{1}{2}}. \quad (10)$$

This formula depends upon the starting phase φ_0. In Appendix I, a discussion of the way in which ions start in the cyclotron is given and it

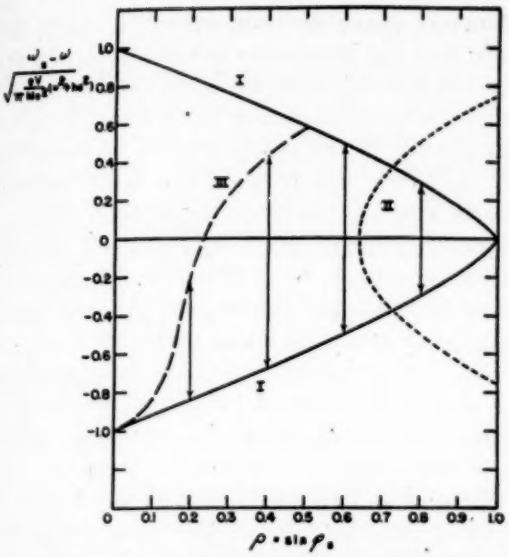

FIG. 1. Starting conditions for capture into stable orbits. Points lying between the two branches of curve I correspond to ions captured into phase stable orbits. Points lying within curve II correspond to ions which are never decelerated. Points lying below curve III correspond to ions which do not return to the origin, while points lying above curve III return to the origin during the first phase oscillation. The vertical arrows designate the range of frequencies for several values of ρ for which ions are captured into phase orbits and do not return to the origin. The ordinate should be

$$\frac{\omega_s-\omega}{\sqrt{\frac{eV}{\pi Mc^2}(\omega_s^2+hc^2)}}$$

is shown that the starting phase is very close to 90°. Thus we shall replace φ_0 by 90° in all subsequent work.

In Fig. 1, curve I, is plotted the maximum deviation of ω_s from ω consistent with phase stability as a function of $\rho=\sin\varphi_s$ assuming $\varphi_0=90°$. It can there be seen that the range of starting frequencies corresponding to phase stability is zero for $\varphi_s=90°$, the reason being, of course, that with φ_s close to 90°, the motion is always near the limit of phase stability. As φ_s decreases, the range of admissable starting frequencies increases reaching its maximum at $\varphi_s=0°$. It is also noteworthy that the range of frequencies leading to stable phase oscillations is proportional to $[V(\omega_s^2+c^2h)]^{\frac{1}{2}}$, which shows that the range may be increased either by increasing the dee voltage or by increasing the curvature of the magnetic field at the origin.

Equation (10) could be used to calculate the efficiency if one could neglect the fact that for small φ_s some of the ions will return to the origin and thus be lost.

7. RETURN OF IONS TO THE ORIGIN

The question of whether or not a particle returns to the origin can be studied qualitatively with the aid of the pendulum model for the motion. In our case the pendulum starts at a phase of 90°. If the equilibrium phase is also close to 90°, a stable oscillation must remain within positive phases even in the most negative part of its swing so that the particle will never be decelerated. Hence there will be no possibility of loss of ions by return to the origin for large values of φ_s. On the other hand the efficiency will be low for large φ_s because of the small range of phase stability, and it will certainly be advantageous to reduce φ_s until loss of ions by return to the origin begins to outweigh the gain in range of phase stability.

As φ_s is reduced the maximum downward swing of the pendulum corresponding to phase stability comes closer and closer to $\varphi=0$; and for small enough φ_s, negative phases will be reached in which ions suffer deceleration. The value of φ_s for which the pendulum just reaches $\varphi=0$ can be calculated by finding the condition that $\dot\varphi=0$ at $\varphi=0$. If these values are substituted into Eq. (6) we obtain, for $\varphi_0=\pi/2$

$$\dot\varphi_0=\pm\left[\frac{eV}{\pi Mc^2}(\omega_s^2+hc^2)(\tfrac{1}{2}\pi\sin\varphi_s-1)\right]^{\frac{1}{2}}. \quad (11)$$

In Fig. 1, curve II, $\pm[\frac{1}{2}\pi\sin\varphi_s-1]^{\frac{1}{2}}=\pm[F_2(\varphi_s)]^{\frac{1}{2}}$ is plotted against $\rho=\sin\varphi_s$. Curve II crosses curve I at about $\rho=0.7(\varphi_s=45°)$ indicating that below this value of φ_s some phase stable orbits involve deceleration of the ions. The fact that curve II crosses the ρ-axis at $\rho=0.63$ $(\varphi_s=39°)$ means that for smaller values of φ_s, all phase stable orbits involve some deceleration.

As φ_s decreases still further, the maximum amplitude of the negative swing increases and particles suffer correspondingly more deceleration. There will finally be reached a critical value of φ_s for which some particles within the range of phase stability begin to be decelerated all the way back to the origin so that they are lost. Calculations which will be discussed later indicate that this critical φ_s is about 30°. Below this value (for constant dee voltage) more and more particles are lost by deceleration to the origin, so many in fact that the gain in range of

phase stability is more than compensated by the increase in number of ions lost by return to the origin. Hence the maximum efficiency at constant dee voltage is at $\varphi_s = 29°(\rho \cong 0.5)$. The range which can be caught below this point is bounded by curve III of Fig. 1. It may be noted that it goes to zero rapidly as ρ approaches zero.

It is helpful to obtain a more detailed qualitative understanding of the factors determining the shape of curve III. As has already been stated, a particle will miss the origin only if the maximum inward swing of the radius occurring when the phase goes negative is less than the amount by which the equilibrium radius has expanded while the swing is taking place. The rate of expansion of the equilibrium radius is proportional to $d\omega_s/dt$ which, according to Eq. (3) is proportional to $\sin\varphi_s$. The total expansion of the equilibrium radius during the time interval t_1 in which the swing takes place will therefore be proportional to the product $t_1 \sin\varphi_s$.

Both t_1 and the maximum amplitude of the inward swing will depend on the starting phase and on the starting value of $\varphi = \omega - \omega_s$. We are interested mainly in the character of the motion for small φ_s since we have already seen that for large φ_s the particle is not even decelerated so that the question of return to the origin does not arise. From the pendulum model it can be seen that when φ_s is small a stable oscillation starting out at $\varphi_0 = 90°$ must reach a maximum negative phase somewhere between a little less than $-90°$ and a little less than $-180°$. Hence

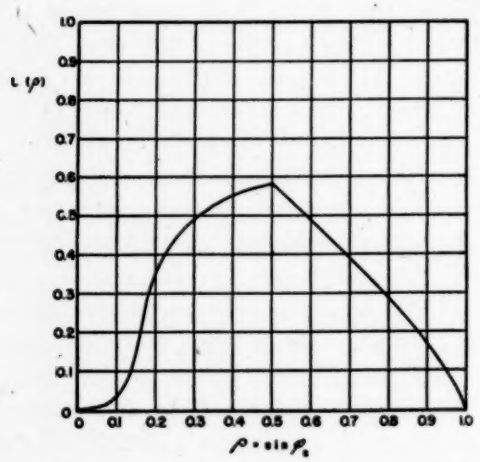

FIG. 2. The function $L(\rho)$ determining the capture efficiency as a function of equilibrium angle for constant dee voltage.

the amount of deceleration experienced by the particle and the maximum inward swing of the radius will depend strongly neither on φ_s nor on $\dot{\varphi}_0$ as long as φ_s is small. For qualitative purposes the amplitude of the swing may be regarded as constant. Hence the question of whether or not the particle misses the origin depends on whether the expansion of the equilibrium radius is greater than this constant. It is therefore adequate to consider only the manner in which the product $t_1 \sin\varphi_s$ depends on the variables involved.

Now t_1 is determined principally by the initial value of $\dot{\varphi}$. If, for example, a particle starts with negative $\dot{\varphi}_0$, it will reach the negative phases more rapidly than if $\dot{\varphi}$ is initially positive, and it will therefore begin to be decelerated sooner. The more negative the initial value of $\dot{\varphi}$, the greater is the deceleration and the greater is the likelihood of striking the origin. Conversely, the most favorable catching conditions occur with the largest possible positive initial $\dot{\varphi}$ consistent with phase stability. For such particles will come close to the point of unstable equilibrium at $\varphi = \pi - \varphi_s$, where they will spend a long time thus allowing the equilibrium radius to expand a great deal before their phase swings negative.

As φ_s is reduced, it is necessary that t_1 increase if the product $t_1 \sin\varphi_s$ is to remain large enough to result in an expansion of the equilibrium orbit which exceeds the maximum inward swing resulting from the phase oscillation. As has already been stated, at $\varphi_s = 30°$ some particles begin to be decelerated back to the origin; these will be the particles with the most negative φ_0 consistent with phase stability. At $\varphi_s = 13°(\rho = 0.225)$ calculations show that particles with $\dot{\varphi}_0 = 0$ will reach the origin and below this value only particles with positive $\dot{\varphi}_0$ can be caught. As φ_s approaches zero the range that misses the origin is progressively narrowed to an ever smaller range of positive $\dot{\varphi}_0$ near the limit of phase stability. This explains the approach of curve III to zero as φ_s approaches zero.

8. RESULTS FOR EFFICIENCY

The actual value of the efficiency taking account of return of ions to the center is calculated in Appendix C. The results will merely be quoted here:

(a) Constant Dee Voltage

If one wishes to compare efficiencies at constant dee voltage when $\rho=\sin\varphi_s$ is varied by varying the rate of frequency modulation (ρ is proportional to rate of rotation of the condenser), the efficiency is most conveniently expressed in the following form:

$$\epsilon=\frac{2}{|\tau d\omega_s/dt|}[eV(\omega_0^2+hc^2)/\pi Mc^2]^{\frac{1}{2}}L(\rho). \quad (12)$$

The function $L(\rho)$ is plotted in Fig. 2.

(b) Constant Rate of Frequency Modulation

For the case where the rate of frequency modulation is held fixed and φ_s is varied by varying the dee voltage, we write $V_s=V\sin\varphi_s$ so that V_s is the actual voltage gain per turn and is determined by the rate of frequency modulation through Eq. (3). It is thus a constant for constant rate of frequency modulation and from (12) it follows that

$$\epsilon=\frac{2}{|\tau d\omega_s/dt|}[eV_s(\omega_0^2+hc^2)/\pi Mc^2]^{\frac{1}{2}} \times L(\rho)/\rho^{\frac{1}{2}}. \quad (13)$$

In Fig. 3, $L(\rho)/\rho^{\frac{1}{2}}$ is plotted against ρ. It should be noted that the maximum efficiency now occurs at ρ in the neighborhood of 0.34. It must be remembered when considering this formula that the operation of the ion source is affected by the dee voltage so that the output current will depend upon the dee voltage both through the variation of the capture efficiency and through the ion source efficiency.

It should be noted that the maximum efficiency available with a particular rotating condenser is proportional to the square root of the dee voltage or alternatively to the square root of the rate of frequency modulation. If for a particular machine, one is limited as to the voltage that can be applied to the dees, then the maximum efficiency is obtained by adjusting the rate of rotation of the condenser so that the equilibrium phase is about 30°. It may be remembered that according to Eq. (3), the actual average energy gain per turn, $eV\sin\varphi_s$, is determined solely by $d\omega_s/dt$ and does not depend on the dee voltage. Hence the statement that $\varphi_s=30°$ means that

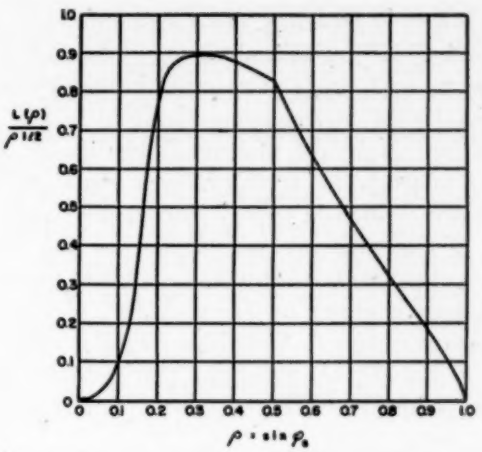

FIG. 3. The function $L(\rho)/\rho^{\frac{1}{2}}$ determining the capture efficiency as a function of equilibrium angle for constant rate of frequency modulation.

the average energy gain per turn is half the maximum available with the given dee voltage. On the other hand, if for a particular machine, one is limited as to the maximum rate of rotation for the condenser, then the maximum efficiency is obtained by adjusting the dee voltage so that the equilibrium phase is about 20°, or that the ratio of the average to the maximum available energy gain per turn is 0.34.

(c) Efficiency with Different Ions

In comparing the efficiency of the same machine for operation with different ions, we may consider two cases; operation with the same rotating condenser and oscillator circuit for both ions and operation with different rotating condensers for the two ions. In the first case $|\tau d\omega_s/dt|$ is the same for both ions, and since the applied frequency must be the same, the field H must be adjusted so that $\omega_0=eH/Mc$ is the same for both. Hence with the same dee voltage and equilibrium phase in the two cases, we see that the efficiency is proportional to $(e/M)^{\frac{1}{2}}$. Thus

$$\epsilon\alpha(e/M)^{\frac{1}{2}}. \quad (14)$$

Hence the efficiency depends only on the ratio e/M for the two ions. The efficiency should therefore be the same for alpha-particles and deuterons but higher by a factor of $\sqrt{2}$ for protons than for these ions.

In the second case where different condensers

are used, it is probably fair to assume that the condensers will be built so as to give a change of frequency with angle of rotation proportional to the total shift in frequency required in the acceleration. Now the fractional change in frequency during the acceleration is equal to the fractional change in energy during the acceleration. If the ions are accelerated to the same radius, then the latter quantity is given for non-relativistic energies by $H^2e^2r^2/2M^2c^4$, where r is the radius attained. Since the frequency is proportional to eH/Mc, it follows that $|\tau d\omega_s/dt|$ will be proportional to $H^3e^3r^2/2M^3c^5$, and the efficiency to

$$(M/e)^{5/2}[(eH/Mc)^2+hc^2]^{\frac{1}{2}}, \qquad (15)$$

for the same dee voltage and equilibrium phase angle. Again the efficiency depends only on e/M, but in this case is proportional to $(M/e)^{5/2}$, if the decrease in magnetic field with radius is primarily responsible for the decrease in angular velocity, and to $(M/e)^{\frac{1}{2}}$ if the increase of mass with velocity is primarily responsible for the decrease in angular velocity with radius. The efficiency for α-particles and deuterons is again the same, but is lower in this case for protons. It should be noted in this comparison that the actual output current will depend not only on the catching efficiency but on other factors (source efficiency, loss of ions by scattering and striking the dees, deflector efficiency, etc.) as well, which will in general be different for different ions, even in the same machine.

9. COMPARISON WITH EXPERIMENT

In this concluding section we shall attempt to compare our results with the small amount of experimental data on the California 37-inch synchro-cyclotron and the California 184-inch synchro-cyclotron.

(a) California 37-inch Synchro-Cyclotron

This machine was intended as a model for the 184-inch synchro-cyclotron. In order to simulate the large relativistic increase of ion mass occurring in the larger machine, the magnetic field was designed to decrease approximately parabolically by a factor of about 15 percent between the center of the magnet and the radius of the final orbit. In this machine the magnetic field is very accurately parabolic near the origin and from field measurements there was obtained the value $h=0.000138$ cm^{-2}.

While no systematic study was made of the absolute value of the catching efficiency, on a typical run a value of about 2 percent was obtained. The conditions on this run were $V=23$ kev, $(-d\omega_s/dt)/\omega_0=1380$ sec^{-1}, $\tau=0.00053$ sec

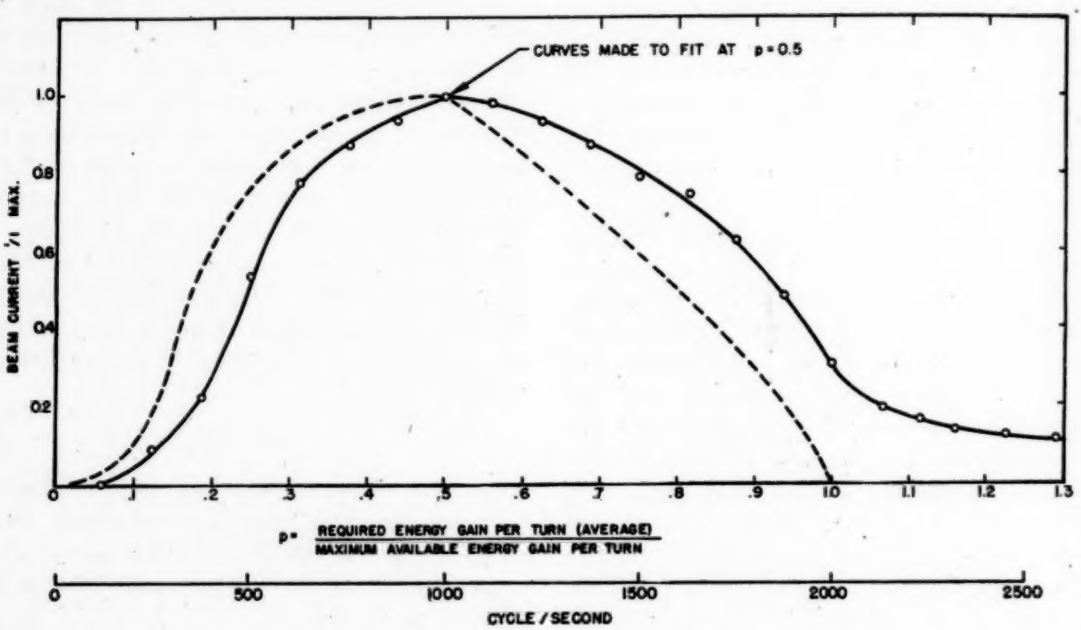

FIG. 4.

and $i_0=\omega_0/2\pi=11$ Mc/sec. At the best phase of 30°, the theoretical value for these conditions is 1.8 percent which is in satisfactory agreement with the rough experimental value.

The relative efficiency was measured systematically as a function of ρ at constant voltage.[10] The results are plotted in Fig. 4; the ordinates are the efficiencies and the abcissae are $\rho=\sin\varphi_s$. Because the absolute values of the efficiencies were not known, the theoretical curve was adjusted to agree at $\varphi_s=30°(\rho=0.5)$. The agreement between theory and experiment is quite satisfactory from $\rho=0$ to $\rho=0.85$. In particular the appearance of the maximum at $\rho=0.5$ is a direct confirmation of the basic assumption of the theory that losses by return of ions to the origin limit the efficiency at small equilibrium phase angles.

It should be noted that the measured efficiency does not approach zero as ρ approaches unity but instead actually has non-zero values when ρ is greater than unity. This seems to indicate that particles are being indefinitely accelerated even though they do not gain enough energy per turn to allow the rate of decrease of rotation frequency to keep up with the rate of decrease of applied frequency. By pulsing the ion source and examining the output current from the cyclotron with an oscilloscope, it was determined that some of the ions which left the source during one frequency modulation cycle did not strike the probe until two or three frequency modulation cycles later. It thus appears that some ions which cannot gain enough energy per turn to remain in synchronism with the applied frequency are accelerated out to some radius. When they there fall out of step with the applied frequency they successively lose and gain energy but on the average remain at about this radius until at the appropriate instant during a succeeding frequency modulation cycle they may again be picked up and further accelerated to a high energy.

(b) California 184-inch Synchro-Cyclotron[11]

In this machine the magnetic field is parabolic only near the center. From a radius of about 8 inches the field then drops off linearly almost to the edge of the pole faces. The radius reached during the first phase oscillation is about 9 inches as calculated for typical operating conditions so that the theory developed here is approximately valid (see Appendix II). The acceptance time for ions was measured under typical operating conditions by applying pulses of voltage to the ion source and measuring the current by means of a probe as a function of the time at which the voltage pulse was applied. From the speed of rotation of the condenser it was thus possible to obtain an experimental value for the capture efficiency.

In order to obtain the theoretical capture efficiency, one would in general have to know the dee voltage. No accurate measurements of this quantity are available at present. To obtain the maximum efficiency at a fixed dee voltage, however, it suffices to know the rate of frequency modulation only. Hence in the measurement the rate of rotation of the condensor was adjusted to give maximum yield. Under typical operating conditions for the acceleration of deuterons ($H_0=14{,}760$ gauss, $h=1.57\times10^{-5}$, $\omega_0=7\times10^7$ radians/sec; $d\omega_s/dt=8.8\times10^9$ radians/sec^2, $\tau=0.0114$ sec) the value 0.33 percent was obtained for the theoretical efficiency. The measured acceptance time was 35 microseconds which combined with $\tau=0.0114$ sec, yields an experimental value for the efficiency of 0.31 percent in satisfactory agreement with the predicted value.

Because of the change in the field from parabolic to linear dependence on radius at about 8 inches, it will be seen from Eq. (2) that K will be a decreasing function of the radius beyond this radius. As a consequence, if the dee voltage and frequency modulation rate do not change during the acceleration period, it follows from Eq. (3) that the equilibrium phase will increase with radius. This will result in a loss of captured particles, since as the equilibrium phase increases, the range of phase stability decreases; hence ions which were initially in phase stable orbits near the limit of stability will pass into unstable orbits and be lost. This effect can be very serious if the equilibrium phase should increase to a value close to 90° since there the region of phase stability is very narrow. Actually, in this ma-

[10] J. R. Richardson, K. R. MacKenzie, E. J. Lofgren, and B. T. Wright, Phys. Rev. 69, 669L (1946).

[11] The measurements on the 184-inch cyciotron were made by a group under the direction of Duane Sewell.

chine, the dee voltage is known to rise somewhat (about 15 percent) during the acceleration period. This tends to prevent the equilibrium phase from rising quite so far. From plots of the magnetic field, the variation of dee voltage with frequency, and the (slight) variation of frequency modulation rate with frequency, it was possible to calculate the required energy gain per turn as a function of radius under typical operating conditions. The result is shown in Fig. 5. It will be noted that the rise in required energy gain per turn is not too serious. Its decrease again at large radii is due to the fact that at these radii the magnetic field again falls off more rapidly than linearly with the distance. The rise in equilibrium phase could, of course, be prevented by continuing the parabolic field dependence to the edge of the pole pieces. The resultant gain in output current, however, would then be obtained at a loss in the maximum energy to which ions could be accelerated, since the initial rate of parabolic decrease is determined by vertical focussing considerations and cannot be appreciably lessened without the sacrifice of particles due to their striking the dees.

ACKNOWLEDGMENTS

It is a pleasure to express our gratitude to Professor E. O. Lawrence for his encouragement of this work. We are also very grateful to Professor Robert Serber, Professor E. M. McMillan, Professor Robert Thornton, and many other members of the staff of the Radiation Laboratory who contributed many helpful discussions and suggestions. This work was carried out under the auspices of the Atomic Energy Commission under Contract No. W-7405-Eng-48 with the University of California.

APPENDIX I. MOTION DURING FIRST FEW TURNS

During the first few turns several of the approximations leading to the phase equation (A-17) are not valid. In the first place the motion is not close enough to circular that it can be described as a circle with small deviations. Secondly, the energy gain per turn is not equal to $eV\sin\varphi$, as this requires that the diameter of the orbit be greater than the spatial extent of the accelerating field.

Just after the particle starts, the motion consists of an expanding spiral within the region of the accelerating electric field. By the time the orbit becomes appreciably larger than the accelerating region, however, the above approximations will apply. It is therefore necessary to integrate the equations of motion without these approximations only over the first few turns. During this time ω_s, ω, and H change so little that they may be set equal to their initial values. The equations of motion then take the form

$$M\ddot{y}=(eH_0/c)\dot{x}-eE_0(\sin\omega_s t+\alpha), \tag{16}$$

$$M\ddot{x}=-(eH_0/c)\dot{y}. \tag{17}$$

Here E_0 is the electric field at the center, which may also be regarded as essentially uniform in this region, and α represents a d.c. bias which may be applied to the dees to improve operation of the oscillator. The quantity α is seldom larger than $\frac{1}{2}$.

The initial conditions are $x=\dot{x}=y=\dot{y}=0$ at $t=t_0$. The solution may be written in the form

$$y=-\frac{eE_0}{M\omega_0^2}\left\{\alpha-\alpha\cos\omega_0(t-t_0)-\frac{\omega_0}{\omega_0+\omega_s}\cos\omega_s t_0\cos\omega_0(t-t_0)\right\}+\frac{2eE_0}{M(\omega_0^2-\omega_s^2)}\sin\left[(\omega_s-\omega_0)\left(\frac{t-t_0}{2}\right)\right]\times\cos\left[\omega_s t+\frac{(\omega_0-\omega_s)}{2}(t-t_0)\right], \tag{18}$$

$$x=-\omega_0\int_{t_0}^{t}y\,dt. \tag{19}$$

Since ω_s is always close to ω_0, it is clear that the last term on the right will become large; that is, it is the "resonant" term. After only four turns, for example it is about 25 times larger than the remaining terms. This means that the main part of the motion corresponds to an expanding spiral with an almost constant fractional increase of radius per turn. As soon as the radius reaches an appreciable size the relative increase becomes small and the motion becomes nearly circular. The remaining terms contribute only small perturbations causing the motion to differ

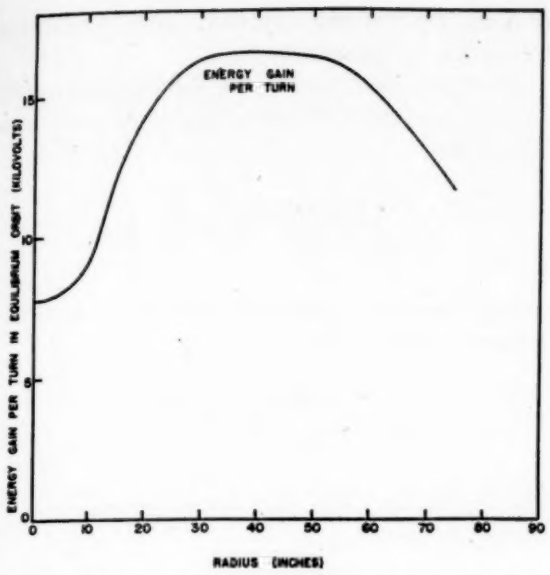

FIG. 5. Variation of energy gain per turn as a function of radius for 184-inch synchro-cyclotron.

slightly from circularity, but in a way which cancels out over a turn. When $(\omega_0-\omega_s)(t-t_0)/2$ is small, as it will be during the first few turns, y is proportional to $\cos\omega_s t$. This means that the ion will cross $y=0$ when $\omega_s t=(n+\frac{1}{2})\pi$ or when the accelerating force is a maximum. Therefore the phase as defined in A is $\pi/2$ and the effect of the accelerating force is always to start ions in a phase close to that at which they gain energy at the maximum rate.

APPENDIX II. PHASE EQUATION AT SMALL RADII

In A the phase equation was derived with the aid of the approximation that the fractional change of energy, momentum, and radius occurring during a phase oscillation is small. Because the particle starts at zero radius and from rest in the synchro-cyclotron, this approximation will break down at the start just when the catching process is taking place. In this section we shall derive the phase equation without this approximation and show that for a parabolic variation of magnetic field with radius, the exact phase equation is the same as the approximate equation obtained in A. If the magnetic field deviates from a parabolic form the phase equation becomes much more complex and, as we shall see, no longer possesses an elementary first integral analagous to (5). The catching problem can then be solved only by numerical integration. Fortunately, the magnetic field is nearly parabolic near the origin in most cyclotrons although it does deviate from parabolic form at larger radii. In order to decide whether these deviations will affect the catching process it is necessary to estimate the range of radii covered during the first phase oscillation. This will be done after the derivation of the phase equation. An approximation will also be given for treating the case in which the first phase oscillation carries the particle into non-parabolic regions of the magnetic field.

We begin with the well known relation between ionic rotation frequency and energy

$$\omega=ecH(r)/E. \tag{20}$$

From this we calculate the energy gain per turn which is $\Delta E=2\pi(dE/dt)/\omega$. Differentiation of (20) yields

$$d\omega/\omega dt=-dE/Edt+(\partial H/H\partial r)dr/dt. \tag{21}$$

To eliminate dr/dt, we write

$$r=v/\omega=c[1-(Mc^2/E)^2]^{\frac{1}{2}}/\omega, \tag{22}$$

so that

$$dr/rdt=-d\omega/\omega dt+\frac{(Mc^2/E)^2}{1-(Mc^2/E)^2}(dE/Edt).$$

Equation (21) then yields

$$-(d\omega/\omega dt)(1+r\partial H/H\partial r)$$
$$=(dE/Edt)\left[1-(r\partial H/H\partial r)\frac{(Mc^2/E)}{1-(Mc^2/E)^2}\right].$$

Writing $(Mc^2/E)^2=1-(v/c)^2$ and using (20), we obtain

$$\frac{\Delta E}{E}=\frac{2\pi}{K\omega^2}\frac{d\omega}{dt}, \tag{23}$$

where K is defined in Eq. (5). To obtain the phase equation we express ω with the aid of Eq. (7) and write $\Delta E=eV\sin\varphi$:

$$\frac{2\pi}{\omega^2}\frac{d^2\varphi}{dt^2}+\frac{KeV}{E}\sin\varphi=-\frac{2\pi}{\omega^2}\frac{d\omega_s}{dt}. \tag{24}$$

If the magnetic field is parabolic so that K is constant, the phase equation may (with the aid of a little algebra) be shown to be exactly the same as Eq. (A–17).

If K is not a constant, it may, in general, be expressed as a power series in r with the aid of the expression for H as a function of r. This yields an expression of the form, $K=K_0+K_1r+K_2r^2/2+\ldots$; similar expansions can then be obtained for E and ω. These latter, however, will normally vary so slowly with r near the origin that the neglect of this variation over the first phase oscillation is permissable. However, if K varies appreciably over this distance, it will be necessary to eliminate r in terms of $\omega=\omega_s+d\varphi/dt$, with the aid of Eqs. (20) and (22). This will introduce terms involving $(\omega_s+d\varphi/dt)\sin\varphi$ into the phase equation and then a first integral of this equation can no longer be obtained. If K does not change too much during the first phase oscillation, a rough value of the efficiency may be obtained simply by averaging K over the range of radii covered during the first phase oscillation. Since the efficiency does not depend critically on K, such a procedure will probably be adequate for a rough estimate even if K changes by as much as a factor of 2 or 3 during the first phase oscillation.

In order to know whether K varies much during the first phase oscillation and to correct for such variation by averaging K, it is necessary to estimate the range of radii covered during the first phase oscillation. To obtain this estimate, we first assume that H varies parabolically and see what radius the particle would reach with such a variation. In the first phase oscillation the non-relativistic approximation for the energy can be used;

$$E=Mc^2+\tfrac{1}{2}Mv^2=Mc^2+\tfrac{1}{2}M\omega^2r^2 \simeq Mc^2(1+\omega_0^2r^2/2c^2), \quad (25)$$

where ω_0 is the angular rotation frequency at the center. With the expansion (4) for H, we get, up to second order in r, with $\omega=\omega_s+d\varphi/dt$

$$\frac{d\varphi}{dt}=\omega_0\left[1+\left(h+\frac{\omega_0^2}{c^2}\right)\frac{r^2}{2}\right]-\omega_s. \quad (26)$$

Now the range of radii covered will depend on the initial value of $d\varphi/dt$; as a typical case we shall take $(d\varphi/dt)_0=0$, or $\omega_0=\omega_s$. Furthermore, for small φ_s, in which we are most interested, ω_s will not change much during a phase oscillation and hence a rough estimate may be obtained by setting $\omega_s=\text{constant}=\omega_0$.

We eliminate dt in (26) by differentiating (25) and setting $(2\pi/\omega_s)dE/dt=M\omega_0^2rdr/dt=eV\sin\varphi$. We obtain

$$\frac{eV}{2\pi M\omega_0^2}\frac{d\cos\varphi}{dr}=\left(h+\frac{\omega_0^2}{c^2}\right)\frac{r^3}{2}.$$

Integration over r with the boundary condition, $\varphi_0=\pi/2$, yields

$$\cos\varphi=\frac{2\pi M\omega_0^2}{eV}\left(h+\frac{\omega_0^2}{c^2}\right)\frac{r^4}{8}.$$

The maximum value of r occurs where $\cos\varphi=1$, whence it is

$$r_{\max}=\left[\frac{4eV}{\pi M\omega_0^2(h+\omega_0^2/c^2)}\right]^{\frac{1}{4}}. \quad (27)$$

APPENDIX III. CALCULATION OF EFFICIENCY

As explained in Section 2, our objective is to solve for the range of $\Delta\omega_s$ corresponding to phase stable motion which never returns to the origin. The range of $\Delta\omega_s$ corresponding to phase stability is already given in Eq. (10). Let us refer to this range as

$$(\Delta\omega_s/2\omega_s)_1=(\dot\varphi_0)_1.$$

Now it has been pointed out that there will be a critical value of $\dot\varphi_0$ for which the ion barely returns to the origin. Let us call this value $(\dot\varphi_0)_2$. It is convenient to express $(\dot\varphi_0)_2$ in terms of $(\varphi_0)_1$ through a dimensionless parameter λ defined as follows

$$(\dot\varphi_0)_2=\lambda(\dot\varphi_0)_1 =\lambda[(eV/\pi Mc^2)(\omega_0^2+hc^2)F_1(\varphi_0,\varphi_s)]^{\frac{1}{2}}, \quad (28)$$

where it will be noted that λ may take on values ranging from -1 to $+1$. For $\lambda=-1$, the range of $(\dot\varphi_0)$ for phase stability and that for particles failing to return to the origin just coincide. This will occur at the intersection of curves I and III in Fig. 1. As $\lambda\to+1$, only particles with positive $(\dot\varphi_0)$ near the limit of phase stability will miss the origin.

The efficiency can then be written from Eq. (28) as

$$\epsilon=\frac{(1-\lambda)}{|\tau d\omega_s|dt|}\left[\frac{eV}{\pi Mc^2}(\omega_0^2+hc^2)F_1(\varphi_0,\varphi_s)\right]^{\frac{1}{2}}$$

$$=\frac{2}{|\tau d\omega_s|dt|}\left[\frac{eV}{\pi Mc^2}(\omega_0^2+hc^2)\right]^{\frac{1}{2}}L(\varphi_0,\varphi_s) \quad (29)$$

where

$$L(\varphi_0,\varphi_s)=\tfrac{1}{2}(1-\lambda)[F_1(\varphi_0,\varphi_s)]^{\frac{1}{2}}. \quad (30)$$

Since $(\dot\varphi_0)_2$ is the initial value of $\dot\varphi$ corresponding to a particle just returning to the origin, we may obtain a formula for $\dot\varphi$ at all times for such a particle by replacing $\dot\varphi_0$ in Eq. (6) by $(\dot\varphi_0)_2$, as given in Eq. (28). We obtain, taking $\varphi_0=\pi/2$:

$$(\dot\varphi)^2=\frac{eV}{\pi Mc^2}(\omega_0^2+hc^2)[\cos\varphi+\lambda^2\cos\varphi_s$$

$$+\{\varphi-(\lambda^2+1)\pi/2+\lambda^2\varphi_s\}\sin\varphi_s] \quad (31)$$

$$=(eV/\pi Mc^2)(\omega_0^2+hc^2)P(\varphi_1,\varphi_s,\lambda).$$

Integration of this equation yields

$$(t-t_0)=[\pi Mc^2/eV(\omega_0^2+hc^2)]^{\frac{1}{2}}$$

$$\times\int_{\pi/2}^{\varphi}d\varphi/[P(\varphi,\varphi_s,\lambda)]^{\frac{1}{2}}, \quad (32)$$

where the path of integration must include all values of φ covered by the particle in its motion. If $\dot\varphi_0$ is negative (λ negative), φ will decrease directly to a minimum value, then increase, etc. If $\dot\varphi_0$ is positive (λ positive), φ will first increase to a maximum, then decrease to a minimum, again increase, etc.

We wish to obtain the time t_1 required for a particle to reach its minimum radius in the first phase oscillation. This may be obtained from Eq. (32) by noting that the minimum radius is reached when φ returns to zero from the negative side. We thus set $\varphi=0$ as the upper limit and keep in mind the range of values of φ actually covered in the integration. The limiting particle will have $r=0$ at $t-t_0=t_1$. From Eq. (7) we see that at $r=0$, $d\varphi/dt=\omega_0-\omega_s=\dot\varphi_0-(t-t_0)d\omega_s/dt=\dot\varphi_0-t_1d\omega_s/dt$. Expressing $\dot\varphi_0$ with the aid of (28) we obtain for the value of $d\varphi/dt$ at $r=r_{\min}$:

$$\left(\frac{d\varphi}{dt}\right)_{r=r_{\min}}=\lambda\left[\frac{eV}{\pi Mc^2}(\omega_0^2+hc^2)F_1(\pi/2,\varphi_s)\right]^{\frac{1}{2}}$$

$$-\frac{d\omega_s}{dt}\left[\frac{\pi Mc^2}{eV(\omega_0^2+hc^2)}\right]^{\frac{1}{2}}\int_{\pi/2}^{0}\frac{d\varphi}{P^{\frac{1}{2}}}.$$

From Eq. (31) we can obtain another value of $d\varphi/dt$ at $r=r_{\min}$ by setting $\varphi=0$. We must choose the positive square root of $d\varphi/dt$ because φ will be increasing from negative values when $r=r_{\min}$:

$$\left(\frac{d\varphi}{dt}\right)_{r=r_{\min}}=\left[\frac{eV}{\pi Mc^2}(\omega_0^2+hc^2)P(0,\varphi_s,\lambda)\right]^{\frac{1}{2}}.$$

Setting the two expressions for $(d\varphi/dt)_{r=r_{\min}}$ equal, and using Eq. (3) we obtain

$$1/2\sin\varphi_s\int_{\pi/2}^{0}\frac{d}{[P(0,\varphi_s,\lambda)]^{\frac{1}{2}}}$$

$$=[P(0,\varphi_s\lambda)]^{\frac{1}{2}}-\lambda[F_1(\pi/2,\varphi_s)]^{\frac{1}{2}}, \quad (33)$$

which implicitly defines λ as a function of φ_s. The quantity λ was obtained from this equation by numerical solution.

Scattering of Protons by Deuterons†

R. SHERR,* J. M. BLAIR,** H. R. KRATZ,*** C. L. BAILEY,** AND R. F. TASCHEK
Los Alamos Scientific Laboratories, Sante Fe, New Mexico

(Received July 7, 1947)

Utilizing a scattering chamber based upon the successful design used by Herb, Kerst, Parkinson, and Plain (HKPP) in the measurement of proton-proton scattering, experimental data on the scattering of protons by deuterons have been obtained. The incident protons were accelerated by the 3.5-Mev Wisconsin generator ("long tank") which was used by the Manhattan Project at Los Alamos, New Mexico. The geometry, and the current and pressure measurements were checked by comparing the measurements of proton-proton scattering at 2.1 Mev with the work of HKPP. Results on proton-deuteron scattering at 0.825, 1.51, 2.08, 2.53, 3.00, and 3.49 Mev were obtained. The absolute cross sections per unit solid angle show the presence at all energies studied of higher order waves. A minimum in the scattering is observed near 90° at the low energies; the minimum shifts to larger angles with increasing energy. The cross sections at all angles decrease with increasing energy but the ratio of the cross section at 150° to the minimum increases gradually from 2.3 at 1.51 Mev to 3.0 at 3.49 Mev. The present results at 825 kev do not show the large anomaly found by Tuve, Heydenburg, and Hafstad at 830 kev.

INTRODUCTION

THE general theoretical interest in the scattering of light particles has led us to perform a series of measurements on the scattering of protons by deuterons. The earlier experimental work by Tuve, Heydenburg, and Hafstad[1] showed a large anomaly at 830 kev. Subsequent theoretical papers have tried to explain this anomaly with little success.[2,3] Measurements were made by Taschek[4] at very low energies. It was decided to perform the present experiments at the high energies available to us in the operation of the 3.5-Mev Wisconsin generator ("long tank") designed by Herb, *et al.*[5] This generator was used by the Manhattan Project at Los Alamos, and was scheduled to be returned to Wisconsin within several months after the present work was begun. It was considered advisable to follow as closely as possible the successful experiments of Herb, Kerst, Parkinson, and Plain[6] (hereafter referred to as HKPP) on the scattering of protons by protons. Several changes were made in the design of the scattering chamber and detecting equipment. For the sake of completeness we shall describe our apparatus in detail.

MECHANICAL DETAILS OF SCATTERING CHAMBER

The scattering chamber (Fig. 1) was turned from a single piece of aluminum 17½ inches in diameter. The inside hollow was 14 inches in diameter and 4 inches deep. Around the wall were several accurately placed holes. The brass tube which held the collimating diaphragms for defining the incoming beam of ions, was inserted into one of these holes. In a diametrically opposite hole was pressed the tube which held the current collecting cup. A port at 90° connected the chamber to the liquid-air trap and vacuum pumps. There were four other holes, at 15°, 135°, 225°, and 345°, into which the defining slit systems of proportional counters used for monitoring could be placed.

The movable proportional counter and its slit system were mounted on a 10-inch diameter disk which was screwed onto a tapered plug fitting

† This paper is based on work performed under U. S. Government Contract No. W-7405-eng-36 at the Los Alamos Scientific Laboratory of the University of California.

* Now at Princeton University, Princeton, New Jersey.
** Now at the University of Minnesota, Minneapolis, Minnesota.
*** Now at General Electric Company, Schenectady, New York.

[1] H. A. Tuve, N. P. Heydenburg, and L. R. Hafstad, Phys. Rev. **50**, 806 (1936).
[2] H. Primakoff, Phys. Rev. **52**, 1000 (1937).
[3] K. Ochial, Phys. Rev. **52**, 1221 (1937).
[4] R. F. Taschek, Phys. Rev. **61**, 13 (1942).
[5] R. G. Herb, C. M. Turner, C. M. Hudson, and R. E. Warren, Phys. Rev. **58**, 579 (1940).
[6] R. G. Herb, D. W. Kerst, D. B. Parkinson, and G. J. Plain, Phys. Rev. **55**, 998 (1939).

into a hole through the bottom of the chamber. The axis of this tapered hole intersected, and was perpendicular to, the line joining the holes mentioned above which held the collimating-diaphragm system and current-collection system. The gas and electrical leads to the movable proportional counter were brought out of the scattering chamber through holes bored through this tapered plug. Outside of the chamber a 6-inch diameter gear was clamped to the plug. This gear was driven by a smaller gear to rotate the disk and counter inside the scattering chamber. The larger diameter of the plug was on the inside of the chamber to allow the plug to be inserted in its hole after the disk had been screwed on. Four springs pressing against the gear on the bottom of the plug prevented the plug from being pushed in by atmospheric pressure when the

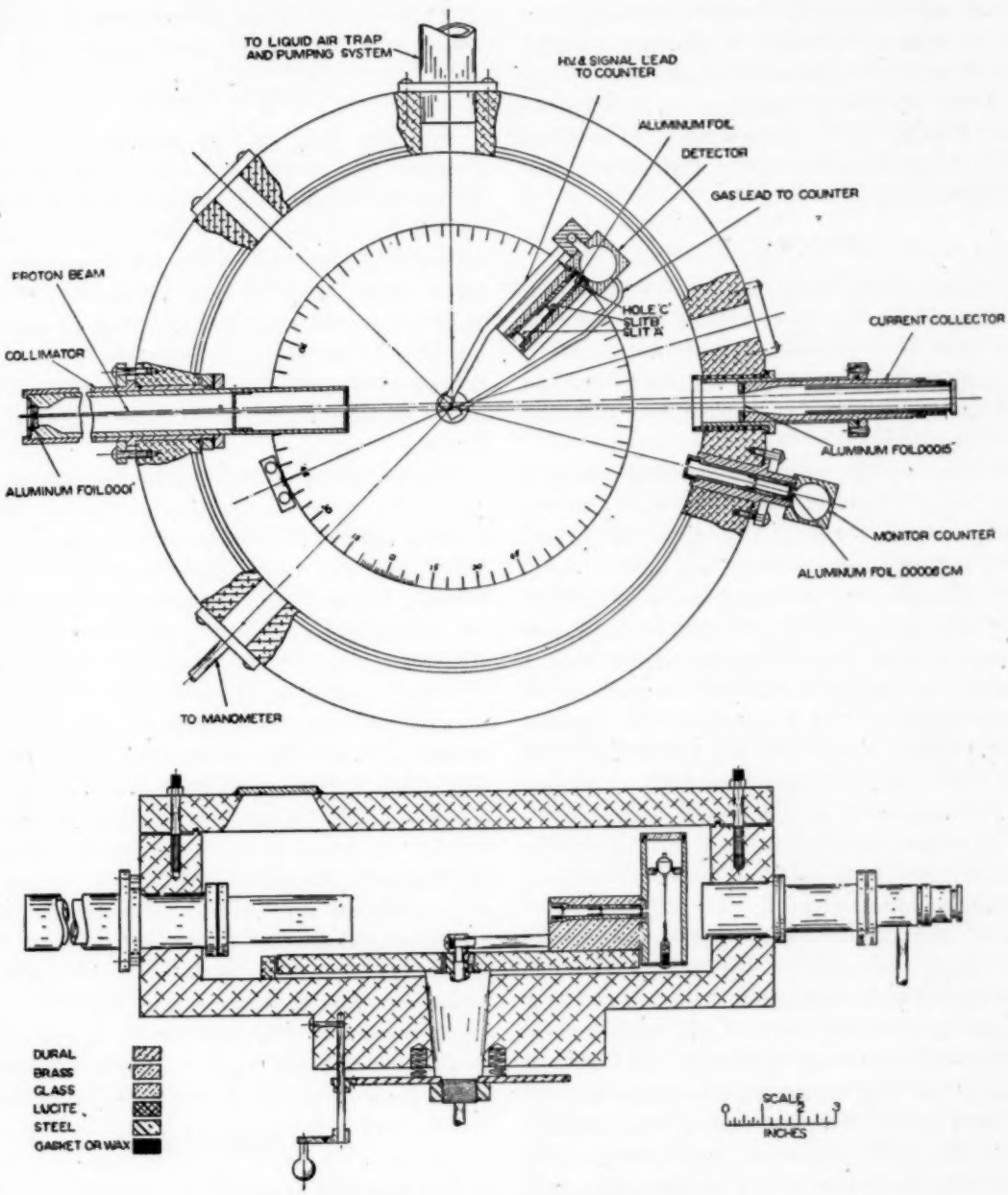

FIG. 1. Views of Scattering Chamber.

chamber was evacuated. The springs fitted into four recesses in the bottom of the chamber.

The periphery of the disk inside the chamber was graduated in degrees. These graduations were read against a vernier marked to tenths of a degree. The graduations were numbered so that the reading was zero when the movable proportional counter was on the side of the chamber opposite the beam-collimating diaphragms.

The lid of the scattering chamber was made of Dural, one inch thick. It had a gasket groove which contained a gasket of silicone material. A tongue projecting from the upper edge of the wall of the scattering chamber fitted into this groove. The lid had a glass window in it which allowed the graduations on the disk and vernier to be read.

COLLIMATOR

The brass tube which held the collimating-diaphragm assembly was pressed into the hole in the wall of the chamber and was sealed in vacuum-tight with glyptal. A section of sylphon tubing connected the brass tube to the target tube of the electrostatic generator.

The defining diaphragms were fastened into another brass tube which was a tight fit into the above mentioned tube. The first diaphragm which the beam encountered had a hole, 0.085 inch in diameter on the front side and tapered slightly to a larger diameter on the back, so that the beam was defined by a sharp edge to reduce scattering. An aluminum foil on the back side of this diaphragm served to separate the chamber from the target tube. This foil was 0.0001 inch thick (70-kev stopping power for 2-Mev protons) and was cemented in place with Glyptal. To facilitate replacement of this foil the diaphragm was removable, being held in place by a Neoprene gasket and a clamp ring.

The second defining diaphragm was ten inches further along the tube. It also had a hole 0.085 inch in diameter, tapered like the first one. These two holes defined the beam of incoming ions so that its total width was limited to 0.215 inch at the center of the scattering chamber, and to 0.355 inch at the foil in front of the current-collector cup. The maximum angle away from the axis of these holes, which an ion path could make, was 0.6 degree.

To prevent the entrance into the chamber of ions which were scattered by the edge of the second diaphragm, a third diaphragm with a 0.175-inch hole was placed at the end of the collimating tube. Tests made with the chamber evacuated indicated that this system effectively eliminated slit-edge scattering for all angular settings of the counter (15° and higher).

The tube which held these diaphragms was sealed into its supporting tube by a gasket of $\frac{1}{16}$-inch-square Neoprene strip and a clamp ring which were just inside the chamber wall.

CURRENT COLLECTOR

Into the hole on the opposite side of the chamber was pressed a Lucite insulating tube of $\frac{1}{8}$-inch wall thickness. A brass tube which supported the insulator for the collector cup slipped into the Lucite tube. With this arrangement the brass tube could be used as a guard ring for testing the efficiency of collection of the beam current. To facilitate the assembly of the current-collection system this tube was made in two parts, sealed together with a Neoprene strip gasket.

The insulator which supported the current-collector cup was a piece of glass tubing, one-inch outside diameter, sealed to the brass with hard wax. The collector cup itself was a piece of brass tubing, $\frac{3}{4}$-inch inside diameter, which extended out through the glass tube insulator and had its rear end covered with a piece of vicor glass .To eliminate charging of this glass plate, it was covered on the inside with a fine-mesh nickel screen. This window on the back of the collector cup was used in order that the chamber as a whole could be more easily lined up with respect to the ion beam of the generator by observing the fluorescent spot on the glass.

To prevent erroneous results in the current collection because of ionization current around the collector, the collector-cup assembly was separated from the rest of the chamber by a thin aluminum foil (0.0015 inch thick). A separate lead to the fore vac and high vac manifolds was provided for evacuating the collector-cup chamber.

DETECTORS

The movable proportional counter was bored out of a brass block. Its inside diameter was one

inch, and its central wire was 0.010 inch in diameter. The wire was supported at one end by a procelain insulator, and at the other end passed out of the counter into a connection box just above through a Kovar-glass seal. To keep the active region of the counter from being too large and yet not distort the field near the center to any extent, the central wire was enlarged for about three-eighths of an inch at each end by placing over it sections of stainless-steel tubing, 0.025-inch outside diameter. These sections reduced the field on the ends to too low a value to cause appreciable multiplication of ions. The section of bare wire in the center was one inch long.

The scattered particles entered the proportional counter through a defining system consisting of two slits and a hole.†† The first slit and the hole defined the space from which scattered particles could enter the counter, while the intermediate slit cut off particles scattered from the walls of the slit system.

To make sure that the slit system of the counter was pointed directly at the center of the chamber, it was lined up by using a pointed mandrel, which was a tight fit into the holder for the slit system, and another pointed rod which was pressed into a hole exactly in the center of the tapered plug. The alignment was checked by setting the counter at zero degrees and sighting into the chamber and counter through the holes which define the original beam of ions entering the chamber. During this process it was found that the axis of the tapered plug was 0.007 inch off of the axis of the beam-collimating system, but seemed to be perpendicular to it nevertheless.

The center of the counter slit system was a little below the axis of the beam-collimating holes so the proportional counter assembly was shimmed up into position. After the position of the counter had been checked for height, orientation, and position with respect to the zero of the disk graduations, it was pinned in place with two tapered pins so that it could be removed and yet replaced exactly as it was. The critical dimensions of the slit system required for conversion of the observed yield to absolute cross sections are, in the notation of HKPP, the width $2b$ of the first detector slit (slit A, Fig. 1), the area A of the last detector hole (hole C, Fig. 1), the separation h between these apertures, and the distance R_0 from the hole C to the center of the beam. Careful measurements were made of each of these quantities, with the following results: $2b=0.2067$ cm; $A=2.094\times10^{-2}$ cm^2; $h=6.988$ cm; and $R_0=12.893$ cm. The slit and hole were somewhat irregular in shape so that the values of $2b$ and A represent the averages of a number of width measurements along the slit and diameter measurements at eight different angles across the hole. These values for the geometrical constants give a value of 4.796×10^{-5} cm for the quantity $G=2bA/R_0h$ (see HKPP). The accuracy of this constant is estimated to be 0.5 percent; the greatest uncertainty is contributed by the irregularity of the hole.

After passing through the last dector hole, the scattered particles passed through a thin window of aluminum 0.00006 centimeter thick into the counter. The aluminum was coated with a 5 percent solution of collodion in order to cover the pinholes in the foil. This combination aluminum and collodion window is thinner than one made of pure aluminum which is without pinholes, and is more reliable than a window made of collodion alone. Such a window easily withstood the 5-cm Hg pressure of the gas inside the counter. The scattered particles passed through the counter in a plane perpendicular to the counter wire and $\frac{1}{8}$ inch away from the wire. Tests of this arrangement with a polonium source gave very satisfactory results. With a gas filling of 5 cm of butane and a multiplication of about 150, the α-particle pulses gave a distribution with a half-width of 5 to 7 percent.

The outside of the proportional counter was at ground potential and the central wire was maintained at high voltage. Since the wire also collects the signal which is to be amplified, it is essential to prevent corona trouble and spark-over to the high voltage lead going to the central wire. The high voltage lead was brought up through the tapered plug and over to the connection box on top of the counter through a tube which was maintained at atmospheric pressure. The connection box at the top of the counter, also at atmospheric pressure, was covered with a brass plate and isolated from the vacuum by a

†† See reference 6, Fig. 3, p. 1000. See also detail in Fig. 1.

Neoprene strip gasket. The lead wire was insulated with a continuous plastic tube from a coaxial cable.

Outside the chamber, the electrical lead passed through a flexible joint to another connection box where the signal was separated from the high voltage by a decoupling resistance of 10 Meg in the high voltage supply line. A coupling capacitance of 100 $\mu\mu$f fed the signals to the preamplifier. From there the signal passed on to the amplifier and discriminator. The gas lead to the counter went through the tapered plug directly to a hole in the counter wall. A piece of rubber tubing connected this lead to the gas-filling system external to the chamber.

The monitor counter, which fitted into a hole in the wall of the scattering chamber at 15° with respect to the proton beam, was essentially the same as the movable counter inside the chamber. Since it was somewhat further away from the center of the chamber, the slit system was a little larger to prevent reduction of its counting rate.

The two counters were enough alike that they could be filled simultaneously and could use the same high voltage supply.

MEASUREMENT OF PROTON ENERGY

To calibrate the electrostatic analyzer[7] of the generator, the $Li^7(p,n)Be^7$ reaction was used. The threshold was assumed to be 1.860 Mev.[8] A small crystal of LiF was placed on a magnetically operated shutter already installed in the target tube of the generator. When the crystal was raised into the proton beam, the neutrons produced could be detected by a BF_3 neutron counter placed beyond the scattering chamber.

To know accurately the energy of the ions inside the scattering chamber a correction must be made for the stopping power of the aluminum foil over the first defining diaphragm. To obtain the stopping power of this foil another LiF crystal was placed in a special holder at the entrance to the current-collector guard ring. When the $Li(p,n)$ threshold is checked first with the crystal in the target tube and then with the one inside the chamber, the difference gives the stopping power of the foil. Measurements at the beginning and at the end of this experiment gave values of 70 and 90 kev, respectively, for the stopping power of the foil at 1.86 Mev. The increase was undoubtedly due to carbon deposited during the course of operation. Measurements on the threshold, before and after the present experiments, indicated no noticeable change in the calibration of the analyzer.

CURRENT MEASUREMENT

In order to check the efficiency of the current collector, a series of tests, similar to those described by HKPP††† were made. A brass tube was inserted in the Lucite sleeve, described above, and was in contact with the brass guard ring. The inserted tube extended to, but did not touch, the exit slit of the collimator. The guard-ring system and the cup were separately connected to sensitive galvanometers and tests on secondary electrons, leakage, foil scattering, and neutralization were carried out. These tests showed that with a vacuum of 4×10^{-6} mm Hg around the cup, a magnetic field at the entrance to the cup of 300 gauss, and a voltage of 45 volts between cup and guard ring (cup negative), the error in measuring the current, introduced by the factors mentioned above, was less than 0.1 percent.

Two methods of measuring the beam current were employed. The generator-current integrator[9] was used in the preliminary measurements. It was calibrated by feeding current from a +400-volt supply through a high resistance onto the input condenser of the integrator. The collector cup and connecting lead had an appreciable capacitance so that they were left connected to the integrator during the calibration. The high resistance box also was left permanently in place. The current was determined by measuring the voltage across a 3-meg. resistor with a type *K* potentiometer. The 3-meg. resistor had been previously calibrated against precision resistances and was inserted between the high voltage

[7] A. O. Hanson, R.S.I. **15**, 57 (1944).

[8] R. O. Haxby, W. E. Shoupp, W. E. Stephens, and W. A. Wells, Phys. Rev. **58**, 1035 (1940); A. O. Hanson and D. L. Benedict, Phys. Rev. **65**, 33 (1944). The former group obtained 1.856 Mev for the threshold while the latter investigators found 1.883 Mev. The value 1.860 Mev has been generally used in this laboratory.

††† See reference 6, p. 1004.

[9] J. M. Blair, Rev. Sci. Inst. **14**, 64 (1943).

supply and the high resistance. This system eliminated the introduction of unwanted capacitances in parallel with the input condenser of the integrator. The integrator was biased so that it operated between −45 volts and ground. Calibration to a fraction of a percent was possible, but was found to be unnecessarily refined, since it was discovered during preliminary scattering measurements that the calibration varied irregularly over the course of time by as much as 5 percent. Since the method of calibration outlined above was too cumbersome for frequent use, it was decided to use a monitor chamber and, in addition, to calibrate the monitor counter with a standard condenser and ballistic galvanometer. For the greater part of each run (angular distributions at a fixed energy) the current integrator was used. Then for several angular settings of the rotating counter the Leeds and Northrup 1-microfarad standard condenser was connected to the collector cup, and the charge corresponding to a given number of monitor counts (6400) was measured. Preceding each such measurement, the ballistic galvanometer was calibrated by charging the standard condenser to an accurately measured voltage and subsequently discharging it through the galvanometer.

Monitor counts were taken at each position of the rotating counter and current-integrator readings were taken except during the calibrations. It was, therefore, possible to compare the number of monitor counts (per microcoulomb per mm of pressure) obtained with the current integrator with the number of monitor counts (per microcoulomb per mm of pressure) obtained with the condenser-ballistic galvanometer. By averaging the former values a number was obtained which agreed within several percent with the latter values but were consistently lower. For the final calculation of the number of scattered particles per microcoulomb per mm of pressure, the current integrator and the condenser-ballistic galvanometer results were averaged. This procedure was adopted since time did not permit a thorough investigation of either method. It is felt that the problem of current measurement is the greatest single course of error in the determination of the absolute cross sections. A reasonable estimate of the probable error in the current measurement is 2 percent.

The number of scattered particles per microcoulomb per mm of pressure was determined by multiplying the ratio of detector counts to monitor counts by the value of monitor counts per microcoulomb per mm of pressure, obtained as outlined in the preceding paragraph. Since the monitor was located at 15°, its counting rate was very high and the accuracy in the ratio of detector to monitor counts was limited by the counting rate of the detector. As mentioned above, the runs were made at constant energy. The relative cross sections at a particular energy are more accurate than the absolute values, since errors in the determination of the "microcoulombs" and the "mm of pressure" are eliminated.

GAS SYSTEM

The scattering chamber was filled with the scattering gas to a pressure of approximately 1-cm Hg through a palladium spiral which was directly heated. The pressure in the chamber was measured with a manometer of 2-cm diameter glass tubing, attached directly to the chamber. The Apiezon B oil used in the manometer was outgassed by torching during evacuation. A microscope with a micrometer screw was mounted on a swinging vertical bar so that, with the aid of fiducial marks, the levels of the oil in both arms of the manometer could be read to an accuracy of 0.1 mm. As the difference in oil levels was usually 150 mm, the pressure could be read to an accuracy of 0.15 percent. A thermometer was placed on top of the scattering chamber to give the chamber temperature.

A stainless-steel liquid-air trap, attached to the chamber, was constantly in use. Because of rapid conduction by the hydrogen-scattering gas, the level of the liquid air changed rapidly and had to be refilled every hour. The pressure in the chamber varied by several millimeters as the liquid-air level changed. Consequently, pressure readings were taken immediately preceding and following each measurement at a particular angle and energy, and the pressure (corrected for temperature to 0°C) was taken to correspond to the mid-time of each measurement. The estimated accuracy in the pressure values is 0.5 percent. This figure includes possible errors introduced by assuming that the oil density was

0.864, whereas the actual density was found to vary from 0.858 at 25°C to 0.864 at 15°.

Tests were made to determine the effect of impurities. Since the chamber was isolated for five or six hours during each run, measurements of scattering of the proton beam were made with the chamber evacuated and isolated, with the liquid-air trap in operation. These measurements showed that impurities built up by gassing of the chamber contributed a negligible amount to the gas-filled yield. The palladium tube was tested for a possible contribution by a simulated filling, with negative results. Before changing from hydrogen to deuterium gas, and *vice versa*, the palladium tube and chamber were flushed several times with the new gas before measurements were begun. The effectiveness of this procedure was adequately checked by the absence of recoil deuterons when hydrogen was substituted for deuterium.

RECORDING APPARATUS

The present experiments were begun shortly after the completion of a new 10-channel amplitude recorder designed by M. Sands of the Electronics group. This instrument was available and proved to be a thoroughly reliable and extremely useful recording device for our measurements. The details of this multi-channeled discriminator will be described in detail in a future publication,[10] but in essence it consists of 10 discriminator and scaling units. The discriminators are successively biased by equal increments. Each channel is connected with its neighbors by anti-coincidence circuits and an incoming pulse is registered in that channel which is in anti-coincidence with the following channel (except for the tenth channel which records all pulses higher than its bias setting.) One, therefore, obtains a "differential bias curve" for the incoming pulses. The width of the channels could be selected to be 2, 5, or 10 volts, and the minimum bias on the set of channels could be varied. With these two adjustments it was possible, in a simple manner, to adjust the resolution of the instrument to our particular requirements.

The time-saving features of the 10-channel discriminator are immediately obvious for the $p-d$ scattering measurements, since both scattered protons and recoil deuterons enter the detector at angles below 90°. The relative and absolute pulse amplitudes of the two groups vary from angle to angle as will be shown below (Fig. 2). The proper settings of the amplifier gain and channel position and width could be determined in a matter of minutes before actual measurements were made. Since the two groups could be adequately resolved at most angles a higher accuracy is achieved by this method of recording over a single discriminator for the same total number of counts. Another simplification was introduced by obtaining the background for each group. At low accelerating voltages, this background was more or less randomly distributed. At higher energies (about 3 Mev), an appreciable background, generated by protons striking the collimator slits, was observed which had a distribution which was high in the lower channels and rapidly decreased. Backgrounds were measured after each run with the scattering chamber evacuated at the same angular, amplifier, and discriminator settings which were used in the scattering measurements.

The linear amplifiers,[11] used with the movable detector and the monitor counter, had a rise time of 0.5 microsecond and were stabilized by inverse feedback. The low frequency response was limited to allow quick recovery (within several microseconds). Since the monitor counter detected the two groups of particles at constant amplitudes for a given energy setting, its pulses were recorded with two "integral-bias" discriminators. Bias curves were taken at each energy and the two groups were found to have excellent plateaus. The two discriminators were then set on the deuteron plateaus, one at the middle and the other at a lower bias as a check for drift of the plateau.

PROTON-PROTON SCATTERING

In the notation of HKPP the yield of detected particles is given by

$$Y = N n \sigma G / \sin\theta, \tag{1}$$

where N is the number of incident particles, n is the number of scattering particles per cm³, and σ is the scattering cross section (in laboratory

[10] Los Alamos Technical Series 1, Part 1, Section 4.5.

[11] Los Alamos Technical Series, 1, Part 1, Section 3.6.

coordinates) per unit solid angle at the angle θ. The factor $G/\sin\theta$ defines the target volume and detector efficiency. In view of the short time available for the present experiment, it was considered advisable to check our experimental arrangement and procedures by measuring proton-proton scattering for comparison with the careful experiment of HKPP. By these measurements it was felt that systematic errors would be discovered quickly. One series of such measurements were made before the proton-deuteron tests, and a second set of data was taken after completion of the latter measurements. These results are summarized in Table I. The incident-

TABLE I. Comparison of proton-proton scattering yields at 2.08 Mev with the yields obtained by HKPP. The upper set was measured before the proton-deuteron experiments, the lower set after the completion of the latter measurements.

Angle (degrees)	15	20	25	30	35	40	45
Yield/μC/mm	5.09	2.38	1.81		1.23		0.887
Corrected yield	3.03	1.42	1.08		0.732		0.528
HKPP yield	2.91	1.405	1.039		0.743		0.525
Percentage difference	+4.1	+1.1	+3.9		−1.4		+0.5
Angle (degrees)	15	20	25	30	35	40	45
Yield/μC/mm	4.90	2.32	1.76	1.46	1.22	1.009	0.880
Corrected yield	2.92	1.38	1.05	0.866	0.725	0.600	0.524
HKPP yield	2.91	1.405	1.039	0.855	0.743	0.604	0.525
Percentage difference	+0.3	−1.8	+1.0	+1.3	−2.4	−0.7	−0.2

proton energy was 2.08 Mev. Measurements made at different pressures gave identical results for the yield per mm. Measurements were also made with angular settings on both sides of the incident beam, but no systematic difference was observed. The first set of data was taken using the current integrator. The second set was taken using the condenser-ballistic galvanometer-monitor counter method of current measurement, in addition to the current integrator; the final results were evaluated as described in the section on "current measurements." For a direct comparison with the data of HKPP, our yields were divided by 1.680, which is the ratio of our value of G to the value of G given by HKPP.

In Table I the first row gives the angular setting (laboratory coordinates); the second row is the yield per microcoulomb per mm of pressure at 0°C. Row three shows the yields corrected by the factor 1.680, while the fourth row gives the data obtained by HKPP. The last row indicates the percentage differences. The improvement in our measurements on using the monitor counter

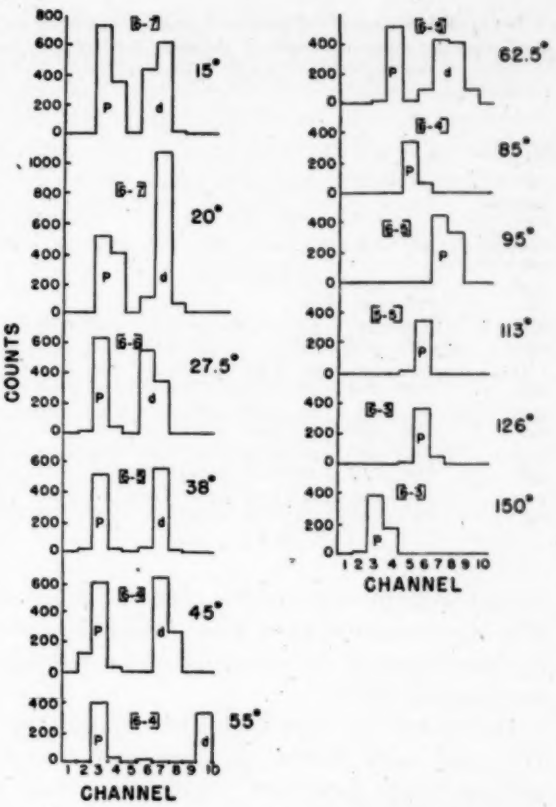

FIG. 2. Scattered-proton (p) and recoil-deuteron (d) yields at 2.08 Mev obtained with the 10-channel amplitude recorder. The ordinates are the observed counting rates, the abscissa are the various channels. The bracketed quantities represent the amplifier gain, larger numbers corresponding to higher gain.

and ballistic galvanometer method of current calibration is apparent from the second set of data in Table I. From the estimates given above for the accuracy in the determination of N, n, and G, one obtains a probable error of 2.2 percent in the determination of NnG. The number of counts taken at each setting in the second experiment was in the neighborhood of 8000, leading to

TABLE II. Conversion factors for determining of absolute cross sections per unit solid angle in the center of mass system from the observed yields of protons and deuterons. The angles ϕ and ϵ are the laboratory angles (degrees) for the protons and deuterons, the values of β are the corresponding center of mass angles.

ϕ	15	20	27.5	38	45	55	62.5	85	95
β	22.5	29.9	40.9	55.9	65.7	79.2	88.8	114.9	124.9
$F(\phi)$	0.1180	0.1592	0.2240	0.3235	0.398	0.520	0.626	1.041	1.273
ϕ	113	126	150						
β	140.4	149.9	164.5						
$F(\phi)$	1.704	1.918	1.991						
ϵ	15	20	27.5	38	45	55	62.5		
β	150	140	125	104	90	70	55		
$F(\epsilon)$	0.0670	0.0910	0.1302	0.1953	0.2500	0.3570	0.4803		

TABLE III. Summary of proton-deuteron scattering experiments. The yield is the number of scattered protons or recoil deuterons per microcoulomb of incident protons per millimeter of oil pressure. The cross section per unit solid angle in center of mass coordinates $\sigma(\beta)$ is given in units of 10^{-24} cm^2.

Proton angle φ	15	20	27.5		38	45		55	62.5			85	95			113	126		150	Energy (Mev)
Deuteron angle ϵ				62.5			55			45	38			27.5	20			15		
Center of mass angle β	22.5	29.9	40.9	55	55.9	65.7	70	79.2	88.8	90	104	114.9	124.9	125	140	140.4	149.9	150	164.5	
Yield	34.0	9.24	2.64											2.18	3.69			5.26		0.825
$\sigma(\beta)$	2.98	1.09	0.439											0.210	0.247			0.261		
Yield	11.18	3.73	1.55		0.765	0.576	0.584	0.387		0.784	1.10	0.228	0.226	2.32	4.37	0.227	0.225	6.72	0.331	1.51
$\sigma(\beta)$	0.980	0.441	0.258		0.184	0.170	0.154	0.149		0.145	0.159	0.176	0.214	0.224	0.294	0.286	0.320	0.334	0.417	
Yield	6.08	2.67	1.29	0.487	0.738	0.527	0.548	0.340	0.258	0.632	0.830	0.180	0.179	1.76	3.69	0.194	0.204	5.94	0.292	2.08
$\sigma(\beta)$	0.533	0.315	0.214	0.174	0.177	0.156	0.145	0.131	0.120	0.117	0.120	0.139	0.169	0.170	0.247	0.245	0.290	0.295	0.367	
Yield	4.97	2.28	1.30	0.503	0.736	0.534	0.537	0.330	0.242	0.588	0.724	0.149	0.150	1.52	3.15	0.171	0.191	5.69	0.272	2.52
$\sigma(\beta)$	0.436	0.270	0.216	0.179	0.177	0.158	0.142	0.127	0.113	0.109	0.105	0.116	0.142	0.147	0.213	0.217	0.271	0.282	0.342	
Yield	3.92	2.05	1.24	0.474	0.688	0.492	0.517	0.316	0.230	0.540	0.603	0.125	0.125	1.26	2.73	0.148	0.175	5.06	0.271	3.00
$\sigma(\beta)$	0.344	0.242	0.207	0.169	0.166	0.145	0.137	0.122	0.107	0.100	0.0878	0.0968	0.118	0.122	0.196	0.187	0.251	0.251	0.343	
Yield	3.48	1.95	1.20	0.404	0.679	0.480	0.474	0.272	0.173	0.499	0.528	0.128	0.117	1.03	2.44	0.126	0.151	4.58		3.49
$\sigma(\beta)$	0.304	0.229	0.198	0.144	0.163	0.141	0.125	0.104	0.0802	0.0922	0.0764	0.0975	0.110	0.0986	0.165	0.160	0.215	0.227		

a total probable error in the yield of 2.5 percent. The agreement between these two independent measurements of the proton-proton scattering is very satisfactory.

Data were taken at angles beyond 45° (up to 70°) and were found to agree well with the measurements below 45°, indicating that our instrumentation would be satisfactory for the larger angular range covered in the proton-deuteron scattering.

PROTON-DEUTERON SCATTERING

In the measurement of proton-deuteron scattering, scattered protons and recoil deuterons enter the detecting counter. It is necessary to separate the two groups in order to determine the angular cross sections. As mentioned above, this separation was accomplished by means of a 10-channel amplitude recorder. Typical results obtained with this device are shown in Fig. 2. The bracketed numbers represent the amplifier gain, higher numbers referring to higher gain settings. Bearing these numbers in mind, we can see the general trend of the amplitudes of the two groups. The counter depth is small compared with the particle range at low angles so that at 15°, the deuteron pulse is roughly twice as large as the proton pulse. The deuteron energy falls off relatively more rapidly with angle than the proton energy, so that both groups increase in amplitude, the deuteron group increasing more rapidly. A maximum separation in the groups occurs at about 55°. Beyond this point the proton pulses continue to increase, but the deuteron pulses begin to decrease as the residual deuteron range (beyond the counter window) becomes smaller than the counter depth. At about 70° the proton and deuteron groups overlap with the latter disappearing rapidly beyond this angle. The proton pulses continue to increase in amplitude to 113° beyond which they decrease. An additional point of interest is the counts observed in channel 6 at 55°. These correspond to protons scattered from hydrogen contamination in the deuterium gas. (The apparent narrowness of the deuterium group at 55° is fictitious, since channel 10 actually records all amplitudes greater than those which would fall in channel 9.) Mass-spectrographic analysis‡ of the deuterium gas gave a composition of 99.1 percent deuterium and 0.9 percent hydrogen.

If β is the angle of scattering of the proton in center of mass coordinates, and ϕ and ϵ are the corresponding angles in the laboratory system of the scattered proton and recoil deuteron, one obtains the following relationships:

$$\epsilon=\pi/2-\beta/2 \tag{2}$$

and

$$\sin(\beta-\phi)=\tfrac{1}{2}\sin\phi. \tag{3}$$

To convert the laboratory angular cross sections, obtained from the yields by Eq. (1),

‡ Analysis was made at the Metallurgical Laboratory in Chicago.

to angular cross sections in the center of mass system, one has

$$\sigma(\beta)\sin\beta d\beta=\sigma(\phi)\sin\phi d\phi.$$

Combining this equation with Eq. (3) one finds

$$\sigma(\beta)=\sigma(\phi)\cos(\beta-\phi)[(\sin\phi)/(\sin\beta)]^2.$$

Since $\sigma(\phi)$ is given by Eq. (1), one obtains

$$\sigma(\beta)=(1/NnG)\,Y(\phi)F(\phi), \tag{4}$$

where

$$F(\phi)=[(\sin^3\phi)/(\sin^2\beta)]\cos(\beta-\phi). \tag{5}$$

Similarly, from the deuteron yields

$$\sigma(\beta)=(1/NnG)\,Y(\epsilon)F(\epsilon), \tag{6}$$

where

$$F(\epsilon)=\tfrac{1}{4}\tan\epsilon. \tag{7}$$

The conversion factors $F(\phi)$ and $F(\epsilon)$ were evaluated from these equations and are listed in Table II. These results were used to convert the measured yields to cross sections per unit solid angle in the center of mass system. The value of $(NnG)^{-1}$ for 1 microcoulomb and 1 mm of oil pressure is 0.742×10^{-24} cm^2.

RESULTS

A series of runs was made to scan the energy interval 0.8 to 3.5 Mev to see if any pronounced dependence on energy was to be observed. The dependence on energy appears to be gradual, so that final results were obtained at intervals of approximately 500 kv. These results are summarized in Table III. The yields have been cor-

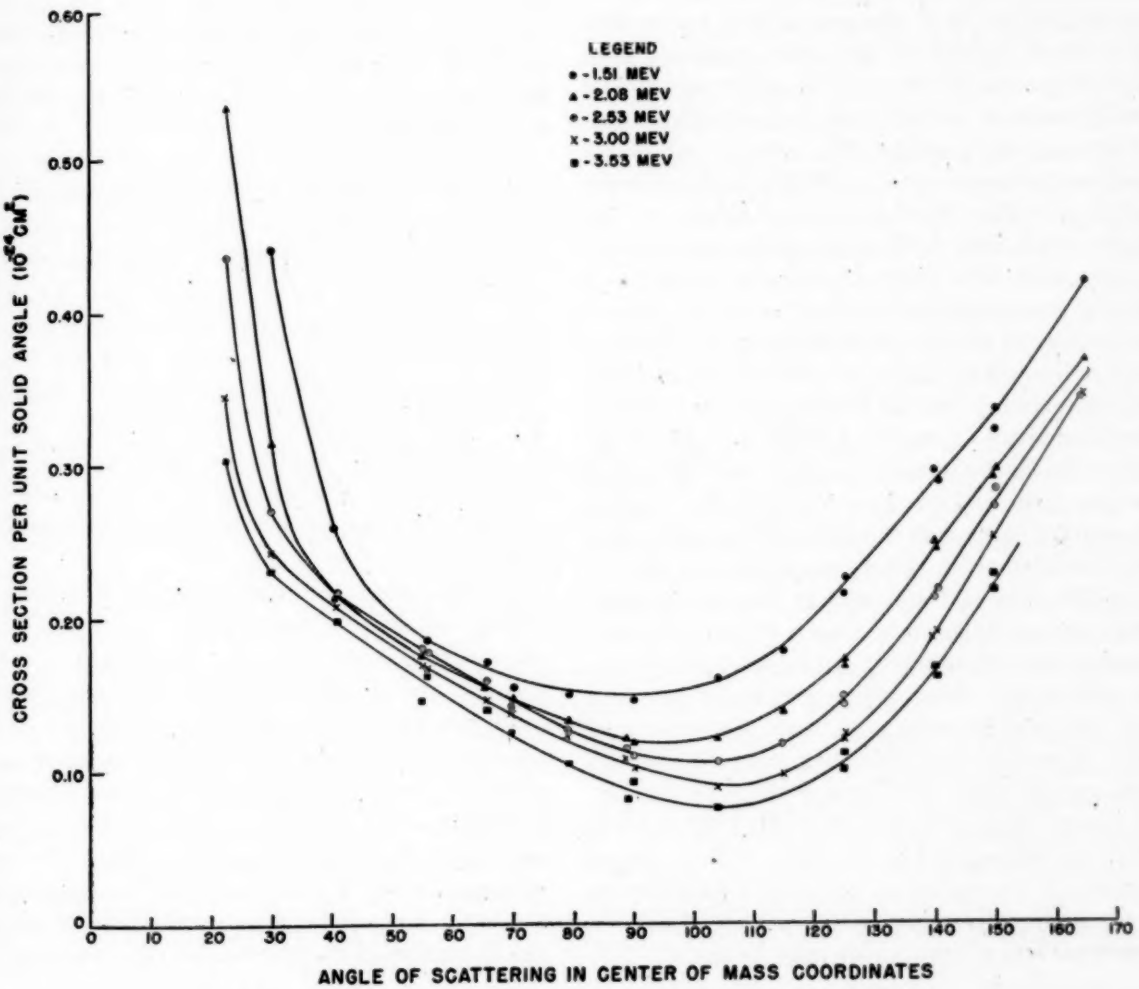

FIG. 3. Angular distribution of protons scattered by deuterons (see Table III).

TABLE IV. Ratio of observed scattering cross sections to Rutherford cross sections for various energies and angles.

E (Mev)	Scattering Angle β 45°	60°	90°	120°	150°
1.51	3.68	8.65	28.3	87	224
2.08	6.44	15.2	43.8	128	377
2.53	9.76	22.9	60.1	158	524
3.00	13.1	30.5	79.3	186	670
3.49	16.6	37.8	89.6	215	798

rected for background and for hydrogen contamination. The latter correction was made for all deuteron angles and for proton angles greater than 55°. At lower angles, the protons scattered by hydrogen and deuterium were indistinguishable. No correction was made at these angles, but since the scattering by the two nuclei is of the same order of magnitude, the negligence introduces a trivial error. No geometrical corrections have been applied to the cross sections; such corrections would increase the value at 15° (for the protons) a few percent, but would be negligible at higher angles. The energy values are believed to be correct to ±30 kev relative to the value of 1.860 Mev for the threshold of the Li(p,n) reaction which was used to calibrate the energy scale. The entrance foil was taken to be 80-kev equivalent at 2.1 Mev, since the rate of deposition of carbon on this foil was unknown. The estimated accuracy of ±30 kev also includes the uncertainty in the linearity of the electrostatic analysis. Counts of 2500 or more were taken at each setting so that the statistical weight of the yields is 2 percent or better, leading to a probable error of the order of 3 percent when the uncertainty in the determination of NnG is included. The last run at 3.49 Mev is considerably less accurate as a result of generator difficulties and the failure to take a background run at this energy. The background was fairly high and an estimate of it was made for this set of data. However, it is felt that the errors of this run are probably not greater than 10 percent. The data taken at 1.51, 2.08, 2.53, 3.00, and 3.49 Mev are shown in Fig. 3, where $\sigma(\beta)$ is plotted against β. The excellent agreement between the cross sections obtained independently from the deuteron and proton yields may be noted.

TABLE V. Proton-deuteron scattering results at 825 kev. The ratio of observed cross section to Rutherford cross section is given in rows labelled R.

(a) Results of present experiment at 825 kev.

β	22.5°	29.9°	40.9°	125°	140°	150°
$\sigma(\beta)$	2.98	1.09	0.439	0.210	0.247	0.261
R	0.997	1.12	1.52	30.4	45.6	53.1

(b) Results obtained by Tuve *et al.* (tabulated by Primakoff) at 830 kev.

β	30°	45°	59°	110°	120°	150°
R	2	5	8	70	124	2275
R theory	2	4	7	35	40	61

The presence of nuclear scattering is quite apparent from these curves. At angles beyond 45° it represents the major fraction of the scattering cross section. The increase of cross section at large angles and the shifting of the minimum show that waves of higher order than the spherically symmetrical S-wave must be effective. The ratios of the observed cross sections to Rutherford cross sections are given in Table IV for several angles.

As was mentioned in the introduction to this paper, Tuve, Heydenburg, and Hafstad[1] obtained very anomalous results in the proton-deuteron scattering at 830 kv which subsequent theoretical work by Primakoff[2] and Occhai[3] attempted to explain. The present data do not agree with these previous results. In Table V our measurements expressed as "ratio to Rutherford" may be compared with the earlier work. The theoretical values of R calculated by Primakoff are in fair agreement with the present measurements at the larger angles, but give too high values at low angles.

In conclusion we take pleasure in acknowledging the helpful suggestions and interest of Drs. A. O. Hanson, J. L. McKibben, C. M. Turner, and J. H. Williams. This experiment could not have been completed within the short time available without the generous assistance of Dr. A. Hemmindinger and Messrs. E. Klema, R. Perry, and L. W. Seagondollar in taking data and operating the electrostatic generator. We are indebted to Mr. E. W. Dexter of the electronics group for his assistance in periodically checking the operation of the 10-channel discriminator.

A Neutron Detector Having Uniform Sensitivity from 10 Kev to 3 Mev

A. O. HANSON* AND J. L. MCKIBBEN
Los Alamos Scientific Laboratory, Santa Fe, New Mexico

(Received July 10, 1947)

A neutron detector having approximately uniform sensitivity from 10-kev neutron energy to 3-Mev energy is described. The arrangement, known as a long counter, consists of a paraffin cylinder about 10″ outer diameter ×12″ long surrounding a long boron trifluoride proportional counter. Sensitivity curves are given for two of the best arrangements. The response is flat over the above range to about 10 percent.

A NEUTRON detector which has a uniform efficiency for neutrons of widely different energies has many advantages for certain types of measurements. A large water bath containing slow-neutron detectors in some form fulfills this requirement and has been very useful in determining the number of neutrons emitted by various neutron sources.[1] The examination of the number of slow neutrons as a function of the distance from the source in such a water bath gives additional information regarding the energy of the neutrons.[2] There are many experiments, however, where the use of a large water bath is either awkward or gives erroneous results because of the effect of the degraded neutrons reflected from the bath into the experimental setup.

In order to achieve a high efficiency in a detector of reasonable size an attempt was made to find a suitable arrangement of paraffin surrounding a boron detector. The analogy with the water bath experiment suggested that a long boron counter embedded in a block of paraffin would have a counting rate which would not depend much on the energy of the neutrons. The first detector constructed consisted of a boron-lined ionization chamber 20 cm long surrounded by a cylinder of paraffin 20 cm long and 17 cm in diameter, this was used with its axis pointed toward the neutron source. Preliminary tests on the sensitivity of this counter showed that the sensitivity was very nearly the same for neutron energies of from 0.4 Mev to 2 Mev; these tests served to encourage the development of counters along the same lines. This type of detector will be referred to as a long counter.

The theoretical treatment of the sensitivity of this type of counter is quite complicated and has not been worked out. There are, however, certain qualitative arguments which may help in understanding the behavior of these counters and which may serve to suggest further improvements.

Examine first an arrangement in which a long thermal-neutron detector is embedded in a large (semi-infinite) slab of paraffin and in which neutrons of various energies are incident upon this slab in the direction parallel to the axis of the detector. The neutrons entering the paraffin will be slowed down primarily by the hydrogen atoms to thermal energies and some of these neutrons will be captured by the central thermal-neutron detector and will be recorded as counts in some manner. If the neutrons have a very high energy, the mean free path of these neutrons is initially large and therefore will be slowed down an appreciable distance from the front face of the slab. After a number of collisions, the mean free path will be reduced to such an extent that these neutrons have a very small chance of escaping out of the front face of the slab. This is not the case, however, for neutrons having energies of the order of 100 kev or less, since in this case the mean free path of the neutrons does not change appreciably as the neutrons approach thermal energies.[3] These neutrons would therefore have a much larger probability of escaping out of the surface of the semi-infinite slab as compared to the high energy neutrons. This effect is partially compensated for by the fact that the less energetic neutrons would need to make fewer collisions before becoming thermal-

* Now at the University of Illinois, Urbana, Illinois.
[1] E. Amaldi, L. R. Hafstad, and M. A. Tuve, Phys. Rev. **51**, 896 (1937).
[2] R. D. O'Neal, Phys. Rev. **70**, 1 (1946).
[3] C. L. Bailey, W. E. Bennett, T. Bergstralh, R. G. Nuckolls, H. T. Richards, and J. H. Williams, Phys. Rev. **70**, 583 (1946); D. H. Frisch, *ibid.*, 589 (1946).

ized, but the effect would be such that the detection efficiency for high energy neutrons would be several times greater than that for very low energy neutrons.

If the sensitivity for low energy neutrons is to be approximately the same as that for neutrons of high energy, some modification of this idealized arrangement must be made. The success of the first long counter must be ascribed to a fortunate choice of the dimensions of the paraffin block such that the increased probability of escape of high energy neutrons from the sides of the block compensated in some degree for the escape of low energy neutrons from the front face. The effect of the size of the paraffin cylinder has been investigated roughly and is indicated in a later section of this report. The size of the central cavity made by the detector is perhaps important although no systematic investigation of its effect was made. It will be shown, however, that the introduction of additional holes in the front face affected the low energy sensitivity of one of the counters appreciably.

DESCRIPTION OF COUNTERS

Two counters were used quite extensively and will be described here in detail. The first consisted of a central BF_3 proportional counter 1 inch in diameter, which had an effective length of 8 inches. This tube was surrounded by paraffin cylinders 12 inches long and 6, 8, and 12 inches in diameter. The counter with the 8 inch paraffin cylinder is shown in Fig. 1. The proportional counter protrudes slightly from the front face of the paraffin block but is protected from direct thermal neutrons by means of a cadmium shield. The proportional counter is supported by means of ceresin wax in the center of an aluminum tube which also serves as an electrical shield. The body of the counter was a $\frac{1}{32}$-inch wall brass tube and was soldered to Kovar glass seals. The central electrode consisted of a 10-mil Kovar wire. The $\frac{1}{4}$-inch intermediate electrode was used as a guard ring and was connected to ground. The counter was filled with enriched BF_3 (80 percent B^{10}) to a pressure of 25 cm Hg. With -2700 volts on the outer shell the proportional counter gives a gas amplification of about 10. The signal was further amplified by means of a model 100 linear amplifier[4] with a R-C time constant of 5 microseconds and the pulse was counted by means of a model 200 discriminator and scale-of-64 circuit.[5] Except in the cases where impure BF_3 was used, because of leaks in the tube or filling system, the bias curves (counting rate against minimum pulse height recorded) were such that a change in the bias voltage by a factor of two in either direction would not change the counting rate by more than 5 percent. The counting rate was not affected by the gamma radiation from an unshielded 500-mg radium source used at a distance of 40 cm from the counter.

The other counter, which will be referred to as the shielded long counter, is shown in Fig. 2. The principal modification is that an additional paraffin and boron shield is used so as to make it less sensitive to neutrons which have been scattered about the room. The proportional counter is similar except that it was 10.5 inches long,

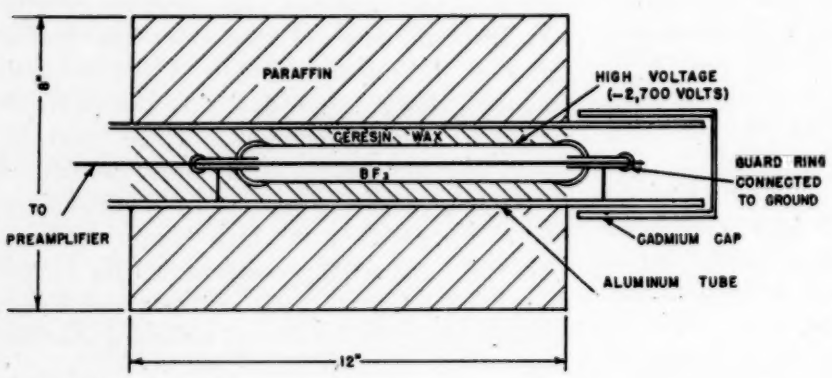

FIG. 1. 8-inch OD long counter.

[4] Designed by M. Sands.
[5] Designed by W. Higinbotham.

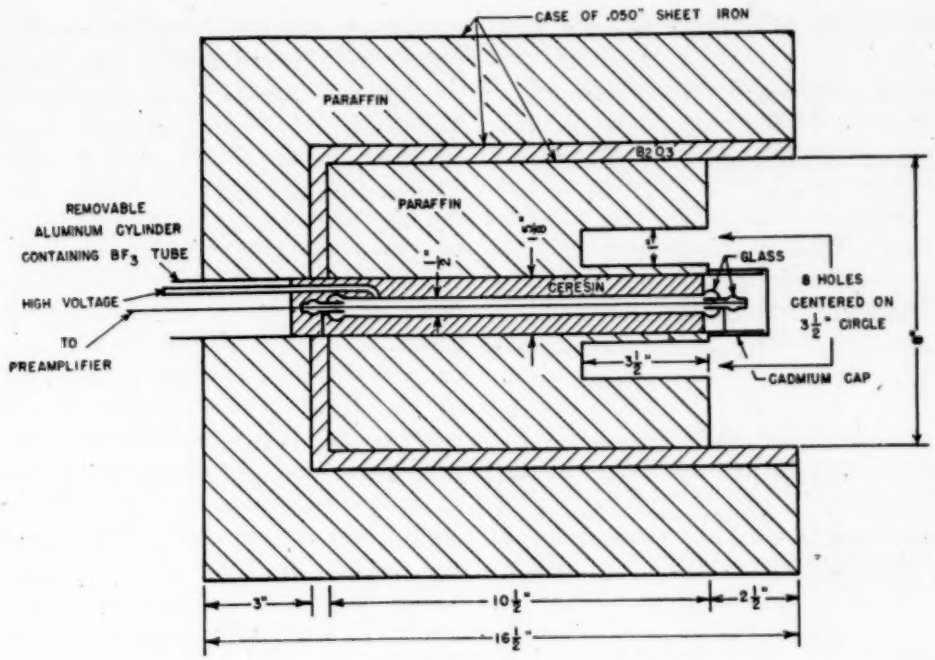

FIG. 2. Shielded long counter.

½ inch in diameter, and was filled with BF_3 to a pressure of 40 cm. For most of the measurements made with these counters it was convenient to use a matched pair of the counters in the arrangement shown in Fig. 3. In addition to increasing the sensitivity of the over-all system, such an arrangement minimizes errors due to exact positioning of sources.

SENSITIVITY CURVES

The data on the sensitivity of the counters to neutrons of various energies were obtained by three methods, namely:

(1) By comparing the counting rates in the counters due to various radioactive neutron sources whose total neutron yield had been compared by some other method such as the water bath technique. Photo neutron sources used were Sb-Be and Y-Be. Alpha neutron sources used were Po-BF_3[6] and Ra-Be. The energies of these sources were taken to be 0.023, 0.16, 2.2 and 5 Mev, respectively. While the energy of the photo neutron sources should be well defined, the alpha neutron sources give a spectrum and the values given represent only average energies. The assignment of an average energy to the neutrons from Ra-Be is especially dubious since the energy spectrum of these neutrons extends out to about 14 Mev. The fraction of neutrons below 0.1 Mev, however, is estimated to be less than 10 percent.[7]

(2) The degradation of the energy of the neutrons from a given source by surrounding the source with spheres of graphite and heavy water. A graphite sphere, 24 cm in diameter, was used which had the effect of reducing the

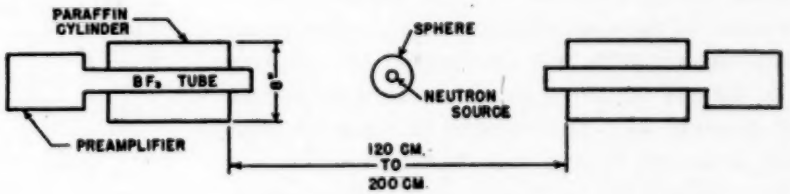

FIG. 3. Experimental arrangement with a pair of 8-inch OD long counters.

[6] H. T. Richards, LADC—288.
[7] A. A. Yalow, R. S. Yalow and M. Goldhaber, Phys. Rev. 69, 253A, 1946.

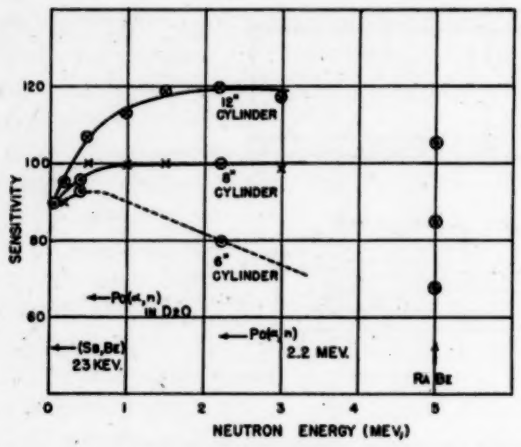

FIG. 4. Sensitivity of 8-inch OD and 12-inch OD long counters. The X's and circled X's represent points obtained with Li^7 (p, n) and D (d, n) neutron sources. Although the curves are not continued beyond 3 Mev the general trends of the curves above this energy are indicated by the points obtained with the Ra-Be source.

average energy of the neutrons by a factor of about 2. A heavy-water sphere, 20 cm in diameter, served to reduce the average energy of the neutrons by a factor of 4 or more. Since neither graphite nor heavy water absorbs neutrons appreciably, the number of neutrons emerging from the sphere would be the same as that emitted from the source. A change in the counting rate with the sphere around the source was therefore taken as a measure of the change in the sensitivity of the counter to the modified spectrum of neutrons. The use of D_2O was, of course, limited by the fact that any source having sufficiently high energy gamma rays would give rise to photo-neutrons from the deuterium. In the case of yttrium it was found that the number of photo-neutrons from deuterium caused by the high energy ray (~2.8 Mev) was only 3 percent of that due to the Be and hence could be accurately taken into account.

(3) The use of homogeneous neutrons of known energy from the Li (p, n) and D (d, n) reactions. In these experiments the flux of neutrons into the counters was determined by counting the fissions occurring in a standardized sample of uranium 235. The energies of these neutrons are accurately known, and the flux measurement are considered to be reliable so that these points should be quite significant.

The summary of the data on the first counter with 6-, 8- and 12-inch cylinders are shown in Fig. 4. Since very few data were obtained with the 6-inch cylinder, the curve is sketched in only to indicate the general trend of the sensitivity curve as the size of the paraffin cylinder is reduced. It is seen that the 8-inch cylinder gives the best approximation to a uniform sensitivity over the region shown. Other tests with neutrons absorbable by cadmium indicated that the sensitivity of the counter to thermal neutrons was about 70 on the scale used in Fig. 4. The sensitivity of this counter would be somewhat affected by the arrangement in which it is used. For most of the tests described here the counters were used as a matched pair in the arrangement shown in Fig. 3 so as to reduce errors caused by the location of the sources. This pair of counters was used in the center of a room approximately 15 by 20 feet at a height of about 50 inches above the floor. In spite of precautions to keep all other material as far from the counters as possible about 15 percent of the counting rate in the counters was due to scattered neutrons when a Ra-Be source was placed at a distance of 1 meter from the front face of the counters. The absolute sensitivity of this counter was such that it would give about 1 count for every 10^5 neutrons emitted from a source placed at a distance of 1 meter from the front face.

The shielded counter is less sensitive to scattered neutrons by a factor of about 3 and hence largely eliminates this objectionable feature of the 8-inch long counter. The sensitivity of this counter to high energy neutrons is considerably

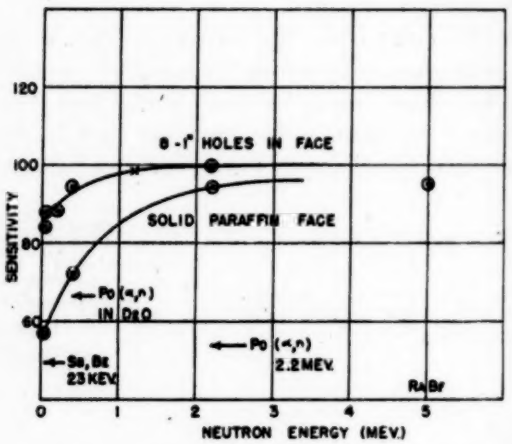

FIG. 5. Sensitivity of shielded long counters.

increased due to the larger mass of paraffin in the shield, and the sensitivity to low energy neutrons is therefore relatively low. The use of holes in the front face, however, increases the sensitivity to low energy neutrons to a sufficient extent so that the response curve of the counter is about as good as that of the previous counter. The effect of these holes is clearly indicated in the sensitivity curves shown in Fig. 5. It seems probable that the sensitivity of this counter would remain fairly constant up to energies of about 5 Mev, but there has been no work done to indicate the trend of the sensitivity curve in this range of energies.[8] No doubt further improvement in the response curve for both high energy neutrons and low energy neutrons can be accomplished by using more suitable paraffin arrangements.

The detectors described here have been found useful in many problems requiring a high and approximately uniform sensitivity to neutrons of various energies. Some of the applications have been the determination of the yield and angular distribution of neutrons from various (p, n) and (d, n) sources as a function of energy, the preliminary measurement of neutron yield from various radioactive sources, and the determination of the number of delayed neutrons accompanying fission.

This paper is based on work performed under Contract No. W-7405-Eng-36 with the Manhattan Project at the Los Alamos Scientific Laboratory of the University of California. The information contained herein will appear in Division V of the Manhattan Project Technical Series as part of the contribution of the Los Alamos Laboratory.

[8] Preliminary measurements with 16.5-Mev neutrons indicate that the sensitivity of the shielded counter for these neutrons is approximately 40 on the scale used in Fig. 5 (R. F. Taschek, private communication).

Further Experiments on the Elastic Single Scattering of Electrons by Nuclei*

W. W. BUECHNER, R. J. VAN DE GRAAFF, A. SPERDUTO, E. A. BURRILL, JR.,** AND H. FESHBACH
Physics Department, Massachusetts Institute of Technology, Cambridge, Massachusetts

(Received July 5, 1947)

The apparatus used in making the observations previously reported has been reassembled, and the measurements have been extended to lower atomic number by using beryllium as a scattering material. These show that, for angles up to 60° and for electron energies of 2.1, 2.2, and 2.3 Mev, the ratio of observed scattering to that predicted by the Mott formula is 0.99, with a standard deviation of 0.04. Measurements have also been made on aluminum in this angular and energy range, and the ratio of observed scattering to that predicted is found to be 0.99 with a standard deviation of 0.05. The earlier results for aluminum at 2.27 Mev, which were reported as anomalous and to be repeated, were presumably due to experimental errors of undetermined origin. The present results, together with those reported earlier, show that, in this angular and energy range, the elastic single scattering of electrons is in good agreement with theory for nuclei ranging in atomic number from 4 to 79 (beryllium to gold).

1. INTRODUCTION

IN an earlier paper,[1] we reported some measurements on the elastic scattering of electrons by nuclei in the energy range from 1.27 to 2.27 Mev. The nuclei investigated in those experiments were aluminum, copper, silver, platinum, and gold. It was found that, except for the case of 2.27-Mev electrons on aluminum, the results were in close agreement with the relativistic theory of electron scattering as developed by Mott. In order to extend the measurements to lower atomic number as well as to check the anomalous results previously obtained for the scattering of 2.27-Mev electrons by aluminum, the apparatus previously used has been modified somewhat and reassembled.

2. APPARATUS

The use of the electrostatic accelerator for other purposes during the war has led to certain improvements in the technique of accelerating and focusing the electron beam. Among these was the installation of an annular focusing magnet at the grounded end of the accelerating tube and the development of a small-area cathode for use as the electron source. This combination allows precise control of the diameter of the electron beam over the range from 0.010 to 0.250 inch. Both the position and the potential of the electron source with respect to the electrodes of the accelerating tube were controlled by selsyn motors located at the remote-control panel. These arrangements were particularly useful in the experiment in insuring that the beam passed completely through the entrance diaphragms to the scattering chamber, thus eliminating a possible source of x-ray background.

Another source of x-ray background is that produced by electrons which are scattered by the foil and which subsequently strike the walls of the scattering chamber. This is principally caused by small-angle scattering. It has been very much reduced in the present experiment by placing a layer of beryllium one-eighth inch thick on the inside cylindrical wall of the scattering chamber. This beryllium covering extended up to an angle of about 30° on both sides of the incident electron beam.

As in the preceding experiments, the target foils were mounted around the rim of an insulated aluminum disk. For the present experiment, selsyn motors were mounted on the lid of the scattering chamber so that this target holder could be both accurately rotated and tipped with respect to the electron beam by using selsyns located at the remote-control panel. This facilitated the changing of targets and the rapid intercomparison of results for different atomic numbers and different foil thicknesses. In addition, rotation of the foil carrier made it possible to make scattering measurements using different areas of the same foil while the effective thickness of the foil was varied by changing its angle with respect to the electron beam.

* A preliminary account of this work was given in an abstract at the November 30, 1946 meeting of the American Physical Society in Minneapolis, Phys. Rev. **71**, 142 (1947).

** Now at the High Voltage Engineering Corporation, Cambridge 38, Massachusetts.

[1] R. J. Van de Graaff, W. W. Buechner, and H. Feshbach, Phys. Rev. **69**, 452 (1946).

The collector assembly with ionization chamber was the one previously employed. The one-eighth inch thick beryllium layer placed over the lower part of the walls of the scattering chamber made it necessary to move the ionization chamber assembly somewhat closer to the scattering foil. The solid angle corresponding to the entrance window to the ionization chamber has thus been increased to 7.87×10^{-3} steradians. As in the previous experiments, a relatively thick absorber was placed immediately in front of the ionization chamber to stop any electrons that might have been scattered from the primary beam with a loss of energy due either to electron-electron or to inelastic nuclear scattering. In the present case, the absorber used was a 0.033 inch thick sheet of copper. The total material in the path of the scattered electrons (absorber plus the window of the ionization chamber) amounted to slightly less than the range of 2.0-Mev electrons, the lowest energy employed in the present measurements.

The experimental procedure followed in calibrating the ionization chamber and in making the experimental measurements was identical with that previously described. Since the reduction in background made it possible to increase the sensitivity of the apparatus, a Lindemann electrometer with calibrated high resistors was used for making the ionization current measurements. This made it possible to extend the angular range of the measurements up to 60°.

3. RESULTS

Measurements have been made with beryllium and aluminum foils as scattering materials. As in the previous paper, the results of these experiments, after the various corrections outlined there were made, have been compared to the predictions of the Mott theory. The ratios of these experimental results to the theoretical predictions are given in Table I.

The measurements on beryllium were made with a foil that was 0.0037 inch thick. This foil was of exceptional purity. The results given in the table show that, for angles up to 60° and for electron energies of 2.1, 2.2, and 2.3 Mev, the ratio of the observed scattering for beryllium to that predicted by the theory is 0.99, with a standard deviation of 0.04.

TABLE I. Ratios of measured elastic scattering of electrons to predictions of Mott's theory.

Energy (Mev)	35°	40°	45°	50°	55°	60°
			Nucleus: beryllium			
2.1	1.02	0.98	0.93	1.00	0.97	0.93
2.2	0.97	0.98	0.96	0.99	0.99	1.11
2.3	0.98	1.00	1.01	1.00	0.99	1.02
			Nucleus: aluminum			
2.1	0.94	0.94	0.94	0.93	0.95	0.91
2.2	1.00	1.02	1.03	1.06	1.02	1.03
2.3	1.02	1.00	1.05	0.99	1.04	1.00

In view of some of our previous results for aluminum, very careful measurements have been made for this element in this angular and energy range. Particular attention was given to the scattering obtained from the same aluminum foils that were used in the previous work. Our present measurements show that, for angles up to 60° and voltages from 2.0 to 2.3 Mev, the scattering from aluminum is in good agreement with theory, the ratio of observed scattering to that predicted being 0.99 with a standard deviation of 0.05.

4. DISCUSSION

In the previous paper, we reported that, except for the case of 2.27-Mev electrons on aluminum, the results obtained over a wide range of experimental variables were in close agreement with theory. This agreement was in marked contrast with the results of most previous observers who have reported wide divergence from theory. The anomalous results with aluminum were among the last obtained before that apparatus was dismantled. In view of the present careful measurements on both the old foils and the new ones, we can only conclude that the anomalous result for this particular element and energy was due to experimental errors, for which we are as yet unable to ascribe an origin. The present results, together with the earlier ones, show that, for angles up to 60° and for energies up to 2.3 Mev, the elastic single scattering of electrons is in good agreement with theory for nuclei ranging in atomic number from 4 to 79 (beryllium to gold).

ACKNOWLEDGMENTS

We are happy to acknowledge the support of the Research Corporation, the Carnegie Corporation of New York, and Navy Contract N5ori-78.

Note on Angular Distributions in Nuclear Reactions*

E. EISNER AND R. G. SACHS
Argonne National Laboratory, Chicago 80, Illinois

(Received July 11, 1947)

A proof is given of the physically plausible theorem that in a nuclear reaction produced with an unpolarized beam of given orbital angular momentum incident on an unpolarized target, the angular distribution of the outgoing intensity cannot be more complicated than that of the incoming intensity.

THE purpose of this note is to give a simple proof, based on symmetry arguments, of a conjecture made by Critchfield and Teller[1] concerning the angular distribution of the outgoing particles in a nuclear reaction. This conjecture, which is at the outset very plausible, may be stated as follows: *In a nuclear reaction produced with an unpolarized beam of given orbital angular momentum incident on an unpolarized target, the angular distribution of the outgoing intensity cannot be more complicated than that of the incoming intensity.* The statement appears plausible since the spins of the incident particle and target nucleus are unpolarized so the only angular effects which can occur are those produced by the incident wave. However, it seems worth while to give a rigorous proof because, in complicated cases, it is not a trivial matter to see how the angular dependence of the incoming wave fixes that of the outgoing intensity.[2]

The statement is obviously correct if the reaction is produced by an incident S-wave since then there is no fixed direction in space to which the angular distribution of outgoing particles could refer. It is also obvious if only two particles are produced in the reaction and if both initial and both final particles have zero spin. Then the incoming and outgoing relative orbital angular momenta must be equal.

When the particles have spin, compound states can be formed with J, the total angular momentum, larger than L, the orbital angular momentum of the incident wave. These states, in general, give rise to outgoing orbital angular momenta, l, larger than L. The content of our theorem is that, although $l>L$, the highest spherical harmonic required to describe the angular dependence of the outgoing intensity is of order $2L$ rather than $2l$ as might be expected. The proof follows.

First a remark on notation. ψ_j^m will be used to represent a function which transforms under rotations like a wave function with angular momentum, j, and magnetic quantum number m. The function is otherwise unspecified. Because of the appearance of sums over uncorrelated spins in the expressions to follow, a special notation for such a sum, $\mathfrak{S}$, is introduced. The implication is that

$$|\mathfrak{S}_m \psi_j^m|^2 = \sum_m |\psi_j^m|^2.$$

The wave function of the incident particle will, in general, contain terms corresponding to many orbital angular momenta. If the energy of the incoming particle is not too high, only the terms of low angular momentum will contribute to the reaction. We consider, in particular, the case for which the only term contributing appreciably corresponds to an orbital angular momentum, L. This L may be greater than zero as a consequence of a selection rule.

For an arbitrary coordinate system the spatial dependence of the incoming wave is given by some linear combination of the ψ_L^m, let us say,

$$\sum_m a_m \psi_L^m. \tag{1}$$

The spin dependence of the incident wave is given by

$$\mathfrak{S}_{m_N, m_I} \psi_N^{m_N} \psi_I^{m_I} \tag{2}$$

where the wave function $\psi_N^{m_N}$ is that of the target nucleus with total angular momentum, N,

* This work has been carried out under the auspices of the Atomic Energy Commission. It was completed and submitted for declassification on June 9, 1947.

[1] C. L. Critchfield and E. Teller, Phys. Rev. 60, 10 (1941).

[2] An implicit proof is contained in the literature, R. D. Myers, Phys. Rev. 54, 361 (1938), but the direct proof given here appears to be somewhat simpler.

and the wave function $\psi_I{}^{m_I}$ is that of the incident particle with spin I. The angular momenta N and I may be combined to form a total spin angular momentum, S, where $S=N+I, \cdots |N-I|$. Then, as shown by Breit and Darling,[3] the function (2) may be replaced by

$$\mathfrak{S}_{s,m_S}\psi_S{}^{m_S}.$$

Combining this with (1), the incident wave function is found to have the form

$$\psi_i=\sum_m a_m \mathfrak{S}_{s,m_S}\psi_L{}^m\psi_S{}^{m_S}. \quad (3)$$

The products $\psi_L\psi_S$ appearing in Eq. (3) may be expressed in terms of the wave functions ψ_J associated with the total angular momenta J. Thus,

$$\psi_i=\sum_J \mathfrak{S}_{s,m_S}\sum_m a_m \times(L, m, S, m_S|J, m+m_S)\psi_J{}^{m+m_S} \quad (4)$$

where $(L, m, S, m_S|J, m+m_S)$ are the usual transformation coefficients.

That term in Eq. (4) with a given total angular momentum, J, will interact only with those states of the compound nucleus with the same J. Thus each such term will contribute to the nuclear reaction to a different extent. The outgoing wave is then similar in form (insofar as transformation properties are concerned) to the incoming wave, Eq. (4), except for a change in the relative amplitudes of the terms with different J values. These relative amplitudes will be indicated by ρ_J. The intensity I_0 of the outgoing wave is proportional to the absolute square of the outgoing wave function or

$$I_0=\sum_{s,m_S}|\sum_J \rho_J \sum_m a_m \times(L, m, S, m_S|J, m+m_S)\psi_J{}^{m+m_S}|^2. \quad (5)$$

This expression contains terms of the type $(\psi_J{}^{m+m_S})^*\psi_{J'}{}^{m'+m_S}$ or, since $(\psi_J{}^m)^*=\pm\psi_J{}^{-m}$, of the type $\psi_J{}^{-(m+m_S)}\psi_{J'}{}^{(m'+m_S)}$. These products transform under rotations like a linear combination of $\psi_j{}^\mu$ where j may have any value from $j=|J-J'|$ to $J+J'$ and $\mu=m'-m$. However, m and m' both range from $-L$ to $+L$ so μ ranges from $-2L$ to $+2L$. Since we are using an arbitrarily oriented coordinate system, the coordinate system can be chosen in such a way that each possible value of μ occurs for a given value of j. In particular, the value $\mu=j$ will appear for every j. Since μ is never greater than $2L$, it follows that j cannot be greater than $2L$.

If there are only two products of the reaction and they both have zero spin, the last statement constitutes a proof of the theorem, since then the orbital angular momentum, l, of the products is equal to J, and their angular distribution is determined by the $\psi_J{}^\mu$. If one of the two particles has a spin, s, then the $\psi_J{}^M$, with $M=m+m_S$, must be analyzed into products $\psi_l{}^{M'}\psi_s{}^{M-M'}$, and the spatial dependence of the outgoing intensity is determined by terms of the form $\psi_l{}^{M'}\psi_{l'}{}^{-M''}$. These products transform like a linear combination of $\psi_{j'}{}^{\mu'}$ and we wish to show that the largest value of j' which can occur is $j'=2L$. To demonstrate this, we note that the product $\psi_l{}^{M'}\psi_{l'}{}^{-M''}$ in the outgoing intensity is multiplied by a spin factor $\psi_s{}^{M-M'}\psi_s{}^{-(M-M'')}$. The latter product may also be analyzed into a linear combination of $\psi_{j''}{}^{\mu''}$. Then the over-all transformation properties of the outgoing intensity are given by a combination of terms of the form $\psi_{j'}{}^{\mu'}\psi_{j''}{}^{\mu''}$ and these may be analyzed into a series of $\psi_j{}^\mu$ with $j=j'+j'', \cdots |j'-j''|$. This final series is identical with our analysis in the preceding paragraph which was made without reference to the distribution of angular momentum between spin and orbit. Therefore, $j\leq 2L$. But $j=j_{max}{}'+j_{max}{}''$ always occurs in the series[4] where $j_{max}{}'$ is the largest value of j', so we must have $j_{max}{}'+j_{max}{}''\leq 2L$ or finally $j_{max}\leq 2L$ as was to be proved. It is to be noted that $j_{max}{}''\leq 2L$ also but it does not appear to be possible to attach a simple physical significance to this result.

The proof for any number of product particles with arbitrary spins follows in similar manner. In general, one comes to a result of the form

$$j_{max}{}'+j_{max}{}''+j_{max}{}'''+\cdots\leq 2L$$

so that $j_{max}{}^i\leq 2L$.

[3] G. Breit and B. T. Darling, Phys. Rev. **71**, 402 (1947).

[4] $j_{max}{}'+j_{max}{}''$ occur only once so there can be no cancellation of this term as there may be for the lower values of $j'+j''$.

On the $^2\Pi_u \rightarrow {}^2\Pi_g$ Bands of CO_2^+. Part III

S. MROZOWSKI
*Department of Physics, University of Chicago, Chicago, Illinois**

(Received February 10, 1947)

The rotational analysis of additional 14 sub-bands of the band system $^2\Pi_u \rightarrow {}^2\Pi_g$ of the molecule of CO_2^+ leads to the identification of vibrational levels $v_1''=3$, 4, 5, 6, and 7 for the ground state of the molecule (Tables I–III). All 48 sub-bands analyzed and reported in Parts I, II, and III are arranged in a vibrational scheme into which many weaker, not analyzed bands (not less than 46) can be fitted. (Tables VI and VII). The distribution of the intensities of the bands corresponds to a Franck-Condon parabola with an extra intensity maximum on the diagonal. All vibrational and rotational constants for this band system (corresponding to different quanta of the symmetric vibration) are given in this and the previous paper, Part II. B'', D'', and p'' values for the levels $v_1''=0$, 1, and 2 and p' values for levels $v_1'=0$ to 6 were given in Part II. B'' and D'' for $v_1''=3$ and 4 are given on pages 682–683 of this paper; B'', D'', and p'' for $v_1''=5$, 6, and 7 are given in Table III. Tables IV and V contain the rotational constants for the excited state $^2\Pi_u$. The dependence of the Λ-doubling on the rotational quantum number J is represented in Fig. 4, Part II and Fig. 1, Part III. The values of B'' (Fig. 2), of B' (Fig. 5, Part II), of the Λ-doubling for $J=30\frac{1}{2}$ (Figs. 3 and 4), and finally of the deviation of the vibrational energy from the calculated values (Figs. 5 and 6) are represented as functions of the vibrational quantum number. From these curves the character of the perturbations occurring for the substate $^2\Pi_{3/2g}$ at $v_1''=1$, for $^2\Pi_{3/2u}$ at $v_1'=4$, for $^2\Pi_{\frac{1}{2}u}$ at $v_1'=7$, and finally for both substates in the ground level at $v_1''=5$ can be conveniently studied. A discussion of these perturbations is included; however, no explanation is given, since this would require a special theoretical investigation.

INTRODUCTION

IN the first two parts of this work[1,2] the results of a rotational analysis of 34 sub-bands of the system of bands $^2\Pi_u \rightarrow {}^2\Pi_g$ of the molecule CO_2^+ were reported. These bands were frequently observed in the past; some progress already had been made in the vibrational analysis by Smyth[3] and in the rotational analysis by Schmid.[4] However, no definite results could be obtained in view of the insufficient resolution. In this work the analysis was made possible thanks to the high resolving power of the Chicago 30-foot grating spectrograph. In Part I a discussion of previous work on the spectrum of CO_2^+, a description of the experimental procedure and the results of the analysis of 10 sub-bands belonging to the progression $v_1''=v_2''=v_3''=0$ of the symmetrical vibration (v_1' varying, $v_2'=v_3'=0$) were presented. In Part II the analysis of bands belonging to the progressions $v_1''=1$ and 2 of the symmetrical vibration was reported. The molecule CO_2^+ appears to be linear for both the excited $^2\Pi_u$ and the ground $^2\Pi_g$ states. For the substate $^2\Pi_{3/2}$ very interesting perturbations were found in the ground state for $v_1''=1$ and in the excited state for $v_1'=4$, the perturbation consisting in a doubling of the energy level accompanied by the operation of a special selection rule forbidding transitions between vibrational levels showing opposite perturbational shifts in the vibrational energy. In this paper the results of the rotational analysis of the remaining progressions of the symmetrical vibration (in all 14 sub-bands) and of the vibrational analysis for the whole system of symmetrical vibrations are reported. Also molecular constants for the whole band system and a discussion of perturbations are included.

RESULTS

The $v_1''=3$ and 4 Progressions of Bands

The wave numbers of the lines of sub-bands and the Δ_2F'' values for the levels $v_1''=3$ and 4 are given in Tables I and II. The molecular constants obtained from Δ_2F_3'' for the ground state of CO_2^+ with three quanta of the symmetrical vibration ($v_1''=3$) are the following:

$$^2\Pi_{3/2g}: \quad B_3''=0.3755\pm0.00015$$
$$D_3''=-(1.1\pm0.2)\times10^{-7}$$

$$^2\Pi_{\frac{1}{2}g}: \quad B_3''=0.3788\pm0.0002$$
$$D_3''=-(1.6\pm0.3)\times10^{-7}.$$

* Now at Research and Development Division, Great Lakes Carbon Corporation, Morton Grove, Illinois.

[1] S. Mrozowski, Phys. Rev. 60, 730 (1941). Part I.
[2] S. Mrozowski, Phys. Rev. 62, 270 (1942). Part II.
[3] H. D. Smyth, Phys. Rev. 38, 2000 (1931).
[4] See the references in Part I.

The Λ-doubling is in both substates anomalous. For $^2\Pi_{3/2g}$ with $v_1''=3$ it is negative as for the level $v_1''=2$, but the absolute values are a little smaller. For $^2\Pi_{1/2g}$ with $v_1''=3$ the Λ-doubling is positive and bigger than for $v_1''=2$.

The molecular constants obtained from Δ_2F_4'' for the ground state with four quanta of symmetrical vibration ($v_1''=4$) are the following:

$$^2\Pi_{3/2g}: \quad B_4''=0.3790\pm0.0002$$
$$D_4''=-(1.4\pm0.3)\times10^{-7}$$

$$^2\Pi_{1/2g}: \quad B_4''=0.3791\pm0.0003$$
$$D_4''=-(1.5\pm0.5)\times10^{-7}.$$

Again the Λ-doubling is in both substates anomalous; however, here it is positive for both substates. The total Λ-doubling for the substate $^2\Pi_{3/2g}$ and the relative increase of the Λ-doubling for the substate $^2\Pi_{1/2g}$ over the values for $v_1''=1$ as function of the rotational quantum number J are given in Fig. 1.

The relatively lower accuracy of the results for $v_1''=4$ is caused by the weakness of the corresponding bands analyzed. Although only one band per substate was analyzed, the rotational analysis definitely points toward the accepted assignment and the latter appears to be well substantiated by the vibrational analysis (see below, Tables VI and VII).

The $v_1''=5$, 6 and 7 Progressions of Bands

The wave numbers of the lines of the bands corresponding to the levels $v_1''=5$, 6 and 7 are given in Table III. The identification of the bands met considerable difficulties. The bands are overlapped by strong bands of CO and the measurements are for this and other reasons less accurate. Some unexplainable irregularities in the

TABLE I. Sub-bands $^2\Pi_{3/2u} \rightarrow {}^2\Pi_{3/2g}$.

$J-\frac{1}{2}$	(1,3) $\nu_0=25920.95$ R	P	(3,3) $\nu_0=28163.8$ R	P	(6,3) $\nu_0=31443.0$ R	P	(7,3) $\nu_0=32540.75$ R	P	$^2\Pi_{3/2g}(v_1''=3)$ Δ_2F_4'' av.	1st diff.	(4,4) $\nu_0=28034.0$ R	P	$^2\Pi_{3/2g}(v_1''=4)$ Δ_2F_4''	1st diff.
3		25918.13						32536.89						
4		17.18						35.80						
5		16.18						34.68						
6		15.11						33.44						
7		13.98												
8		12.80			31446.76 h		32544.33 h	32.16			28037.77 h			
9		11.57	28168.05 h		46.76 e		44.33 e	30.80	14.89		37.77 e			
10	25925.57 h	10.38	68.05 e	28152.96	46.76 a		44.33 a	29.44	16.43	1.54	37.77 a			
11	25.57 e	08.97	68.05 a	51.59	d	31430.24	d	27.93	17.98	1.55	37.77 d		18.08	
12	25.57 a	07.55	68.05 d	50.10	46.57	28.78	44.10	26.47	19.46	1.48	37.65	28019.69	19.74	1.66
13	25.57 d	06.11	67.85	48.60	46.29	27.16	43.81	24.80	21.00	1.54	37.41	18.03	21.23	1.49
14	25.41	04.57	67.74	47.07	45.93	25.45	43.55	23.03	22.52	1.52	37.16	16.42	22.74	1.51
15	25.29	03.01	67.53	45.42	45.55	23.69	43.10	21.26	24.03	1.51	36.84	14.57	24.23	1.49
16	25.05	01.38	67.23	43.73	45.14	21.95	42.71	19.46	25.54	1.51	36.42	12.93	25.82	1.59
17	24.73	25899.70	66.85	42.02	44.57	20.10	42.07	17.53	27.05	1.51	35.92	11.02	27.26	1.44
18	24.41	97.96	66.40	40.22	44.10	18.13	41.51	15.57	28.54	1.49	35.39	09.16	28.79	1.53
19	23.95	96.17	66.01	38.35	43.41	16.09	40.85	13.53	30.04	1.50	34.73	07:13	30.27	1.48
20	23.51	94.32	65.47	36.45	42.67	14.04	40.26	11.48	31.53	1.49	34.13	05.12	31.83	1.56
21	22.98	92.40	64.95	34.49	41.87	11.86	39.20	09.24	33.02	1.49	33.29	02.90	33.35	1.52
22	22.41	90.45	64.26	32.47	41.04	09.69	38.35	07.03	34.53	1.51	32.57	00.78	34.84	1.49
23	21.78	88.45	63.53	30.38	40.14	07.37	37.40	04.67	36.03	1.50	31.58	27998.44	36.38	1.54
24	21.06	86.35	62.80	28.27	39.19	05.02	36.34	02.38	37.53	1.50	30.73	96.19	37.87	1.49
25	20.37	84.24	61.96	26.01	38.14	02.65	35.30	32499.81	39.04	1.51	29.63	93.71	39.41	1.54
26	19.53	82.01	61.02	23.72	37.00	00.23	34.12	97.34	40.55	1.51	28.65	91.32	40.97	1.56
27	18.70	79.81	60.11	21.40	35.77	31397.63	32.83	94.74	42.03	1.48	27.38	88.66	42.48	1.51
28	17.77	77.49	59.05	19.02	34.58	94.97	31.55	92.08	43.52	1.49	26.26	86.18	43.97	1.49
29	16.78	75.16	58.00	16.63	33.15	92.24	30.19	89.31	45.03	1.51	24.83	83.41	45.50	1.53
30	15.78	72.74	56.86	14.05	31.72	89.50	28.71	86.51	46.51	1.48	23.59	80.76	46.99	1.49
31	14.73	70.34	55.74	11.51	30.24		27.25	83.65	48.02	1.51	22.03	77.84	48.54	1.55
32	13.52	67.73	54.44	08.86	28.78		25.71	80.74	49.53	1.51	20.64	75.05	50.05	1.51
33	12.41	65.20	53.18	06.20	27.16		24.10	77.67	51.03	1.50	18.93	71.98	51.54	1.49
34	11.10	62.51	51.77	03.46			22.38	74.58	52.52	1.49	17.45	69.10	53.04	1.50
35	09.87	59.87	50.44	00.74			20.60	71.47	54.02	1.50	15.60	65.89	54.57	1.53
36	08.41	57.07	48.90	28097.76			18.68	68.30	55.52	1.50	14.00	62.88	56.06	1.49
37	07.04	54.33	47.47	94.92			16.70	64.91	57.01	1.49	12.06	59.54	57.53	1.47
38	05.51	51.40	45.78				14.84	61.67	58.51	1.50	10.31	56.47		
39	04.05	48.53	44.29				12.75		60.03	1.52	08.19			
40	02.30	45.47							61.55	1.52				
41	00.82	42.50							62.93	1.38				
42	25899.03	39.37							64.52	1.59				
43	97.49	36.30							66.02	1.50				
44	95.42	33.02												
45	93.67													
46	91.63													
47	89.81													
48	87.61													
49	85.74													
50	83.31													
51	81.33													
52	78.81													

TABLE II. Sub-bands $^2\Pi_{\frac{1}{2}u} \rightarrow {}^2\Pi_{\frac{1}{2}g}$.

$J-\frac{1}{2}$	(1,3) $\nu_0=25821.55$ R	P	(3,3) $\nu_0=28058.45$ R	P	(6,3) $\nu_0=31385.70$ R	P	$^2\Pi_{1/2g}(v_1''=3)$ Δ_2F_3'' av.	1st diff.	(4,4) $\nu_0=27919.4$ R	P	$^2\Pi_{1/2g}(v_1''=4)$ Δ_2F_4''	1st diff.
1	25823.18	25820.41	28060.11									
2	23.75	19.57	60.58	28056.42			4.54					
3	24.26	18.64	61.11	55.56			6.03	1.49				
4	24.68	17.68		54.60			7.58	1.55				
5	25.08	16.67		53.53			9.09	1.51				
6	25.39	15.59		52.47	31389.34		10.63	1.54				
7		14.45	62.49	51.31	89.34		12.15	1.52				
8		13.24	62.49	50.07	89.57 h	31377.13	13.65	1.50				
9		12.01	62.65 h	48.80	89.57 e	75.78	15.10	1.45	27923.26 h			
10	26.10 h	10.71	62.65 e	47.40	89.57 a	74.42	16.65	1.55	23.26 e			
11	26.10 e	09.40	62.65 a	46.06	89.57 d	72.87	18.16	1.51	23.26 a			
12	26.10 a	07.93	62.49 d	44.56	89.34	71.24	19.65	1.49	d		19.41	
13	d	06.48	62.49	43.06	89.34	69.83	21.15	1.50		27903.85		
14	25.88	04.94	62.25	41.43	88.98	68.20	22.69	1.54	22.95	02.16		
15	25.74	03.34	62.09	39.80	88.78	66.58	24.20	1.51	22.80	00.64	24.09	
16	25.48	01.72	61.66	38.04	88.24	64.74	25.77	1.57	22.48	27898.87	25.64	1.55
17	25.19	00.00	61.34	36.33	87.89	63.99	27.22	1.45	22.12	97.15	27.21	1.57
18	24.85	25798.24	60.84	34.45	87.20	61.02	28.77	1.55	21.65	95.27	28.68	1.47
19	24.41	96.38	60.38	32.57	86.75	59.13	30.27	1.50	21.19	93.44	30.19	1.51
20	23.92	94.54	59.76	30.61	85.88	56.94	31.80	1.53	20.59	91.46	31.79	1.60
21	23.37	92.58	59.17	28.58	85.44	55.00	33.26	1.46	19.94	89.40	33.32	1.53
22	22.80	90.64	58.42	26.48	84.44	52.69	34.84	1.58	19.21	87.27	34.88	1.56
23	22.15	88.52	57.69	24.33	83.90	50.50	36.33	1.49	18.39	85.05	36.33	1.45
24	21.48	86.45	56.83	22.10	82.70	48.12	37.86	1.53	17.54	82.87	37.94	1.61
25	20.66	84.24	55.96	19.83	82.20	46.10	39.36	1.50	16.55	80.45	39.34	1.40
26	19.89	82.09	55.01	17.52	80.77	43.35	40.96	1.60	15.65	78.20	40.92	1.58
27	18.95	79.74	54.00	15.11	79.90	41.00	42.42	1.46	14.46	75.63	42.44	1.52
28	18.07	77.48	52.95	12.67	78.36	38.25	43.99	1.57	13.42	73.21	44.00	1.56
29	17.00	74.96	51.80	10.11	77.43	35.82	45.53	1.44	12.03	70.47	45.46	1.46
30	16.04	72.64	50.59	07.56	75.78	32.91	47.00	1.57	10.97	67.96	46.96	1.50
31	14.80	69.96	49.32	04.86	74.70	30.41	48.42	1.42	09.35	65.07		
32	13.77	67.54	48.06	02.25	72.87	27.36	50.01	1.59	08.15			
33	12.38	64.73	46.60	27999.38	71.72	24.69	51.43	1.42				
34	11.26	62.27	45.23	96.65		21.48	53.02	1.59				
35	09.68	59.31	43.62	93.65		18.71	54.47	1.45				
36	08.54	56.72	42.16	90.82		15.37	56.04	1.57				
37	06.84	53.56	40.36	87.65		12.45	57.44	1.40				
38	05.58		38.81	84.73		08.99	58.98	1.54				
39	03.67			81.39		05.97	60.41	1.43				
40	02.34			78.40		02.40						
41				74.92								
42				71.78								
43				68.08								
44				64.98								
45				61.84								
46				58.56								
47				54.36								

dispersion curve in the region λ4090–λ4140 were observed which made a definite decision about the assignment impossible in view of the small differences in B' values for the excited state $^2\Pi_u$. However, it was found that by slightly correcting the correction curves for the dispersion the Δ_2F' values can be brought into agreement with the Δ_2F' values for the corresponding vibrational levels of the excited state. At first this assignment was considered only as tentative, since it gives a very strong vibrational perturbation for the level $v_1''=5$ for both substates and, what seemed more peculiar, no other bands for this progression could be detected. Further it was expected that for such a strong perturbation a doubling of the level should occur, but no bands belonging to the other component level could be identified in spite of a very careful search. However the vibrational analysis for the higher levels $v_1''=6$, 7, 8, and 9 gives such a good agreement with the observations that the author feels reasonably certain the assignment after all is correct.

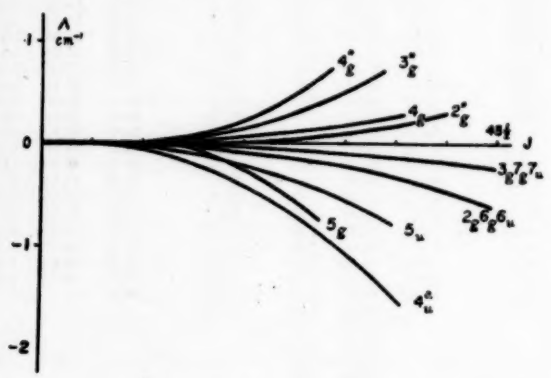

FIG. 1. Λ-doubling of rotational states in the ground substate $^2\Pi_{3/2g}$ of the CO_2^+ molecule for $v_1''=2$ to 7 and in the excited substate $^2\Pi_{3/2u}$ for $v_1'=4^a$, 5, 6, and 7. The three curves for the ground substate $^2\Pi_{1/2g}$ and $v_1''=2$, 3, and 4 are marked by asterisks and represent the excess of the Λ-doubling over the value of the Λ-doubling for the level $v_1''=1$.

The molecular constants obtained from $\Delta_2 F''$ for the ground state $^2\Pi_g$ for $v_1''=5$, 6, and 7 of the symmetrical vibration are given in the lower part of Table III. In view of the uncertainties in the dispersion curve the results naturally are still less exact than for $v_1''=3$ and 4. The anomalous negative Λ-doublings for $^2\Pi_{3/2g}$, $v_1''=5$, 6, and 7 are given in Fig. 1. The Λ-doublings for $^2\Pi_{1/g}$, $v_1''=5$ and 6 are normal, that is are linear with J. The linear coefficients p'' are given in the lower part of the Table III.

The Ground State $^2\Pi_g$

The dependence of the rotational constant B'' on the quantum number of the symmetrical vibration is represented in Fig. 2. The values were taken from Part II and from the preceding sections of this paper. The broken line corresponds to the formula $B_v''=B_0''-0.0014\cdot v_1''$. In order to visualize the type of perturbation occurring for both substates at $v_1''=5$, the Λ-doubling for an arbitrarily chosen rotational

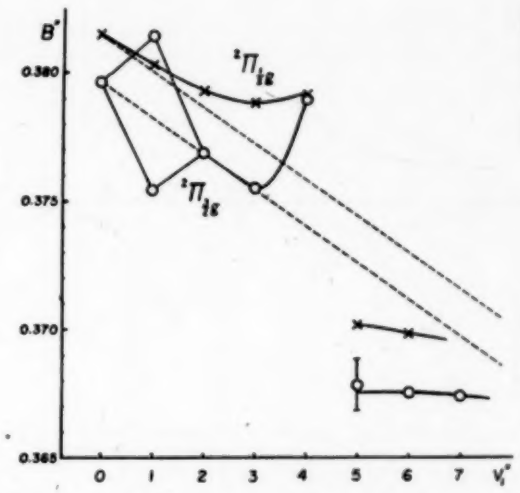

FIG. 2. Graphical presentation of the change of the B''-value with the vibrational quantum number v_1'' for the ground state $^2\Pi_g$.

TABLE III.

	Sub-bands $^2\Pi_{3/2u} \rightarrow {}^2\Pi_{3/2g}$						Sub-bands $^2\Pi_{1/u} \rightarrow {}^2\Pi_{1/g}$			
	(2,5) $\nu_0=24404.0$		(3,6) $\nu_0=24327.45$		(4[b],7) $\nu_0=24250.2$		(2,5) $\nu_0=24321.25$		(3,6) $\nu_0=24240.2$	
$J-\frac{1}{2}$	R	P	R	P	R	P	R	P	R	P
2				24325.50						
3			24330.20	24.64	24252.89					
4			30.70	23.75	53.37			24317.55		24236.25
5			31.15	22.94	53.84			16.68		35.20
6			31.57	21.74				15.71		34.21
7		24397.93	31.93	20.89	54.71			14.64		33.18
8		96.85	32.26	19.78	55.13			13.63		32.16
9		95.75		18.67	55.48			12.52		31.00
10		94.59		17.55				11.40		29.86
11		93.40		16.33				10.15		28.69
12		92.08		15.09				08.99		27.43
13		91.00	33.20 h	13.81	55.70 h	24236.38		07.67	24245.62 h	26.16
14	24410.50 h e	89.67	33.20 e	12.52	55.70 e	34.97	24327.40 h	06.46	45.62 e	24.81
15	10.50 a	88.34	33.20 a	11.12	55.70 a	33.66	27.40 e	05.10	45.62 a	23.45
16	10.50 d	86.90	33.20 d	09.70	55.70 d	32.17	27.40 a	03.58	45.62 d	22.00
17		85.51		08.24		30.78	27.40 d	02.20		20.58
18	10.32	84.13	32.95	06.72		29.10		00.71		19.04
19	10.20	82.30	32.78	05.10	55.55	27.66	27.15	24299.20		17.55
20	09.95	80.89	32.59	03.57	55.33	26.14	26.94	97.61		15.89
21	09.77	79.30	32.40	01.98	54.92	24.37	26.72	96.05		14.32
22	09.29	77.40	32.07	00.27	54.52	22.83	26.48	94.39	44.58	12.56
23	09.02	75.80	31.78	24298.50	54.14	21.02	26.20	92.75	44.30	10.93
24	08.40	73.65	31.33	96.77	53.66	19.23	25.86	90.95	43.80	09.03
25	08.20	72.40	30.92	95.11	53.19	17.35	25.50	89.24	43.31	07.40
26	07.45	70.20	30.39	93.32	52.68	15.49	25.08	87.35	42.78	05.27
27	07.20	68.24	29.95	91.25	52.09	13.53	24.64	85.41	42.24	03.62
28	06.22	66.20	29.35	89.25	51.49	11.56	24.16	83.65	41.51	01.23
29			28.78	87.35	50.84	09.52	23.57	81.69	40.76	
30			28.06	85.40	50.15	07.39	23.06		40.13	
31			27.40	82.21	49.36	05.27	22.33		39.39	
32			26.72	81.03	48.64	03.18	21.59		38.62	
33			25.86	78.91	47.74	00.98	20.89		37.71	
34			25.08	76.68	46.91	24198.71	20.19		36.72	
35			24.16	74.47			19.39		35.71	
36			23.28	72.14			18.52		34.75	
37			22.33	69.75			17.55		33.66	
38			21.19	67.39					32.57	
39			20.19	64.72					31.46	
40			19.01						30.32	
41			17.99							
42			16.68							
43			15.44							
44			14.06							
	$B_0''=0.3678\pm0.0010$ $D_0''=1.5\cdot10^{-7}$ assumed		$B_1''=0.3675\pm0.0003$ $D_1''=-(1.3\pm0.4)10^{-7}$		$B_2''=0.3674\pm0.0004$ $D_2''=-(1.4\pm0.5)10^{-7}$		$B_5''=0.3702\pm0.0004$ $D_5''=-(1.2\pm0.4)10^{-7}$ $p_5''=0.0090\pm0.0006$		$B_6''=0.3698\pm0.0005$ $D_6''=-(1.2\pm0.7)10^{-7}$ $p_6''=0.0106\pm0.0006$	

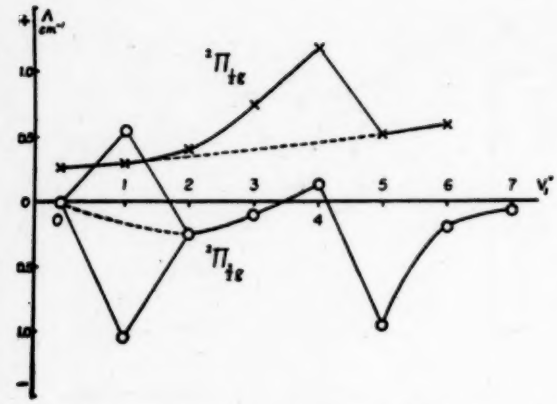

FIG. 3. Λ-doubling for the rotational level $J=30\frac{1}{2}$ in dependence on the vibrational quantum number v_1'' of the ground state $^2\Pi_g$ of the molecule CO_2^+.

quantum number ($J=30\frac{1}{2}$) is given in Fig. 3 as a function of the vibrational quantum number. For all levels of the substate $^2\Pi_{3/2g}$, except $v_1''=0$, an anomalous Λ-doubling is observed. On the contrary, in $^2\Pi_{\frac{1}{2}g}$ the anomalous Λ-doubling is observed only for levels below the perturbation, that is $v_1''=2$, 3, and 4. The value of the contribution of the anomalous Λ-doubling is given for $^2\Pi_{\frac{1}{2}g}$ by the distance from the broken curve, corresponding to the normal Λ-doubling effect. This latter Λ-doubling is linear with J and is probably caused by the interaction with an hypothetical excited state $^2\Sigma_g^+$.[5] For both substates a similar trend in curves Fig. 3 is observed, with the difference that strong anomalous

TABLE IV. Combination differences for $^2\Pi_{3/2u}$.

	$v_1'=0$		$v_1'=1$		$v_1'=2$		$v_1'=3$		$v_1'=4^a$		$v_1'=4^b$		$v_1'=5$		$v_1'=6$		$v_1'=7$	
$J-\frac{1}{2}$	Δ_2F_0' av.	1st diff.	Δ_2F_1' av.	1st diff.	Δ_2F_2' av.	1st diff.	Δ_2F_3' av.	1st diff.	Δ_2F_{ee}'	1st diff.	Δ_2F_{eb}' av.	1st diff.	Δ_2F_5' av.	1st diff.	Δ_2F_6' av.	1st diff.	Δ_2F_7'	1st diff.
2	4.16		4.23															
3	5.59	1.43	5.60	1.37	5.55													
4	6.96	1.37	6.96	1.36	6.93	1.38												
5	8.39	1.43			8.31	1.38												
6	9.75	1.36			9.70	1.39												
7	11.14	1.39			11.03	1.33	11.08				11.07		10.95					
8	12.55	1.41			12.42	1.39	12.41	1.33			12.26	1.19	12.22	1.27	12.14		12.17	
9	13.89	1.34	13.83		13.80	1.38	13.74	1.33	13.53		13.73	1.47	13.57	1.35	13.45	1.31	13.53	1.36
10	15.28	1.39	15.20	1.37	15.22	1.42	15.13	1.39	14.86	1.33	15.18	1.45	14.94	1.37	14.85	1.40	14.89	1.36
11	16.66	1.38	16.60	1.40	16.55	1.37	16.58	1.45	16.42	1.56	16.48	1.30	16.46	1.52				
12	18.07	1.41	18.02	1.42	18.00	1.45	17.96	1.38	17.79	1.37	17.95	1.47			17.79		17.84	
13	19.48	1.41	19.46	1.44	19.42	1.42	19.32	1.36	19.09	1.30	19.33	1.38	19.20		19.12	1.33	19.01	1.37
14	20.88	1.40	20.88	1.42	20.80	1.38	20.71	1.39	20.44	1.35	20.75	1.42	20.55	1.35	20.50	1.38	20.52	1.51
15	22.30	1.42	22.27	1.39	22.17	1.37	22.08	1.37	21.80	1.36	22.10	1.35	21.96	1.41	21.83	1.33	21.83	1.31
16	23.70	1.40	23.67	1.40	23.57	1.40	23.45	1.37	23.25	1.45	23.47	1.37	23.32	1.36	23.19	1.36	23.25	1.42
17	25.10	1.40	25.05	1.38	24.96	1.39	24.85	1.40	24.54	1.29	24.86	1.39	24.71	1.39	24.55	1.36	24.54	1.29
18	26.48	1.38	26.42	1.37	26.36	1.40	26.25	1.40	26.02	1.48	26.25	1.39	26.05	1.34	25.96	1.41	25.94	1.40
19	27.87	1.39	27.82	1.40	27.73	1.37	27.66	1.41	27.35	1.33	27.63	1.38	27.41	1.36	27.32	1.36	27.34	1.39
20	29.27	1.40	29.20	1.38	29.12	1.39	29.03	1.37	28.73	1.38	29.00	1.37	28.74	1.33	28.65	1.33	28.78	1.54
21	30.67	1.40	30.60	1.40	30.50	1.38	30.41	1.38	30.00	1.36	30.39	1.39	30.13	1.39	30.01	1.36	29.96	1.18
22	32.04	1.37	31.98	1.38	31.89	1.39	31.78	1.37	31.47	1.38	31.76	1.37	31.50	1.37	31.40	1.39	31.32	1.36
23	33.43	1.39	33.37	1.39	33.26	1.37	33.16	1.38	32.95	1.48	33.14	1.38	32.87	1.37	32.76	1.36	32.73	1.41
24	34.83	1.40	34.74	1.37	34.63	1.37	34.54	1.38	34.13	1.18	34.54	1.40	34.26	1.39	34.15	1.39	33.96	1.23
25	36.25	1.42	36.12	1.38	36.01	1.38	35.95	1.41	35.50	1.37	35.91	1.37	35.62	1.36	35.50	1.35	35.49	1.53
26	37.62	1.37	37.53	1.41	37.43	1.42	37.33	1.38	36.95	1.45	37.31	1.40	36.99	1.37	36.82	1.32	36.79	1.30
27	39.03	1.41	38.91	1.38	38.81	1.38	38.71	1.38	38.42	1.47	38.72	1.41	38.35	1.36	38.21	1.39	38.09	1.30
28	40.40	1.37	40.29	1.38	40.18	1.37	40.08	1.37	39.73	1.31	40.09	1.37	39.76	1.41	39.60	1.39	39.47	1.38
29	41.81	1.41	41.66	1.37	41.58	1.40	41.45	1.37			41.44	1.35	41.11	1.35	40.93	1.33	40.88	1.41
30	43.20	1.39	43.04	1.38	42.98	1.40	42.84	1.39			42.85	1.41	42.45	1.34	42.28	1.35	42.20	1.32
31	44.59	1.39	44.42	1.38	44.38	1.40	44.23	1.39			44.21	1.36	43.78	1.33	43.76	1.38	43.60	1.40
32	46.00	1.41	45.81	1.39	45.72	1.34	45.61	1.38			45.61	1.40	45.16	1.38	45.07	1.31	44.97	1.37
33	47.40	1.40	47.21	1.40	47.09	1.37	47.00	1.39			46.97	1.36	46.55	1.39	46.48	1.41	46.43	1.46
34	48.77	1.37	48.59	1.38	48.47	1.38	48.38	1.37			48.32	1.35	47.96	1.41	47.76	1.28	47.80	1.37
35	50.16	1.39	49.99	1.40	49.88	1.41	49.70	1.32			49.71	1.39	49.33	1.37	49.09	1.33	49.13	1.33
36	51.55	1.39	51.37	1.38	51.23	1.35	51.14	1.44			51.12	1.41			50.55	1.46	50.38	1.25
37	52.96	1.41	52.75	1.38	52.62	1.39	52.55	1.41			52.52	1.40			51.92	1.37	51.79	1.41
38	54.34	1.38	54.14	1.39	53.97	1.35					53.84	1.32			53.27	1.35	53.17	1.38
39	55.72	1.38	55.53	1.39	55.33	1.36									54.65	1.38		
40	57.09	1.37	56.90	1.37	56.72	1.39												
41	58.50	1.41	58.29	1.39	58.08	1.36												
42	59.87	1.37	59.68	1.39	59.48	1.40												
43	61.28	1.41	61.11	1.43														
44	62.64	1.36	62.43	1.32														
45	64.07	1.43																
46	65.44	1.37																
47	66.84	1.40																
48	68.28	1.44																
49	69.62	1.34																
50	71.00	1.38																

$B_0'=0.3485_8\pm0.0001$ $B_1'=0.3475_8\pm0.00015$ $B_2'=0.3466\pm0.00015$ $B_3'=0.3457\pm0.0002$ $B_{ee}'=0.3421\pm0.0003$
$D_0'=-(1.0\pm0.2)10^{-7}$ $D_1'=-(1.5\pm0.2)10^{-7}$ $D_2'=-(1.7\pm0.3)10^{-7}$ $D_3'=-(1.3\pm0.4)10^{-7}$ $D_{ee}'=+(0.6\pm0.3)10^{-7}$
$B_{eb}'=0.3454\pm0.0001$ $B_4'=0.3426_8\pm0.0001$ $B_4'=0.3417\pm0.00015$ $B_4'=0.3408\pm0.0002$
$D_{eb}'=-(0.1\pm0.1)10^{-7}$ $D_4'=-(0.4\pm0.15)10^{-7}$ $D_4'=-(1.7\pm0.2)10^{-7}$ $D_4'=-(0.5\pm0.2)10^{-7}$

[5] S. Mrozowski, Rev. Mod. Phys. **14**, 216 (1942). The discussion of the vibrational perturbations given there on p. 217 requires modifications.

TABLE V. Combination differences for $^2\Pi_{\frac{1}{2}u}$.

$J-\frac{1}{2}$	$v_1'=0$ Δ_2F_0' av.	1st diff.	$v_1'=1$ Δ_2F_1' av.	1st diff.	$v_1'=2$ Δ_2F_2' av.	1st diff.	$v_1'=3$ Δ_2F_3' av.	1st diff.	$v_1'=4$ Δ_2F_4' av.	1st diff.	$v_1'=5$ Δ_2F_5' av.	1st diff.	$v_1'=6$ Δ_2F_6' av.	1st diff.
1			2.77		2.80									
2			4.22	1.45	4.20	1.40	4.17							
3			5.65	1.43	5.67	1.37	5.55	1.38						
4	6.90		7.02	1.37	7.03	1.36								
5			8.43	1.41	8.37	1.34								
6	9.58		9.80	1.37			9.79		9.75		9.70		9.73	
7			11.34	1.54	11.14		11.10	1.31	10.92	1.17	10.92	1.22	10.91	1.18
8	12.71		12.53	1.19	12.51	1.37	12.48	1.38	12.49	1.57	12.48	1.56	12.44	1.51
9	14.07	1.36	13.96	1.43	13.91	1.40	13.85	1.37	13.78	1.29	13.75	1.27	13.79	1.35
10	15.41	1.34	15.36	1.40	15.28	1.37	15.26	1.41	15.26	1.48	15.17	1.42	15.20	1.41
11	16.80	1.39	16.76	1.40	16.70	1.42	16.65	1.39	16.63	1.37	16.54	1.37	16.65	1.45
12	18.22	1.42	18.17	1.41	18.09	1.39	18.04	1.39	17.94	1.31	17.90	1.36	18.02	1.37
13	19.66	1.44	19.73	1.46	19.59	1.50	19.47	1.43	19.44	1.50	19.40	1.50	19.44	1.42
14	21.05	1.39	20.99	1.26	20.89	1.30	20.85	1.38	20.81	1.37	20.70	1.30	20.72	1.28
15	22.45	1.40	22.37	1.38	22.30	1.41	22.28	1.43	22.22	1.41	22.14	1.44	22.17	1.45
16	23.85	1.40	23.77	1.40	23.69	1.39	23.65	1.37	23.60	1.38	23.52	1.38	23.44	1.27
17	25.27	1.42	25.17	1.40	25.11	1.42	25.05	1.40	24.97	1.37	24.91	1.39	24.93	1.49
18	26.66	1.39	26.58	1.41	26.52	1.41	26.42	1.37	26.36	1.39	26.28	1.37	26.21	1.28
19	28.08	1.42	27.98	1.40	27.90	1.38	27.83	1.41	27.74	1.38	27.68	1.40	27.64	1.43
20	29.49	1.40	29.38	1.40	29.29	1.39	29.19	1.36	29.12	1.38	29.03	1.35	28.99	1.35
21	30.89	1.41	30.77	1.39	30.69	1.40	30.61	1.42	30.51	1.39	30.45	1.42	30.47	1.48
22	32.31	1.42	32.16	1.39	32.06	1.37	31.97	1.36	31.91	1.40	31.74	1.29	31.75	1.28
23	33.70	1.39	33.58	1.42	33.46	1.40	33.39	1.42	33.30	1.39	33.20	1.46	33.26	1.51
24	35.10	1.40	34.98	1.40	34.84	1.38	34.75	1.36	34.68	1.38	34.51	1.31	34.57	1.31
25	36.51	1.41	36.40	1.42	36.26	1.42	36.17	1.42	36.06	1.38	36.01	1.50	36.06	1.49
26	37.89	1.38	37.78	1.38	37.63	1.37	37.52	1.35	37.44	1.38	37.28	1.27	37.42	1.36
27	39.31	1.42	39.17	1.39	39.04	1.41	38.93	1.41	38.83	1.39	38.72	1.44	38.91	1.49
28	40.69	1.38	40.57	1.40	40.43	1.39	40.34	1.41	40.20	1.37	40.08	1.36	40.13	1.22
29	42.11	1.42	41.96	1.39	41.81	1.38	41.72	1.38	41.57	1.37	41.54	1.46	41.59	1.46
30	43.49	1.38	43.36	1.40	43.20	1.39	43.08	1.36	42.96	1.39	42.84	1.30	42.87	1.28
31	44.90	1.41	44.76	1.40	44.59	1.39	44.49	1.41	44.36	1.40	44.28	1.44	44.28	1.41
32	46.28	1.38	46.16	1.40	45.98	1.39	45.90	1.41	45.75	1.39	45.67	1.39	45.57	1.29
33	47.70	1.42	47.57	1.41	47.37	1.39	47.26	1.36	47.12	1.37	47.08	1.41	47.02	1.45
34	49.08	1.38	48.95	1.38	48.73	1.36	48.62	1.36	48.49	1.37	48.38	1.30	48.31	1.29
35	50.49	1.41	50.38	1.43	50.15	1.42	50.02	1.40	49.89	1.40	49.81	1.43	49.84	1.53
36	51.87	1.38	51.77	1.39	51.55	1.40	51.42	1.40	51.22	1.33	51.09	1.28	51.08	1.24
37	53.28	1.41	53.20	1.43	52.95	1.40	52.84	1.42	52.62	1.40	52.53	1.44	52.59	1.51
38	54.76	1.38	54.46	1.26	54.36	1.41	54.22	1.38	54.00	1.38	53.87	1.34		
39	56.15	1.39	55.93	1.47	55.75	1.39	55.63	1.41	55.42	1.42	55.32	1.45		
40	57.51	1.36	57.36	1.43	57.12	1.37	56.98	1.35	56.73	1.39	56.65	1.33		
41			58.69	1.33	58.52	1.40	58.40	1.42	58.18	1.45	58.10	1.45		
42			60.09	1.40	59.90	1.38	59.75	1.35	59.46	1.28	59.42	1.32		
43			61.50	1.41	61.31	1.41	61.15	1.40	60.90	1.44	60.77	1.35		
44			62.85	1.35	62.67	1.36	62.55	1.40	62.25	1.35	62.24	1.47		
45			64.22	1.37	64.05	1.38	63.97	1.42	63.66	1.41	63.47	1.23		
46			65.60	1.38	65.42	1.37	65.31	1.34	65.05	1.39				
47					66.80	1.38	66.66	1.35	66.41	1.36				
48					68.20	1.40	68.03	1.37	67.80	1.39				
49					69.58	1.38	69.42	1.39	69.24	1.44				
50					70.93	1.35			70.61	1.37				
51					72.38	1.45			72.01	1.40				

$B_0'=0.3509\pm0.0001$	$B_1'=0.3498_6\pm0.0001$	$B_2'=0.3488\pm0.0001$	$B_3'=0.3478\pm0.0001$	$B_4'=0.3468\pm0.0001$	$B_5'=0.3460\pm0.0001$	$B_6'=0.3460\pm0.0002$
$D_0'=-(0.5\pm0.2)10^{-7}$	$D_1'=-(0.8\pm0.1)10^{-7}$	$D_2'=-(1.3\pm0.2)10^{-7}$	$D_3'=-(1.1\pm0.2)10^{-7}$	$D_4'=-(1.4\pm0.2)10^{-7}$	$D_5'=-(1.3\pm0.2)10^{-7}$	$D_6'=-(1.3\pm0.3)10^{-7}$
$p_0'=0.0077\pm0.0002$	$p_1'=0.0084\pm0.0002$	$p_2'=0.0096\pm0.0002$	$p_3'=0.0112\pm0.0002$	$p_4'=0.0133\pm0.0003$	$p_5'=0.0161\pm0.0004$	$p_6'=0.0201\pm0.0006$

Λ-doublings for $^2\Pi_{\frac{1}{2}g}$ are occurring below, and for $^2\Pi_{3/2g}$ above the perturbation. For $^2\Pi_{3/2g}$ there is a general tendency for a negative Λ-doubling, which is only overbalanced by strong positive perturbations at $v_1''=1$ and $v_1''=4$.

The Excited State $^2\Pi_u$

In Tables IV and V the values of Δ_2F' for the excited state are collected. They were calculated as weighted averages of differences of frequencies of the band lines given in Parts I–III. In the lower part of the tables the values of the rotational constants determined from these Δ_2F' values by application of usual methods are collected.

A drawing corresponding to Fig. 2 but for the excited state $^2\Pi_u$ was already given in Part II, Fig. 5, where the broken lines were drawn accord-

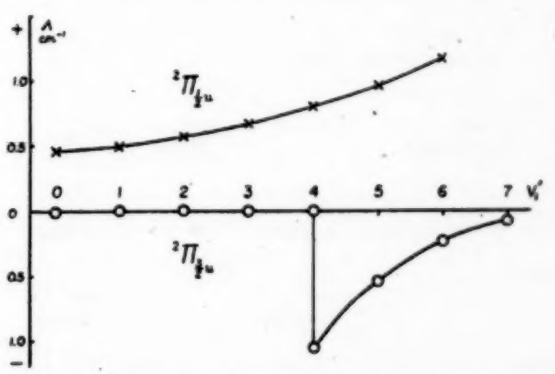

FIG. 4. Λ-doubling for the rotational level $J=30\frac{1}{2}$ in dependence from the vigrational quantum number v_1' of the excited state $^2\Pi_u$ of the molecule CO_2^+.

ing to the equation $B_v' = B_0' - 0.0011 \cdot v_1'$. The dependence of the Λ-doubling (for $J = 30\frac{1}{2}$) on the vibrational quantum number is represented in Fig. 4. It seems very interesting that for $^2\Pi_{3/2u}$ no doubling below the perturbation $v_1' = 4$ is observed at all. Λ-doublings as function of J are given for anomalous levels of the substate $^2\Pi_{3/2u}$ and $v_1' = 4^a$, 5, 6, and 7 in Fig. 1. For $^2\Pi_{\frac{1}{2}u}$ the Λ-doubling up to $v_1' = 6$ is perfectly normal, that is linear with J, although it seems quite certain that some kind of perturbation is occurring for this substate at $v_1' = 7$ (see below). The normal Λ-doubling in $^2\Pi_{\frac{1}{2}u}$ is caused by the interaction with the $^2\Sigma_u^+$ state.[5] Since the $^2\Sigma_u^+$ state is at a distance of only about 6050 cm^{-1} above the $^2\Pi_{\frac{1}{2}u}$ substate, for $v_1' = 6$ the substate $^2\Pi_{\frac{1}{2}u}$ is already above the state $^2\Sigma_u^+$ with $v_1' = 0$. However, no perturbation occurs between $v_1' = 5$ and 6, and no excessive Λ-doublings are observed for the substate $^2\Pi_{\frac{1}{2}u}$. The Λ-doubling is increasing relatively slowly up to $v_1' = 6$. This shows very conclusively that for the occurrence of perturbations (namely, the Λ-doubling) the Franck-Condon condition has to be satisfied in the same manner as for the occurrence of radiational transitions.

The Vibrational Scheme

In Tables VI and VII the vibrational schemes for the systems of sub-bands $^2\Pi_{3/2u} \rightarrow {}^2\Pi_{3/2g}$ and $^2\Pi_{\frac{1}{2}u} \rightarrow {}^2\Pi_{\frac{1}{2}g}$ are given. For all bands with boldface zero line frequencies the assignment was obtained by the rotational analysis. For many bands which are too weak to be analyzed the position of the head was measured, and the frequencies thus obtained are given in parentheses. For a few bands not observed with the big grating spectrograph, the band head frequencies obtained by Smyth[3] are given (values in parentheses denoted by a letter *S*). From the known B' and B'' values and the measured positions of heads, the frequencies of the zero lines were calculated and are given in the tables for a considerable number of bands. For all progressions

TABLE VI. Vibrational scheme sub-bands $^2\Pi_{3/2u} \rightarrow {}^2\Pi_{3/2g}$.

v_1' \ v_1''	0	1241.77	1	45.55	1	1209.55	2	1241.50	3	1249.80	4	1390.0	5	1196.7	6	1197.25	7	~1224	8
	λ3503		λ3663		λ3669		λ3839		λ4030										
0	**28532.60**		**27290.80**		**27245.25**		**26035.67**		24794.0(98.84)										
	4	a_2	4	c_2?	3	b_1	5	n_1	2										
1126.76																			
	λ3370		λ3517		λ3523		λ3680		λ3856		λ4051			λ4526					
1	**29659.31**		**28417.6**		28372.0(75.7)		**27162.45**		**25920.95**		24671.2(76.2)			*c*					
	5	a_3	<1		<1	b_2	3		4	c_2	3	k_1							
1122.72																			
	λ3247				λ3389		λ3534		λ3696		λ3875		λ4095	λ4306		λ4541		λ4809	
2	**30781.97**				**29494.70**		**28285.20**		27043.8(48.3)		25794.0(98.9)		**24404.0**	(23217.6)		*c*		*c*	
	5	a_4			3	b_3	4	n_2	0		1		2	k_2 1	f_2				
1120.12																			
	λ3133				λ3265		λ3399		λ3549					λ4108		λ4320		λ4563	
3	**31902.19**				**30614.75**		29405.4(09.4)		**28163.8**					**24327.45**		(23140.5)		*c*	
	3	a_5			4	b_4	0		2	c_4				3		2			
1062.50																			
	λ3032		λ3151																
4[a]	32964.0(68.02)		**31722.9**																
	0		3																
57.50																			
	λ3027				λ3150		λ3275		λ3413		λ3565					λ4122		λ4340	
4[b]	**33022.15**				**31734.90**		30525.4(29.3)		29283.8(87.93)		**28034.0**					**24250.2**		(23036.0)	
	1	a_6			4	b_5	0		1	c_5	2					3		3	
1055.25																			
	λ2933		λ3044				λ3165												
5	34077.0(80.5)		**32835.65**				**31580.50**												
	1		3	b_6			3	g_8											
1103.97																			
			λ2945				λ3058		λ3179										
6			33939.5(43.0)				**32684.55**		**31443.0**										
			2	b_7			2	g_9	1	r_4									
1097.73																			
							λ2959		λ3072										
7							33782.5(86.0)		**32540.75**										
							0	g_{10}	1	k_3									

TABLE VII. Vibrational scheme sub-bands $^2\Pi_{\frac{1}{2}u} \rightarrow {}^2\Pi_{\frac{1}{2}g}$.

v_1' \ v_1''	0	1	2	3	4	5	6	7	8	9
	1265.75		1256.89	1250.21	1250.78	1370.25	1197.06	1217	1220	1230
	λ3511	λ3674	λ3852	λ4047						
0	28468.46	27202.65	25945.78	24695.7(00.4)						
	4 c_3	5 d_3	5 j_2	2 r_0						
1125.99										
	λ3378	λ3528	λ3692	λ3871	λ4068		λ4540.5			
1	29594.41	28328.65	27071.75	25821.55	24570.8(75.3)		*c*			
	5 c_4	1 d_4	4 $c_2 j_3$	4 r_1	2					
1120.87										
	λ3254	λ3394	λ3545		λ3891	λ4109	λ4321.5	λ4561	λ4830	
2	30715.20	29449.55	28192.65		25691.5(95.8)	24321.25	(23133.9)	*c*	*c*	
	5 c_5	3 d_5	4 j_4		1	3 f_3	2 m_1			
1116.01										
	λ3140	λ3270		λ3562			λ4123	λ4341.5	λ4583	λ4858
3	31831.29	30565.55		28058.45			24240.2	(23037.3)	*c*	*c*
	4 c_6	4 d_6		3 $r_2 k_4$			3 m_2			
1111.79										
	λ3034	λ3156	λ3286	λ3427	λ3580			λ4141	λ4361	λ4608
4	32943.05	31677.35	30420.35(24.35)	29170.2(74.3)	27919.4			(24142.9)	(22925.0)	*c*
	3 c_7	4 d_7	1 j_5	1 k_5	1			3	1.5	
1108.50										
	λ2936	λ3049	λ3170	λ3301	λ3443				λ4160	λ4384
5	34051.5(55.1)	32785.82	31582.95	(30279 S)	29028.0(31.6)				(24030.7)	*c*
	1 c_8	3 d_8	3 $c_3 j_7$	1 k_6?	1 l_4				3	
1106.99										
		λ2949	λ3063	λ3185						λ4182
6		33893.0(96.5)	32635.95	31385.70						(23906.2)
		1 d_9	2 $c_4 j_8$	1 k_7						2
?~1015										
		λ2863	λ2971							
7[a]		(34916 S)	(33649 S)							
		00 n_0	0 (r_3)							
1~ 96										
		λ2856	λ2962	λ3075						
7[b]		(35008 S)	(33750 S)	(32510 S)						
		1 d_{10}	0 j_9	1 k_8						

$v_1'' = 0$ to 4 an excellent agreement is obtained (differences smaller than 0.1 cm^{-1}).

In Tables VI and VII for many bands in the right-hand lower corner the letter designations of Smyth[3] are inserted. It is interesting to note how successful Smyth was in spite of the low dispersion of his spectrograph in picking out several progressions. In the left-hand lower corners the relative intensities of the bands are given, estimated on a scale of 5. The intense bands form a typical Franck-Condon parabola, with a subsidiary maximum along the diagonal. For the sub-bands $^2\Pi_{\frac{1}{2}u} \rightarrow {}^2\Pi_{\frac{1}{2}g}$ a tentative assignment for 5 bands observed by Smyth is given by ascribing them to a perturbed double level $v_1' = 7^{a,b}$.

The vibrational scheme for $v_1'' \geqslant 5$ is very incomplete. The CO_2^+ spectrum obtained by the author was in the longer wave-length region strongly overlapped by bands of CO and in general was very weak—no rotational analysis could be performed for bands beyond λ4130. Only band heads for the λ4300 group were measured; this was the last group observable on my spectrograms. Smyth[3] reported the existence of many bands at longer wave-lengths, but he did not measure their positions exactly and did not include the frequencies of those bands in his tables. However, he included in this paper a photograph of the spectrum as far as λ5000, and this photograph constitutes at present the only available source of information about those bands. The wave-lengths of several long wave-length bands were calculated from the vibrational scheme (values denoted by *c* in Tables VI and VII), and in comparing them with the photograph in Smyth's paper a reasonably good agreement can be observed.

Perturbations

In the band system studied several vibrational perturbations are observed in the lower and in the upper states. In Figs. 5 and 6 the deviations of

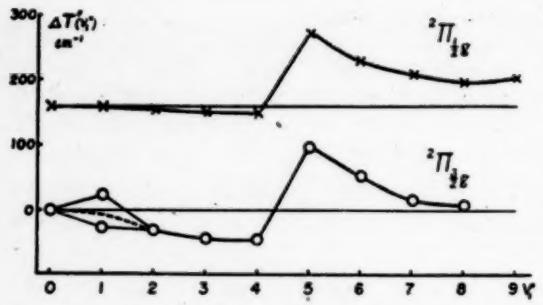

FIG. 5. Deviations of the positions of the vibrational levels from positions calculated according to the formula $T''(v_1'') = T''(0) + 1271v_1'' - 2.5v_1''(v_1''+1)$ as a function of the vibrational quantum number v_1'' for the ground state $^2\Pi_g$.

the vibrational levels from calculated values are presented as functions of the vibrational quantum number. The calculated values were obtained on the basis of the formulas $T''(v_1'') = T''(0) + 1271v_1'' - 2.5v_1''(v_1''+1)$, and $T'(v_1') = T'(0) + 1131v_1' - 3.0v_1'(v_1'+1)$, where $T'(0) - T''(0)$ are equal to 28532.57 and 28468.42, respectively, for the sub-bands $^2\Pi_{3/2u} \rightarrow {}^2\Pi_{3/2g}$ and $^2\Pi_{\frac{1}{2}u} \rightarrow {}^2\Pi_{\frac{1}{2}g}$. The formulas were chosen so as to give the smallest deviations for levels which show little perturbation in Λ-doubling and in the B values. The distances of the crosses from corresponding circles for a given vibrational quantum number indicate directly the splitting of the state $^2\Pi$ in the given vibrational state. The following perturbations are observed:

(1) Splitting of the substate $^2\Pi_{3/2g}$ into two levels for $v_1''=1$, $v_2''=v_3''=0$ which is undoubtedly caused by the interaction with the level $v_2''=2$, $v_1''=v_3''=0$ (double bending vibration).

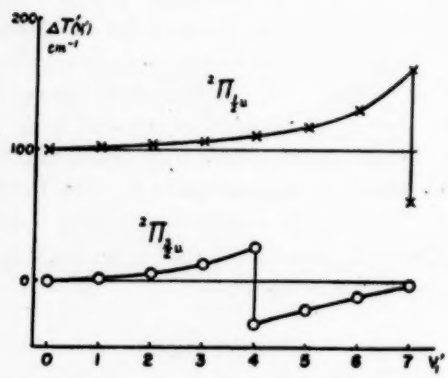

FIG. 6. Deviations of the positions of the vibrational levels from positions calculated according to the formula $T'(v_1') = T'(0) + 1131v_1' - 3.0v_1'(v_1'+1)$ as a function of the vibrational quantum number of v_1' for the excited state $^2\Pi_u$.

Sublevel a shows a vibrational perturbation downwards, possesses a lower B'' value and an anomalous negative Λ-doubling. Sublevel b shows exactly opposite perturbations.

(2) Splitting of the substate $^2\Pi_{3/2u}$ into two levels for $v_1'=4$ is similar in general character to the previous perturbation, with the exception that no anomalous Λ-doubling for sublevels b is observed. The corresponding vibronic levels perturbing the levels $v_1' \leqslant 3$ and $v_1' \geqslant 5$ are in a greater distance and the corresponding perturbations are decreasing in moving away from $v_1'=4$.

(3) The perturbation of the substate $^2\Pi_{\frac{1}{2}u}$ at $v_1'=7$ seems to be similar to the perturbation 2. No anomalous Λ-doubling for levels below the perturbation is observed. The levels become with increasing vibrational quantum number predominantly of the b-type.

(4) The perturbation occurring between $v_1''=4$ and 5 for both substates of the ground state $^2\Pi_g$ shows a reversed correlation between the vibrational shift on the one hand, and the B'' value and the Λ-doubling on the other. Levels showing vibrational perturbation downwards have excessively big B-constants and anomalously high Λ-doubling, and *vice versa*. There is, however, the similarity with cases 2 and 3 in that the levels $^2\Pi_{\frac{1}{2}g}$ with upward vibrational perturbation do not show any anomalous Λ-doubling. From the vibrational analysis of the subbands $^2\Pi_{3/2u} \rightarrow {}^2\Pi_{3/2g}$ it can be seen that no bands corresponding to transitions $v_1'=4^a$, 5, $6 \rightarrow v_1''=7$, 8 are observed; the levels of $^2\Pi_{3/2g}$ for $v_1'' \geqslant 5$ should therefore be classified according to the selection rule formulated in Part II ($a \rightarrow b$ forbidden) as levels of a b-type, in spite of their reversed perturbations in rotational constants. However for $v_1'' \leqslant 4$ the levels are also not of the a-type as can be seen from the vibrational scheme, since they are also combining only with the levels of $^2\Pi_{3/2u}$ of a b-type. It seems therefore that maybe the classification into levels of an a- and b-type has a meaning relative only to perturbations of the type described under 1 and 2 (maybe 3) and only because such perturbations lead to the prohibition of mixed $a \rightarrow b$ transitions.

An interesting feature of the perturbation now under discussion is that it leads to a very

weak emission of bands of the progression $v_1'' = 5$. It should be pointed out also, that with the exception of the perturbation 1 very little influence of the perturbations on the values of the D-constants is noticeable.

CONCLUDING REMARKS

In this work a very complete analysis of the band system $^2\Pi_u \rightarrow {}^2\Pi_g$ of the molecule CO_2^+ is given for the system of symmetrical vibrations. A rotational analysis of all strongest and some of the weaker bands in all of 48 sub-bands was reported. In the vibrational scheme 94 (possibly 99) sub-bands are classified. Almost all vibrational and rotational constants for this array of symmetrical vibrations are contained in this paper and should be supplemented only by the following data from Part II: B'', D'', and p'' values for the levels $v_1'' = 0$, 1, and 2, p'-values for the levels $v_1' = 0$ to 6 and by the data contained in Figs. 4 and 5. In several instances strong perturbations are observed, the explanation of which seems to require a thorough theoretical investigation of the rotational structure of the vibronic states of such a molecule and their mutual interaction. In the band system the long wave-length bands were not investigated with sufficient accuracy, and in order to get better data for the higher vibrational levels of the ground state $^2\Pi_g$ a reinvestigation of the bands in the region beyond λ4000 seems necessary. A source emitting a purer spectrum of CO_2^+, perhaps of the kind used by Smyth,[3] should be applied for this purpose.

PHYSICAL REVIEW VOLUME 72, NUMBER 8 OCTOBER 15, 1947

On the $^2\Pi_u \rightarrow {}^2\Pi_g$ Bands of CO_2^+. Part IV

S. MROZOWSKI
*Department of Physics, University of Chicago, Chicago, Illinois**

(Received February 10, 1947)

In this last part of the work on the $^2\Pi_u \rightarrow {}^2\Pi_g$ bands of the CO_2^+ molecule all data are collected on bands for which no classification could be found or for which the classification suggested is for any reason considered as hypothetical. Bands belonging to two groups around λ3760 and λ3915 are classified tentatively as transitions $v_1' = 0$, 1, 2, 3, 4; $v_2' = v_3' = 0 \rightarrow v_1'' = 0$, 1, 2, 3; $v_2'' = v_3'' = 1$. The upper states are probably identical with the vibrational levels of the symmetrical array discussed in the first three parts of this work. The rotational analysis of the bands (8 sub-bands) is given in Tables I and II, the vibrational schemes for the two systems of sub-bands (12 in all) are presented in Tables III and IV. Very weak bands around λ3245 and λ3370 are classified as transitions $v_1' = 0$, 1, 2; $v_2' = 0$; $v_3' = 1 \rightarrow v_1'' = 0$, 1, 2; $v_2'' = 1$; $v_3'' = 0$. The rotational analysis of the bands (10 sub-bands) is given in Tables V and VI, the vibrational schemes for the two systems of sub-bands are presented in Tables VII and VIII. The tentative classification of these four groups of bands leads to provisional values for the frequencies of the antisymmetric vibration ν_3. These values are included in the following table presenting a comparison for the ground state of the molecule CO_2 with the corresponding frequencies for the ground state $^2\Pi_g$ and the excited state $^2\Pi_u$ of the molecule CO_2^+.

	CO_2	$^2\Pi_g CO_2^+$	$^2\Pi_u CO_2^+$
ν_1	1361	1280	1131
ν_2	673	~ 632	<560?
ν_3	2379	~2305?	~1895?

The rotational constants in the first approximation for the ground state of the ion are thus: $B_{v_1 v_2 v_3}'' = B_{000}'' - 0.0014 v_1' - 0.0042(v_2'' + v_3'')$; $B_e'' = 0.3849$ and 0.3867 for the substates $^2\Pi_{3/2g}$ and $^2\Pi_{1/2g}$, respectively. In Table IX the rotational analysis is presented for 8 sub-bands from the region λ3500−λ3850. No classification for these bands could be found. In Table X the remainder of observed but not classified weak band edges, groupings of lines and bands of a more complicated structure are listed. Several of them present special features of interest for future investigations.

INTRODUCTION

IN the first three parts of this work (see the preceding paper) the results of an extensive and quite complete rotational and vibrational analysis of the band system $^2\Pi_u \rightarrow {}^2\Pi_g$ of the molecule CO_2^+ were presented for the array of symmetrical vibrations ($v_1' v_1''$ array, for $v_2' = v_3' = v_2'' = v_3'' = 0$). Not less than 94 bands were

* Now at Research and Development Division, Great Lakes Carbon Corporation, Morton Grove, Illinois.

TABLE I. Sub-bands $^2\Pi_{3/2u} \rightarrow {}^2\Pi_{3/2g}$.

$J-\frac{1}{2}$	(B_0, A_0) $\nu_0=25593.5$ R	P	(B_1, A_0) $\nu_0=26720.9$ R	P	(B_2, A_1) $\nu_0=26607.7$ R	P
6				26715.46		26601.35
7				14.44		00.24
8		25585.34		13.30		26599.08
9		84.27		12.18		97.87
10		83.09		10.93	26611.82 h	96.59
11		81.86		09.72	11.82 e	95.27
12	25598.67 h	80.54	26726.49 h	08.37	11.82 a	93.88
13	98.67 e	79.31	26.49 e	07.04	d	92.45
14	98.67 a	77.90	26.49 a	05.62	11.71	90.93
15	d	76.50	d	04.17	11.48	89.31
16		75.09		02.69	11.29	87.72
17	98.55	73.55	26.29	01.13	11.02	85.89
18	98.40	72.02	26.07	26699.56	10.68	84.38
19	98.17	70.41	25.82	97.88	10.19	82.46
20	97.90	68.81	25.51	96.21	09.82	80.72
21	97.63	67.11	25.13	94.49	09.27	78.68
22	97.30	65.37	24.74	92.70	08.74	76.88
23	96.89	63.63	24.28	90.83	08.16	
24	96.48	61.76	23.77	89.00	07.43	
25	96.00	59.93	23.26	87.04	06.45	
26	95.35	58.04	22.67	85.06	05.59	
27	94.90	56.04	21.98	83.05	04.71	
28	94.30	54.07	21.28	80.97	03.73	
29	93.61	51.98	20.55	78.80	02.77	
30	92.92	49.85	19.80	76.67		
31	92.15	47.75	18.94	74.42		
32	91.41	45.61	18.07	72.17		
33	90.47	43.37	17.13	69.85		
34	89.62	41.08	16.16	67.50		
35	88.64	38.73	15.13	65.06		
36	87.60		14.07	62.60		
37	86.49		12.90	60.10		
38			11.74			
39			10.48			
40			09.29			
41			07.89			
42			06.60			
43			05.06			
44			03.64			
	$B_0'=0.3470?(0.3485)$		$B_1'=0.3477$		$B_2'=0.3465$	
	$B_0''=0.3700?(0.3717)$		$B_0''=0.3720$		$B_1''=0.3740$	

classified. All the most prominent bands of CO_2^+ in the region $\lambda 2900-\lambda 5000$ were shown to belong to this array. However, there are many weaker bands in the same region, which show a similar rotational structure and undoubtedly correspond to the same electronic transition $^2\Pi_u \rightarrow {}^2\Pi_g$ but definitely cannot be included into the array of the pure symmetrical vibrations. A rotational analysis of quite a number of them (26 in all) was performed, and positions of many weak band edges were determined. In view of the smaller intensity of the bands the results are of a relatively lower accuracy. For this and also other reasons no final correlation to vibrational quantum numbers v_1, v_2, and v_3 could be established. Since with the observational material at present available no better results can be obtained, and since the solution of difficulties can only be expected from a reinvestigation of this band spectrum with an improved technique, it seems appropriate to present in this paper all results obtained in this work in spite of their incompleteness, with the hope that these data will facilitate the solution of the problem in the future. For the same reason tentative classifications for some groups of bands will be given.

RESULTS

Groups of Bands Around λ3760 and λ3915

Two groups of bands are always observed by investigators of the CO_2^+ spectrum at the same time with the main system of bands (array of symmetrical vibrations). The intensity of the bands in these groups around λ3760 and λ3915 is relatively quite high; it is comparable to the weaker bands in the symmetrical sequence around λ3850. The two groups of bands seem to form two double sequences of sub-bands of the same structure as the main bands. The wave numbers of the lines of these bands are given in Tables I and II. The rotational quantum number assignments can be in error not more than by one unit for the R branches; of the correctness of the numbering in the P branches the author feels reasonably confident. For the sub-band λ3775 in which only the R branch was recorded, the numbering can be in error as much as by ± 2. The B' and B'' values determined by the usual procedure are given in the lower part of the tables. Slightly higher values are obtained by increasing the numbering in the R branches by one unit, but the B-values do not seem to be in such good general agreement, and therefore they are not included. However the possibility of such a correction should be kept in mind.

By comparing the B' and B'' values and the general structure of the two band groups, the vibrational schemes for the two arrays of sub-bands $^2\Pi_{3/2u} \rightarrow {}^2\Pi_{3/2g}$ and $^2\Pi_{\frac{1}{2}u} \rightarrow {}^2\Pi_{\frac{1}{2}g}$ given in Tables III and IV were obtained. These tables are arranged similarly to and all designations are the same as in Tables VI and VII of the preceding paper. First of all it should be noted that the B' values for all sub-bands of the λ3760 group are almost exactly equal to the B' values obtained for vibrational levels of the excited state from the main system of bands (symmetrical array, see Part III, Tables IV and V). Secondly, the vibrational frequency differences for the upper B differ very little from the differences reported previously for the upper substates $^2\Pi_{3/2u}$ and $^2\Pi_{\frac{1}{2}u}$. They differ not more than 0.7

cm^{-1}. If the assumption is made that these differences are due to a slightly erroneous dispersion curve for the region λ3915 and that for the same reason the B' values for sub-bands of the λ3915 group are deviating from the values found in Part III, Tables IV and V, a perfect agreement can be obtained between the vibrational schemes Tables III and IV and the B' and B'' values given in Tables I and II. If the B'' values are increased by amounts corresponding to the necessary corrections of the B' values (all corrected values are given in parentheses), the new B'' values become almost exactly equal to the values obtained for the same vibrational levels from the sub-bands of the λ3760 group. The limits of error and the D' and D'' values are not given in Tables I and II, since in general all constants are of a relatively low accuracy. The accuracy is the lowest for sub-bands with short P branches. An approximate idea of the accuracy can be obtained by inspection of Table III in Part III. Unfortunately, because of unforeseen circumstances no new photographs of the CO_2^+ spectrum could be obtained with the big grating spectrograph, and the supposition of an erroneous dispersion curve in the region λ3915 could not be tested. However this view is strongly supported by the consistency of the results presented above and also by the fact that the region around λ3915 is the only region for which a correction curve strongly deviating from a parabolic shape was obtained.

It follows from the probable identification of the vibrational levels $B_0 \cdots B_4$ with the levels reported in Part III that $y=0$ in Tables III and IV and $v_2'=v_3'=0$. The vibrational levels

TABLE II. Sub-bands $^2\Pi_{\frac{1}{2}u} \rightarrow {}^2\Pi_{\frac{1}{2}g}$.

$J-\frac{1}{2}$	(B_2, A_2) $\nu_0=25531.7$ R	P	(B_1, A_2) $\nu_0=26658.4$ R	P	(B_1, A_1) $\nu_0=25447.8$ R	P	(B_2, A_1) $\nu_0=26569.2$ R	P	(B_2, A_2) $\nu_0=\sim 26476$ R
2									26478.30*
3									78.83
4		25527.98						26565.40	79.53*
5		26.96						64.48	80.05
6		26.02						63.44	80.53*
7		24.99		26651.55				62.38	81.02
8		23.84		50.62				61.28	81.37*
9		22.76		49.53		25438.95		60.16	81.74
10		21.59		48.27		37.69		58.95	81.99*
11		20.42		47.04		36.45		57.73	
12		19.07		45.75		35.24		56.39	
13	25537.45 h	17.86	25663.98 h	44.46		33.99	26574.64 h	55.10	82.65 h
14	37.45 e	16.48	63.98 e	43.05	25453.48 h	32.58	74.64 e	53.71	82.65 e
15	37.45 a	15.11	63.98 a	41.63	53.48 e	31.20	74.64 a	52.30	82.65 a
16	d	13.67	d	40.16	53.48 a	29.77	d	50.80	d
17		12.20	63.85	38.64	d	28.28	74.53	49.32	82.43
18	37.24	10.67	63.63	37.06	53.30	26.74	74.24	47.72	82.19
19	37.09	08.94	63.47	35.45	53.07	25.22	74.07	46.13	81.99*
20	36.90	07.49	63.16	33.77	52.86	23.64	73.73	44.44	81.60
21	36.67	05.87	62.89	32.11	52.67	21.94	73.48	42.76	81.37*
22	36.37	04.13	62.51	30.33	52.26	20.23	73.02	40.96	80.85
23	36.13	02.43	62.16	28.53	51.95	18.49	72.68	39.22	80.53*
24	35.70	00.63	61.72	26.66	51.51	16.85	72.16	37.30	79.82
25	35.18	25498.83	61.23	24.79	51.10	14.87	71.68	35.47	79.53*
26	34.70	96.95	60.60	22.81	50.59	12.97	71.08	33.47	78.56
27	34.23	95.01	60.09	20.88	50.12	11.09	70.55	31.55	78.30*
28	33.58	93.07	59.36	18.81	49.50	09.09	69.86	29.45	
29	33.02	91.06	58.75	16.75	48.90	07.07	69.20	27.39	
30	32.35	88.99	58.04	14.62	48.14	05.00	68.44	25.22	
31	31.64	86.95	57.30	12.45	47.59	02.92	67.68	23.11	
32	30.90	84.63	56.38		46.74	00.67	66.76	20.80	
33	30.15	82.60	55.61		45.96	25398.54	65.94	18.59	
34	29.26	80.38	54.75		45.06	95.99	64.94	16.23	
35	28.34	78.11	53.77		44.16	93.80	64.00	13.92	
36	27.48	75.72	52.79		43.19		62.92	11.42	
37	26.50	73.40			42.25		61.92	09.03	
38	25.49	70.95			41.20		60.74	06.46	
39	24.49	68.59			40.19		59.62	03.98	
40	23.35	65.95					58.33	01.29	
41	22.27	63.55							
42	20.95	60.98							
43	19.86	58.40							
44	18.49	55.86							
45	17.33								
46	15.85								
47	14.44								
48	12.98								
49	11.43								
50	09.81								
	$B_2'=0.3506?(0.3509)$ $B_2''=0.3725?(0.3729)$		$B_1'=0.3500$ $B''=0.3732$		$B_1'=0.3485?(0.3498)$ $B_1''=0.3702?(0.3717)$		$B_2''=0.3486$ $B_1''=0.3722$		

TABLE III. Sub-bands $^2\Pi_{3/2u} \rightarrow {}^2\Pi_{3/2g}$.

v_1' \ v_1''		A_0 x	1235	A_1 $x+1$	1245?	A_2 $x+2$
B_0	y	λ3905 25593.5 1.5 p_2?				
1127.4						
B_1	$y+1$	λ3741 26720.9 1		λ3922 (25491) 0		
1122						
B_2	$y+2$			λ3757 26607.7 <1		λ3942 (25363)? <0 (m_3)
1120?						
B_3	$y+3$					λ3774 (26487.4) 0

$A_0, A_1 \cdots$ present a set of new vibrational levels situated slightly above the vibrational levels $v_1''=2, 3\cdots; v_2''=v_3''=0$ discussed in Part III. It seems probable there is no corresponding level above $v_1''=1$, $v_2''=v_3''=0$, since no bands of comparable intensity are observed in the region below λ3740. Hence the vibrational level A_0 is probably the lowest level of this type. The vibrational frequency for A_0 measured from the level $v_1''=v_2''=v_3''=0$ is around 2937 cm^{-1}, the level A_0 can only be interpreted, therefore, as a level $v_1''=0(x=0)$, $v_2''=v_3''=1$. Since for the ground state the bending vibration frequency is around 632 cm^{-1} (see Part II, resonance of $v_2''=2$ with $^2\Pi_{3/2g}v_1'=1$), the proposed classification leads to a frequency of the antisymmetric vibration $\nu_3''=2305$ cm^{-1}. This value seems quite reasonable, maybe a little too high (see the comparison of vibrational frequencies for CO_2 and CO_2^+ below). The simple rotational structure of a type $^2\Pi \rightarrow {}^2\Pi$ does not seem to be in agreement with the fact of the presence of one quantum of bending vibration. However, the rotational structure of the level with a double bending vibration which is in resonance with the level $v_1''=1, v_2''=v_3''=0$ does not have a very different structure (see Part II), and maybe there is little interaction between the electronic state and the molecular vibration for the CO_2^+ molecule. It seems also hard to see why a transition $v_1'', v_2''=v_3''=0 \rightarrow v_1'', v_2''=v_3''=1$ should appear in the spectrum with such a relatively high intensity. It should be finally noted that the interaction with the new levels $A_0, A_1 \cdots$ cannot be the cause of the perturbation for the symmetrical levels around $v_1''=5$, $v_2''=v_3''=0$ discussed in Part III, since the perturbing levels should lie below and not above the corresponding symmetrical levels (for $v_1'' \leqslant 5$).

By shifting the rotational quantum numbering in Tables I and II for R branches by one unit lower and in P branches by one unit higher the bands could be interpreted as a system of bands corresponding to a new higher excited state $^2\Pi_g$* combining with the excited state $^2\Pi_u$. The B' values for the new state $^2\Pi_g$ would be then considerably smaller than for $^2\Pi_u$, which seem reasonable, but the frequency of the symmetrical vibration would be much too high for such large interatomic distances in the molecule. This alternative classification should be discarded also in view of the similarity in the excitation conditions of these bands and of the main system.

Groups of Bands Around λ3245 and λ3370

Two groups of very weak bands are observed around λ3245 and λ3370. Their rotational structure and the relative positions of band heads are very much like those of the main progressions of bands around λ3265 and λ3385; their intensity, however, is of a different order of magnitude. The groups are shifted toward shorter wavelengths relative to the main progressions. Their rotational analysis and the B' and B'' constants are collected in Tables V and VI. The vibrational schemes are given in Tables VII and VIII. Some time ago it was believed* that these bands could be classified as transitions $v_1', v_2'=0$, $v_3'=1 \rightarrow v_1'', v_2''=0, v_3''=1$. This classification would require that $n=1$ and $m=0$ in Tables

TABLE IV. Sub-bands $^2\Pi_{\frac{1}{2}u} \rightarrow {}^2\Pi_{\frac{1}{2}g}$.

v_1' \ v_1''		A_0 x	1210.6	A_1 $x+1$	1210?	A_2 $x+2$	1212?	A_3 $x+3$
B_0	y	λ3915 25531.7 1.5 h_3						
1126.7								
B_1	$y+1$	λ3749 26658.4 1 h_4		λ3928 25447.8 1 f_4				
1121.4								
B_2	$y+2$			λ3762 26569.2 1.5 f_5		λ3942 (~25363)? <0 (m_3)		
1116?								
B_3	$y+3$					λ3775 (26492.6) <1 (m_4)		
1112?								
B_4	$y+4$							λ3790 (26381.3) <1

* S. Mrozowski, Rev. Mod. Phys. 14, 216 (1942), and Part I.

TABLE V. Sub-bands $^2\Pi_{3/2u} \rightarrow {}^2\Pi_{3/2g}$.

	(D_0, C_0) $\nu_0 = 29793.8$		(D_1, C_0) $\nu_0 = 30904.0$		(D_1, C_1) $\nu_0 = 29638.7$		(D_2, C_1) $\nu_0 = 30749.5$		(D_2, C_2) $\nu_0 = 29553.2$	
$J-\frac{1}{2}$	R	P	R	P	R	P	R	P	R	P
8										
9	h	29784.38	30907.84 h	30894.10	29643.11 h	29630.42	30753.41 h	30740.87	29557.21 h	
10	29797.88 e	83.35	07.84 e	92.67	43.11 e	29.10	53.41 e	39.53	57.21 e	29543.28
11	97.88 a	81.36	07.84 a	91.32	a	27.81	53.41 a	38.17	57.21 a	42.05
12	d	79.92	d	89.92	d	26.38	d	36.81	d	40.80
13		78.41	07.60	88.37	42.78	24.91		35.33	56.97	39.13
14		76.89	07.39	86.76	42.43	23.31	52.88	33.65	56.77	37.40
15	97.45	75.30	07.15	85.16	42.03	21.80	52.47	32.05	56.48	35.73
16	97.10	73.58	06.85	83.44	41.64	20.00	52.07	30.26	56.22	34.12
17	96.70	71.86	06.37	81.68	41.15	18.45	51.58	28.47	55.90	32.24
18	96.42	70.06	06.01	79.84	40.66	16.43	51.05	26.66	55.37	30.52
19	95.88	68.19	05.51	77.97	39.92	14.76	50.47	24.73	54.77	28.68
20	95.40	66.29	04.91	76.03	39.09		49.80	22.72	54.18	26.72
21	94.74	64.39	04.30	73.98	38.16		48.99	20.59	53.50	24.67
22	94.13	62.28	03.58	71.92	37.61		48.31	18.21	52.80	22.63
23	93.46	60.20	02.73	69.78	36.83		47.49	15.84	52.01	20.51
24	92.68	58.10	01.97	67.58	36.03		46.64	13.56	51.12	18.35
25	91.83	55.87	01.05	65.35	34.96		45.54		50.12	16.06
26	90.91	53.58	00.13	62.98	33.92		44.34		49.24	13.68
27	89.94	51.24	30899.10	60.60	33.01		43.38		48.19	11.37
28	88.96	48.80	98.03	58.06	31.80		41.99		47.06	08.91
29	87.85	46.31	96.81	55.55					46.01	06.46
30	86.61	43.74	95.42	52.87					44.88	03.84
31	85.25	40.95	94.10	49.89						01.22
32	84.00		92.67	47.18						29498.51
33	82.66									
	$B_0' = 0.3462$		$B_1' = 0.3444$		$B_1' \cong 0.3440$		$B_2' = 0.3415$		$B_2' = 0.3425$	
	$B_0'' = 0.3760$		$B_0'' = 0.3760$		$B_1'' \cong 0.3745$		$B_1'' = 0.3748$		$B_2'' = 0.3740$	

VII and VIII and further that the frequency of the antisymmetric vibration for the excited state $^2\Pi_u$ should be higher than for the ground state. Since $\nu_3'' = 2305$ cm^{-1} (see preceding section) for ν_3' a value of about 2435 cm^{-1} is obtained. An increase in antisymmetric frequency with increase of interatomic distances is contrary to expectations. If we accept the explanation of the origin of the bands discussed in the preceding section as correct, a similar general structure of bands with and without bending vibration has to be assumed. A satisfactory explanation of the

TABLE VI. Sub-bands $^2\Pi_{\frac{1}{2}u} \rightarrow {}^2\Pi_{\frac{1}{2}g}$.

	$(\pm_0, C_0)$ $\nu_0 = 29731.8$		(D_1, C_0) $\nu_0 = 30841.3$		(D_1, C_1) $\nu_0 = 29616.6$		(D_2, C_1) $\nu_0 = 30682.4$		(D_2, C_2) $\nu_0 = 29518.6$	
$J-\frac{1}{2}$	R	P	R	P	R	P	R	P	R	P
6		29725.72				29610.28		30676.08		
7		24.88				09.21	h	74.93		
8		23.73		30832.97	h	07.98	30686.47 e	73.69	h	29510.01
9		22.39	h	31.76	29620.53 e	06.67	86.47 a	72.20	29522.85 e	08.91
10	29736.36 h	21.14	30845.63 e	30.37	20.53 a	05.25	86.35 d	70.93	22.85 a	07.66
11	36.36 e	19.71	45.63 a	29.07	d	03.84	86.23	69.50	d	06.13
12	36.36 a	18.37	d	27.55	20.34	02.32	86.01	67.87		04.87
13	d	16.76	45.53	26.07	20.00	00.80	85.76	66.40	22.63	03.18
14		15.28	45.33	24.49	19.80	29599.03	85.38	64.80	22.36	01.39
15	35.92	13.64	45.09	22.88	19.41	97.53	85.05	63.06	21.84	29499.79
16	35.72	12.04	44.84	21.14	18.93	95.57	84.50	61.21	21.47	
17	35.33	10.36	44.40	19.41	18.45	93.86	84.06	59.48	21.08	
18	35.04	08.67	44.05	17.59	17.86	91.98	83.49	57.43	20.51	
19	34.55	06.68	43.49	15.71	17.29		82.88	55.53	20.09	
20	34.15	04.78	43.01	13.84	16.64		82.23	53.50	19.60	
21	33.51	02.95	42.31	11.83	15.85		81.41	51.40	18.90	
22	32.99	00.98	41.75	09.80	15.12		80.63	49.15	18.35	
23	32.23	29698.84	40.92	07.68	14.20		79.65	46.90	17.36	
24	31.63	96.82	40.27	05.51	13.25		78.72	44.72	16.69	
25	30.76	94.58	39.34	03.25	12.19		77.70	42.38	15.62	
26	30.01	92.22	38.49	01.06	11.13		76.54	39.91	14.57	
27	28.99	90.05	37.47	30798.57	10.02		75.44	37.40	13.68	
28	28.18	87.59	36.43	96.27	08.76		74.09	34.84	12.52	
29	27.01	85.30	35.33	93.71	07.37		72.94	32.08	11.37	
30	26.02	82.97	34.28	91.32	06.15		71.44	29.54	10.01	
31		80.32			04.67		70.06	26.73		
32		77.46			03.34		68.56	23.92		
33		75.03			01.88		66.99	21.05		
34		70.90			00.26		65.37			
35					29598.30		63.63			
36							61.92			
37							59.94			
38							58.14			
39							56.22			
	$B_0' = 0.3485$		$B_1' = 0.3475$		$B_1' \cong 0.3450?$		$B_2' = 0.3440$		$B_2' \cong 0.3440?$	
	$B_0'' = 0.3772$		$B_0'' = 0.3773$		$B_1'' \cong 0.3755?$		$B_1'' = 0.3760$		$B_2'' \cong 0.3765?$	

TABLE VII. Sub-bands $^2\Pi_{3/2u} \rightarrow {}^2\Pi_{3/2g}$.

v_1' \ v_1''		C_0 m	1265.3	C_1 $m+1$	1196.3	C_2 $m+2$
		λ3355				
D_0	n	29793.8				
		0				
1110.2						
		λ3234		λ3372		
D_1	$n+1$	30904.0		29638.7		
		0		0		
1110.8						
				λ3251		λ3382
D_2	$n+2$			30749.5		29553.2
				0		0

TABLE VIII. Sub-bands $^2\Pi_{\frac{1}{2}u} \rightarrow {}^2\Pi_{\frac{1}{2}g}$.

v_1' \ v_1''		C_0 m	1224.7	C_1 $m+1$	1163.8	C_2 $m+2$
		λ3362				
D_0	n	29731.8				
		0				
1109.5						
		λ3241		λ3375		
D_1	$n+1$	30841.3		29616.6		
		0		0		
1065.8						
				λ3258		λ3386
D_2	$n+2$			30682.4		29518.6
				0		0

weak bands λ3245 and λ3370 can be obtained by assuming $m=n=0$ and classifying as transitions $v_1'=0, 1, 2$; $v_2'=0$, $v_3'=1 \rightarrow v_1''=0, 1, 2$; $v_2''=1$, $v_3''=0$. The important feature of this classification is the assumption that $n=0$, which would furnish a good explanation why no corresponding bands are observed on the short wave-length side of the progression of main bands around λ3500. As in the former case, the new levels C and D cannot be the cause of the perturbations observed in the main system.

For the suggested classification the frequency of the antisymmetric vibration in the excited state is obtained as $\nu_3'=1895$ cm^{-1}, a value which seems a little low in comparison to the ground state $^2\Pi_g$ of CO_2^+, but which compares more favorably with the data for the CO_2 molecule. A comparison of the frequencies of vibrations following from the proposed classifications with the corresponding values for CO_2 is given below.

	CO_2 ground state	$CO_2^+ - {}^2\Pi_g$	$CO_2^+ - {}^2\Pi_u$
$\nu_1=$	1361	1280	1131
$\nu_2=$	673	~ 632	<560?
$\nu_3=$	2379	~2305?	~1895?

The value of ν_2 for $^2\Pi_u$ is obtained by observing that there is no resonance splitting of the level $v_1'=1$, $v_2'=v_3'=0$ by interaction with the double bending vibration and assuming for this reason $2\nu_2<\nu_1$. It must be emphasized again that the values of ν_3 for CO_2^+ are hypothetical and based on classifications which are only tentative. It might be of interest to note that the suggested classifications for both groups of bands correspond to a change in the sum of the quantum numbers v_2 and v_3 equal to an even number.

From the suggested classifications and the B'' values for levels of the type A and C an approximate formula for B'' can be deduced: $B_{v_1v_2v_3}'' = B_{000}'' - 0.0014v_1'' - 0.0042(v_2''+v_3'')$. From this formula the rotational constant B_e'' for the non-vibrating CO_2^+ molecule is found to be 0.3849 and 0.3867 for the substates $^2\Pi_{3/2g}$ and $^2\Pi_{\frac{1}{2}g}$, respectively. It should be again pointed out however that the whole suggested classification of the levels A, B, C, and D is a very hypothetical one, and a classification involving totally symmetrical vibration states of the non-totally symmetrical vibrations (for instance combinations involving $2\nu_3$, or $2\nu_2$ with $l=0$) would be preferred for theoretical reasons.

Unclassified Bands

In Table IX are given the wave-lengths of the lines of weak bands observed in the region λ3500–λ3850. No reasonable classification could be found for these bands. In the lower part of the table two sets of B values are given, namely, for

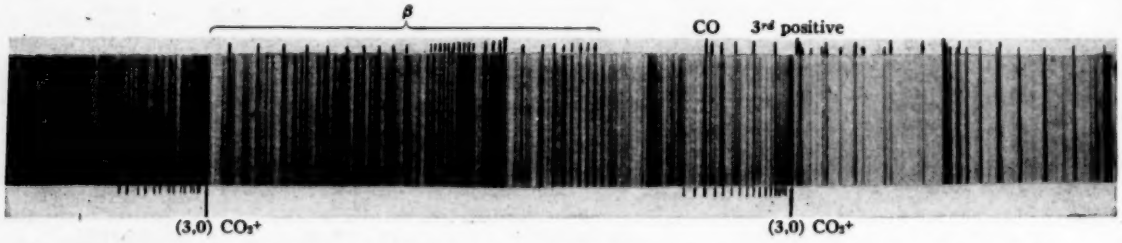

FIG. 1. Unclassified band β of CO_2^+ in the region around λ3137. Main branches marked on top. Bands of the main system of CO_2^+ are marked below, and of CO (third positive) above the picture.

TABLE IX. Unclassified sub-bands.

J−½	λ3307 ν_0=28502.6 R	P	λ3510 ν_0=28481 R	P	λ3540 ν_0=28237.5 R	P	λ3544 ν_0=28202 R	λ3553 ν_0=28125.2 R	P	λ3572 ν_0=27979.4 R	P	λ3651 ν_0=27376.2 R	P	λ3832 ν_0=26085.8 R	P
1				28479.41?											
2				78.47?											
3				77.62											
4				76.57											
5				75.60											
6				74.48											
7				73.47											
8	28506.62		28484.76		28241.68	28227.71		28129.28		27983.57		27380.57			
9	06.62		84.76		41.68	26.40	28206.30	29.28		83.57		80.57	27366.30	2609056.	
10		28491.50	84.76			24.94	06.30	23.28	28112.55	83.57		80.57	65.18	90.56	
11		90.18				23.56	06.30		11.08				63.62	90.56	
12	06.37	88.60										80.33	62.07		
13	06.28	86.72	84.38		41.37	22.00		29.05	09.50	83.41	27963.73	80.11	60.63		26070.77
14	06.03	85.18	84.05		41.16	20.43	06.06	28.83	07.87	83.17	62.20	79.80	58.77	90.35	69.27
15	05.67	83.27	83.78		40.84	18.62	05.70	28.64	06.19	82.85	60.54	79.40	56.94	90.21	67.71
16	05.27	81.60	83.39		40.43	17.11	05.41	28.27	04.47	82.47	58.75	79.03	55.18	89.88	66.03
17	04.68		82.93		39.97	15.35	05.02	27.86	02.67	82.05	56.89	78.49	53.22	89.59	64.44
18	04.27		82.43		39.61	13.57	04.57	27.34	00.74	81.54	55.06	77.99	51.36	89.18	62.55
19	03.71		81.78		39.00	11.68	03.96	26.84	28098.81	80.98	53.13	77.35	49.26	88.91	60.81
20	02.98		81.16		38.37	09.72	03.27	26.22	96.51	80.37	51.13	76.76	47.29	88.22	58.77
21	02.29		80.38		37.90	07.74	02.65	25.68	94.50	79.70	49.09	75.94	45.04	87.85	56.98
22	01.35		79.72		37.06	05.70	01.99?	24.81	92.64	78.96	46.94	75.24	42.83	87.11	54.76
23	00.57		78.96		36.22	03.46	01.36?	24.06	90.49	78.16	44.72	74.28	40.55	86.62	52.86
24	28499.70		77.99		35.45	01.02	00.32?	23.14	88.23	77.30	42.44	73.50	38.42	85.68	50.57
25	98.75		77.04		34.47	28198.32	28199.76?	22.28	85.97	76.33	40.09	72.40	35.84	85.21	48.59
26	97.69		76.26		33.56		98.50?	21.37	83.50	75.35	37.72	71.50	33.62	84.07	46.10
27	96.62		74.98		32.46			20.26		74.30	35.26	70.29	30.96	83.41	44.08
28	95.36		73.72		31.35			19.02		73.18	32.72	69.26	28.56	82.19	
29	94.23				30.21			18.02		71.98	30.15	67.96	25.83	81.53	
30	92.80				28.90			16.63		70.70		66.79	23.33	80.00	
31								15.44				65.37	20.43	79.41	
32								14.05				64.17	17.68	77.71	
33								12.86				62.15	14.83	77.00	
34								11.31				61.22			
35								09.80							
36								08.20							
37								06.65							
38								05.09							
39								03.42							
	$B'=0.3500$		$B'=0.3440$		$B'=0.3500$			$B'=0.3485$		$B'=0.3510$				$B'=0.3510$	
	$B''=0.3820$		$B''=0.3760$		$B''=0.3820$			$B''=0.3810$		$B''=0.3840$				$B''=0.3800$	
	$B'=0.3440$		$B'=0.3360$		$B'=0.3440$			$B'=0.3410$		$B'=0.3410$				$B'=0.3465$	
	$B''=0.3760$		$B''=0.3705$		$B''=0.3740$			$B''=0.3730$		$B''=0.3770$				$B''=0.3720$	

the given numbering of lines in branches and for an alternative numbering, for which J numbers in the R branches are decreased by one unit. In Table X are collected the wave numbers of weak band edges, grouping of lines which in some earlier papers were reported as band edges, and finally of bands of a more complicated structure.

Especially interesting are the six band regions denoted with Greek letters α, β, γ, δ, ϵ, and η, since they are wide groups containing a great number of lines which probably constitute bands of a more complicated character. Group α is composed of two bands shaded in opposite directions with a space free from lines between the two band heads; between α and the band head (4, 0) of the main system ($\nu_0=33022$ cm^{-1}) a complicated structure of several band heads is observed. Group β is a band composed of several branches; it is reproduced in Fig. 1. In the upper part of Fig. 1 some branches of this band are indicated. Group γ is a very complicated and weak group on the short wave-length side of the main sequence around λ3370. Very little can be said about the group δ since it is strongly overlapped by bands of CO. It seems to be a rather strong band with numerous branches. The band ϵ around λ3961 has a very strong main central

TABLE X. Band heads and groupings of lines.

	34087.5			27951.04	
	33778.4	gr.		27821.43	
Sm_{10}?	~33125	α	Sm_4	~27600	δ
S	32990	gr.		~27270	gr.
	32954.46			27238.20	
S	32860.99			27141.52	gr.
	32678.46			27000.40	gr.
Sr_7	32587	gr.		26915.00	
S	~31890	β		26659.0	
	31568.48			26576.5	
	31559.86			25701.0	
S	~31490	gr.		25519.1	
S	~31402	gr.		25380.6	
S	~30831	gr.	S	~25240	ε
	30653.82			24810.9	
	30640.53			24690.5	gr.
	30496.77			24155.0	
F	30446.30		S	~24152	η
	30436.40		F	23201.3	
S	~29700	γ		23158.1	

S—observed by Smyth (Phys. Rev. **38**, 2000, 1931), and his designations (m_{10}, r_7, m_4).

F—not observed by Smyth, but observed earlier by Fox, Duffendack, and Barker (Proc. Nat. Acad. **13**, 302, 1927).

gr.—grouping of lines, α, β, γ, δ, ε, and η see text; all others—probably weak band edges.

part and several side branches. Group η is mixed with the bands of the main sequence around $\lambda 4140$; it seems to have a quite complicated structure. All the bands given in Table X are either too weak or insufficiently resolved or hopelessly overlapped by other bands and require reinvestigation with a much more powerful and purer spectral light source and at least equally high dispersion. It can be expected that a successful analysis of all the weaker band systems described in Part IV, and of the more complicated bands, will lead to a deeper understanding of the electronic spectrum of a triatomic molecule.

In conclusion I should like to express my sincere thanks to Professor R. S. Mulliken for his continued interest in this work and to Professor H. D. Smyth for putting kindly at my disposal unpublished data and photographs of the spectrum of CO_2^+ obtained by him some time ago with a 21-foot grating spectrograph. The careful study of these photographs revealed very good agreement with my results; the higher purity of the spectrum obtained by Professor H. D. Smyth was an important factor in strengthening my confidence in the correctness of the results reported in this and the preceding paper. I am also very much indebted to Mr. T. J. Kinyon for assistance in computations.

PHYSICAL REVIEW VOLUME 72, NUMBER 8 OCTOBER 15, 1947

The Conservation of Momentum in the Disintegration of Li^8

R. F. CHRISTY, E. R. COHEN, W. A. FOWLER, C. C. LAURITSEN, and T. LAURITSEN
Kellogg Radiation Laboratory, California Institute of Technology, Pasadena, California

(Received July 11, 1947)

Apparatus for the introduction of radioactive materials into a cloud chamber has been employed to investigate the conservation of momentum in the β-decay of Li^8 to Be^8, which subsequently breaks up into two α-particles. The projection on the plane of measurement of the angle between the two α-particles is a measure of one component of the recoil momentum of the Be^8. Additional information is obtainable from the momentum of the electron but relatively few cases occur where both α-particles and the electron are in the plane of the cloud chamber. The Li^8 is produced by bombarding with deuterons a thin deposit of LiOH on beryllium or gold foils. The mean squares of the observed momenta relative to the maximum possible momenta were 0.247 (Be foil) and 0.349 (Au foil). Corrected for scattering and other errors these become 0.197 ± 0.025 and 0.207 ± 0.034, respectively, the probable errors quoted being statistical in origin. The weighted mean, rounded off to two figures, is 0.20 ± 0.02. This value is roughly twice that obtained taking into account only the emitted electrons, and approximately equal to that calculated for an electron and neutrino emitted with no preferred angle of ejection between them.

1. INTRODUCTION

THE conservation of momentum in the disintegration of radioactive nuclei by electron and positron emission and by the capture of electrons from extra-nuclear levels has been the subject of numerous experimental investigations.[1–5] These investigations have generally consisted in measuring the energy of the recoiling daughter nucleus either by counting the number of ions formed as the nucleus is brought to rest in a gas or by determining the retarding potential necessary to bring the nucleus to rest in vacuum. As the atomic weight of the daughter nucleus is usually known, its momentum can be calculated and compared with that to be expected theoretically. These experiments have shown that the maximum momentum of the recoiling nucleus is equal to that to be expected from the maximum observed energy of the emitted electron or positron but that the momentum of recoil is

[1] A. I. Leipunski, Proc. Camb. Phil. Soc. **32**, 301 (1936).
[2] H. R. Crane and J. Halpern, Phys. Rev. **56**, 232 (1939).
[3] L. W. Alvarez, A. C. Helmholtz, and B. T. Wright, Phys. Rev. **60**, 160 (1941); B. T. Wright, *ibid.* **71**, 839 (1947).
[4] J. S. Allen, Phys. Rev. **61**, 692 (1942).
[5] J. C. Jacobsen and O. Kofoed-Hansen, D. Kgl. Danske Vidensk. Selskab Mat.-fys. Medd **23**, 12 (1945).

greater, on the average, than that of the electron or positron. Furthermore, nuclear recoil has even been observed in the capture of extra-nuclear electrons, Allen[4] having observed and measured such a recoil in the disintegration of Be^7.

The results are consistent with the suggestion made by Pauli that a neutrino is emitted in these disintegrations. If the neutrino be assumed to have an energy given by the amount available in the transition between the mother and daughter nucleus minus that of the electron and the small energy of the recoiling nucleus, and if it is also assumed to have very small rest mass, its momentum can be computed. This suggestion, coupled with Fermi's[6] assumptions concerning the distribution in momentum between electron and neutrino, is sufficient to account for the observed distributions in momenta of the recoiling nuclei although the quantitative agreement has not been nearly as exact as in the determination of the maximum momentum. Perhaps the most critical tests are those of Jacobsen and Kofoed-Hansen[5] who found by means of retarding potentials a distribution in the momenta of daughter nuclei from the decay of Kr^{88} which was not consistent with the recoil from the decay electrons alone, and which even indicated qualitatively that the neutrino is emitted in this particular disintegration mainly in the same direction as the electron.

The disintegration of Li^8 by electron emission[7] is unique in that it is followed by the breakup of the daughter nucleus,* Be^8 into two alpha-particles.[8–10] The initial electron decay has a half-life of 0.88 second[11] and is followed by the alpha-particle decay in a time of the order of 10^{-21} second as indicated by the spread (uncertainty) in the alpha-particle energies.[9,12–14] The Be^8 nucleus is probably formed in one of several broad excited states extending up to 12 Mev in excitation. The observed energy spectrum of the emitted electrons extends at least to 12.0 ± 0.6 Mev and has been shown to be consistent[15,16] with the energy spectrum of the alpha-particles and with the fact that approximately 16.0 Mev is available in the complete transition from Li^8 to two alpha-particles. The mass of Li^8 is determined from the threshold bombarding energy[12] ($\sim$0.2 Mev) in the reaction $Li^7+H^2\rightarrow Li^8+H^1$.

In a coordinate system moving with the center of mass of the two alpha-particles the momenta of the alpha-particles are equal and oppositely directed. In laboratory coordinates the motion of this mass center will be observable in that there will be, in general, a small deviation from 180° in the angle between the two alpha-particles and in that the momenta, and hence energies and ranges of the two particles, will not, in general, be identical. These effects will be discussed quantitatively below but at this point it will suffice to note their orders of magnitude. The recoil momentum of the Be^8 will be at most the maximum electron energy divided by the velocity of light:

$$p_r \leq E_{\max}/c, \tag{1}$$

giving 5×10^7 cm/sec. for the maximum value of the recoil velocity, v_r. The velocity of the alpha-particles, v_α, in the center of mass system is approximately 10^9 cm per sec. for the decay of the 3.0-Mev excited state in Be^8, so that the angular deviation from 180° in the angle between the two alpha-particles in laboratory coordinates is

$$\theta \sim 2\frac{v_r}{v_\alpha}\sin\varphi \leq 2\frac{v_r}{v_\alpha} \leq \frac{1}{10} \text{ radian or } 6°, \tag{2}$$

where φ is the angle between the recoil of the Be^8 and its line of breakup in the center of mass system. For a given amount of recoil the maximum deviation from 180° occurs when the Be^8

[6] E. Fermi, Zeits. f. Physik **88**, 161 (1934).
[7] H. R. Crane, L. A. Delsasso, W. A. Fowler, and C. C. Lauritsen, Phys. Rev. **47**, 971 (1935); L. H. Rumbaugh and L. R. Hafstad, Phys. Rev. **50**, 681 (1936).
* Throughout this paper the formation of Be^8 as an intermediate stage in the ultimate decay of Li^8 into two alpha-particles will be assumed. This has been done primarily for convenience in discussing the disintegration. Considerations regarding the conservation of energy and momentum in the over-all process are independent of any assumptions concerning intermediate stages.
[8] P. I. Dee and C. W. Gilbert, Proc. Roy. Soc. **A154**, 279 (1936).
[9] W. A. Fowler and C. C. Lauritsen, Phys. Rev. **51**, 1103 (1937).
[10] E. Wigner and G. Breit, Phys. Rev. **50**, 1191 (1936); G. Breit and E. Wigner, Phys. Rev. **51**, 593 (1937).
[11] W. B. Lewis, W. E. Burcham, and W. Y. Chang, Nature **139**, 24 (1937).
[12] L. H. Rumbaugh, R. B. Roberts, and L. R. Hafstad, Phys. Rev. **51**, 1106 (1937) and **54**, 657 (1938).
[13] C. Smith and W. Y. Chang, Proc. Roy. Soc. **A166**, 415 (1938).
[14] T. W. Bonner, Phys. Rev. **72**, 163 (1947).
[15] D. S. Bayley and H. R. Crane, Phys. Rev. **52**, 604 (1937).
[16] Charles Kittel, Phys. Rev. **55**, 515 (1939).

breaks up in a plane normal to its direction of recoil. When the Be^8 breaks up parallel to its direction of recoil the maximum difference in velocity and range of the two alpha-particles occurs. For the velocity difference we have:

$$\Delta v_\alpha \sim 2v_r \cos\varphi \leq 2v_r. \quad (3)$$

For low energy alpha-particles the range varies approximately as the square of the velocity so that

$$\frac{\Delta R_\alpha}{R_\alpha} \sim 2\frac{\Delta v_\alpha}{v_\alpha} \sim 4\frac{v_r}{v_\alpha}\cos\varphi \leq 4\frac{v_r}{v_\alpha} \leq 20 \text{ percent}. \quad (4)$$

Hence range differences of as much as 20 percent and angular deviations from 180° of as much as 6° are to be expected.

It is the purpose of this paper to describe experiments in which cloud-chamber photographs of the beta-decay of Li^8 and the subsequent alpha-particle breakup of Be^8 have been obtained.** In a few cases photographs in which all three particles lie in the plane of the cloud chamber have been obtained and some analysis of these photographs has been attempted. In the main, however, emphasis has been placed on those more numerous photographs in which only the two alpha-particles occurred in such locations as to make measurements possible. Attempts were made to determine in general the deviation of the angle between the two alphas from 180° and the difference in their ranges. Scattering and loss of energy of the alpha-particles in the target in which the Li^8 was produced and in the gas of the cloud chamber introduced errors into these determinations. Uncertainty in the energy losses was such as to preclude the possibility of accurate determinations from the observed range differences, while the scattering corrections were found to introduce mean errors of the order of 25 percent in the determination of the angle. The most reliable information is believed to be that determined from the angular deviations measured on tracks in which the range differences were at most that to be expected from Eq. (4). Measurements of the projection of this angle on a vertical plane were not attempted for reasons described below, and so these measurements in principle are concerned with the determination of one component in a Cartesian coordinate system of the recoil momentum of the Be^8. In most cases this component lay in a horizontal plane. In those cases where measurements on the electron as well as on the alpha-particles could be obtained it was possible to specify one component of the resultant momentum of the three observable particles. Any component should of course be zero if momentum is conserved among these particles. However, all other cases could be treated only on a statistical basis by employing Fermi's equation for the distribution in momenta of the electrons.

Attempts to obtain cloud-chamber photographs of both the beta- and alpha-disintegrations of Li^8 were first made in this laboratory in 1937 at about the same time that the alpha-radioactivity was under investigation.[9] In a method devised by H. R. Crane, a small pump was utilized to transfer into a cloud chamber a sample of gas which contained recoils from a lithium target bombarded by deuterons. In a second method a lithium target was mounted on a stopcock in such a way that it could be rapidly rotated into a cloud chamber after bombardment in vacuum. Neither of these attempts was successful, the reason for the most part being that the cloud chamber was usually fogged by small amounts of impurities or by ionized gases introduced into it during the operations. No experiments on this problem were carried out during the war years and it was not until late in 1945 that a new attack was started. It was believed that the most promising line of attack would be to produce Li^8 directly in the cloud chamber by neutron irradiation, and the reaction first chosen was

$$B^{11} + n^1 \rightarrow Li^8 + He^4, \quad (5)$$

as it has been shown[17] that Li^8 is produced by fast neutrons in this way. Boron was introduced into the chamber in the form of methyl borate*** and it was found possible to obtain a large

** It has come to our attention that numerous investigators have proposed the study of the conservation of momentum in the decay of Li^8 and we are grateful in particular to Doctor E. R. Gaerttner, Professor H. R. Crane, and Professor Nicholas Feather for correspondence on the subject.

[17] A. M. Lawrance, Proc. Camb. Phil. Soc. **35**, 304 (1939).

*** We are grateful to Professor H. J. Lucas and Mr. C. N. Scully who prepared the methyl borate used in these experiments.

number of tracks in the chamber gas which corresponded to the disintegration[18] of B^{10} by slow neutrons to form Li^7 and He^4. No evidence for the formation of Li^8 was found, however, and it was concluded that the cross section for this reaction must be very small. A second reaction was also tried, namely,

$$Li^7+n^1\rightarrow Li^8+\gamma, \qquad (6)$$

but again no activity could be detected in agreement with the small cross section (10^{-27} cm^2) for this reaction which has been recently measured.[19] It was finally decided to produce the Li^8 by bombardment of Li^7 by deuterons according to the reaction

$$Li^7+H^2\rightarrow Li^8+H^1, \qquad (7)$$

and to attempt again to transfer the Li^8 into the chamber. This was done successfully in the manner described below. Preliminary results[20] of these experiments were first reported at the Stanford meeting of the American Physical Society in July, 1947.

2. EXPERIMENTAL ARRANGEMENT

The Li^8 was produced by bombardment of a LiOH target by 1-Mev deuterons from the electrostatic generator, previously described.[21] After bombardment of the target for about 0.5 second, the target was introduced into the cloud chamber by the automatic mechanism shown in Fig. 1. The target is mounted at the end of a $\frac{5}{16}$" diameter stainless-steel rod which, with an interlocking extension rod, passes through a series of locks connecting the bombardment position and the cloud chamber. Immediately after bombardment of the target, an air cylinder advances the target rod, pushing the target into a socket in the end of the extension rod and passing the assembly successively through a rough vacuum region, a region at cloud-chamber pressure, and into the cloud chamber. Once the target is in the cloud chamber, a second air cylinder retracts the extension rod, exposing the target. A rotation of one and one-quarter turns is provided by a helix in the advancing air cylinder to facilitate passage through the seals and to present the target in the proper orientation in the cloud chamber. When the target is in the center of the chamber, the chamber is expanded and a photograph taken. The sheath is then advanced to cover the target and the assembly is passed back through the locks and opened in the bombarding position. Seals between the locks are provided by Koroseal sleeves lubricated with stopcock grease. The elapsed time for a 10" motion of the target into the cloud chamber is about 1.5 seconds with a somewhat longer interval allowed on the return stroke to permit pumping out in the rough vacuum lock. The entire cycle is repeated every 45 seconds.

The target material was sprayed from a LiOH solution to a just visible thickness (usually in the form of partially coalesced droplets) on a backing of gold leaf (0.176 mg/cm^2 or $\sim 10^{-5}$ cm) or of beryllium foil**** (0.092 mg/cm^2 or $\sim 5\times 10^{-5}$cm)

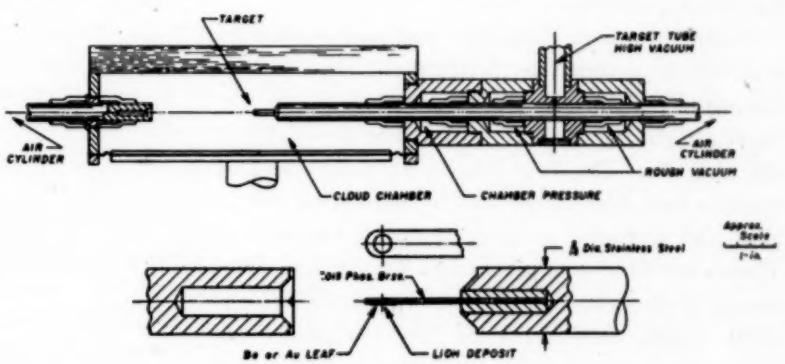

FIG. 1. Apparatus for the introduction of short-lived radioactivity into a cloud chamber.

[18] J. K. Bøggild, D. Kgl. Danske Vidensk. Selskab Mat.-fys. Medd **23**, 4 (1945).
[19] M. J. Poole and E. B. Paul, Nature **158**, 482 (1946).
[20] W. A. Fowler, C. C. Lauritsen, and T. Lauritsen, Phys. Rev. **72**, 738(A) (1947).
[21] T. Lauritsen, C. C. Lauritsen, and W. A. Fowler, Phys. Rev. **59**, 241 (1941).
**** We are indebted to Dr. Hugh Bradner of the Radiation Laboratory of the University of California for the beryllium foils.

which was mounted over a 2.5-mm hole in a light phosphor bronze strip attached to the sliding rod. Quite frequent replacement of targets was necessitated by the deposition of oil films from the lubricant. The stopping power of the foil and target is estimated to be equivalent to approximately 1 mm of standard air or 2 to 3 mm of the gas-vapor mixture used in the chamber.

The cloud chamber was filled with helium gas. In the gold-foil measurements the chamber also contained vapor in equilibrium with a liquid mixture of 65 percent ethyl alcohol and 35 percent water. The total pressure was 0.9 atmospheres in the expanded position so that the calculated stopping power[22] for 2-Mev alpha-particles was 0.267. In the beryllium-foil measurements the vapor was in equilibrium with a liquid mixture of equal parts of ethyl and methyl alcohol. The total pressure was 1.5 atmospheres so that the stopping power was 0.447. The variation of stopping power with energy was taken into account.[22] The stopping-power calculations were checked satisfactorily by measuring on the photographs the range of alpha-particles from a polonium source located at one side of the chamber. An aluminum foil of 1.8-cm air equivalence reduced the lengths of the tracks from the polonium so that they terminated in the chamber. The ranges were measured to the nearest half-millimeter and were thus known to approximately 0.2 mm in standard range. Errors in energy measurement from this source were less than 2 percent.

Turbulence near the target and loss of pressure was largely avoided by holding the final lock at the same pressure as the chamber, allowing the cavity in the sheath rod to fill before passing into the chamber. The best tracks were obtained by using a fast expansion and by providing ample time (45 seconds) to clear between expansions. The sweep field was intensified by two fine wires strung across the top glass. A magnetic field of 2300 gauss was used in the beryllium-foil measurements and fields of 1700 and 2300 gauss were used at different times in the gold-foil measurements.

[22] M. S. Livingston and H. A. Bethe, Rev. Mod. Phys. 9, 271 (1937).

3. MEASUREMENTS

Photography was accomplished by two Sept cameras, one located directly above the chamber and one set off at 18° from the vertical. The off-vertical camera was used solely in the preliminary observations for determining stereoscopically the orientation of the various tracks in space. In reprojection through the original negatives, with the same cameras and mounts, it was possible to locate points in a vertical plane to within one or two millimeters. However, in most cases the angle between the alpha-particles differed so little from 180° that their actual plane could not be determined. Hence photographs of usable tracks were printed on a tilting stage adjusted to lie in a plane containing the mean line of the alpha-particle pair and a horizontal line at right angles to this mean line. Photographs in which electron tracks could be associated with an alpha-particle pair were printed in the plane containing the initial direction of the electron (tangent to the curved path arising from the magnetic field) and the mean line of the alphas. Prints were made in this way only of the negative obtained by the camera mounted directly above the chamber.

The angle between the alpha-pairs was measured on the prints by means of a vernier protractor and it is believed that the limit of error was $\pm 0.5°$. For the most part the tracks were not visible within 7.5 mm (3-mm standard range) of the target support. In the angle measurements the portions of the tracks nearest the support were bisected by fine lines drawn on the prints and the angle between the extension of these lines measured. In this way the effect of large angle scatterings near the end of the tracks was eliminated.

It will be noted that angle measurements as described here do not yield the actual angle between the two alpha-particles since only the projection of this angle on the print is obtained and the projection on a vertical plane is completely neglected. In the photographic method employed in which one camera was directly above the cloud chamber and the other nearly so, practically no information about the projection on a vertical plane is obtained for small angles. It was felt that more elaborate photographic techniques employed to measure this projection would not

have yielded useful results. The reason for this is the fact that the motion of the gas in the chamber during the expansion is largely vertical, and so some distortion in the vertical plane arises from the presence of the target support. A downward displacement of the end of tracks relative to the portion near the target is to be expected except for tracks of particles entering after completion of the expansion. Measurements were confined to tracks showing little diffusion of droplets in order to minimize this and other distortions, but it was not felt that measurements of the vertical projection could be made in a trustworthy manner.

Approximately 10,000 cloud-chamber photographs were taken during these experiments and photographs of about 500 pairs were printed after preliminary inspection of the projected images. In further selection after the prints were available about 200 pairs were rejected for one or more of the following reasons:

(1) The tracks were diffused, distorted, or exhibited large scatterings.

(2) The tracks passed out of the light beam near the end of their range.

(3) One of the tracks lay within 30° of the axis of the metal rod supporting the target and thus had possibly been subject to distortions arising from the flow of gas around this rod.

(4) The mean line through the pair made an angle greater than 30° with the horizontal.

(5) More than two pairs appeared on the photograph making association of the proper pair members somewhat uncertain. There was little doubt in most cases as to which tracks were to be associated in pairs, but it was felt wise not to employ photographs on which the existence of more than two pairs made association in principle uncertain.

Among the remaining 300 pairs it was found that about 30 percent showed range differences which were too large to be ascribed to the maximum possible recoil of the Be^8, while only about 10 percent showed angles too large to be ascribed to this recoil. The appearance on some photographs of single alpha-particle tracks indicated there were two possible explanations for the large range differences. In the first place, the single tracks indicated that pair members could be stopped in the LiOH target or in the supporting foils. Hence some large energy differences were to be expected where one pair member suffered a considerable energy loss but not enough to be completely stopped. This was felt to be the main explanation of the observed range differences. In the second place, apparent pairing of two tracks, each of which had lost its true pair member, could occur accidently although this was clearly rather improbable. In any case it was not felt that the range differences gave a reliable

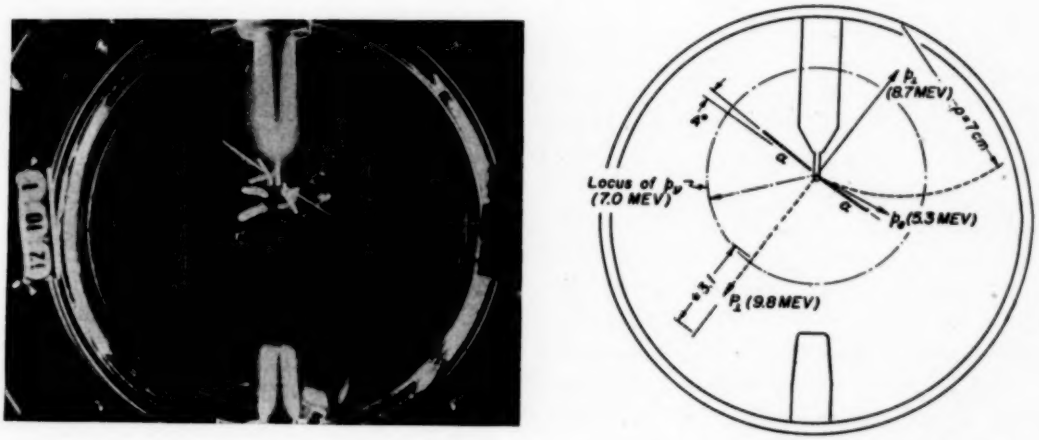

FIG. 2. Film No. 95062. The sharp alpha tracks and the electron track are assumed to arise from the decay of a single Li^8 nucleus produced in the target. A line extending roughly from the upper left hand corner to the lower right can be drawn in such a way that the momentum vectors of all three particles lie to the right of it. The resultant momentum of the three particles is 9.8 ± 3.1 in Mev units where the the uncertainty arises from the possibility of scattering of the alpha-particles. A neutrino with the remaining available energy of 7.0 Mev (16.0 Mev minus the alpha and electron energies) could have this momentum within the probable error. The magnetic field was directed upward. The electron and neutrino momenta are designated by p_e and p_ν, respectively. The momentum of the alpha-particles normal to their mean line of break-up in the plane of the print is $p_\perp$. The resultant momentum of the alpha-particles and the electron is $P_\perp$ (shown in opposite direction in the figure).

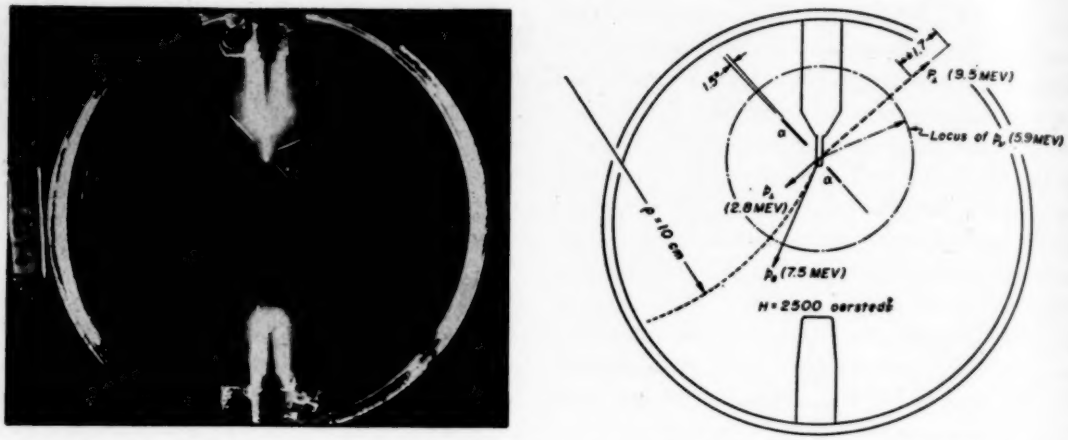

FIG. 3. Film No. 97952. This photograph is illustrative of the difficulty arising in cases where more than one alpha-pair occurred on the same film. In this instance the members of one pair pass out of the illuminated portion of the chamber and thus cannot be used for quantitative measurements. The assumption that the electron is associated with the other pair leads to a resultant momentum of the observable particles greater than that which can be had by a neutrino with the remaining energy. The magnetic field was directed downward.

measurement of the recoil, and it did not seem that the measurement of angles between tracks showing large differences in range was acceptable. For this reason the final analysis of results was confined to the angular measurements on those pairs which did not differ in range by an amount more than that to be expected from the maximum possible recoil of the Be^8. This criterion resulted in the final acceptance of 130 pairs in the photographs obtained using the beryllium foils and 87 pairs on photographs obtained using gold foils.

In 28 cases it was found possible to associate measurable electron tracks with the alpha-particle pairs. This number is considered reasonable in view of the small probability of an electron track lying close enough to the horizontal plane to remain in the illuminated portion of the chamber for a distance comparable to its radius of curvature. On these photographs the orientation of the tangent to the electron track with one member of the alpha-pair was measured. The radii of curvature of the electron tracks were measured in projection on a horizontal plane (normal to the magnetic field). The momentum of the electron is proportional to the product of this radius with the known value of the field and hence it and the energy can be simply computed.

4. ANALYSIS OF THE MEASUREMENTS

(a) Alpha-Particle Pairs with Electrons

Reproductions of photographs showing electrons and pairs of alpha-particles are shown in Figs. 2–4. It will be recalled that these photographs were printed in a plane containing the initial direction of the electron and the mean line of the alpha-particles. Photographs were only made in those cases in which this plane did not make an angle of more than 35° with the horizontal plane and in which the plane of the electron track itself did not make an angle of more than 10° with the horizontal. A graphical analysis of each case is shown with each reproduction. In each analysis we have computed the component of the momentum of the electron normal to the mean line of the alpha-particles and lying in the plane of the print. The electron path is not exactly a circle in these prints and so the radii of curvature were measured in separate projections on the horizontal plane. In addition we have computed the recoil momentum of the Be^8 as indicated by the angle between the alpha-particles as measured on the print. This momentum is also the component normal to the mean line of the alpha-particles lying in the plane of the print. It is obtained from the angle and observed range of the alpha-particles by first determining the mean velocity $\bar{v}_\alpha$ of the two alphas, using the range-velocity relation for the gas-vapor mixture as calibrated with alphas from the polonium source. In part (b) of this section it is shown that the momentum is given by

$$p_\perp = M_\alpha \theta \bar{v}_\alpha, \tag{8}$$

where θ is the deviation from 180° of the angle

between the two alpha-particles. By adding this algebraically to the corresponding component of the momentum of the electron, $p_\perp(e)$, we obtain $P_\perp$, the resultant momentum of the three observable particles normal to the mean line of the alpha-particles and lying in the plane of the alphas and electron. We have compared this with the possible total momentum of a neutrino of zero rest mass which has an energy given by 16 Mev minus the observed energy of the two alpha-particles and the electron. This total momentum of the neutrino should not be less than any one component of the resultant momentum of the observed particles. We have indicated the probable error of this resultant momentum because it is the least accurately determined quantity due primarily to the large probabilities of scattering of the alpha-particles (see final section). Twenty-eight cases in all have been analyzed and are tabulated in Table I. The association of electron tracks with alpha-particles is in some cases doubtful because of the appearance of other alpha-particles on the same picture. In addition the selection criteria in these cases were considerably relaxed compared to those used in the statistical study of alpha-particle pairs in Section (b) below. In Fig. 2, for example, these are many diffuse alpha-particle tracks which apparently entered the cloud chamber some time before the photograph was taken. It is argued that electrons associated with these tracks would also be diffuse and thus not

TABLE I. Analysis of photographs showing electrons and alpha-particle pairs. Components of momentum normal to Be^8 breakup.

Film number	E_α Mev	θ degrees	E_e Mev	$p_\perp$ Mev	$p_\perp(e)$ Mev	$P_\perp$ Mev	$E_p=p_p$ Mev
				Beryllium foil			
97338	5.0	0.5	5.1	−1.2	2.8	1.6±1.3	5.9
97688	3.5	0.0	5.2	0.0	0.0	0.0±1.6	7.3
97952	3.1	1.5	7.0	2.8	6.7	9.5±1.7	5.9
97959	4.1	1.5	5.5	3.2	6.0	9.2±1.5	6.4
97995	2.3	2.9	7.1	4.7	7.6	12.3±2.0	6.6
98001	4.8	1.7	4.8	−3.9	4.1	0.2±1.4	6.4
98002	4.2	2.0	6.3	4.4	0.5	4.9±1.5	5.5
98041	3.2	2.6	8.2	4.9	0.0	4.9±1.7	4.6
98092	6.1	6.0	0.8	15.8	−1.2	14.6±1.2	9.1
98145	3.5	2.7	6.3	5.4	−1.5	3.9±1.6	6.2
98244	4.5	5.0	6.3	11.3	−5.9	5.4±1.5	5.2
98312	3.1	1.1	7.8	2.0	8.1	10.1±1.7	5.1
98490	5.3	2.0	7.1	4.9	1.8	6.7±1.3	3.6
98588	6.6	1.3	3.7	3.6	−2.9	0.7±1.2	5.7
98623	5.9	2.6	5.9	6.9	−6.4	0.5±1.2	4.2
98634	2.8	2.9	5.6	−5.2	6.0	0.8±1.8	7.6
				Gold foil			
91551	2.8	0.9	6.3	1.7	−1.1	0.6±3.8	6.9
91603	4.5	2.8	9.2	6.3	−0.3	6.0±3.0	2.3
91644	5.1	3.3	4.1	8.1	−2.6	5.5±2.8	6.8
91811	2.7	7.1	8.6	12.4	−6.4	6.0±3.9	4.7
94734	1.9	1.3	7.1	−2.0	7.6	5.6±4.6	7.0
94899	5.2	1.5	3.7	−3.7	4.2	0.5±2.8	7.1
95046	4.3	2.0	3.3	4.4	−2.6	1.8±3.1	8.4
95060	2.7	6.3	5.9	11.1	−5.4	5.7±3.9	7.4
95062	4.2	4.0	4.8	8.7	1.1	9.8±3.1	7.0
95063	1.9	1.6	3.7	2.1	3.7	5.8±4.6	10.4
95282	1.5	8.5	3.7	11.6	4.0	15.6±5.2	10.8
95478	4.6	2.0	6.3	4.6	5.0	9.6±3.1	5.1

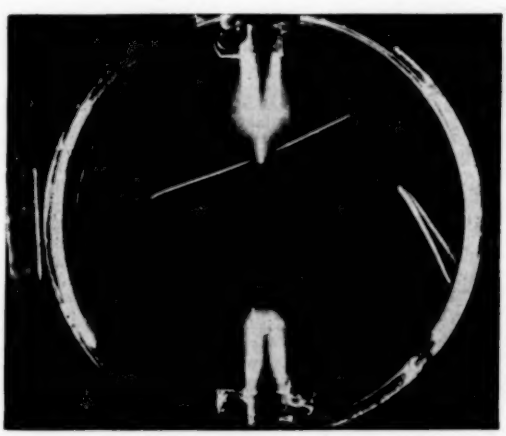

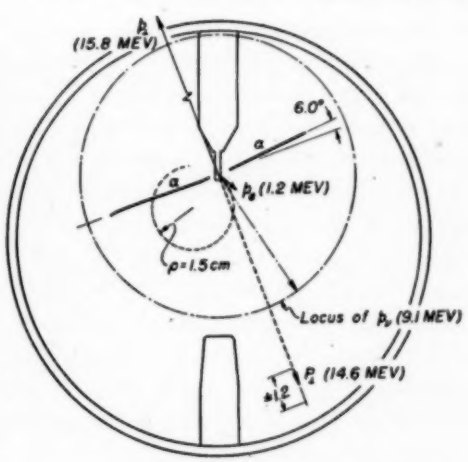

FIG. 4. Film No. 98092. In this photograph the angle between the two alpha-particles deviates by 6° from 180°. This cannot be caused by recoil from the low energy electron also appearing. On the other hand, the expected scattering is only about ½°. Recoil from a neutrino with the available energy will account for an angle of about 4° and the remainder can be attributed to a scattering several times that to be expected on the average. The difference in range of the two alphas indicates that the right-hand particle has suffered a large energy loss, probably in an unusually thick part of the target. The magnetic field was directed downward.

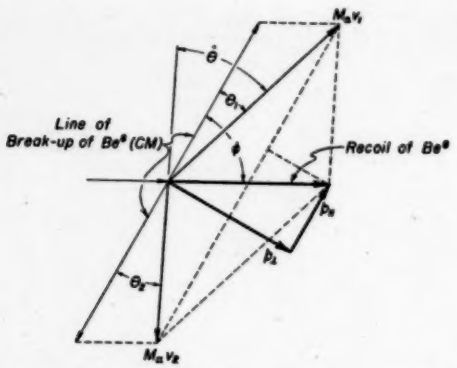

FIG. 5. Analysis of the resultant momentum of the two alpha-particles. The angle $\theta=\theta_1+\theta_2$ is in general much smaller than the angle φ. *CM* indicates the center of mass system.

in general visible and that the electron is most probably the one associated with the sharp pair. At one time in the experiments, shutters were mounted on either side of the target position in the chamber and were opened by the piston motion only at the end of the expansion. These were found to introduce considerable turbulence and to scatter considerable light into the camera and so were eventually discarded. In Fig. 3 the situation is even worse since a sharp pair which passed almost vertically through the chamber, each member leaving the illuminated region, occurs on the photograph in addition to the pair used in the measurements. The analysis was made in this case solely to determine if the neutrino hypothesis was consistent with the assumption that the electron was associated with the pair used in the measurements. In Fig. 4 these difficulties do not occur. In this photograph the angle between the alpha-particles is more than twelve times that to be expected from scattering or from recoil from the observed low energy electron.

An examination of the data on these 28 pictures shows that in the majority of cases the observed resultant momentum of alpha-particles and electron is much larger than can be accounted for by scattering alone. In many of these cases the momentum can be understood on the neutrino hypothesis although in some the resultant momentum is larger than can be explained on the assumption that the electron and neutrino have no preferred angle of emission. As a result, although there is observed an unbalanced momentum such as would be given by a neutrino, the data are not sufficient for a meaningful numerical comparison with any definite assumption concerning the angular distribution of electron and neutrino.

(b) Alpha-particle Pairs without Electrons

In cases where it is not possible to associate electrons with the alpha-particle pairs it is still useful to make an analysis of the resultant momentum of the two alpha-particles in laboratory coordinates. This resultant momentum can be resolved into components parallel and perpendicular to the line of breakup of the alphas in a system moving with their center of mass. From Fig. 5 we have

$$p_\perp = M_\alpha v_1 \sin\theta_1 + M_\alpha v_2 \sin\theta_2, \tag{9}$$

$$p_{\parallel} = M_\alpha v_1 \cos\theta_1 - M_\alpha v_2 \cos\theta_2, \tag{10}$$

where θ_1 and θ_2 are the angles between the velocity of the alpha-particles in the center of mass coordinates and their velocity in laboratory coordinates. The velocities in laboratory coordinates are v_1 and v_2. The velocities of alpha-disintegration are in all observable cases large compared to the recoil velocities. Hence v_1 and v_2 are approximately equal as are θ_1 and θ_2. Then, in terms of the average velocity $\bar{v}_\alpha=\frac{1}{2}(v_1+v_2)$ and the velocity difference $\Delta v_\alpha=v_1-v_2$, we have

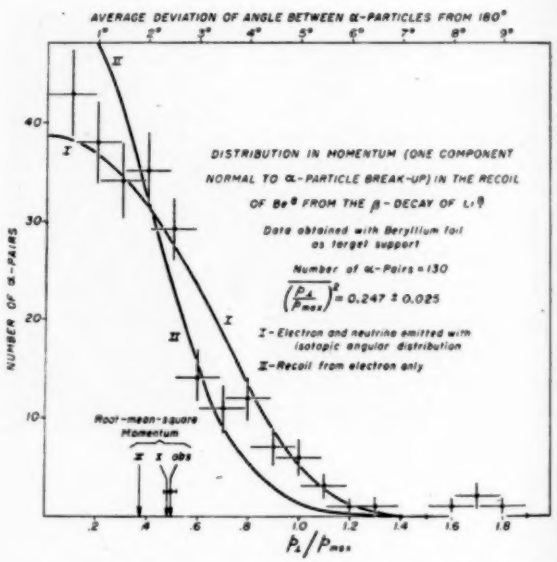
AVERAGE DEVIATION OF ANGLE BETWEEN α-PARTICLES FROM 180°
DISTRIBUTION IN MOMENTUM (ONE COMPONENT NORMAL TO α-PARTICLE BREAK-UP) IN THE RECOIL OF Be⁸ FROM THE β-DECAY OF Li⁸
Data obtained with Beryllium foil as target support
Number of α-Pairs = 130
Σ-Electron and neutrino emitted with isotopic angular distribution
Σ-Recoil from electron only
Root-mean-square Momentum
NUMBER OF α-PAIRS
p⊥/pmax

FIG. 6. Distribution in $p_\perp/p_{\max}$ for 130 alpha-pairs obtained with a beryllium foil for target support.

Eq. (8) which was employed above:

$$p_\perp = M_\alpha \bar{v}_\alpha \theta,$$

where

$$\theta = \theta_1 + \theta_2. \tag{11}$$

We also have

$$p_{11} = M_\alpha \Delta v_\alpha. \tag{12}$$

In terms of the energy of the two alpha-particles $E_\alpha = E_1 + E_2$ and the energy difference $\Delta E_\alpha = E_1 - E_2$ we have

$$p_\perp = \theta(M_\alpha E_\alpha)^{\frac{1}{2}} = 1.07 E_\alpha^{\frac{1}{2}} \theta \tag{13}$$

and

$$p_{11} = \Delta E_\alpha (M_\alpha / E_\alpha)^{\frac{1}{2}} = 61 E_\alpha^{-\frac{1}{2}} \Delta E_\alpha, \tag{14}$$

where in the numerical expressions, energies and momenta† are in Mev and angles in degrees. The maximum resultant momentum of the two alpha-particles can be computed from the maximum energy available in the electron-neutrino decay. This will be the total energy Q available in the disintegration of Li^8 minus the disintegration energy of the alpha-particles. We have

$$p_{\max} = (Q - E_\alpha)/c, \tag{15}$$

where Q is 16.0 Mev. We normalize the two components of momentum to this value so that

$$\frac{p_\perp}{p_{\max}} = \frac{M_\alpha c^2}{Q - E_\alpha} \frac{\bar{v}_\alpha}{c} \theta = \frac{(M_\alpha c^2 E_\alpha)^{\frac{1}{2}}}{Q - E_\alpha} \theta$$

$$= 1.07 \frac{E_\alpha^{\frac{1}{2}}}{16 - E_\alpha} \theta, \tag{16}$$

and

$$\frac{p_{11}}{p_{\max}} = \frac{M_\alpha c^2}{Q - E_\alpha} \frac{\Delta v_\alpha}{c} = \frac{(M_\alpha c^2 / E_0)^{\frac{1}{2}}}{Q - E_\alpha} \Delta E_\alpha$$

$$= 61 \frac{\Delta E_\alpha}{E_\alpha^{\frac{1}{2}}(16 - E_\alpha)}. \tag{17}$$

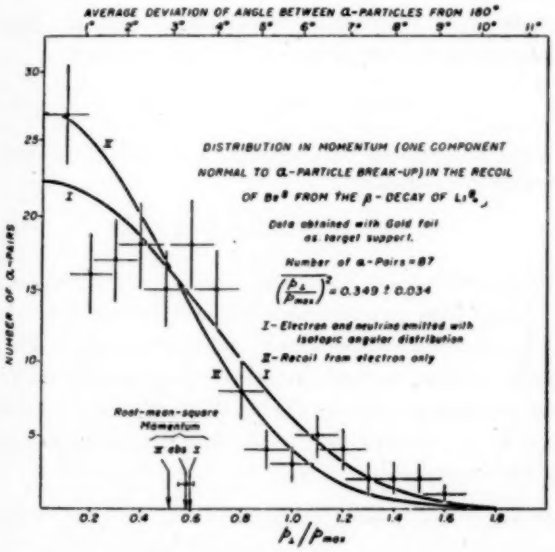
AVERAGE DEVIATION OF ANGLE BETWEEN α-PARTICLES FROM 180°
DISTRIBUTION IN MOMENTUM (ONE COMPONENT NORMAL TO α-PARTICLE BREAK-UP) IN THE RECOIL OF Be^8 FROM THE β-DECAY OF Li^8
Data obtained with Gold foil as target support.
Number of α-Pairs = 87
$\left(\frac{p_\perp}{p_{max}}\right)^2$ = 0.349 ± 0.034
I - Electron and neutrino emitted with isotopic angular distribution
II - Recoil from electron only
Root-mean-square Momentum
II obs I
NUMBER OF α-PAIRS
$p_\perp/p_{max}$

FIG. 7. Distribution in $p_\perp/p_{\max}$ for 87 alpha-pairs obtained with a gold foil for target support.

† The convenient energy unit, the Mev, can be used for momenta if the momenta are always considered to be multiplied by the velocity of light.

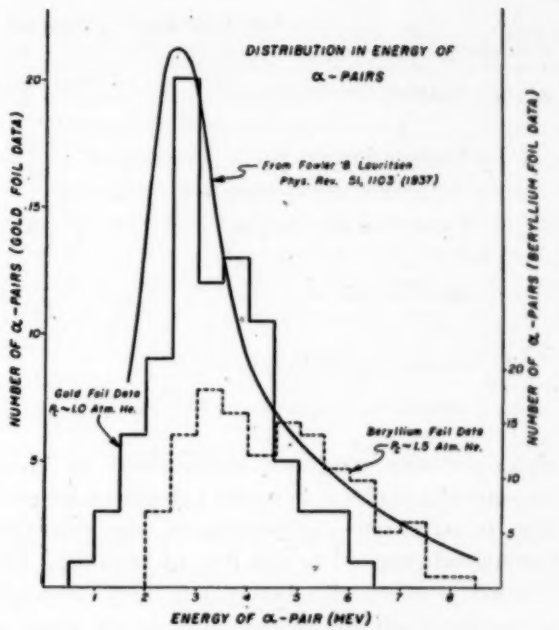
DISTRIBUTION IN ENERGY OF α-PAIRS
From Fowler & Lauritsen Phys. Rev. 51, 1103 (1937)
Gold Foil Data
Beryllium Foil Data
NUMBER OF α-PAIRS (GOLD FOIL DATA)
NUMBER OF α-PAIRS (BERYLLIUM FOIL DATA)
ENERGY OF α-PAIR (MEV)

FIG. 8. Distribution in energy of the alpha-pairs employed in these measurements with the distribution in energy of all pairs from Li^8 shown for comparison.

These expressions were employed in analyzing about 300 alpha-particle pairs. As discussed above, all those cases for which $p_{11}/p_{\max} > 1$ were excluded from the final analysis. These final results are shown in Figs. 6 and 7 in which are plotted the number of alpha-particle pairs having specified values of $p_\perp/p_{\max}$. The distribution in energy of the pairs included in these measurements is shown in Fig. 8. The distribution in energy of all the alpha-pairs from Li^8 as originally measured by Fowler and Lauritsen[9] is also shown for comparison. Since the projection on a vertical plane of the angle between the two

TABLE II. Calculated momentum distribution and mean-square momenta.

Neutrino distribution	Distribution of ⊥ component of recoil momentum $p_\perp$	$\langle p_\perp^2\rangle_{Av}$	$\langle p^2\rangle_{Av}$
Neutrino anti-parallel to electron	$\frac{15}{8}\left[\ln\frac{1}{p_\perp}-\frac{1}{4}(1-p_\perp^2)(3-p_\perp^2)\right]$	$\frac{1}{21}$	$\frac{1}{7}$
Recoil from electron only	$\frac{5}{2}(1-p_\perp)^2(1+3p_\perp)$	$\frac{2}{21}$	$\frac{2}{7}$
$\Theta(\theta)=1+\alpha\cos\theta$	$\frac{5}{16}(1-p_\perp^2)\left[(5-\alpha)-(1-5\alpha)p_\perp^2\right]$	$\frac{4+\alpha}{21}$	$\frac{4+\alpha}{7}$
Neutrino parallel to electron	1	$\frac{7}{21}$	1

alpha-particles was not determined in these measurements the $p_\perp$ actually calculated for each pair is only one component of the resultant momentum normal to the line of breakup. The relation between this component and the angle as measured on the photographs is the same as given in Eq. (16) above.

5. CALCULATIONS

(a) Recoil Momentum Distributions

The distribution of recoil momentum of the excited Be^8 nucleus will depend on the momentum (or energy) distribution of the electrons and if the existence of the Pauli neutrino is supposed, on the relative angular distribution of electron and neutrino. The over-all electron energy distribution was measured directly[15] and was found to be consistent with the supposition that, associated with each observed alpha-particle pair there is an electron-neutrino pair with total energy equal to 16 Mev$-E_\alpha$ and distributed in energy according to the simple Fermi distribution. The existence of a copious gamma-ray following the beta-decay is ruled out by the above energy considerations. Furthermore, delayed gamma-rays have been looked for[12,15] without success. Consequently, in what follows we shall suppose that all the energy not appearing in the alpha-pair is distributed between electron and neutrino with a Fermi distribution. Since this energy is usually large compared to mc^2, we shall equate E for the electron to pc. We also assume that all beta-transitions have the same characteristics, i.e., they correspond to transitions to the same type of excited state of Be^8. This is made plausible by the apparent absence of irregularities in the final alpha-spectrum but is particularly justified in this experiment where almost all the alpha-pairs have an energy corresponding to the disintegration of a single broad excited state of Be^8 at about 3 Mev. With the above assumptions we are able to normalize the recoil momentum of Be^8 in each disintegration to the maximum recoil available from parallel electron and neutrino. Writing all momenta in these units we have the momentum of Be^8 given by

$$p^2=p_e^2+p_\nu^2+2p_ep_\nu\cos\theta, \tag{18}$$

where θ is the angle between $\mathbf{p}_e$ and $\mathbf{p}_\nu$. The probability distribution of p_e, p_ν is given by

$$W(p_e)dp_e=30p_e^2(1-p_e)^2dp_e. \tag{19}$$

For the angular distribution of electron and neutrino we take

$$\Theta(\theta)d\theta=\tfrac{1}{2}(1+\alpha\cos\theta)\sin\theta d\theta, \tag{20}$$

where, with $p_ec\approx E_e$, α may take on values from -1 to 1 and in particular[23] takes the values -1, 1, $\frac{1}{3}$, $-\frac{1}{3}$, -1, respectively, for the simple scalar, polar vector, tensor, axial vector, and pseudoscalar allowed interactions. With the above and $p_\nu=1-p_e$, we obtain the probability distribution of Be^8 momentum recoil

$$P(p)dp=(5/4)p^2[3(1-\alpha)-(1-5\alpha)p^2]dp. \tag{21}$$

In addition we consider two limiting angular distributions: p_ν parallel to p_e or $\theta=0$.

$$P(p)dp=\delta(1-p)dp \tag{22}$$

[23] D. R. Hamilton, Phys. Rev. 71, 456 (1947).

where δ is the delta-function of the argument $(1-p)$ and p_ν antiparallel to p_e or $\theta=180°$.

$$P(p)dp=(15/8)(1-p^2)^2dp. \quad (23)$$

Finally we consider the case $p_\nu=0$ (recoil due to electron only) but retain (19) as an observed fact

$$P(p)dp=30p^2(1-p)^2dp. \quad (24)$$

As already indicated, the observations of the Be^8 momentum are restricted to a single component normal to the direction of its disintegration into two alpha-particles. We must then know the disintegration probability of the Be^8 as a function of the angle between $\mathbf{p}$ and the direction of the alphas. This can only be known by knowing the initial state of Li^8, the beta-decay coupling, and the final state of Be^8, none of which is known for sure. According to the most probable description of these transitions, however, the disintegration probability of Be^8 will be independent of the relative directions of alpha-particles and recoil. We have used this "symmetry of breakup of Be^8" assumption in calculating the distribution of component momentum.

According to Wheeler,[24] the excited state of Be^8 involved here is not the $J=0$ state found in $\alpha-\alpha$ scattering at 3 Mev, which would, of course, lead to symmetry in the breakup of the Be^8. On the contrary, it is probably described as $^1D_2$ and the ground state of Li^8 as $^3P_2$.[25] As Konopinski[26] points out, the beta-transition to the $^1D_2$ state is then of the allowed type but unfavored since it proceeds by means of the non-conservation of orbital angular momentum. The symmetry of breakup of Be^8 then follows from the fact that the electron and neutrino are emitted in an S state since the first term in the expansion of $\exp[(i/\hbar)(\mathbf{p}_e+\mathbf{p}_\nu)\cdot\mathbf{r}]$ is responsible for the transition. The transition to the ground state of Be^8 is doubly forbidden by the parity-angular momentum-selection rules.

It is to be noted that the formation of Li^8 by deuteron bombardment on Li^7 presumably involves a change in parity, and since it is a threshold reaction, this probably means that it is only the p-wave deuterons that are effective, the low energy emitted protons being s wave. This should show up in any careful analysis of the excitation function for the reaction which has not, however, been attempted here.

The assumption of spherical breakup thus appears more probable than any other definite assumption we could make. The probability distributions of a single component of the recoil momentum of Be^8 is then easily made giving the distributions and average squares of $p_\perp$, the component of p in Table II and Fig. 9. It is to be noted that $\langle p_\perp^2\rangle_{Av}$ is just $\frac{1}{3}\langle p^2\rangle_{Av}$ for obvious reasons.

(b) Corrections

In order to evaluate the correction to $\langle p_\perp^2\rangle_{Av}$ arising from scattering, we need only $\langle\theta^2\rangle_{Av}$, the mean-square projected angle of Rutherford scattering. This is given, for small angles, by

$$\langle\theta^2\rangle_{Av}=\left(\frac{2Ze^2}{E}\right)^2\pi Nt\ln\frac{\theta_{\max}}{\theta_{\min}}, \quad (25)$$

where E is the energy of the alpha-particle and Z, N the atomic number and number of particles/cc, respectively, of the scatterer. The

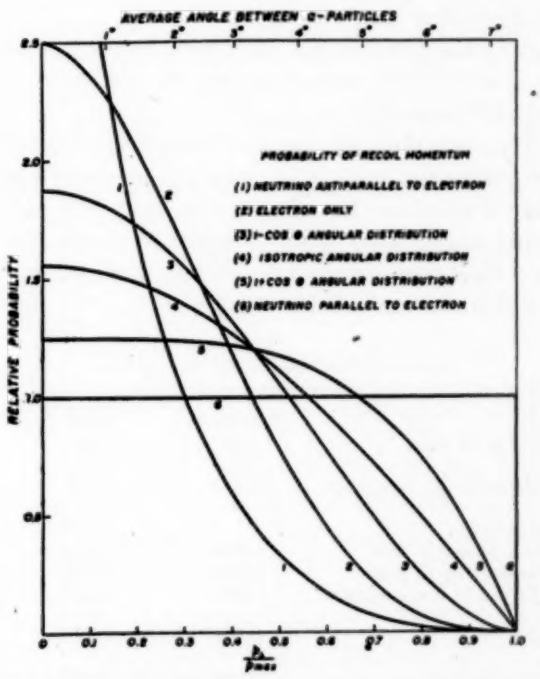
AVERAGE ANGLE BETWEEN α-PARTICLES
PROBABILITY OF RECOIL MOMENTUM
(1) NEUTRINO ANTIPARALLEL TO ELECTRON
(2) ELECTRON ONLY
(3) 1−COS θ ANGULAR DISTRIBUTION
(4) ISOTROPIC ANGULAR DISTRIBUTION
(5) 1+COS θ ANGULAR DISTRIBUTION
(6) NEUTRINO PARALLEL TO ELECTRON
RELATIVE PROBABILITY

FIG. 9. Theoretical distributions of one component of the recoil momentum of Be^8 for various angular orientations of electron and neutrino.

[24] J. A. Wheeler, Phys. Rev. **59**, 27 (1941).
[25] E. Feenberg and E. Wigner, Phys. Rev. **51**, 95 (1937).
[26] E. J. Konopinski, Rev. Mod. Phys. **15**, 209 (1943).

thickness, t, was taken to be the average foil path traversed by the alpha-particles which was 0.215 mg/cm² for the gold foil and 0.102 mg/cm² for the beryllium foil. θ_{max} is the maximum observed angle between two alpha-particles associated as a pair. This was 10° to 15° in this experiment. θ_{min} is a minimum angle of scattering determined by the electronic screening of the nuclear field. For 1-Mev alpha-particles in beryllium this may be taken to be $\theta_{min}=\lambda\!\!\!^{-}/a$ whereas in gold, the Born approximation is invalid and

$$\theta_{min}\approx Ze^2/Ea \qquad (26)$$

from the classical scattering calculation. a is the atomic radius given approximately by $a_0Z^{-\frac{1}{3}}$. The scattering angle $\langle\theta^2\rangle_{Av}$ is related to the equivalent $\Delta\langle p_\perp^2\rangle_{Av}$ and is averaged over the energy distribution of the observed alpha-pairs to give the correction for scattering in the foil. The result is uncertain by about 20 percent for the gold foil because of approximations in the logarithm.

The correction for scattering in the cloud-chamber gas is handled similarly. In this case t was taken to be 1.3 cm—a measure of distance near the foil where the track was unobservable plus one-half the track length used to determine its direction.

A suitably averaged correction in $\langle p_\perp^2\rangle_{Av}$ was also introduced corresponding to an error of angular measurement of 0.5°.

The correction of the momentum distribution for scattering, etc., is in principle more difficult since it requires the use of a distribution in scattering angle. This could roughly be represented by a Gaussian distribution for small angles, with a width determined by $\langle\theta^2\rangle_{Av}$, with θ_{max} the limit of multiple scattering, and a single scattering tail. This calculation was performed however with a simple Gaussian distribution function of suitable width, so that the tail of the corrected distribution for $p_\perp>1$ may be somewhat underestimated.

TABLE III. Mean-square momenta.

Foil Number of pairs	Beryllium 130	Gold 87
Observed $\langle(p_\perp/p_{max})^2\rangle_{Av}$	0.247	0.349
Corrections		
Scattering in foil	0.006	0.110
Scattering in gas	0.032	0.020
Errors in measurement	0.012	0.012
Total	0.050	0.142
Corrected $\langle(p_\perp/p_{max})^2\rangle_{Av}$	0.197±0.025	0.207±0.034
Weighted mean	0.20±0.02	

It had been intended to obtain the component of momentum parallel to the alpha-particle direction from the difference in range of the two members of a pair. From the equality of the two components of $p_\perp$ in the average, this would give $\langle p^2\rangle_{Av}=\langle p_{11}^2\rangle_{Av}+2\langle p_\perp^2\rangle_{Av}$ independent of the assumption of spherical breakup of Be^8. The difference between $\langle p_{11}^2\rangle_{Av}$ and $\langle p_\perp^2\rangle_{Av}$ would measure any asymmetry in this break up. The difference in range of the alphas would arise from penetration of the foil by one of them (known ≈2 mm of the chamber mixture), from straggling (~0.4 mm of chamber mixture), and from the actual difference in energy of the alphas. There resulted $\langle p_{11}^2\rangle_{Av}\approx 0.8$ after subtracting the straggling correction of ~1 percent. This led to $\langle p^2\rangle_{Av}>1$ which is impossible. The cause of this result is uncertain but it might be due to accumulation of oil on the target or to thick spots of LiOH on the target. If it is explained in this manner it should be noted that the scattering corrections should be increased. However, if due to an element of atomic number about equal to that of carbon, the thickness represented by the observed range difference of about (4 mm) would only add 0.03 to the scattering correction. These data were actually used however to exclude certain tracks from measurement as discussed before. The resulting effect on $\langle p_\perp^2\rangle_{Av}$ was comparable to the estimate above. Furthermore if the observed p_{11} were real, the large p_{11} should mean small $p_\perp$ and the exclusion should increase $\langle p_\perp^2\rangle_{Av}$.

6. CONCLUSIONS

The theoretical distributions to be expected on the basis of various angular correlations of the electron and neutrino in the decay of the Li^8 are calculated in the preceding section. The distortion of the distributions due to scattering and errors in measurement is also calculated there. In Figs. 6 and 7 we include the results of these calculations giving corrections for two cases: I, recoil from the electron and neutrino emitted with no preferred orientation and II, recoil from

the electron only. It will be noted that the experimental points fit curve I slightly better than curve II but that the difference is by no means conclusive.

The best comparison with theory is made by comparing the observed mean-square values of $p_\perp/p_{max}$ with the theoretical values. In Table III are given the experimental values of $\langle(p_\perp/p_{max})^2\rangle_{Av}$ and the corrections as calculated in the previous section. The corrected experimental values are given with the probable errors listed being purely statistical in origin. It will be noted that the final result, $\langle(p_\perp/p_{max})^2\rangle_{Av}=0.20\pm0.02$, is slightly more than twice that to be expected from the recoil from the electron alone ($2/21=.095$). The theoretical considerations assume no correlation in the angle between the line of breakup of the Be^8 and the line of its recoil. Even if the Be^8 is assumed, as is unlikely, to breakup always in a direction normal to its recoil, the theoretical value is only three-quarters of the observed value. The result is not very selective with respect to the type of interaction in the Fermi theory, favoring, perhaps, the Tensor interaction, for which $\alpha=\frac{1}{3}$.

It will be noted that the corrections reduce the observed values by 20 percent and 40 percent in the beryllium-foil data and gold-foil data, respectively. Furthermore, the result of the exclusion of all pairs having p_{11}/p_{max} greater than unity reduced the observed values of $\langle(p_\perp/p_{max})^2\rangle_{Av}$ by about 25 percent. These corrections are of course much larger than the statistical probable errors which have been quoted, and certainly make these experiments a much less critical test of the neutrino hypothesis than is to be desired. On the other hand, the final result quoted contains all the corrections which we consider reasonable and we conclude that momentum is not conserved among the observable particles, alphas and electrons. On the other hand, the results seem not to violate the conservation of momentum if the emission of a neutrino is postulated and in particular if the neutrino emission shows no very preferred orientation with that of the electron. The experimental evidence supports this last point but by no means constitutes a conclusive proof of its validity. A more precise experimental determination and a more complete investigation of sources of error will be necessary before questions concerning the angular distribution in the electron-neutrino decay can be answered. The theoretical calculations given in Section 5 show that the recoils expected in the most extreme cases of forward or backward correlations, which are theoretically reasonable, differ only by 25 percent from the recoil expected in the case of no correlation. We have reduced our probable statistical errors to less than one-half of this difference but the scattering and selection corrections are of just this order of magnitude. Further data should be obtained from cloud-chamber photographs in which the Li is produced directly in the chamber gas and the scattering and loss of energy in target foils are avoided.

This work was carried on under contract with the Office of Naval Research.

Rate of Electron Production in the Ionosphere

S. L. SEATON
Little Silver, New Jersey

(Received May 15, 1947)

Methods are developed for determination of the rate of electron production in the ionosphere throughout the 24 hours. Application of the theory to experimental data shows that the rate of electron production varies more or less systematically from zero before sunrise to values around 800 electrons cm^{-3} $sec.^{-1}$ near noon at the equator for an equinoctial interval at sunspot minimum. The results are in general agreement with values determined over restricted time intervals during eclipse of the sun.

THE rate of electron production in the ionosphere has been examined over restricted time intervals by Appleton,[1] Mohler,[2] Gilliland,[3] Berkner and Seaton,[4] and others. It seems worth while, with the extensive ionospheric measurements now available, to attempt an

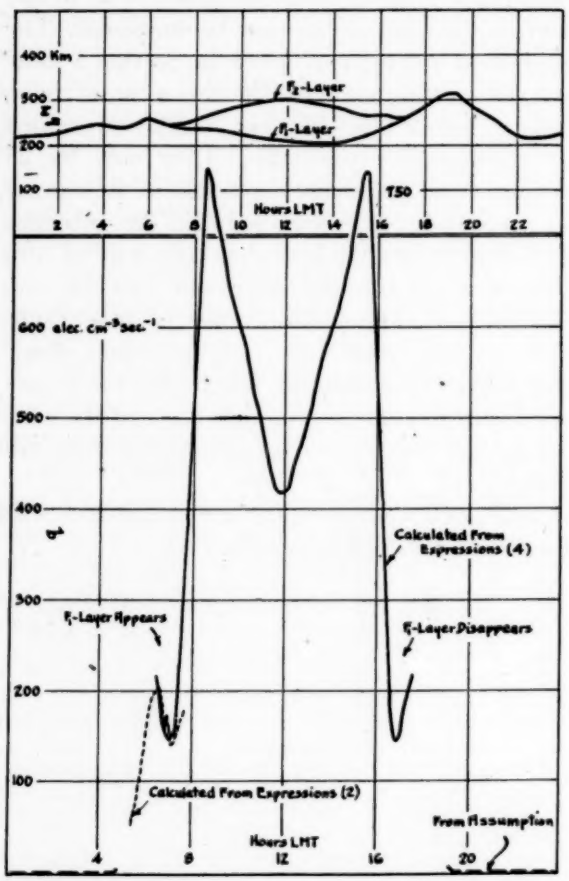

FIG. 1A. Calculated values of q for F_2-layer, and experimental values of height of maximum electron density, Huancayo, Peru.

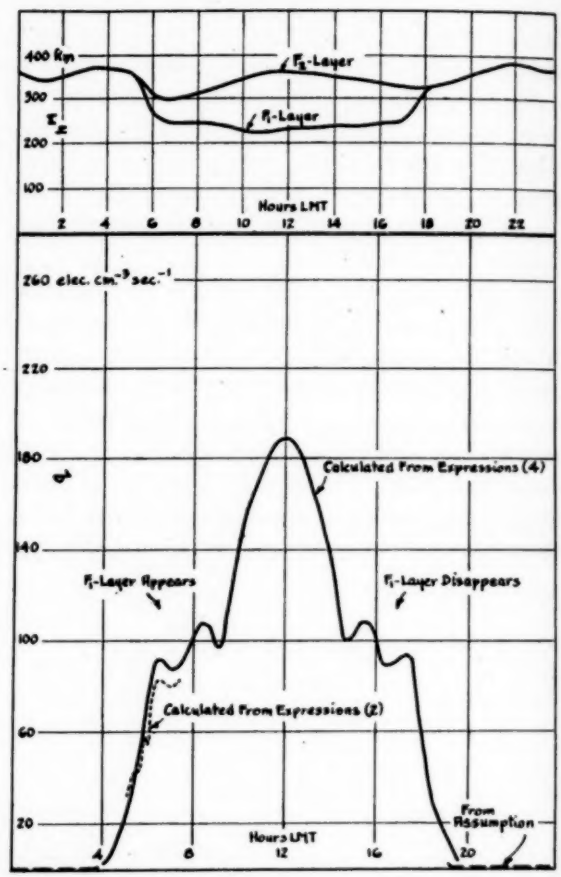

FIG. 1B. Calculated values of q for F_2-layer, and experimental values of height of maximum electron density, Watheroo, W. Australia.

[1] E. V. Appleton, Proc. Phys. Soc. **45**, 673–687 (September 1, 1933) and Proc. Roy. Soc. **A162**, 451 (1937).
[2] F. Mohler, J. Research Nat. Bur. Stand., Research Paper No. RP-1342 **25**, 507–518 (November 1940).
[3] T. K. Gilliland, Nat. Geog. Soc., Solar Eclipse Series No. 2, Washington, D. C. (1942).
[4] L. V. Berkner and S. L. Seaton, Terr. Mag. **45**, 393–418 (December 1940).

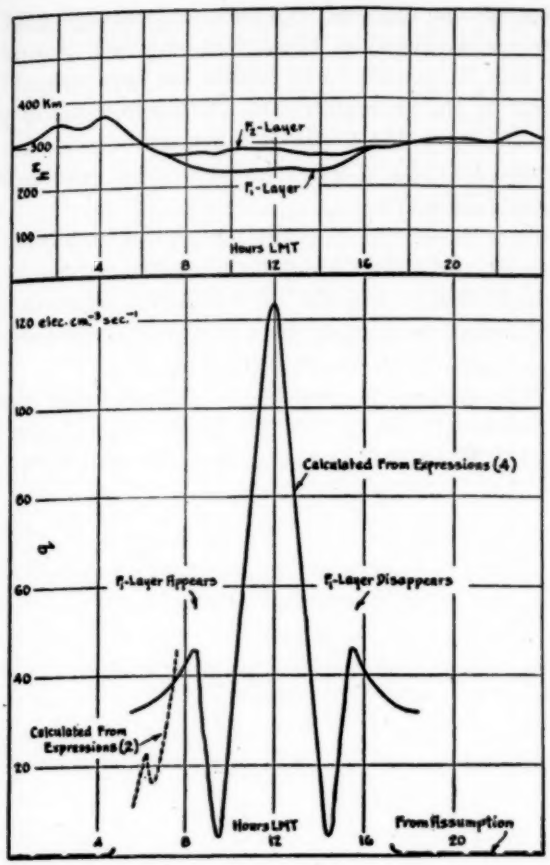

FIG. 1C. Calculated values of q for F_2-layer, and experimental values of height of maximum electron density, College, Alaska.

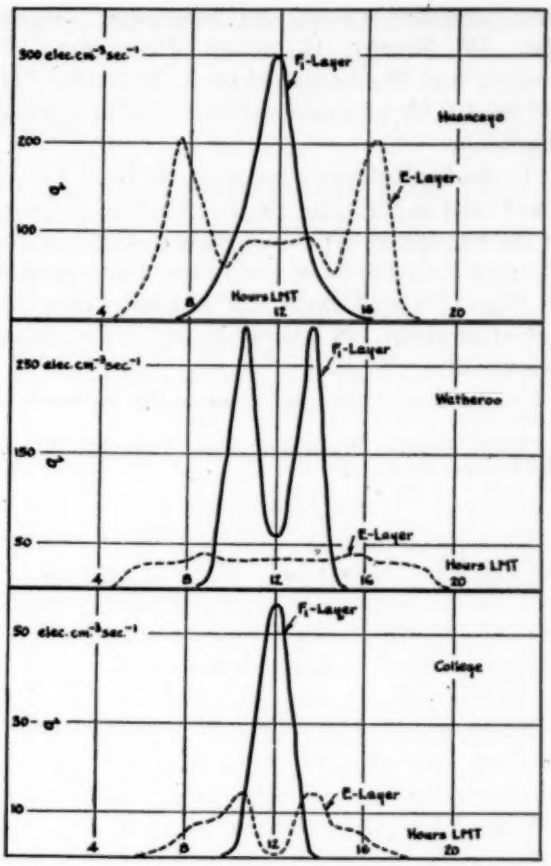

FIG. 2. Calculated values of q for E- and F_1-layers.

evaluation of this important quantity throughout the 24 hours for several typical latitudes.

The following well-known expression will be used as a basis for this evaluation:

$$dN/dt = q - \alpha N^2, \tag{1}$$

where dN/dt is the time rate of change of free electron concentration in the ionosphere; q is the rate of electron production; α is the generalized destruction factor having the characteristic of the recombination coefficient.

At night $q \equiv 0$ and hence, after the postulates of Appleton, if α before sunrise is set equal to α after sunrise, and if values of $(dN/dt)_1$ before sunrise and $(dN/dt)_2$ after sunrise are measured for equal values of N, then:

$$\left.\begin{aligned}(dN/dt)_1 &= -\alpha N^2\\ (dN/dt)_2 &= q_2 - \alpha N^2\end{aligned}\right\} \tag{2}$$

whence:

$$q_2 = (dN/dt)_2 - (dN/dt)_1. \tag{3}$$

The same argument holds after and before sunset.

It is now necessary to set up corresponding expressions to carry evaluation of q forward through the mid-day interval. Invoking Appleton's second postulate, i.e., that for times equally spaced either side of noon q and α are likely to be equal, the following pair of expressions may be written:

$$\left.\begin{aligned}(dN/dt)_3 &= q - \alpha N_3^2\\ (dN/dt)_4 &= q - \alpha N_4^2\end{aligned}\right\}. \tag{4}$$

Solving expressions (4) first for α and then for q, where the subscripts are in order before and after noon respectively, the tools are at hand for evaluation of q throughout the 24 hours. Basic ionospheric data for numerical use were taken

from published information[5] for College, Alaska (lat. 64° North), Huancayo, Peru (lat. 12° South), and Watheroo, Western Australia (lat. 30° South) for an equinoctial interval at sunspot minimum.

Typical calculations are given in Figs. 1A, B, and C and in Fig. 2 for the F_2-, F_1-, and E-layers of the ionosphere. For convenience heights of the F_2- and F_1-layers are given in the upper portion of Fig. 1. The E-layer has a nearly constant height of about 108 kilometers and is not shown graphically.

For the F-layer around 7 hours the methods of expressions (2) and (4) permit overlapping of determinations of q. The agreement, as indicated in Fig. 1, appears to be within the experimental error of the measurements. Determinations of q by the foregoing methods agree quite well with determinations made over restricted intervals from eclipse data.

It is necessary to point out that just around sunrise and sunset q applies to the combined F_2- and F_1-layers. For the interval after separation and before merging of these two layers each layer has a separately determined value of q.

The author is pleased to acknowledge the helpful criticism of Drs. O. Wulf, Fred Mohler, and G. R. Wait in preparation of the manuscript.

[5] CRPL F-Series Ionospheric Data, Nat. Bur. Stand., Washington, D. C.

The Hyperfine Structure and the Stark Effect of the Ammonia Inversion Spectrum

J. M. JAUCH
Department of Physics, The State University of Iowa, Iowa City, Iowa
(Received June 30, 1947)

The expressions for the hyperfine structure separations and the relative intensities in the ammonia inversion spectrum are derived with quantum mechanics under the assumption that the splitting is caused by the interaction of an electric quadrupole moment of the N^{14} nucleus with the electric charge distribution in the rest of the molecule. Furthermore, we consider the displacement of the absorption lines in an electric field E of variable strength. General formulas for the positions of energy levels for weak ($E<E_c$) and strong ($E>E_c$) fields ($E_c\sim500$ volt/cm) are given and the methods outlined for obtaining solutions of the secular equation for intermediate fields ($E\sim E_c$). The intensities and selection rules for longitudinal and transverse transitions are determined and one particular case ($J=K=3$) is worked out in detail.

1. INTRODUCTION

IT is well known that the NH_3 molecule has the form of a pyramid with the three H atoms at the base of a regular triangle and the N atom at the top. The fact that there exist two equilibrium positions of the N-atom on either side of the base, separated by a potential will give rise to a doubling of each energy level of the whole system of rotational and vibrational states.[1] The transitions from one of the pair of energy levels to the other for all the rotational states and the vibrational ground state can be observed directly since they give rise to a strong absorption in the region of 24,000 megacycles.[2]

With improved techniques of radiofrequency absorption measurements it has recently been possible to separate and identify the lines which arise from different rotational states.[3] W. E. Good observed for the first time the existence of a hyperfine structure with a separation of the four satellites from the main line of several megacycles which was interpreted by various authors as due to the electric quadrupole moment of the N^{14} nucleus.[4] In this paper we shall treat the Stark effect of the inversion spectrum of the NH_3 molecule. The hyperfine structure causes the pattern for intermediate values ($E_c\sim300$–1000 volt/cm) to be quite complicated and a general solution of the secular equation does not seem to be feasible although it could in principle be obtained. It is possible, however, to give generally valid expressions for all of the energy levels for very weak fields ($E\ll E_c$) and very strong fields ($E\gg E_c$). For these cases the intensities for both the transverse and longitudinal effects can also be calculated. For intermediate values of the electric field ($E\sim E_c$) one can obtain good approximations for each individual level system by numerical or graphical interpolation.

Although the theory resembles in many respects that of the transition from the weak-field Zeeman effect to the Paschen-Back effect in atomic spectra, there is a characteristic difference for the type of problem considered here. This is due to the fact that a uniform electric field does not interact with the spin of the nucleus (at least not in the approximation considered here). For this reason the spin is never completely decoupled from the orbital angular momentum and thus a splitting of the energy levels with different orientation of the nuclear spin with respect to the orbital angular momentum prevails even for arbitrarily strong fields. This situation holds true for other kinds of radiofrequency absorption spectra as well.

One of the applications of these absorption experiments is the measurement of nuclear spins.[5]

[1] D. M. Dennison and G. E. Uhlenbeck, Phys. Rev. **41**, 313 (1932); D. M. Dennison and J. P. Hardy, Phys. Rev. **39**, 938 (1932); H. Y. Sheng, E. F. Barker, and D. M. Dennison, Phys. Rev. **60**, 786 (1941).

[2] C. E. Cleeton and N. H. Williams, Phys. Rev. **45**, 234 (1934).

[3] W. E. Good, Phys. Rev. **70**, 213 (1946); W. E. Good and D. K. Coles, *ibid.* **71**, 383 (1947); D. K. Coles and W. E. Good, *ibid.* **70**, 979 (1946); C. H. Townes, *ibid.* 665 (1946); B. Bleaney and R. P. Penrose, Nature **157**, 339 (1946).

[4] B. P. Dailey, R. L. Kyhl, M. W. P. Strandberg, J. H. Van Vleck, and E. B. Wilson, Jr., Phys. Rev. **70**, 984 (1946); W. Gordy and M. Kessler, *ibid.* **71**, 639 (1947).

[5] I am indebted to Dr. A. Roberts for numerous discussions on these questions. The electric field is used to modulate the absorption frequency and thus to increase

Since all nuclei with spin values equal to, or greater than, unity seem to have an electric quadrupole moment, it follows that such spin values can be measured in the case of a strong electric field, which simplifies considerably the interpretation of the results.

2. THE HYPERFINE STRUCTURE OF THE INVERSION SPECTRUM

The rotational state of the NH_3 molecules is given by the well-known formula for the energy levels of the symmetric top.[6] Each level is characterized by three quantum numbers J, K, M, corresponding to the three degrees of freedom of a freely rotating rigid body. The inversion doubling introduces a new quantum number ($s=\pm 1$) which is essentially the symmetry character of the wave function of the molecule under reflection on the base plane. For the energy of a rotational state we have therefore an expression of the form

$$E_{JK_s}=J(J+1)/2A+\tfrac{1}{2}(1/C-1/A)K^2 -\tfrac{1}{2}s\Delta(J,K). \quad (1)$$

Here A and C are the two principal moments of inertia;[7] $\Delta(JK)$ is the term for the inversion doubling. The frequency of a particular line in the inversion spectrum is then given by $\Delta(J, K)$. The quantum number J represents the value of the total angular momentum and K is the projection of the angular momentum in the direction of the figure axis. Owing to the rotational symmetry the energy is independent of M, the projection of J in a fixed direction in space. The numbers K and M are restricted by the inequalities

$$-J\leqslant M\leqslant +J, \quad -J\leqslant K\leqslant J.$$

We consider now the case in which the nitrogen nucleus has an electric quadrupole moment. Let $\mathbf{i}$ represent the operator of the nuclear spin vector and $\mathbf{J}$ the angular momentum vector of the rotational motion of the molecule. The vector $\mathbf{F}=\mathbf{i}+\mathbf{J}$ represents then the total angular momentum of the system. The energy for the electric quadrupole interaction is given by[8]

$$H_q=\frac{e^2q'Q}{2J(2J-1)i(2i-1)} \times\{3(\mathbf{i}\cdot\mathbf{J})^2+\tfrac{3}{2}(\mathbf{i}\cdot\mathbf{J})-i(i+1)J(J+1)\}. \quad (2)$$

In this expression Q is the nuclear quadrupole moment and the quantity q' represents the expression

$$q'=\langle\sum(3\cos^2\vartheta-1)/r^3\rangle_{J,\,M_J=J}, \quad (3)$$

where the summation is to be extended over all the charges in the molecule other than the nucleus under discussion and the expression thus obtained to be averaged over the rotational state J, $M_J=J$. The angle ϑ is the angle of the radius vector with the fixed 3-direction in space. The expression eq' represents simply the gradient of the 3-component of the electric field in the 3-direction. The expression for q' is not a constant characteristic of the molecule since its value will, in general, still depend on the rotational state of the molecule. We can separate this latter dependence by introducing the characteristic molecular constant q which when multiplied with e represents the gradient of the electric field in the direction of the figure axis. The relationship between q and q' is then given by[9]

$$q'=q\langle\tfrac{3}{2}\cos^2\theta-\tfrac{1}{2}\rangle_{J,\,M_J=J}, \quad (4)$$

where θ is the angle of the figure axis with the 3-axis. Introducing the normalized wave function[10] for the rotational states

$$\left.\begin{aligned} U_{JKM}(\theta,\phi,\psi)&=\frac{1}{2\pi}\Theta_{JKM}(\theta)e^{i(K\phi+M\psi)}\\ \Theta_{JKM}&=C(1+\cos\theta)^{\frac{1}{2}(J+K)}\\ &\quad\times(1-\cos\theta)^{\frac{1}{2}(J-K)}\end{aligned}\right\}, \quad (5)$$

with the normalization constant given by

$$C^2=(2J+1)!/2^{2J}(J+K)!(J-K)!.$$

---

the sensitivity of the absorption measurements. See also R. M. Hughes and E. B. Wilson, Jr., Phys. Rev. **71**, 562 (1947).

[6] C.f. D. M. Dennison, Rev. Mod. Phys. **3**, 311 (1931).

[7] We use here the units $\hbar=c=1$ and cm. The energy is then expressed in wave numbers cm^{-1} and the dimension of A and C is cm.

[8] H. B. G. Casimir, *On the Interaction between Atomic Nuclei and Electrons* (Taylor's Tweede Genootschap, Haarlem, 1936).

[9] See the similar calculation given by A. Nordsieck, Phys. Rev. **58**, 310 (1940).

[10] R. de Kronig and I. I. Rabi, Phys. Rev. **29**, 262 (1927).

We obtain for the average of $\frac{1}{2}(3\cos^2\theta-1)$

$$\langle\tfrac{1}{2}(3\cos^2\theta-1)\rangle_{J,M_J=J}=\tfrac{1}{2}C^2\int_0^\pi(1+\cos\theta)^{J+K}\times(1-\cos\theta)^{J-K}(3\cos^2\theta-1)\sin\theta d\theta. \quad (6)$$

This integral can be reduced to three integrals of the type

$$\int_0^1 x^p(1-x)^q dx=p!q!/(p+q+1)!$$

by introducing the substitution $x=\frac{1}{2}(\cos\theta+1)$, $dx=-\frac{1}{2}\sin\theta d\theta$.

$$\tfrac{1}{2}\int_0^\pi(\cos\theta+1)^\alpha(\cos\theta-1)^\beta(3\cos^2\theta-1)\sin\theta d\theta$$

$$=2^{\alpha+\beta}\int_0^1 x^\alpha(1-x)^\beta(6x^2-3x+1)dx$$

$$=2^{2J}\left\{6\frac{(\alpha+2)!\beta!}{(\alpha+\beta+3)!}-3\frac{(\alpha+1)!\beta!}{(\alpha+\beta+2)!}+\frac{\alpha!\beta!}{(\alpha+\beta+1)!}\right\}$$

$$=2^{2J}\frac{\alpha!\beta!}{(\alpha+\beta+3)!}\{(\alpha+\beta)^2-(\alpha+6\alpha\beta+\beta)\}.$$

This gives finally for Eq. (6)

$$\langle\tfrac{1}{2}(3\cos^2\theta-1)\rangle_{J,M_J=J}=\frac{J}{2J+3}\left\{\frac{3K^2}{J(J+1)}-1\right\}. \quad (7)$$

The eigenvalues of the expression in brackets in Eq. (2) are known,[8] and we have

$$\{3(i\cdot J)^2+\tfrac{3}{2}(i\cdot J)-i(i+1)J(J+1)\}=\tfrac{3}{4}N(N+1)-i(i+1)J(J+1)$$

with

$$N=F(F+1)-i(i+1)-J(J+1)$$

and $F=J+i, J+i-1, \cdots, |J-i|$. We finally obtain for the quadrupole energy

$$E_q(J,K,F)=e^2qQ\left(\frac{3K^2}{J(J+1)}-1\right)\times\frac{\frac{3}{4}N(N+1)-i(i+1)J(J+1)}{2(2J+3)(2J-1)i(2i-1)}, \quad (8)$$

with q defined by Eq. (4). This is identical with the formula given by Dailey *et al* in reference 4.

The intensities and selection rules are obtained from the well-known formula[11] for the matrix elements of the electric dipole vector $\mathbf{P}$ in the representation scheme (J, i, F, M).

Since we shall use later the dependence of the intensities on M, we shall give the intensities for the transition to different values of M although they are of course unobservable as long as we have degeneracy with respect to M.

(a) *Longitudinal transitions*, electric field parallel to the 3-axis. Selection rules: $\Delta F=0, \pm1$, $\Delta M=0$. The transition probabilities A are proportional to the squares of the matrix elements of P_3

$\Delta F=0$ (center line)

$$A=\frac{K^2}{J^2(J+1)^2}M^2\frac{[J(J+1)-i(i+1)+F(F+1)]^2}{4F^2(F+1)^2}, \quad (9)$$

$F\to F+1$ (satellite)

$$A=\frac{K^2}{J^2(J+1)^2}[(F+1)^2-M^2]\frac{(F+1-i+J)(F+1+i-J)(i+J+2+F)(i+J-F)}{4(F+1)^2(2F+1)(2F+3)}. \quad (10)$$

(b) *Transverse transition*, electric field perpendicular to 3-axis. Selection rules: $\Delta F=0, \pm1, \Delta M=\pm1$. In this case the transition probabilities are proportional to the squares of the matrix elements of P_1.

$\Delta F=0$, $M\to M\pm1$

$$A=\frac{1}{4}\frac{K^2}{J^2(J+1)^2}(F\mp M)(F\pm M+1)\frac{[J(J+1)-i(i+1)+F(F+1)]^2}{4F^2(F+1)^2}, \quad (11)$$

[11] Condon and Shortley, *The Theory of Atomic Spectra* (Cambridge University Press, Cambridge, 1935).

$F\to F+1,\ M\to M\pm 1$

$$A=\frac{1}{4}\frac{K^2}{J^2(J+1)^2}(F\mp M+1)(F\mp M)\frac{(F+1-i+J)(F+1+i-J)(i+J+2+F)(i+J-F)}{4(F+1)^2(2F+1)(2F+3)}. \tag{12}$$

In addition to the above selection rules we have for the inversion spectrum of course for all transitions $\Delta J=0$, $\Delta K=0$.

We shall now specialize these formulas for the case of the ammonia inversion spectrum. For this case $i=1$. Furthermore we shall sum over all the initial and final states which have the same energy in the field-free case. Making use of the formulas

$$\sum_{-F}^{+F} M^2=\tfrac{1}{3}F(F+1)(2F+1)$$

we obtain for the total transition probabilities:

Center line:

$$A_{J,J}=[K^2(2J+1)/3J^3(J+1)^3]Q(J)$$

with

$$Q(J)=(J+1)^4+J^4+[J(J+1)-1]^2.$$

Satellites:

$$F:\ J-1\to J,\quad A_{J-1,J}=K^2(2J-1)/3J^3(J+1)^3,$$
$$F:\ J\to J+1,\quad A_{J,J+1}=K^2(2J+3)/3J^3(J+1)^3.$$

The magnitudes of these quantities for different values of J and K have no direct relation to the relative intensities of the different absorption lines since they must be multiplied with the statistical weight factor, ($=1$ for $K=1,2,4,5,\cdots$ and $=2$ for $K=3,6,9,\cdots$) and the Boltzmann factor $\exp[-E(J,K)/kT]$. Since we are primarily interested in the relative intensities within one and the same hyperfine structure-level system we calculate instead the ratios of the intensities of the satellites to the intensity of the center line, which is given by

$$\left.\begin{aligned}\alpha_{J-1,J}&=A_{J-1,J}/A_{J,J}\\&=(J+1)^2(2J-1)/(2J+1)Q(J)\\ \alpha_{J,J+1}&=A_{J,J+1}/A_{J,J}\\&=J^2(2J+3)/(2J+1)Q(J)\end{aligned}\right\}. \tag{13}$$

In Table I we summarize these ratios for some values of J.

TABLE I. Ratios of the intensities of the hyperfine components to the main lines for different values of J.

J	$\alpha_{J-1,J}$	$\alpha_{J,J+1}$
1	7.4×10^{-2}	9.3×10^{-2}
2	4.42	4.6
3	2.5	2.53
4	1.56	1.58
5	1.06	1.07
6	0.769	0.769

3. THE STARK EFFECT OF THE INVERSION SPECTRUM, WEAK FIELD[12]

We consider now the modification of the hyperfine structure when the absorbing molecule is brought into a uniform electric field E. Let the field direction be the 3-direction of the fixed-space coordinate system. The total Hamiltonian for the system is then

$$H=H_0+H_q+H',$$

where H_0 is the energy for the rotational levels (we disregard the vibrational-level system and consider only the vibrational ground state) given by Eq. (1) including the inversion splitting (last term of Eq. (1)). H_q is the quadrupole energy of Eq. (2) and H' is the interaction energy of the electric dipole moment with the external electric field.

$$H'=(\mathbf{E}\cdot\mathbf{P})=EP_3. \tag{14}$$

Here P_3, as before, is the 3-component of the electric dipole vector of the molecule. Since the symmetry character of P is odd under a reflection of the molecule on its base (the dipole moment has the direction of the figure axis) the matrix elements of the form $(s|P|s)$ are zero. We shall write for $P_3=\mu\cos\theta$, where μ is the strength of the electric dipole moment and $\cos\theta$ is the operator with the squares of its matrix elements in the (J,i,F,M) representation given by (9), (10).

Two methods of solution suggest themselves:

(a) In the case of sufficiently weak field the splitting due to H' will be small compared to the

[12] I wish to express my appreciation to Professor J. H. Van Vleck for correspondence and a discussion on the content of this and the following section.

splitting due to H_q. In this case one should choose the representation (J, i, F, M) which makes H_q diagonal and treat H' as a perturbation.

(b) For strong fields the Stark-effect splitting is more important than the quadrupole splitting and we start with the representation $(J, i, M_J M_i)$ for which H' is diagonal and treat H_q as a perturbation.

In this section we shall discuss case (a).

The perturbation matrix is then a 6×6 matrix. According to the foregoing remark on the matrix elements of P_3, H' will be, with respect to the symmetry character s, a matrix of the form

$$H' = \begin{pmatrix} 0 & G \\ G & 0 \end{pmatrix},$$

i.e. the only matrix elements different from zero are those which connect states with different symmetry. The matrix $G_{FF'}$ is a 3×3 matrix which, for each value of (K, J, M), has the following non-vanishing matrix elements (see Eqs. (9)

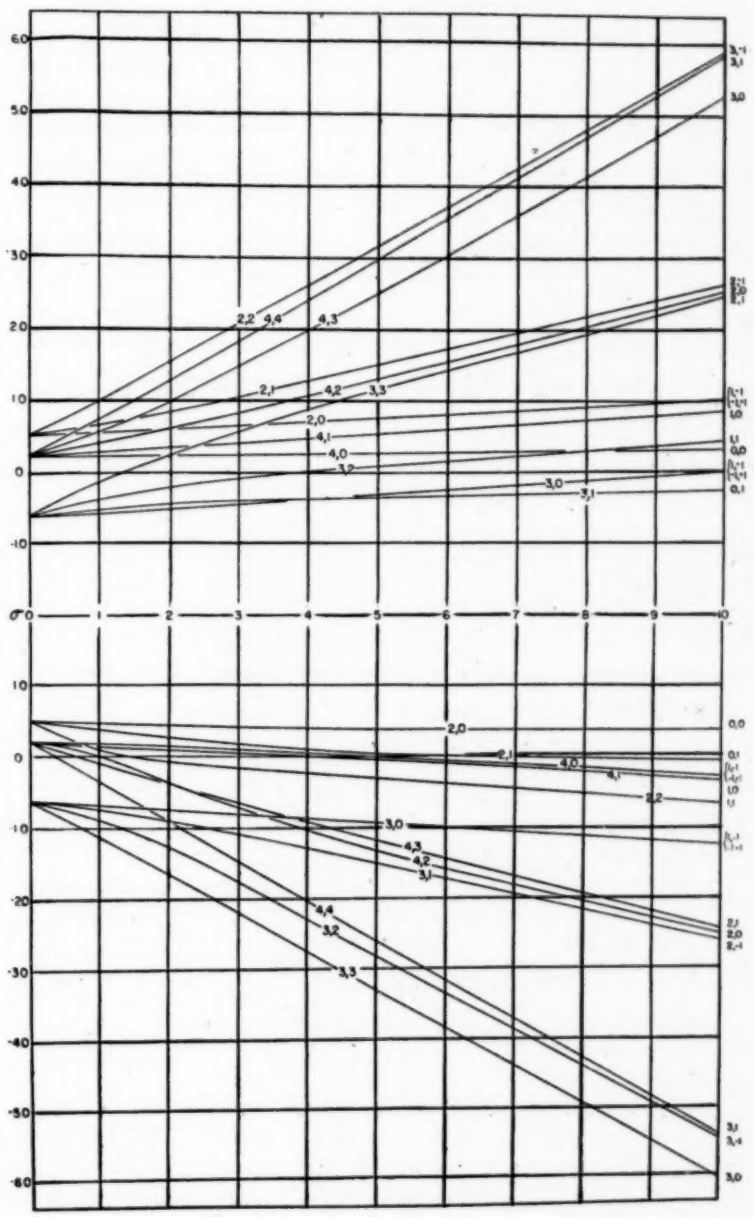

FIG. 1. Energy levels in units e^2qQ for the ammonia inversion line $J=K=3$ as a function of the parameter

$$\sigma = \mu^2E^2/[\Delta(J, K)e^2qQ].$$

The numbers at the right-hand edge denote M_J, M_i. The numbers in the figure give F, M_F for each line.

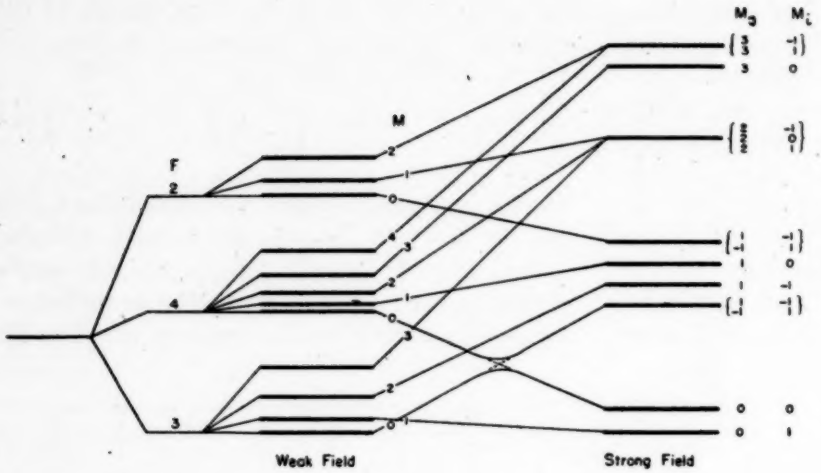

FIG. 2. Coordination of energy levels in the Stark effect of the ammonia inversion line $J=K=3$ for weak and strong fields. Upper state (schematic).

and (10)):

$$\left.\begin{aligned} &|M|\leqslant J-1\\ &G_{J-1,J-1}=\mu EKM/J^2\\ &G_{J-1,J}=G_{J,J-1}=\mu E(K/J^2)\\ &\times[(J+M)(J-M)/(J+1)(2J+1)]^{\frac{1}{2}} \end{aligned}\right\}, \quad (15a)$$

$$\left.\begin{aligned} &|M|\leqslant J\\ &G_{J,J}=\mu EKM[J(J+1)-1]/J^2(J+1)^2\\ &G_{J+1,J}=G_{J,J+1}=\mu EK(M/(J+1)^2)\\ &\times[(J+M+1)(J-M+1)/J(2J+1)]^{\frac{1}{2}} \end{aligned}\right\}, \quad (15b)$$

$$|M|\leqslant J+1$$
$$G_{J+1,J+1}=\mu EKM/(J+1)^2. \quad (15c)$$

The eigenvalue problem leads to a secular equation of the sixth degree. The fact that the separation of the unperturbed levels with different values of s is very much larger than the hyperfine structure splitting (the ratio is about 10^5), allows the application of Van Vleck's transformation[13] after which the hamiltonian has the form

$$H=H_0+H_q+\bar{H}, \quad (16)$$

where

$$\bar{H}=\begin{pmatrix}\Gamma & 0\\ 0 & -\Gamma\end{pmatrix},$$

and where Γ is a 3×3 matrix given by

$$\Gamma_{FF'}=(1/\Delta(J,K))\sum_{F''}G_{FF''}G_{F''F'}.$$

Here $\Delta(J,K)$ according to (1) is the energy difference (taken positive) between upper and lower state. The secular equation for the eigenvalue problem is now of third degree. The $\Gamma_{FF'}$ are functions of M as seen from (15).

In the following we shall find it convenient to introduce e^2qQ as unit of energy. Further, we

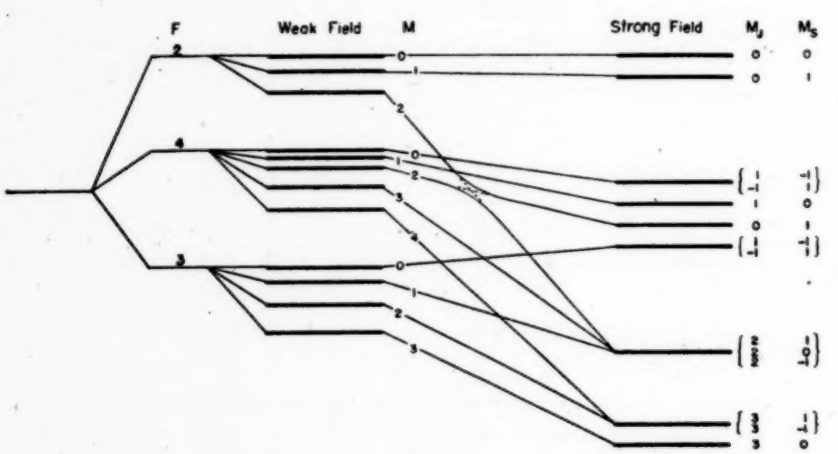

FIG. 3. Coordination of energy levels in the Stark effect of the ammonia inversion line $J=K=3$ for weak and strong fields. Lower state (schematic).

[13] See E. Kemble, *Principles of Quantum Mechanics* (McGraw-Hill Book Company, New York), p. 395.

TABLE II. The Stark effect of the inversion line $J=K=3$ for an electric field $E\sim 300$ volt/cm in units of e^2qQ.

Level F	M	Upper state	Lower state
4	4	0.771	−0.355
	3	0.563	−0.101
	2	0.390	+0.010
	1	0.270	0.150
	0	0.232	0.181
3	3	−0.167	−1.127
	2	−0.404	−0.904
	1	−0.526	−0.745
	0	−0.562	−0.687
2	2	0.991	0.090
	1	0.666	0.380
	0	0.539	0.479

introduce the parameter

$$\sigma=[(\mu E)^2/\Delta(J,K)]1/e^2qQ$$

which is a measure of the relative strength of the electric field. σ is about equal to unity for a field $E\sim 300$ volt/cm $=1$ e.s.u. If we assume for the dipole moment the value $\mu=1.45\times10^{-18}$ e.s.u. $=2.58\times10^{-6}$ cm. We may treat the upper and lower states simultaneously by letting $\sigma>0$ for the upper and $\sigma<0$ for the lower state.

The formula for the perturbation theory gives then in general an expression for the level displacement due to H_q and H'.

$$\epsilon(J,F,M)=\epsilon_q(J,F)+\sigma\Gamma_{FF}+\sigma^2\sum_{F'\pm F}\frac{\Gamma_{FF'}\Gamma_{F'F}}{\epsilon_q(F)-\epsilon_q(F')}$$

$$=\epsilon_q{}^0+\epsilon^{(1)}+\epsilon^{(2)}. \qquad (17)$$

The general formulas for these eigenvalues are rather complicated. It is more convenient to evaluate them for each level separately. It may be noted however that for some special values of M the cubic secular equation degenerates into a quadratic and a linear term which can be easily solved. This is the case for $M=J+1$ and $M=J$ and also for $M=0$.

Thus for the line $J=K=3$ there will be twelve levels of which six can be calculated by solving merely a quadratic equation. For the other six the formula (17) must be used for $\sigma<\sim 1$. The case $J=K=3$ is treated explicitly and the results are plotted in Fig. 1 for σ ranging from 0 to 10. For the special value $\sigma=1$ the energy values are also given in Table II. Figures 2 and 3 show the coordination of the levels for weak and strong field.

TABLE III. Stark effect of inversion spectrum for $E\sim 300$ volt/cm.

Initial F	M	Final F	M	Energy (arb. units)	Relative intensity
4	4	4	4	1.126	0.563
4	3	4	3	0.664	0.316
4	2	4	2	0.334	0.141
4	1	4	1	0.120	0.035
3	3	3	3	0.960	0.473
3	2	3	2	0.500	0.210
3	1	3	1	0.219	0.053
2	2	2	2	0.926	0.444
2	1	2	1	0.286	0.111
4	3	3	3	1.690	0.0117
4	2	3	2	1.294	0.0201
4	1	3	1	1.015	0.0251
4	0	3	0	0.919	0.0268
3	2	2	2	0.494	0.0198
3	1	2	1	−0.906	0.0317
3	0	2	0	−1.041	0.0357
2	2	3	2	1.895	0.0198
2	1	3	1	1.411	0.0317
2	0	3	0	1.226	0.0357
3	3	4	3	−0.066	0.0117
3	2	4	2	−0.414	0.0201
3	1	4	1	−0.676	0.0251
3	0	4	0	−0.743	0.0268

The general expressions for the intensities for longitudinal and transverse absorption spectrum are given by the formulas (9), (10) and (11), (12). In Table III the weak-field spectrum is given for the case of longitudinal transition for the line $J=K=3$.

4. THE STARK EFFECT FOR A STRONG FIELD

In the case of strong electric field ($\sigma\gg1$) we diagonalize first the operator $\bar{H}$ in Eq. (16). The representation which makes $\bar{H}$ diagonal is the (J, i, M_J, M_i) representation. For in this system the matrix G has the simple form

$$G_{M_JM_J'}=\sigma^{\frac{1}{2}}(K/J(J+1))M_J\delta_{M_JM_J'}$$

and

$$\Gamma_{M_JM_J'}=\sigma(K^2/J^2(J+1)^2)M_J{}^2\delta_{M_JM_J'}.$$

Since $M=M_J+M_i$, M_J may assume for any given M the values $M_J=M+1$, M, $M-1$. The quadrupole interaction in this representation may best be obtained by using the form of H_q in terms of the operators J and i given by Casimir.[8]

TABLE IV. Longitudinal spectrum of the $J=K=3$ NH_3 inversion line for strong electric fields ($\sigma \gg 1$).

Transitions: Initial M_J	Initial M_i	Final M_J'	Final M_i'	Relative line position	Relative intensity
3	+1	3	+1	9σ	9
3	0	3	0	9σ	9
3	−1	3	−1	9σ	9
2	+1	2	+1	4σ	4
2	0	2	0	4σ	4
2	−1	2	−1	4σ	4
$\begin{pmatrix}+1\\-1\end{pmatrix}_+$	$\begin{pmatrix}-1\\+1\end{pmatrix}_+$	$\begin{pmatrix}+1\\-1\end{pmatrix}_-$	$\begin{pmatrix}-1\\+1\end{pmatrix}_-$	$\sigma+16$	$\frac{1}{2}$*
1	0	1	0	σ	1
1	+1	1	+1	σ	1
$\begin{pmatrix}+1\\-1\end{pmatrix}_-$	$\begin{pmatrix}-1\\+1\end{pmatrix}_-$	$\begin{pmatrix}+1\\-1\end{pmatrix}_+$	$\begin{pmatrix}-1\\+1\end{pmatrix}_+$	$\sigma-16$	$\frac{1}{2}$*

* The two states (22) are distinguished by a ± sign.

$$H_e=\Lambda\{(J_3^2-\tfrac{1}{2}J_1^2-\tfrac{1}{2}J_2^2)(i_3^2-\tfrac{1}{2}i_1^2-\tfrac{1}{2}i_2^2)$$
$$+\tfrac{3}{8}[J_3(J_1+iJ_2)+(J_1+iJ_2)J_3]$$
$$\times[i_3(i_1-ii_2)+(i_1-ii_2)i_3]$$
$$+\tfrac{3}{8}[J_3(J_1-iJ_2)+(J_1-iJ_2)J_3]$$
$$\times[i_3(i_1+ii_2)+(i_1+ii_2)i_3]$$
$$+\tfrac{3}{8}(J_1+iJ_2)^2(i_1-ii_2)^2$$
$$+\tfrac{3}{8}(J_1-iJ_2)^2(i_1+ii_2)^2, \quad (18)$$

with

$$\Lambda=2[3K^2-J(J+1)]/J(J+1)(2J-1)(2J+3).$$

Explicitly written out, the matrix elements are the following (we use the abbreviation (M_JM_J') for $\Lambda^{-1}(H_e)_{M_JM_J'}$)

$$\left.\begin{aligned}(M+1,\,M+1)&=\tfrac{1}{4}\{3(M+1)^2-J(J+1)\}\\(M,\,M)&=-\tfrac{1}{2}\{3M^2-J(J+1)\}\\(M-1,\,M-1)&=\tfrac{1}{4}\{3(M-1)^2-J(J+1)\}\end{aligned}\right\}, \quad (19)$$

$$\left.\begin{aligned}(M+1,\,M)&=(M,\,M+1)\\&=-\sqrt{2}\tfrac{3}{8}(2M+1)\\&\quad\times[J(J+1)-M(M+1)]^{\frac{1}{2}}\\(M+1,\,M-1)&=(M-1,\,M+1)\\&=\tfrac{3}{4}[J(J+1)-M(M+1)]^{\frac{1}{2}}\\&\quad\times[J(J+1)-M(M-1)]^{\frac{1}{2}}\\(M,\,M-1)&=(M-1,\,M)\\&=\sqrt{2}\tfrac{3}{8}[J(J+1)-M(M-1)]^{\frac{1}{2}}(2M-1)\end{aligned}\right\}. \quad (20)$$

With this matrix one can apply perturbation theory in the usual way for any level except the case $M=0$. In this case, as is easily seen from (19), the zeroth-order energy levels are degenerate for the two states $M_J=+1$, $M_i=-1$ and $M_J=-1$, $M_i=+1$. The first-order correction in the energy is thus not simply the diagonal matrix element of the perturbation energy (18) but must be calculated in the usual way by solving the secular equation of that submatrix which contains all the elements connecting the same energy. If we denote the two states mentioned above for short with α and β, and an eigenstate of the eigenvalue problem with

$$\psi=x\alpha+y\beta, \quad (21)$$

then the eigenvalue problem is

$$-\tfrac{1}{8}x+\tfrac{1}{2}y=\epsilon x,$$
$$\tfrac{1}{2}x-\tfrac{1}{8}y=\epsilon y.$$

The secular equation for ϵ is

$$(1+8\epsilon)^2-16=0$$

with the solutions

$$\epsilon_1=+\tfrac{3}{8}, \quad \epsilon_2=-\tfrac{5}{8}.$$

TABLE V. Transverse spectrum of the $J=K=3$ NH_3 inversion line for strong electric field ($\sigma \gg 1$).

Transitions: Initial M_J	Initial M_i	Final M_J'	Final M_i'	Relative line position	Relative intensity
3	−1	2	−1	$\frac{1}{2}13\sigma+15/4$	3
3	+1	2	+1		
3	0	2	0	$\frac{1}{2}13\sigma-15/8$	$\frac{3}{4}$
		+1	−1		
2	−1			$\frac{3}{2}\sigma-3$	5/4
		−1	$+1_+$		
		+1	−1		
2	−1			$\frac{3}{2}\sigma+5$	5/4
		−1	$+1_-$		
2	0	1	0	$\frac{3}{2}\sigma-2$	5/2
2	1	1	1	$\frac{3}{2}\sigma+1$	5/2
$\begin{pmatrix}+1\\-1\end{pmatrix}_+$	$\begin{pmatrix}-1\\+1\end{pmatrix}_+$	0	−1	$\sigma+13/3$	3/2
		0	+1		
1	0	0	0	$\sigma-2/3$	3
1	1	0	1	$\sigma+1/3$	6
$\begin{pmatrix}1\\-1\end{pmatrix}_-$	$\begin{pmatrix}-1\\+1\end{pmatrix}_-$	0	−1	$\sigma-11/3$	3/2
		0	+1		

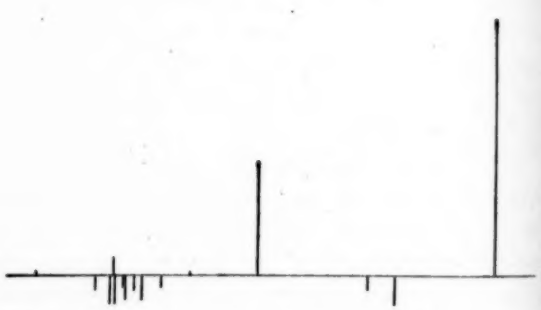

FIG. 4. Stark spectrum of the inversion line $J=K=3$ for a field $E\sim1000$ volt/cm. Upper lines: longitudinal spectrum; lower lines: transverse spectrum.

The corresponding solutions for x and y are:

$$\left.\begin{aligned} x^{(1)}&=1/\sqrt{2}, \quad y^{(1)}=1/\sqrt{2} \\ x^{(2)}&=1/\sqrt{2}, \quad y^{(2)}=-1/\sqrt{2} \end{aligned}\right\}. \tag{22}$$

The eigenstates which represent the zeroth-order wave functions are thus the symmetrical and antisymmetrical combinations of the states $M_J=+1$, $M_i=-1$; $M_J=-1$, $M_i=+1$.

The transition probabilities in this case are given by the square of the matrix elements of P_3 and P_1 for longitudinal and transverse transitions respectively. In the coordinate system characterized by the quantum numbers (J, M_J) we have the matrix elements

$$(M_J|P_3|M_J)=KM_J/J(J+1), \tag{23}$$

$$(M_J|P_1|M_J+1)=(K/2J(J+1)) \times[(J-M_J)(J+M_J+1)]^{\frac{1}{2}}. \tag{24}$$

Together with the selection rules $\Delta M_i=0$ these matrix elements determine the strength and character of each transition uniquely. In the longitudinal case we have for each $|M_J|\geq 2$ six functions corresponding to the six states $M=\pm M_J+1, \pm M_J, \pm M_J-1$.

The total intensity of these transitions is thus given by

$$A=[KM_J/J(J+1)]^2 \quad \text{for} \quad |M_J|\geq 2.$$

For $|M_J|=1$ we have the two states ψ_+, ψ_- determined by (21), (22). It is readily seen that only the matrix elements $(+|P_3|-)$ and $(-|P_3|+)$ are different from zero and are given by

$$(+|P_3|-)=(-|P_3|+)=[K/J(J+1)]^2.$$

There are four other transitions corresponding to the states

$$M_J=+1, \quad M_i=0, +1; \quad M_J=-1, \quad M_i=0, -1.$$

The total transition probability for these is then

$$A=[2K/J(J+1)]^2.$$

The transitions for the longitudinal spectrum together with their intensities are given in Table IV.

The transverse spectrum is somewhat more complicated. The transitions and their relative intensities are calculated with the matrix elements (11), (12), and (24) and are tabulated in Table V. In Fig. 4 the longitudinal and transverse spectrum is plotted for a strong field ($E\sim 1000$ volt/cm). For the transverse case only half of the transitions (those with $M_J\doteq -1$) are given. The others are symmetrically situated with respect to the origin (i.e. the undisplaced position of the line).

It is seen from Tables IV and V and also in Fig. 4 that for arbitrarily strong fields there always remains a hyperfine structure with a constant separation. The pattern is particularly simple for the longitudinal case in which only the last component ($M_J=1$) has a hyperfine structure in the form of two satellites on either side of the outer line with one-fourth the intensity of the center line. The transverse spectrum is more complicated and may be not so suitable for an investigation of nuclear spins since it may be difficult to separate all the hyperfine components.

On the Mass and the Disintegration Products of the Mesotron

CARL D. ANDERSON, RAYMOND V. ADAMS, PAUL E. LLOYD, AND R. RONALD RAU*
California Institute of Technology, Pasadena, California

August 25, 1947

A photograph has been obtained of a mesotron of positive charge which comes to rest in the gas of a cloud chamber and ejects a positron of 24-Mev energy. Several possible interpretations of this photograph are discussed.

I. EXPERIMENTAL DATA

IN a recent series of cloud-chamber observations made at an elevation of 9200 meters in a B-29 airplane, a photograph (Fig. 1) was obtained in which a mesotron of positive charge was observed to come to rest in the gas of the cloud chamber and at the end of its path to produce a lightly-ionizing particle of positive charge. In two previous cases, cloud-chamber photographs have shown the track of a particle resulting from the disintegration of a mesotron.[1] Other observations have shown that mesotrons of negative charge may undergo absorption into a nucleus before disintegration, in the case of nuclei of high atomic number.[2] Recent observations of tracks produced by slow mesotrons in photographic emulsions show that secondary-charged mesotrons are also sometimes produced.[3] In no previous case, however, has it been possible to obtain an accurate measurement of the magnetic curvature of the disintegration particle.

In the photograph here reported, the disintegration particle has an $H\rho = 8.0 \times 10^4$ gauss cm in a magnetic field of 7500 gausses. The curvature of this particle is accurately measurable and is not influenced by multiple scattering in the gas. The incoming mesotron is increasingly scattered toward the end of its path. It has an apparent $H\rho = 2.0 \times 10^4$ gauss cm, a range in argon of 4.4 cm (reduced to N.T.P.), and makes an angle of about 60° with the magnetic field. The angle between the track of the disintegration particle and the incoming mesotron is approximately 90°.

If the disintegration particle is assumed to be a positron, its $H\rho$ corresponds to an energy of 24 Mev. The magnetic curvature of this particle, together with the low value of its specific ionization, places an upper limit on its mass equal to about 25 electron masses, and so is quite consistent with the assumption that it has a mass equal to that of an electron.

II. DISINTEGRATION RESULTING IN PRODUCTION OF ELECTRON AND NEUTRINO

The mass of the mesotron is directly related to the energy of disintegration. It usually has been assumed that the mesotron disintegrates into an electron and a neutrino, and that the loss in rest mass which occurs in the transformation appears as additional kinetic energy of the electron and neutrino (or photon) in conformance with conservation of energy and momentum.

The disintegration of a mesotron into an electron (+ or −) and a neutrino has been compared with ordinary β-disintegration, but one difference should be noted. In the case of ordinary β-disintegration, for a given available disintegration energy, the electron may be emitted with any energy between zero and the available disintegration energy, with the emission of a single neutrino. Charge and spin are conserved. Conservation of energy and momentum are satisfied because a daughter nucleus is always present to absorb the recoil and thus balance the momenta of the electron and neutrino. In the case of mesotron disintegration, however, the assumption has usually been made that the mesotron disappears entirely, and so for a given available disintegration energy (here dependent upon the mass of the mesotron) the disintegration electron can

---

* Now at Princeton University, Princeton, New Jersey.
[1] Williams and Roberts, Nature 145, 102 (1940); Shutt, de Benedetti, and Johnson, J. Frank. Inst. 235, 637 (1943).
[2] See Conversi, Pancini, and Piccioni, Phys. Rev. 71, 209 (1947).
[3] Lattes, Muirhead, Occhialini, and Powell, Nature 159, 694 (1947).

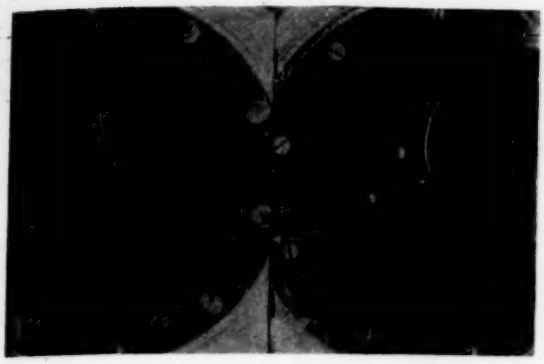

FIG. 1. A mesotron enters the cloud chamber through the rear wall and disintegrates in the gas giving rise to a positron of 24 Mev. The terminus of the mesotron track is at *A*. The disintegration particle leaves the right-hand photograph at *B*, and the left-hand photograph at *C*. The faintness of the positron track is due to its position near the edge of the illuminated region of the chamber. (The track passing from top to bottom of the photograph was produced by the particle which triggered the cloud chamber, the mesotron disintegration occurring by chance at about the same time.)

appear only with a unique energy, on the assumption that only one other known particle (neutrino or photon) is emitted. Thus in the case here reported, the assumption that two known particles, *viz.*, an electron and a neutrino (or photon), are produced in the disintegration requires that the mass of the mesotron lie between the limits of 90 and 110 electron masses.

It is possible, of course, that the mesotron disintegrated in the proximity of a nucleus under conditions such that the nucleus could absorb an appreciable recoil. In this way an energy of the disintegration electron of 25 Mev and a mesotron mass of 200 electron masses could be brought into harmony with conservation of momentum and energy. Such a possibility, however, seems quite unlikely, since the incoming mesotron is of positive charge and has a very low energy, as shown by its heavy degree of ionization, by its large curvature, and by the large degree of scattering in the gas.

III. THE MASS OF THE MESOTRON

Direct determinations of the mass of the mesotron have been reported, usually based on experiments in which two of the following parameters were measured: range, specific ionization, and magnetic curvature. In many cases these experiments could not lead to reliable numerical values of the mass of the mesotron because it was not possible to obtain accurate measurements of at least two of the above parameters in any given case. The specific ionization was often only a rough estimate, or the effects of multiple scattering of the particle under the conditions of the experiment were often sufficiently large to impair the measurement of the magnetic curvature.[4]

Data which have been obtained so far, and which are not subject to the above criticism, lead to a value for the mass of the mesotron of about 200 electron masses. The first and most accurate such determination,[5] in which a mesotron was observed to pass through a Geiger counter placed horizontally across the diameter of a cloud chamber, and come to rest in the gas of the cloud chamber, gave a value for the mass of 220 electron masses with a possible error conservatively estimated as ± 35 electron masses. In this case multiple scattering of the mesotron was not an important error, and both the magnetic curvature and range were accurately determined.

Additional determinations,[6] and in particular a set involving 26 individual cases,[7] by a method similar in principle to the above, and made under conditions where multiple scattering is not an important error, are also consistent with a mass equal to about 200 electron masses.

An accurate, direct determination of the mass of the mesotron in the present case cannot be made. Although the radius of curvature and the range of the particle would seem to indicate a mass of about 100 electron masses, the probable effects of multiple scattering on the observed curvature are such that a mass as large as 200 electron masses cannot be excluded. The probability of occurrence of sufficient multiple scattering to make a mass of 200 electron masses appear to be 100 electron masses is 20 percent. For an assumed mass of 300, the probability is 5 percent.[4]

---

[4] H. A. Bethe, Phys. Rev. **70**, 821 (1946).
[5] Neddermeyer and Anderson, Phys. Rev. **54**, 88 (1938); Rev. Mod. Phys. **11**, 201 (1939).
[6] Donald J. Hughes, Phys. Rev. **71**, 387 (1947).
[7] William B. Fretter, Phys. Rev. **70**, 625 (1946).

IV. THE GENERAL CASE OF DISINTEGRATION INTO TWO PARTICLES

In view of the fact that the reliable and direct determinations of the mass of the mesotron seem in all cases to indicate a mass considerably greater than 100 electron masses, and that the curvature and range of the incoming mesotron in the present case are not inconsistent with a larger mass, one may assume that the mass of the mesotron here observed is actually considerably greater than 100 electron masses. For the sake of discussion let us take a mass equal to 200 electron masses. We shall assume, further, that only two particles, one charged and one neutral, are produced in the disintegration. The observed curvature and specific ionization of the charged particle produced in the disintegration place an upper limit on its mass equal to about 25 electron masses. If, for the time being, we dismiss the possibility that the mass of the charged particle lies between 1 and 25 electron masses, and assume it has electronic mass, then the mass of the neutral particle, computed on the basis of conservation of momentum and energy, must have a value of about 140 electron masses, and its kinetic energy must be about 4 Mev.

The difference between the masses of the primary particle and of the secondary "heavy" particle, namely, about 60 electron masses, and also the kinetic energy of the secondary particle are relatively insensitive to the assumed mass of the primary particle; e.g., if a mass of 300 electron masses is chosen for the primary particle, the mass difference between the primary mesotron and the secondary neutral mesotron is 55 electron masses, and the kinetic energy of the secondary neutral mesotron is about 2 Mev.

The above interpretation shows an analogy with the recent observations by Lattes, Muirhead, Occhialini, and Powell[3] of tracks of secondary charged mesotrons in photographic emulsions. In two instances, the track of a secondary mesotron was observed to originate at the terminus of the track of another mesotron which comes to rest. If, among the interpretations suggested by the authors, we choose the fundamental one in which a charged mesotron disintegrates into another charged mesotron and a photon (or neutrino), we note that, in each case, the difference in mass between the primary and secondary mesotron is "not greater than 100 electron masses," its kinetic energy is about 2 Mev, and the total disintegration energy is "of the order of 25 Mev." The following points of similarity between the results of Lattes, Muirhead, Occhialini, and Powell and our own observation are now apparent: the mass difference between the original and the secondary mesotrons, the kinetic energy of the secondary mesotron, and the total disintegration energy of the process.

V. DISINTEGRATION INTO MORE THAN TWO PARTICLES

The possibility that the mesotron actually has a mass greater than about 100 electron masses and disintegrates into more than two particles should not be overlooked. If the spin of the mesotron is either zero or unity, it may disintegrate, for example, into an electron, a photon, and a neutrino. If the spin of the mesotron is one-half, the disintegration products may be an electron and two neutrinos, or an electron and two photons. In terms of an assumption of this kind, the electron may be emitted with any energy within a range between zero and an upper limit which depends upon the mass of the mesotrons, and still permit the conservation of both energy and momentum. In such a case, then, there would be no contradiction between an energy of 25 Mev for the disintegration electron, and a value of mass of the mesotron greater than 100 electron masses.

VI. MESOTRON OF NEGATIVE CHARGE

Inasmuch as the lower half of the mesotron track exhibits considerably more scattering than the upper half, it seems very unlikely that the mesotron could be of negative charge and traveling upward. Any interpretation based on this possibility will not be discussed at this time.

VII. CONCLUSION

Until more data are obtained it is not possible to state with certainty which of the interpretations discussed above represents the correct one. This is particularly true since the present ex-

periments were carried out at a higher elevation above sea level than most previous work.

Our present knowledge of the properties of mesotrons, however, would seem to support the view that the photograph here described represents the disintegration of a charged mesotron into an electron and a neutral particle smaller in mass than the charged mesotron by 50 to 60 electron masses. In terms of this interpretation, the mass of the incoming mesotron can well be of the order of 200 electron masses, a value which is in complete accord with the best previous mass determinations. There is also a quantitative agreement, within the uncertainty of the measurements, between the data of Lattes, Muirhead, Occhialini, and Powell, in the only two cases so far reported by them, and our own observation, with respect to (a) the kinetic energy of the secondary mesotron, (b) the mass difference between the initial and secondary mesotron, and (c), the disintegration energy. The mechanism of disintegration of a charged mesotron into an electron and a neutral mesotron is closely analogous to that of a charged mesotron into a photon (or neutrino) and a secondary-charged mesotron. In the former case the electric charge is associated with the "light" secondary particle, and in the latter with the "heavy" secondary particle. The disintegration of a mesotron into an electron and a neutral mesotron would, of course, escape detection by the photographic emulsion technique, since neither of these particles would there produce an observable track.

The existence of neutral mesotrons would aid in removing the present difficulties in explaining the proton-proton and proton-neutron scattering experiments which imply a charge independence of nuclear forces. The existence of two types of mesotrons of different masses already has been suggested on theoretical grounds.[8]

In any case, it is very strongly suggested that a complete interpretation of the experimental data is not to be found in the simple assumption of unstable particles with unit charge and a *unique* mass of the order of 200 electron masses.

It will be of great interest to obtain further measurements of the energy of the disintegration particles and, in particular, under conditions where the mass of the primary mesotron can be determined directly.

It is a pleasure to express our indebtedness to the Office of Naval Research, from which source, through Contract N6onr–102, Task Order No. III, have come the major funds. We are also indebted to the Army Air Forces for the use of a B-29 airplane, and to the U. S. Naval Ordnance Test Station at Inyokern, California, for laboratory and ground facilities. We wish to thank Major W. A. Gustafson, AAF, and his officers and men for their very willing assistance, and to offer to Commander E. Bollay, ONR, our warmest appreciation for the very able assistance he has given on so many occasions.

---

[8] J. Schwinger, Phys. Rev. 61, 387 (1942).

Letters to the Editor

PUBLICATION of brief reports of important discoveries in physics may be secured by addressing them to this department. The closing date for this department is five weeks prior to the date of issue. No proof will be sent to the authors. The Board of Editors does not hold itself responsible for the opinions expressed by the correspondents. Communications should not exceed 600 words in length.

On the Possibility of Observing Beat Frequencies between Lines in the Visible Spectrum

A. THEODORE FORRESTER, WILLIAM E. PARKINS, AND EDWARD GERJUOY
University of Southern California, Los Angeles, California
August 29, 1947

IF two waves of very nearly the same frequency are superposed, the peak amplitude of the combination oscillates in magnitude with a frequency equal to the difference of the two original frequencies, giving rise to so-called beats. It is to be expected that under the proper circumstances such effects should be observable with light waves.

Consider two spectral lines centered at frequencies f_1 and f_2, whose widths are each δ. In each line the electric vector of the light is a superposition of an infinite number of components whose phases and amplitudes determine all details of the time variation of the electric vector. Most of the energy in the line is included in a frequency band equal to the width, and within this band the phases of the various components are random. Nonetheless the vibrations of the electric vector bear a certain resemblance to a sine wave. At any instant the various components of the line f_1 have definite phase relations, which will be retained for a time interval τ so short that the change in phase of the frequency $f_1-\delta/2$ differs by only a fraction of a radian from the change in phase of the frequency $f_1+\delta/2$. In other words, for time intervals τ small compared to $1/\delta$, the electric vector of the line vibrates much like a pure sine wave of frequency f_1. If f_1 and f_2 are polarized in the same plane and superposed, they will show beats, provided that the time intervals during which f_1 and f_2 retain their periodicity are large enough to include a reasonable number of beats. Writing $f_2-f_1=\Delta$, this condition can be expressed $\Delta>2\delta$. The beats can also be considered as resulting from the combination of each component in f_1 with each component in f_2, producing a beat pattern made up of frequencies lying in a band of width 2δ about frequency Δ. Thus the condition $\Delta>2\delta$ assures a relatively well-defined beat-frequency spectrum.

Line widths in the visible region can be made as small as 10^9 cycle/sec. Well-defined beats can therefore be produced with a Δ of 10^{10} cycles/sec., which is within the range of present day UHF techniques. To detect the beats or difference frequency a non-linear device of some kind must be employed. Such a device is a photo-surface, which yields a current proportional to the intensity of the incident light. The fluctuations in photo-current can be detected with a resonant cavity tuned to the frequency Δ. A projected apparatus for observing beat frequencies between lines in the visible spectrum is shown in Fig. 1.

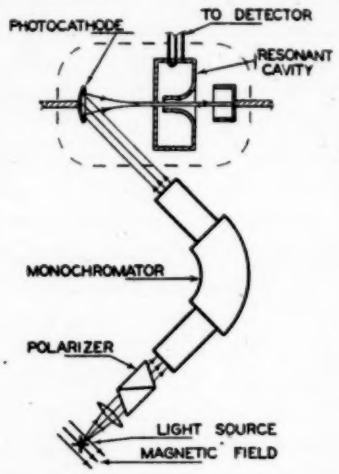

FIG. 1. Projected apparatus for observing beat frequencies. The polarizer eliminates the central component of the Zeeman spectrum of a line and the monochromator all lines except one, whose two outside components reach the photo-cathode with equal intensity.

Beats are produced between two Zeeman components of some chosen spectral line. This has the advantage of providing a variable frequency separation so that the cavity may have a fixed frequency, and of providing two lines of equal intensity, for which the beats are most pronounced. With fields of the order of 10,000 gausses, the two outside components of a normal Zeeman pattern provide separations of the correct order of magnitude.

Calculations indicate that the signal-to-noise ratio will probably be poor, the principal limitations being thermal noise in the cavity and the shot noise fluctuations in the photo-current. However, techniques for measuring signals against a high noise background have been developed,[1] and the prospects are fair that the beats will be detectable.

The possibility of performing this experiment is predicated upon the validity of certain assumptions regarding the nature of the photoelectric process. In particular, it is necessary to assume that the probability of emission of an electron from any point on the cathode is proportional to the average light intensity averaged over a time small compared to $1/\Delta$, and that the lifetime for photo-emission is small compared to $1/\Delta$. Evidently, if these assumptions are not satisfied, the photo-current will show little or no trace of the periodicity $1/\Delta$. Thus, detection of the beats should permit the inference that the lifetime for photo-emission is small compared to 10^{-10} second. Previous measurements have at most been able to show that this time is less than 3×10^{-9} second.[2]

[1] R. H. Dicke, Rev. Sci. Inst. 17, 268 (1946).
[2] E. O. Lawrence and J. W. Beams, Phys. Rev. 32, 478 (1928).

The Absorption Cross Section of Gold for Neutrons of Energies from 0.01 to 0.3 Ev*

B. D. McDaniel,[1] R. B. Sutton,[2] Leo S. Lavatelli,[3] and E. E. Anderson[4]
University of California, Los Alamos Scientific Laboratory, Santa Fe, New Mexico
August 25, 1947

THE neutron transmission of a gold sheet, 3.01 g/cm² thick, has been measured for neutron energies from 0.01 to 0.3 ev. Neutrons of high energy were produced by bombardment of a Be target with deuterons from the 42-inch Los Alamos cyclotron. The neutrons were slowed down in a moderating medium near the cyclotron chamber. The moderator consisted of a 5-cm thickness of a solution of 7 g of B_2O_3 per liter of water, boron being used to shorten the mean life of the source. Neutron energies were determined by measuring their time of flight over a 7.6-meter path from the moderator to a BF_3-ion chamber. The time of flight was measured by means of the Cornell neutron velocity spectrometer.[5] Corrections, which amounted to less than 3 percent of the time of flight, were made to take account of the 68-microsecond mean life of the moderator.

Figure 1 shows the total cross section, obtained from the transmission data, plotted as a function of the neutron time of flight expressed in microseconds per meter. A corresponding scale of neutron energies is also included for comparison. It can be seen that the relation between cross section and time of flight is approximately linear. However, because of the resonance in gold, which is located at about[6] 4.8 ev, the cross-section dependence on time of flight is expected to depart slightly from a linear relation. One may assume that the Breit-Wigner one-level formula describes the variation of the cross section from 4.8 ev down to zero energy and that contributions from higher resonances are not significant. Under this assumption, the total cross section in the region investigated is expected to follow the approximate relation given below.

$$\sigma_T=\alpha(E_r/E)^{\frac{1}{2}}(1+2E/E_r)+\sigma_s,$$

σ_T=total cross section, E=neutron energy, E_r=resonance energy=4.8 ev.

The scattering cross section σ_s is assumed to be approximately constant, while α is a constant depending on the Breit-Wigner parameters of the 4.8-ev resonance as is given below.

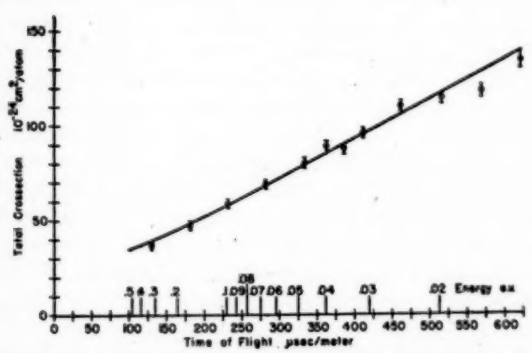

Total cross section of gold as a function of neutron time of flight. Corresponding energy scale also given on the abscissa.

$$\alpha=\sigma_0\Gamma^2/4E_r^2,$$

σ_0=cross section at resonance, and Γ=resonance width.

The curve in Fig. 1 is drawn in accordance with the approximate relation given above, and uses a choice of the constants which provides a good fit to the data. The values of α and σ_s which were chosen are 6.80 and 9.0 barns, respectively (one barn equals 10^{-24} cm²/atom). Substitution of these values in the equation above yields the following expression for σ_T when the neutron energy is expressed in ev:

$$\sigma_T=\{(14.9\pm0.3)E^{-\frac{1}{2}}(1+0.42E)+(9.0\pm2)\}\quad\text{barns.}$$

The corresponding value of $\sigma_0\Gamma^2$ is 625 barns-ev², in agreement with that given by Havens.[6] The value of the total cross section observed at 0.025 ev is (104±2) barns.

* This work was carried out under contract between the University of California and the Manhattan District, Corps of Engineers, War Department.
[1] Now at Cornell University, Ithaca, New York.
[2] Now at Carnegie Institute of Technology, Pittsburgh, Pennsylvania.
[3] Now at Harvard University, Cambridge, Massachusetts.
[4] Now at Milwaukee-Downer College, Milwaukee, Wisconsin.
[5] B. D. McDaniel, Phys. Rev. 70, 832 (1946).
[6] Havens, Wu, Rainwater, and Meaker, Phys. Rev. 71, 166 (1947).

Gamma-Rays from Cu^{64}, Annihilation of Swift Positrons, and Experiments on Orbital-Electron Capture

Martin Deutsch
Massachusetts Institute of Technology, Cambridge, Massachusetts
September 8, 1947

BRADT, *et al*[1] have reported that Cu^{64} emits one gamma-ray of 1.2 Mev for every ten positrons emitted. About a year ago, before the Swiss work came to our attention, we observed a feeble hard radiation from Cu^{64} and believed it to be due to the annihilation of moving positrons. According to Heitler,[2] about three percent of the positrons should be annihilated before stopping, and somewhat more than half of the resulting continuous gamma-ray spectrum should be above 0.51 Mev, with an end point of about 1.35 Mev. The existence of nuclear gamma-rays of the energy and abundance reported by the Zurich group would be of importance to our understanding of the orbital-electron capture process, since the results of Good, Peaslee, and Deutsch,[3] which showed excellent agreement with the theory for allowed transitions, in several cases were based on the use of Cu^{64} as a source of pure annihilation radiation.

The gamma-rays from a sample of copper obtained from Oak Ridge were therefore investigated in the magnetic lens spectrometer. Secondary electrons caused by a feeble 1.35-Mev gamma-ray were found and decayed with the half-life of Cu^{64}. The K-photoelectron line was slightly more than 0.005 times as intense as the K-line caused by the annihilation radiation, as shown in Fig. 1. Evaluation of relative gamma-ray intensities from this ratio is not too easy, because of the relatively thick radiator (50 mg/cm²) used. A gamma-ray spectrum of Na^{22} was there-

fore observed under the same conditions as the Cu^{64} spectrum. Na^{22} is known[3] to emit very nearly one nuclear gamma-ray per positron. The height of the K-line caused by the 1.28-Mev gamma-ray was 0.24 times that caused by annihilation radiation, as seen in Fig. 1. After minor corrections, we conclude that Cu^{64} emits one 1.35-Mev

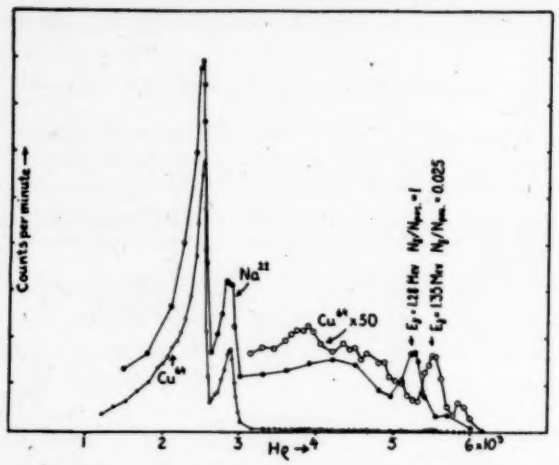

FIG. 1. Secondary-electron spectra produced by the gamma-rays of Cu^{64} (open circles) and of Na^{22} (solid circles). The thick radiatos causes the broadening of the photoelectron lines towards low energier but serves to emphasize the high energy gamma-rays.

nuclear gamma-ray from every 40 ± 5 positrons. This is about equal to the expected intensity of the hard component of the annihilation radiation. It may be seen in Fig. 1 that the secondary-electron distribution of Cu^{64}, instead of dropping for momenta below 4700-oersted-cm as one should expect from the Na^{22} spectrum, continues to rise to a maximum near 3800-oersted-cm and then falls off quite slowly. This is almost certainly caused by the hard annihilation radiation. The order of magnitude of the energy and abundance of the secondary electrons agrees with expectation, but the accuracy of the data is insufficient to allow quantitative comparison with theory. Further experiments in this connection are planned.

The very feeble nuclear gamma-radiation of Cu^{64} causes only insignificant corrections to the results of Good, *et al.* The hard annihilation radiation does not affect their results because the energies of the several positron spectra are all in the same range. In particular the result that an empirically second forbidden transition—Na^{22}—shows an "allowed" relative capture probability remains unchanged.

The author wishes to thank Dr. L. F. Curtiss of the Bureau of Standards for the uranium foil used as secondary-electron radiator. This work was supported in part by the Office of Naval Research.

[1] Bradt, Gugelot, Huber, Medicus, Preiswerk, Scherrer, and Steffen Helv. Phys. Acta 19, 219 (1946).
[2] W. Heitler, *The Quantum Theory of Radiation* (Oxford University Press, London, 1944), p. 231.
[3] W. M. Good, D. Peaslee, and M. Deutsch, Phys. Rev. 69, 313 (1946).

Mass Spectrographic Assignment of Activities to Re^{186} and Re^{188}

DAVID C. HESS, JR., RICHARD J. HAYDEN, AND MARK G. INGRAHAM
Argonne National Laboratory, Chicago, Illinois
August 25, 1947

A SAMPLE of ammonium-pyrrhenate solution was bombarded in the Argonne heavy-water pile to produce the 18- and 90-hour activities summarized by Seaborg.[1] In order to verify the assignment of the activities to certain isotopes, the activated material was analyzed by a mass spectrograph. This was done in the following manner:

A portion of the activated solution was placed in a tungsten crucible and evaporated to dryness. This crucible was then placed in the source system of the mass spectrograph, where it was heated and the emergent vapor ionized by electron bombardment. By operation of the spectrograph the ions were separated according to mass and deposited on a photographic plate.

Before development, two successive radio-autographs were made from this plate, the first for 36 hours and the second for 180 hours. The plate was then developed to provide mass markers.[2] Development of the transfer plates showed weak lines at masses 186 and 188 on the first plate. On the second plate only the line at 186 was observed, showing that the activity causing the exposure at 188 had a shorter half-life than that causing the exposure at 186.

A second portion of the original irradiated sample was followed by counting it concurrently with the production of the radio-autographs. This showed the presence of 18- and 90-hour half-lives. Therefore, the 18-hour half-life is assigned to mass 188, and the 90 hour assigned to mass 186, in agreement with Goodman's assignment.[3]

In order to determine which isotope of rhenium is responsible for the resonance absorption for neutrons of 2.3-volts energy, two additional samples of ammonium pyrrhenate were bombarded, one inside an aluminum cylinder with negligible neutron absorption and the other inside a cadmium cylinder of thickness such that the 0.18-volt cadmium resonant neutrons were reduced to less than 0.1 percent of the initial flux, while the flux of neutrons of 2.3-volt energy was reduced to 88 percent of the initial flux. By counting the resulting activity it was found that the ratio of initial activities of 18-hour half-life to 90-hour half-life was about 7 for the sample which had been bombarded in aluminum, and 2.5 for that in cadmium. As the half-lives have a ratio of five, the ratio of the number of 18-hour isotopes to the number of 90-hour isotopes is 1.4 to 1 for aluminum shielding and 0.5 to 1 for cadmium shielding. Since the production of the 18-hour activity is thus reduced by the cadmium, it appears that the 2.3-hour resonance absorption leads to the 90-hour activity at mass 186.

[1] G. T. Seaborg, Rev. Mod. Phys. 16, 1 (1944).
[2] M. G. Inghram, R. J. Hayden, and D. C. Hess, Jr., Phys. Rev. 71 270 (1947).
[3] L. J. Goodman and M. L. Pool, Phys. Rev. 71. 288 (1947).

On the Double Focusing Beta-Ray Spectrometer

EARL S. ROSENBLUM
Department of Physics, Case Institute of Technology, Cleveland, Ohio
August 25, 1947

IN a recent article,[1] Shull and Dennison developed a mathematical analysis of the double focusing beta-ray spectrometer. By means of this analysis, as corrected by the same authors,[2] a study has been made of the focused images for several values of β, under the same initial conditions: $a=10$ cm, slit size 20×2 mm, $(\phi_r^2+\phi_z^2)^{\frac{1}{2}}\leqslant 0.1$ radian. It was found that for $\beta=\frac{1}{4}$, the image width is a minimum, being 2.67 mm as against 3.33 mm for $\beta=\frac{1}{8}$ or $\frac{1}{2}$. The image area was also found to be smaller, so that both intensity and resolving power are increased. A point source at $\delta r=\delta z=0$ has a triangular image, with apex at $\delta r=\delta z=0$ and center of gravity at a radius less than the equilibrium radius a. A line source 20 mm long at $\delta r=0$ has, roughly, a rectangular image of width 0.67 mm, as compared to 1.33 mm for $\beta=\frac{3}{8}$ or $\frac{1}{2}$, and of half-height 10.7 mm, compared to 10.0 mm for $\beta=\frac{3}{8}$ and 11.3 mm for $\beta=\frac{1}{2}$. An incidental result with $\beta=\frac{1}{4}$ is that the correction term $[-(\beta-\alpha/2)Z^2H_0/a^2]$ in H_s becomes zero.

[1] F. Shull and D. Dennison, Phys. Rev. **71**, 681 (1947).
[2] F. Shull and D. Dennison, Phys. Rev. **72**, 256 (1947).

On the Proton-Proton Scattering at 14.5 Mev

J. LEITE LOPES AND J. TIOMNO
Faculdade Nacional de Filosofia, University of Brazil, Rio de Janeiro, Brazil
September 2, 1947

AN investigation of the recent experiments[1] on the anisotropy of proton-proton scattering at 14.5 Mev was made by superimposing the nucleonic potentials, as given by the current meson theories, on the Coulombian one. A preliminary indication of the theoretical character of this anisotropy was obtained by the Born approximation. The scalar, pseudoscalar, and vector (in the single-force assumption) symmetrical meson theories give too low values for $\sigma(\theta)$ as compared to the experimental points, $\sigma(\theta)$ being the differential cross section in the center-of-mass system. If one assumes the pseudoscalar and vector meson masses equal to 177m, the Møller-Rosenfeld theory gives too large values for $\sigma(\theta)$, the experimental values being less than one-half the theoretical ones, except for $\theta=90°$ where they are in agreement. This theory gives a better curve for a meson mass of the order 250m. If one assumes the meson masses and the coupling constant as calculated by Jauch and Hu[2] for the deuteron problem, the symmetrical Schwinger theory is the one which is in better agreement with the experimental points. The values of $\sigma(\theta)$ in this theory, together with those of the Møller-Rosenfeld theory for $\mu=250$m, are listed in Table I. It is seen that in the Schwinger theory $\sigma(\theta)$ is larger for small θ than the experimental values. Since, however, Born's approximation overestimates the P-wave contribution to the scattering cross section in comparison with the S-wave scattering, one may expect $\sigma(\theta)$ to be smaller for small θ than the values indicated in Table I. If this is true, our results indicate that there probably exists a non-singular tensor force acting between protons in the triplet P state. Experiments at higher energies are needed for a definite conclusion about this point. We should also remark that the symmetrical Schwinger theory predicts[3] an anisotropy for the neutron-proton scattering at 14 Mev which is probably in good agreement with the latest experiments.[4]

TABLE I. Proton-proton scattering anisotropy according to M-R and Schwinger theories (at 14.5 Mev and in Born approximation).

	$\sigma(\theta)\cdot10^{26}$ (in cm²)		
		Schwinger	
θ	M-R ($\mu=250$ m)	($K=177$ m; $\mu=283$ m)	experim.
90°	1.5	2.9	3.34 ±0.2
36	2.7	4.1	3.0 ±0.3
28	3.3	4.4	3.5 ±0.4
24	3.9	4.8	3.0 ±0.2
20	5.2	5.6	4.4 ±0.3

[1] R. R. Wilson, *et al.*, Phys. Rev. **71**, 560 (1947).
[2] J. M. Jauch and N. Hu, Phys. Rev. **65**, 289 (1944).
[3] J. M. Jauch, Phys. Rev. **67**, 125 (1945).
[4] J. S. Laughlin and P. G. Kruger, Phys. Rev. **71**, 736 (1947).

Proton-Proton Scattering at 10 Mev

LESLIE L. FOLDY
Department of Physics, University of California, Berkeley, California
September 2, 1947

IN a recent letter to the editor of the Physical Review,[1] R. E. Peierls and M. A. Preston present an analysis of the recent experimental results of R. R. Wilson[2] on proton-proton scattering at 10 Mev which they find to be at variance with preliminary conclusions of Wilson based on independent calculations of L. B. Eisenbud and myself. Since the analysis of these results is of considerable importance and since a check of my calculations has not uncovered any error, I should like to comment briefly on this matter.

Peierls and Preston begin their analysis with a determination of the S-wave phase shift from the scattering cross section at 90° given by Wilson. However, this value is not an *experimental* value. Wilson states that the experimental points were adjusted to give this value at 90°. This value was, in fact, computed on the basis of a square well of range $e^2/mc^2=2.8\times10^{-13}$ cm and a depth of 10.5 Mev, without interior Coulomb potential for which the phase shift has indeed the value $K_0=52.5°$, as found by Peierls and Preston from the cross section. From this phase shift in combination with that derived from the data of Wilson and Creutz[3] at 8 Mev, the above authors then calculate the range of the proton-proton force, obtaining a value of 2.48×10^{-13} cm. While this value is not ruled out by any available information, since it if based on a theoretical rather than an experimental cross section at 10 Mev, it has no more claim to validity than the value 2.8×10^{-13} cm derived by Breit[4] from low energy proton-proton scattering data.

It is in connection with P-wave phase shift K_1 that a

discrepancy is present whose source is difficult to determine. Peierls and Preston determine from the experimental points a value approximately $-0.8°$, while the calculations of Eisenbud and myself indicate a value in the neighborhood of $-0.4°$. Again, the above authors derive from the theoretical curve for the repulsive P-well in Wilson's paper a value $K_1=-2.1°$. Actually, this curve was computed for a value of $K_1=-1.4°$. A check of the calculations relative to this point has not disclosed any error. The difference between $K_1=-1.4°$ and the value $K_1=-0.8$, calculated by Peierls and Preston for a well of the same depth, is easily accounted for by the different ranges employed in the two computations. Since K_1 varies approximately as the fifth power of the range, we have $(2.8/2.5)^5\times 0.8°=1.7°$, which within the limited validity of the fifth-power law is in satisfactory agreement with 1.4°.

In addition, it was not found possible to verify the statement of Peierls and Preston that a repulsive potential of 12 Mev for the ^3P interaction of two protons is to be expected from a preponderance of charge independent "Majorana" and "Heisenberg" forces; on the contrary, a value of about 22 Mev was obtained. The value of 12 Mev would appear to follow from a preponderance of charge independent "Majorana" and "Bartlett" forces, however. This question is somewhat academic in consequence of the importance of the tensor force in the binding of the deuteron.

This brings us to perhaps the main purpose of this letter, which is to point out the fact that it is doubtful that an unambiguous analysis of the experimental results available at present on proton-proton scattering in terms of internucleonic potentials is possible in view of the limited accuracy of the experiments. This is due principally to the possibility of a tensor force between two protons in the ^3P state. Meson theories in fact predict the existence of such a force. Preliminary calculations indicate that Wilson's results would also be in substantial agreement with the charge and parity dependence of nuclear forces predicted by the symmetrical meson theories, though not with that predicted by the neutral meson theories. These questions will be dealt with in more detail in a forthcoming paper of the author.

[1] R. E. Peierls and M. A. Preston, Phys. Rev. 72, 250 (1947).
[2] R. R. Wilson, Phys. Rev. 71, 384 (1947).
[3] R. R. Wilson and E. C. Creutz, Phys. Rev. 71, 339 (1947).
[4] G. Breit, H. M. Thaxton, and L. Eisenbud, Phys. Rev. 55, 1018 (1939).

Radioactivity of Cu^{60}

C. E. Leith, A. Bratenahl, and B. J. Moyer
Radiation Laboratory, Department of Physics, University of California, Berkeley, California
August 25, 1947

A POSITRON activity with a half-life of 24.6 ± 0.3 minutes has been assigned to Cu^{60}. γ-radiation associated with this decay has an energy of 1.50 ± 0.05 Mev, and two positron groups have energies of 1.8 ± 0.2 and 3.3 ± 0.2 Mev. This activity has been produced in three ways, using separated isotopes of Ni. These are listed with the cyclotron and particle energies used as follows:

$Ni^{60}(p, n)$	37-in. frequency-modulated cyclotron	5–15 Mev p
	60-in. cyclotron	9 Mev p (18 Mev H_2^+)
$Ni^{60}(d, 2n)$	60-in. cyclotron	18 Mev d
$Ni^{58}(\alpha, pn)$	60-in. cyclotron	36 Mev α.

In the 37 in. frequency-modulated cyclotron the Ni^{60} sample was mounted on a probe, and hence could be bombarded at an arbitrary distance from the cyclotron center. The threshold energy observed for the $Ni^{60}(p, n)$ reaction was 5.1 ± 0.2 Mev.

The decay of the activity was observed with an ionization chamber and Ryerson-Lindemann electrometer. By exciting the activity in a Ni^{60} target with 5.5-Mev protons, the decay could be measured through six half-lives with no evidence of a foreign activity. That the particles emitted were positrons was determined by bending them in a magnetic field into a counter. Penetrating γ-radiation was also observed.

Chemical separation of normal nickel targets after bombardment with 15-Mev and 6-Mev protons into Cu, Ni, and Co fractions, accomplished within one hour, showed in each case that more than 99 percent of the 24.6-minute activity followed the Cu-separation chemistry. Mass separation in a calutron, accomplished within one hour of the end of a proton bombardment, showed without question that this activity belonged to Cu^{60}.

The energy of γ-radiation was measured by absorption in lead. The absorption of Co^{60}, 1.1-and 1.3-Mev γ-radiation was used for calibration of the geometry which was similar to that of Cork and Pidd.[1] The absorption coefficient in lead for the γ-radiation of Cu^{60} decay was measured as 0.546 ± 0.013 cm^{-1}, corresponding to an energy of 1.50 ± 0.05 Mev.

From consideration of the (p, n) threshold energy a positron group of energy 1.8 Mev is expected to accompany the γ-radiation, with the possibility of a second group with energy 3.3 Mev providing a transition directly to the ground state. Rough data of absorption in aluminum are consistent with this expectation. The determination of the lower energy end point is made difficult by the presence of the higher energy group. The branching ratio of the 3.3-Mev positron group is less than 0.05.

The 81-second and 7.9-minute positron activities produced by proton bombardment of Ni, observed by Delsasso, *et al.*,[2] and tentatively assigned to either Cu^{58} or Cu^{60}, correspond to 81-second and 10-minute activities after bombarding Ni^{58} with protons in the 37-in. cyclotron. These are tentatively assigned to Cu^{59} and Cu^{58}, respectively, on the basis of threshold and excitation considerations. The longer life was shown to be a Cu activity by chemical separation. The 3.4-hour half-life activity assigned[3] to Cu^{61} was verified by being produced in a Ni^{61} (p, n) reaction. The 10.5-minutes half-life activity assigned[4] to Cu^{62} was also verified, but the half-life was found to be 10.1 ± 0.1 minutes in measurements made through six half-lives.

Acknowledgment is due Dr. E. H. Huffman and Robert Lilly of the Radiation Laboratory for the chemical separations. R. E. Butler contributed to the early research, and

the mass separations on the calutron were performed by Keith Pierce.

This paper is based on work performed under Contract No. W-7405-eng-48, with the Atomic Energy Commission in connection with the Radiation Laboratory, University of California.

[1] J. M. Cork and R. W. Pidd, Phys. Rev. **66**, 227 (1944).
[2] Delsasso, Ridenour, Sherr, and White, Phys. Rev. **55**, 113 (1939).
[3] L. N. Ridenour and W. J. Henderson, Phys. Rev. **52**, 889 (1937).
[4] F. A. Heyn, Physica **4**, 1244 (1937).

The Latitude Effect of the Hard Component as a Function of Altitude

PIARA SINGH GILL,* MARCEL SCHEIN, AND VICTOR YNGVE
Department of Physics, University of Chicago, Chicago, Illinois
September 3, 1947

EIGHT counter-coincidence sets were installed in a B-29 plane for the purpose of measuring the vertical intensity of the penetrating component through 8, 14, and 20 cm of lead, and for studying the production of mesotrons by non-ionizing rays in 2 cm of lead. The measurements were made up to an altitude of 40,000 feet at a geomagnetic latitude of 40° N and at the equator. The geometry of the counters is shown in Fig. 1. The upper three and the lower three counters were each connected in a threefold coincidence. This arrangement is very similar to that used by Schein, Jesse, and Wollan.[1] The coincidence circuits had a resolving time of 5×10^{-6} second. As a consequence, accidentals were negligible at all altitudes reached. The upper coincidence set registered particles passing through 20 cm of Pb, while the lower one recorded particles through 22 cm of Pb, plus those produced by non-ionizing radiation in the upper 2 cm of Pb. All coincidence pulses were recorded on a rotating film. This paper deals only with the data obtained with 20 and 22 cm of Pb. The quantitative measurements with smaller thickness of lead will be reported at a later date.

It was found that at altitudes up to 40,000 ft. the upper and lower threefold coincidence set gave the same counting rate within a precision of 3 percent. It should be mentioned here, however, that this was not the case with smaller thicknesses of lead between the counters. In particular, with a lead absorber of 8-cm thickness a considerably higher counting rate was registered in the lower threefold set than in the upper one at altitudes above 25,000 feet. This leads to the conclusion that a considerable fraction of the penetrating particles produced by non-ionizing rays is capable of traversing 8 cm, whereas it is absorbed by 22 cm of Pb. Since most of the particles passing through large thicknesses of lead were found to be mesotrons, it follows that in the upper 2 cm of Pb only mesotrons of momenta smaller than 3.8×10^{8} ev/c are produced with a large cross section by non-ionizing radiation. This result is in agreement with data obtained in balloon experiments[2] up to an altitude of 80,000 ft.

In Fig. 1, curves *A*, *B*, and *C* represent the latitude effect of the hard component as a function of altitude. Curve *A* refers to the equator, curve *B* to a geomagnetic latitude of

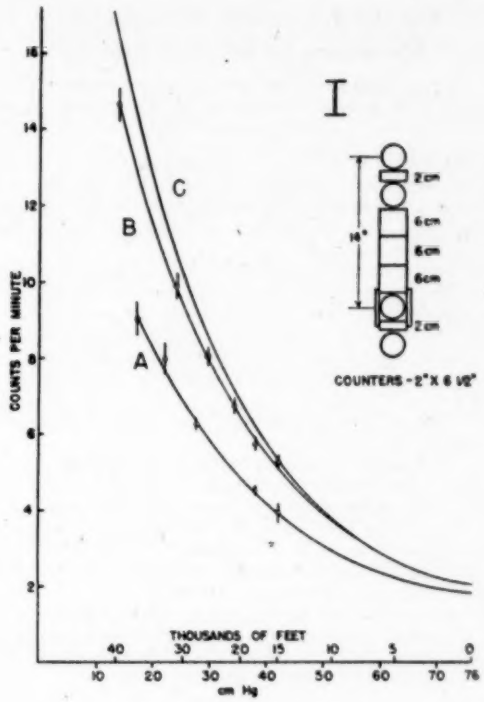

FIG. 1.

40° N, and curve *C* to balloon data obtained at 52° N by using 18 cm of Pb between the counters.[3] The curves show very clearly that the latitude effect of the hard component increases very considerably with elevation. At 33,000 ft. the difference between 40° N and 0° is 30 percent, which is in satisfactory agreement with recent measurements of Swann.[4] On the other hand, Bhabha and his collaborators[5] found a somewhat smaller latitude effect. This might be due to the fact that the latitude curves given in their paper were deduced from experiments in which the geometry of the counter assembly was not the same at the various latitudes.

It is obvious from Fig. 1 that the difference between curves *C* and *B* is considerably smaller than the corresponding difference between *B* and *A*. This fact strongly indicates that the large majority of the mesotrons present at altitudes below 35,000 ft. are produced by primaries of energies considerably higher than 5×10^{9} ev (magnetic cut-off energy at 40°).

We wish to express our sincere appreciation to Dr. Urner Liddel from the office of Naval Research for his valuable assistance in securing a B-29 plane. We are also greatly indebted to Commander Bollay for his cooperation during the flights and to Major Boyse for piloting the plane.

* Now at the Tata Institute of Fundamental Research, Bombay, India.
[1] Marcel Schein, William P. Jesse, and E. O. Wollan, Phys. Rev. **57**, 847 (1940).
[2] Marcel Schein and D. J. Montgomery, *Problems in Cosmic Ray Research* (Princeton University Press, Princeton, New Jersey, 1946).
[3] Marcel Schein and F. A. Allen, private communication.
[4] W. F. G. Swann and Peter A. Morris, Phys. Rev. **71**, 462 (1947).
[5] Bhabha, Chandrashekhar Aiya, Hoteko, and Saxena, Phys. Rev. **68**, 147 (1945).

On the Production of Cosmic-Ray Mesotrons by Primary Protons*

MARCEL SCHEIN AND J. STEINBERGER
Department of Physics, University of Chicago, Chicago, Illinois
September 3, 1947

CALCULATIONS have been made on the difference between the number of mesotrons in the vertical direction at a geomagnetic latitude 40° N, and the number at the equator, as a function of altitude, on the basis of the following assumptions:

(1) The primary particles producing mesotrons are protons. The cut-off energies for vertically moving protons for geomagnetic latitude 40° and 0° are 6 and 16, respectively. Here, and in what follows, the rest mass is included, and proton energies E are given in units of the proton rest mass, mesotron energies ϵ in units of the mesotron rest mass.

(2) The differential energy spectrum of the primary protons is $(E-1)^{-2.8}$.

(3) The mesotrons are produced at a height X_0 by the collision of a primary proton with a nucleon.

(4) This collision, when viewed in its center of mass system, results in a complete stopping of the nucleons, and in the emission of N mesotrons of equal energy, uniformly distributed in space. N is assumed to be constant in the energy range between 6 and 16.

By using (4) and performing a relativistic transformation, it follows that the energy of the mesotrons produced by a primary proton of energy E will be initially distributed uniformly between the two limits:

$$\epsilon=\epsilon_0\pm\epsilon_0\left(\frac{E-1}{E+1}\right)^{\frac{1}{2}}\left[1-\frac{N^2\mu^2}{4M^2}\frac{1}{\left(\left(\frac{E+1}{2}\right)^{\frac{1}{2}}-1^2\right)}\right]^{\frac{1}{2}},$$

$$\epsilon_0=\frac{M}{N\mu}\{E+1-[2(E+1)]^{\frac{1}{2}}\}.$$

μ is assumed to be 200 times the mass of the electron. M is the proton mass.

In the calculations for primary energies between 6 and 16, the lower limit was approximated by 0 and the upper limit by $2\epsilon_0$.

According to Hamilton, Heitler, and Peng,[1] the number of mesotrons of energy ϵ at height x can be written as follows:

$$f(\epsilon, x)=\left(\frac{\epsilon}{X}\right)^{10.7/\epsilon+x}\int_0^x S(\eta, \xi)\left(\frac{\eta-\xi}{\xi}\right)^{-10.7/\eta}d\xi. \quad (1)$$

In this expression, 2×10^{-6} sec. was used for the lifetime of the mesotron at rest.

$S(\epsilon, x)$ is the expression for the number of mesotrons of energy produced at height x. In our case

$$S(\epsilon, X)=\frac{\mu}{M}\frac{N^2}{2}\int_{E_{\min}}^{16}\frac{(E-1)^{-2.8}}{E+1-[2(E+1)]^{\frac{1}{2}}}dE\delta(X-X_0), \quad (2)$$

where $E_{\min}$ is either 6, or $\frac{\mu N}{2M}\epsilon\left[\left(\frac{\mu N}{M}\right)\epsilon+1\right]^{\frac{1}{2}}$, depending on which one is the greater quantity, and X_0 is the height of the mesotron producing layer. $\delta(X-X_0)$ is a Dirac delta-function.

On substituting (2) into (1) we obtain:

$$f(\epsilon, X)=\left[\frac{X_0\epsilon}{(\epsilon+X-X_0)X}\right]^{10.7/\epsilon+X}\times\frac{N^2\mu}{2M}\int_{E_{\min}'}^{16}\frac{(E-1)^{-2.8}dE}{E+1-[2(E+1)]^{\frac{1}{2}}}, \quad (3)$$

where $E_{\min}'$ is either 6 or

$$\frac{\mu}{M}\frac{N}{2}(\epsilon+X-X_0)+\left[\frac{\mu N}{M}(\epsilon+X-X_0)+1\right]^{\frac{1}{2}},$$

depending on which one is the greater quantity.

The unit of distance X is that distance in which a mesotron loses an energy μc^2 by ionization.

Finally, by using (3), the total number of mesotrons capable of penetrating 20 cm of lead at a height X is given by:

$$I(X)=\int_4^{\infty}f(\epsilon, X)d\epsilon.$$

$I(X)$ has been calculated numerically for several values of N and X_0. The results, normalized to the experimental data of Gill, Schein, and Yngve,[2] at $X=4$ (138-mm Hg), are reproduced in Fig. 1 and Table I.

Figure 1 shows that the theoretical curve for $X_0=0.6$ (2-cm Hg) and $N=5$ is in satisfactory agreement with the experimental curve over the atmosphere between 35,000 feet and sea level.

The theoretical value of $X_0=0.6$ for the average altitude where mesotrons are produced corresponds to a cross section, ϕ, for multiple mesotron production of 5.8×10^{-25}

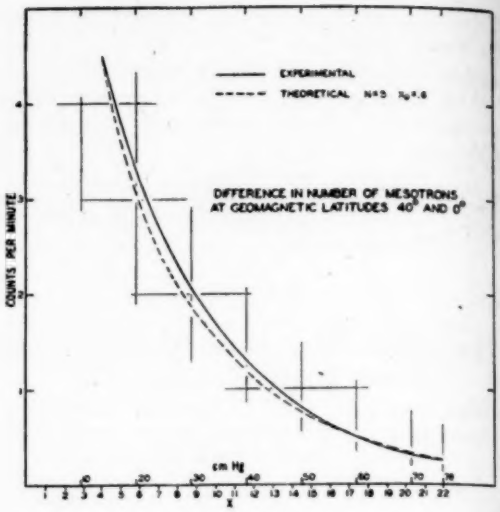

FIG. 1.

TABLE I. Shows that the values $N=5$, $X_0=0.3$ result in too large a latitude effect at sea level; the value $N=6$ gives too small a latitude effect at the lower altitudes.

	Number of counts per minute				
X	Experiment	$N=5$ $X_0=0.3$	$N=5$ $X_0=0.6$	$N=6$ $X_0=0.3$	$N=6$ $X_0=0.6$
4	4.5	4.5	4.5	4.5	4.5
8	2.31	2.22	2.07	1.88	1.66
12	1.22	1.25	1.10	0.95	0.80
17	0.53	0.64	0.53	0.40	0.31
22	0.25	0.30	0.25	0.13	0.11

TABLE II. $\frac{\text{(Total number of primaries of energy between 6 and 16)}}{\text{(Number of mesotrons at sea level at geom. lat. 40°N)}}$.

N	X_0	
5	0.3	6.8
5	0.6	4.08
6	0.3	8.34
6	0.6	4.61

cm² per air nucleus. This is in rough agreement with the experimental results on mesotron production in paraffin.[3] The normalization also determines the number of protons in the energy range 6 to 16 which produce mesotrons. Table II gives the ratio of these protons to the hard component at sea level.

* This work was supported in part by Navy Contract N6-ori-20, Task Order 18.

[1] J. Hamilton, W. Heitler, and H. W. Peng, Phys. Rev. 64, 78 (1943).
[2] P. S. Gill, M. Schein, and V. Yngve, Phys. Rev. 72, 733 (1947).
[3] M. Schein and D. J. Montgomery, *Problems in Cosmic Ray Physics* (Princeton University Press, Princeton, New Jersey, 1946).

On the Generation in Paraffin of Ionizing Penetrating Particles by a Neutral Component of the Cosmic Radiation

CARMELO MILONE AND VANNA TONGIORGI*
Institute of Physics, University of Catania, Catania, Italy
August 18, 1947

DE Vos and du Toit[1] have recently found at sea level, with the counter-set drawn in Section *a* of Fig. 1, a ratio $R=1.03$ between the threefold coincidences $A+B+C$, recorded with a paraffin layer 1.3 cm thick in π, and the ones recorded with the same layer in π'. In their opinion the effect is outside the experimental uncertainty, and the increase in the frequencies when paraffin is in π is due to the generation in the paraffin layer of mesons or protons by some neutral component of the cosmic radiation.

This result is very interesting, because experiments[1,2] like the above-mentioned, performed at sea level also, but with layers of lead instead of paraffin, did not show the same effect; therefore one is compelled to think of a particular phenomenon characteristic of the low atomic number materials.

In order to look into this point the following experiments were performed:

Series 1: (see Section *b* Fig. 1) with the telescope *ABCD* arranged under a thin deck (0.5-cm wood), the fourfold coincidences $A+B+C+D$ were recorded with 2 cm of paraffin alternatively in π and in π'. (Counter surface: 4×40 cm², counter walls: 1-mm brass, resolving time of the recording apparatus: 2.10^{-5} sec.) The penetrating particles were selected by 12.5-cm Pb and the side showers stopped by 5-cm Pb around the counters *D*.

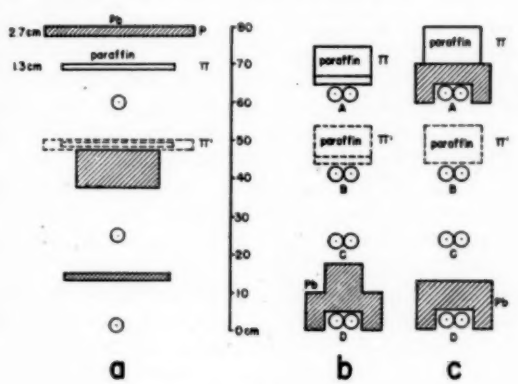

FIG. 1.

As the Table (series 1) shows, no changes in frequencies were recorded by changing the position of the paraffin.

TABLE I. Measurements on the generation of ionizing particles by a neutral component of cosmic rays.

Series	Lead coinc.	Lead min.	Lead coinc./min.	Paraffin coinc.	Paraffin min.	Paraffin coinc./min.	Ratio R
1	69,172	7836	8.827 ±0.034	61,016	6922	8.815 ±0.036	1.0013 ±0.0080
2	43,205	4940	8.746 ±0.042	45,792	5358	8.546 ±0.040	1.023 ±0.010
3	71,394	8225	8.680 ±0.033	68,708	7881	8.718 ±0.034	0.995 ±0.008
4	61,655	7784	7.922 ±0.033	66,219	8338	7.942 ±0.031	0.997 ±0.008

Series 2: counters and screens as in series 1, but paraffin layer: 10 cm.

As it appears in the Table (series 2), a ratio $R=1.02 \pm 0.01$ was found in this case.

Series 3: with the arrangement drawn in Section *c* of Fig. 1, we tried to test whether or not the result of series 2 was a real effect, or a spurious one caused by soft secondary particles generated in the paraffin while in π; such particles could give rise to spurious coincidences in association with penetrating particles hitting only counters *B*, *C*, and *D*. This possibility was removed by arranging a screen of lead 5 cm thick around the counters *A* (paraffin layer: 10 cm).

As the Table (series 3) shows, in this case we found $R=1$ within the experimental uncertainty, which indicates that the positive result of series 2 was really caused by such a spurious effect.

Series 4: In order to make our data more comparable with De Vos and du Toit's result, we performed a last experiment arranging above the counter-set used in series 3 a layer of 2.5-cm Pb, like that (2.7 cm) placed above the counter-set in De Vos and du Toit's experiment (see Fig. 1a).

In this case also no changes in frequencies were recorded when the position of the paraffin was changed (see Table: series 4).

We think our experimental arrangements (series 3 and 4) afford the following advantages with regard to De Vos and du Toit's experiment: (a) screening against side showers (Pb screens surrounding *D* and *A*); (b) removal of soft secondary particles generated in the materials above the telescope (Pb screen surrounding *A* and shapes of paraffin layers so chosen to cover only the solid angle of the telescope); (c) large efficient surface of the telescope and therefore short recording times (our frequencies were about 17 times larger than De Vos and du Toit's); and (d) statistical errors in every series about one-half the error in the result of the above-mentioned observers.

The results obtained compel us to point out that our experiments do not confirm the effect found by De Vos and du Toit, both for thin and thick paraffin layers. Therefore we reach the conclusion that, at sea level, the phenomena of generation in paraffin of penetrating ionizing

particles by neutral radiation are not detectable, or, in any case, their amount is less than ~1 percent.

A fuller discussion of these experiments will be found elsewhere.[3]

We wish to emphasize that our negative conclusion about generation in paraffin of penetrating particles by neutral radiation refers only to experiments performed at sea level. In higher stations, the generation of penetrating particles in low atomic number materials seems to have been found by several experimenters.[4]

* Now at the Laboratory of Nuclear Studies, Cornell University, Ithaca, New York.

[1] P. J. G. De Vos and S. J. du Toit, Phys. Rev. **70**, 229 (1946).
[2] Rossi, Janossy, Rochester, and Bound, Phys. Rev. **58**, 761 (1940).
[3] C. Milone and V. Tongiorgi, Nuovo Cimento, in press.
[4] D. K. Froman and J. C. Stearn, Phys. Rev. **54**, 969 (1938); M. Schein, M. Jona, and J. Tabin, Phys. Rev. **64**, 253 (1943); O. Salo and G. Wataghin, Phys. Rev. **67**, 55 (1945).

Energy Levels of O^{17} Obtained from $O^{16}(d, p)O^{17}$ and $N^{14}(\alpha, p)O^{17}$

ERNEST POLLARD AND PERRY W. DAVISON
Sloane Physics Laboratory, Yale University, New Haven, Connecticut*
August 25, 1947

THE measurement of nuclear energy change (Q) values in transmutation experiments enables the positions of deep nuclear levels to be observed. These levels are not yet explained and there is some question as to whether they are characteristic of the reaction process or of the product nucleus. In any event, the observation of the same levels in different reactions is of interest.

The nucleus O^{17} can be formed in the $O^{16}(d, p)O^{17}$, $F^{19}(d, \alpha)O^{17}$, and $N^{14}(\alpha, p)O^{17}$ reactions. The first has been studied by Cockcroft and Lewis, and Guggenheimer, Heitler, and Powell,[1] the second by Burcham and Smith,[2] and the third by Haxel.[3] A well-defined group occurs for the ground state (Q_0) value for the first two reactions and the first excited state (Q_1) is clearly found at about 0.85-Mev excitation in both cases. The third reaction does not show the presence of an excited state at 0.85 Mev in previous work. Since the geometry of natural source work is rather poor, we have studied the $N^{14}(\alpha, p)$ reaction using cyclotron alpha-particles and good geometry. In order to remove systematic errors, we have also studied the $O^{16}(d, p)O^{17}$ reaction using the same absorption cell.

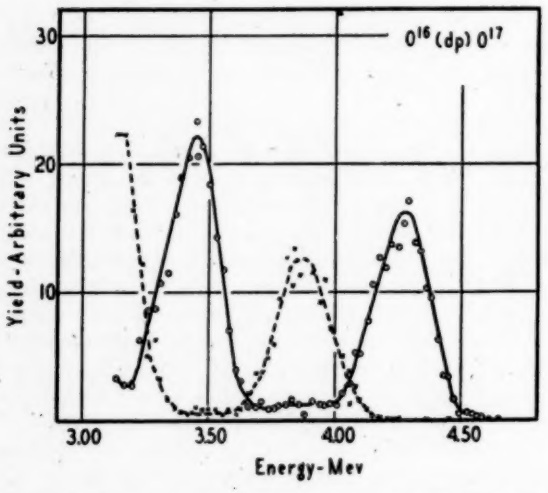

FIG. 1. Yield of protons plotted against energy from $O^{16}(d, p)O^{17}$, using a high counter bias to give differentiation. Two groups are present. The dotted curve is for a reduced bombarding energy. The same groups appear, but with a different relative yield.

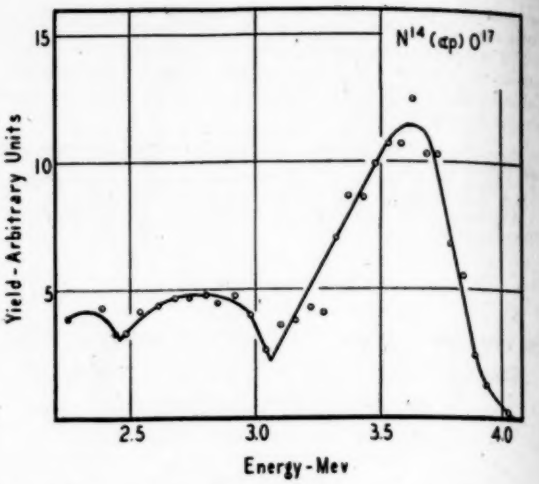

FIG. 2. Yield of protons plotted against energy from $N^{14}(\alpha, p)O^{17}$. Two groups appear corresponding to the same excitation level as found in the reaction of Fig. 1.

The results of the bombardment of oxygen by deuterons of two energies are shown in Fig. 1. It can be seen that the two proton groups are clearly resolved. The ratio of the yields changes as the bombarding energy changes, there being less relative yield in the excited state as the bombarding energy increases. Table I shows the ratio at four energies, the highest being taken from the paper of Guggenheimer, Heitler, and Powell, the lowest, Cockcroft and Lewis, and the other two from our new data. The ratios found by Burcham and Lewis for the (d, α) reaction and our own figures for the (α, p) reaction are included.

TABLE I.

Beam energy	0.575	2.9	3.3	6.2	(d, α)	(α, p)
Ratio yield of Q_1 to Q_0	2.28	1.87	1.43	0.94	1.00	0.3

The alpha-particle bombardment of nitrogen gave the results of Fig. 2. The target was urea. The beam homogeneity is rather worse for alpha-particles, and the yield is less. Nevertheless, two groups of energy 3.93 and 3.15 are present, corresponding to Q-values of -1.31 Mev and -2.12 Mev. The ratio of yields is about 0.3.

We find for the reaction $O^{16}(d, p)O^{17}$, $Q_0 = 1.75$, $Q_1 = 0.89$, difference 0.86 Mev, for $N^{14}(\alpha, p)O^{17}$, $Q_0 = -1.31$, $Q_1 = -2.12$ Mev, difference 0.81 Mev. The two are identical within the experimental error.

The reaction process clearly influences the relative yield as the excited-state group in the (α, p) reaction is one-third as prolific as in the (d, p) or (d, α) reaction. Bombardment by alpha-particles seems to be similar to high energy deuteron bombardment.

A third group of $Q-2.90$ Mev appears in the (α, p) reaction. This perhaps may be due to a second excited state in O^{17}, but other explanations, notably scattered deuterons or $N^{14}(\alpha, d)O^{16}$, are possible.

* Assisted by the Office of Naval Research under Contract N6ori-44.
[1] J. D. Cockcroft and W. B. Lewis, Proc. Roy. Soc. A130, 463 (1936); K. M. Guggenheimer, H. Heitler, and C. F. Powell, Proc. Roy. Soc. A190, 196 (1947).
[2] W. E. Burcham and C. L. Smith, Proc. Roy. Soc. A168, 176 (1938).
[3] O. Haxel, Zeits. f. Physik 93, 400 (1935).

A Note on the Paper "Second Quantization and Representation Theory"[1]

V. Fock
Academy of Sciences of the U.S.S.R., Moscow, U.S.S.R.
April 10, 1947

IN a recent number of this journal[1] Dr. E. M. Corson published a paper with the above title. On examination this paper turns out to bear a striking resemblance to a paper of mine[2] entitled "Konfigurationsraum und Zweite Quantelung," which was published in 1932. Without exception, all of the results which Dr. Corson finds are contained in my paper. There is a close parallelism not only between the formulas, but also between the texts of the two papers.

Through the courtesy of the editor I have had the opportunity of seeing a copy of the letter by Dr. Corson which follows this one, in which he explains that his paper was intended to be expository in nature. It is singularly unfortunate that he neglected to state this in his paper, and also that he neglected to state the source of the material used. My paper was quoted by Dr. Corson, but only in connection with a trivial identity, and no indication was given of the dependence of his paper on my reasoning and on my results.

IN a recent communication from Professor Fock, which has been brought to my attention, Professor Fock points out that my recent article on second quantization is similar in content to his paper in *Zeits. f. Physik* **75**, 622 (1932).

I should like to explain that my paper was intended to be expository in nature. I regret that this aim was not brought out clearly, because of insufficient reference to earlier publications on second quantization. In particular, inadequate acknowledgment was made of the debt to Professor Fock's article, whose general plan my exposition followed, and from which several examples were adapted.

The author sincerely hopes that his work, far from detracting from the credit which is due Fock, will rather serve to direct attention to the very important contribution Fock has made in this field.

E. M. Corson,
The Institute for Advanced Study, Princeton, New Jersey,
June 26, 1947

[1] E. M. Corson, Phys. Rev. **70**, 728 (1946).
[2] V. Fock, Zeits. f. Physik **75**, 622 (1932); *ibid.* **76**, 852 (1932).

Proceedings of the American Physical Society

Minutes of the Meeting at Stanford University, California July 11–12, 1947

ONE of the largest Pacific Coast meetings in the history of the American Physical Society was its 280th, held at Stanford University on Friday and Saturday, July eleventh and twelfth, 1947. Most of the sessions were held in the beautiful Education Auditorium, which was admirably suited (for this meeting) in size and facilities. The Department of Physics at Stanford University, ably led by Dr. Paul Kirkpatrick, at one time Local Secretary for the Pacific Coast, did an outstanding job in arranging for the reception and entertainment of the large number of physicists who attended. All of the sessions were well attended. The maximum attendance at any one session was about 350. Representatives of the press were present in unusually large numbers, and the director of public information of Stanford University was very effective in establishing good press relations. The help of the public information representative from the University of California, in connection with releases of news from the Radiation Laboratory, is acknowledged. It was felt by many that this meeting was marked by excellent publicity in newspapers and magazines.

It is interesting to note that many Eastern physicists were present at this meeting, and a number of them participated in the program. The meeting was also distinguished by the presence of President L. A. DuBridge, and Dr. K. K. Darrow, Secretary of the American Physical Society. The invited papers were excellent, and the symposium on underwater sound, arranged by Dr. Carl Eckart, added greatly to the success of the meeting. Dr. Henry Margenau substituted for Dr. L. B. Loeb as chairman of this symposium. The chairmen at the other meetings were Paul Kirkpatrick, L. A. DuBridge, K. K. Darrow, and J. Kaplan.

J. Kaplan
Local Secretary for the Pacific Coast,
University of California,
Los Angeles, California

Symposium on Underwater Sound

Sounds in the Ocean. Vern O. Knudsen, *University of California, Los Angeles.*

Reverberation in the Sea. Carl F. Eyring, *Brigham Young University.*

Transmission of Sound in the Sea. R. W. Young, *U. S. Navy Electronics Laboratory, San Diego.*

Coherence of Scattered Sound. Carl Eckart, *University of California (Marine Physical Laboratory).*

Fluctuation of Transmitted Sound. Peter G. Bergmann, *National Research Council (Research Analysis Group).*

Invited Papers

Nuclear Radiospectroscopy. Felix Bloch, *Stanford University.*

Some Applications of Microwaves to Physics. J. C. Slater, *Massachusetts Institute of Technology.*

Cosmic Rays. R. B. Brode, *University of California at Berkeley.*

Contributed Papers

A2. Conservation of Momentum in the Disintegration of Li^8. I. W. A. Fowler, C. C. Lauritsen, and T. Lauritsen, *California Institute of Technology.*—Apparatus[1] for the introduction of radioactive materials into a cloud chamber has been employed to investigate the conservation of momentum in the β-decay of Li^8 to Be^8, which subsequently breaks up into two α-particles. The projection on the plane of measurement of the angle between the two α-particles is a measure of one component of the recoil momentum of the Be^8. Additional information is obtainable from the momentum of the electron but relatively few cases occur where both α-particles and the electron are in the plane of the cloud chamber. The Li^8 is produced by bombarding with deuterons a thin deposit of LiOH on beryllium or gold foils. The mean square of the observed momenta relative to the maximum possible momenta were 0.247 (Be foil) and 0.349 (Au foil). Corrected for scattering these become 0.204 ± 0.025 and 0.184 ± 0.034, respectively, with an average value of 0.197 ± 0.020, the probable errors quoted being statistical in origin. It will be noted (see next abstract) that the mean square momentum is twice that obtained taking into account only the emitted electrons and approximately equal to that calculated for an electron and neutrino emitted with no preferred angle of ejection between them ($\alpha=0$).

[1] T. Lauritsen, W. A. Fowler, and C. C. Lauritsen, Phys. Rev. 71, 275 (1947).

A3. Conservation of Momentum in the Disintegration of Li^8, II. E. Richard Cohen and R. F. Christy, *Cali-*

fornia Institute of Technology.—Calculations in connection with the experiment of Fowler, Lauritsen, and Lauritsen on the recoil of Be^8 will be presented. The recoil momenta were normalized to the maximum recoil consistent with conservation of energy. The Fermi distribution was used for the electron energy. Distributions of recoil momentum and the corresponding mean squares were calculated for various angular correlations of electron and neutrino.

Angular correlation of electron and neutrino	$\overline{p^2}$	$\overline{p_\perp{}^2}$
Anti-parallel	1/7	1/21
Electron only	2/7	2/21
$1+\alpha\cos\theta(-1<\alpha<1)$	$(4+\alpha)/7$	$(4+\alpha)/21$
Parallel	7/7	7/21

The mean square of one component assumes no correlation of the α-particle and recoil directions. This is certainly true if the excited state of Be^8 has $J=0$ as suggested by Wheeler's analysis of $\alpha-\alpha$ scattering. Alternatively it is also true if the β-decay is allowed but unfavored as suggested in Konopinski's review article. Reasons for preferring the latter explanation will be presented. The evaluation of scattering corrections will also be discussed. This work (I and II) was carried on under contract with the Office of Naval Research.

A4. Gamma-Radiation from Be^9+H^1. C. C. LAURITSEN, T. LAURITSEN, AND W. A. FOWLER, *California Institute of Technology.*—Further investigations have been made of the resonances in the production of gamma-radiation by bombarding Be^9 with protons. Employing an electrostatic analyzer, the narrow resonance at 1060 kev has been found to have a width of 3 kev when corrections are made for target thickness (3 kev) and the spread in energy of the beam (<1 kev). No resolution of the broad resonance at 972 kev has been found and the width at half-maximum is 95 kev. Measurements of the absorption of electron secondaries using coincidence counters indicate maximum ranges in aluminum of 14 mm at 972 kev and 12.5 mm at 1060 kev. The corresponding gamma-ray energies are 7.5 ± 0.1 and 6.7 ± 0.2 Mev. Evidence has also been obtained for soft radiation of energy between 0.5 and 1.0 Mev at the 1060-kev resonance and it is assumed that the transition to the ground state of B^{10} from the compound state produced in the reaction is a double one through an excited state of B^{10} at 0.8 ± 0.3 Mev, evidence for which has been obtained before.[1] This work was carried on under contract with the Office of Naval Research.

[1] Bonner and Brubaker, Phys. Rev. **50**, 308 (1936).

A5. Proton Scattering from Be^9. SYLVAN RUBIN, *California Institute of Technology.*—The angular distribution of protons scattered from a thin beryllium foil has been measured in the energy range 840 to 1110 kev, using a photographic-type scattering camera, to investigate the effect of the two γ-ray resonances of $Be^9(p,\gamma)B^{10}$ at 972 and 1060 kev. The data include the elastically scattered protons; the deuterons from $Be^9(p,d)Be^8$; and the alphas from $Be^9(p,\alpha)Li^6$. The ratio of observed yield to Coulomb scattering increases with scattering angle to a factor of 12, at 160° for 1060 kev, and to smaller values at lower or higher energy. The yield in addition to Coulomb scattering, on the other hand, decreases with scattering angle to a roughly constant value at each energy at large angles. This increased yield cannot be due to the alphas, which are about 20 percent of the total yield at 1060 kev, at 90°. The behavior of the yield in addition to Coulomb scattering indicates probable interference effects with the Coulomb scattering at small scattering angles, where they are of equal magnitude, and is evidence for this yield being resonance scattered protons. The relation of this data to the γ-ray resonances is being studied. This work was carried on under contract with the Office of Naval Research.

A6. Some Operating Phenomena Associated with the 184-Inch Cyclotron. D. C. SEWELL, L. HENRICH, AND J. VALE, *University of California at Berkeley.*—Two experiments have been performed on the 184-inch cyclotron which give a better understanding of the operation of a frequency modulated cyclotron.

First, to explain the disappearance of the beam at the radius of 82 inches several radio autographs of specially constructed probes were made. They show that the vertical height of the beam increases rapidly near the 82 inch radius, where the value of n is approximately 0.2 ($n=-(r/H)(dH/dr)$; r=radius, H=vertical component of the magnetic field). At this value of n a coupling exists between the radial and vertical oscillations of the ions which appears to be strong enough to cause the energy of the radial oscillations to be converted into the energy of vertical oscillations, thus causing the beam to be intercepted by the dee at the 82-inch radius. Second, a number of studies have been made using a synchroscope to observe the time structure of the beam current collected by the probe. The multiple pulse nature of each beam pulse seems to be explained by the radial oscillations of the beam. These oscillations are caused by the precession of the center of rotation of the ions about the true center of the system. This paper is based on work performed with the support of the Atomic Energy Commission.

A7. Cloud Chamber Study of the Particles in the Neutron Beam of the 184-Inch Cyclotron. WILSON M. POWELL, *University of California at Berkeley.*—Recoil protons and disintegrating atoms in oxygen, nitrogen, helium, and carbon appear in cloud chamber photographs made in the neutron beam from 200 million electron volt deuterons. Frequently oxygen splits up into four doubly charged particles which may be alpha-particles. In some cases a large part of the energy of the neutron appears in one of the star particles. An attempt has been made to discover the maximum energy of the neutrons in the neutron beam by observing the maximum energy of the recoil protons. Some of the protons show energies far in excess of the maximum of 120 Mev expected. The cloud chamber is 16 inches in diameter with a magnetic field of 10,000 oersteds. This paper is based on work performed with the support of the Atomic Energy Commission.

A8. Transmutations with High-Energy Deuterons in the 184-Inch Cyclotron. B. B. CUNNINGHAM, H. H. HOPKINS, M. LINDNER, D. R. MILLER, P. R. O'CONNOR, I. PERLMAN, G. T. SEABORG, AND R. C. THOMPSON, *University*

of California at Berkeley.—The successful operation[1] of the Berkeley 184-inch cyclotron to produce useful beams of deuterons and helium ions of approximately 200 and 400 Mev, respectively, has made possible the radiochemical identification of many of the transmutation products of nuclei excited to very high energies. Products with atomic numbers considerably lower than that of the target were observed in every case. Thus, with 200-Mev deuterons on $_{33}As^{75}$, activities were found representative of all elements from $_{34}Se$ to $_{25}Mn$ with lower elements not excluded. Both negative beta-particle and positron (or orbital electron capture) activities are noted, indicating reactions both of multiple neutron ejection and multiple charged particle ejection. For instance, with deuterons on $_{51}Sb$ (isotopes 121 and 123) both 6.7-hour $_{48}Cd^{107}$ and 2.5-day $_{48}Cd^{115}$ were produced. For the formation of light isotopes, several different reactions are possible, since in most cases the products will not be shielded from formation through a chain of short-lived positron (or orbital electron capture) ancestors following the ejection of different combinations of neutrons and charged particles in the primary reaction. As an example from deuterons on copper, the formation of a new 8-hour iron positron emitter assigned to $_{26}Fe^{52}$ implies that four units of charge and thirteen of mass are lost in arriving at this product.

[1] W. M. Brobeck *et al.*, Phys. Rev. 71, 449 (1947).

A9. Transmutations with High-Energy Helium Ions in the 184-Inch Cyclotron. G. T. Seaborg, B. B. Cunningham, H. H. Hopkins, M. Lindner, D. R. Miller, P. R. O'Connor, I. Perlman, and R. C. Thompson, *University of California at Berkeley.* In continuation of the work reported in the previous abstract, uranium was bombarded with 400-Mev helium ions, and a wide range of activities was identified both in the heavy-element region and in the region of the fission products. Representative of the heavy isotopes observed were $_{88}Ra^{223}$ (AcX), $_{88}Ra^{224}$ (ThX), and $_{85}At^{211}$. The fission-product distribution is characterized by a much shallower dip between the maxima than occurs with slow-neutron fission, and the yields of the lightest among the observed fission-products are much higher. The various aspects of this work will be published more fully by the individual groups of investigators. This work and that reported in the previous abstract were performed with the support of the Atomic Energy Commission.

A10. Angular Distribution of Neutrons From Targets Bombarded by 190-Mev Deuterons. A. C. Helmholz, Edwin M. McMillan, and Duane Sewell, *University of California.*—When deuterons accelerated by the 184-inch synchro-cyclotron at Berkeley to an energy estimated at 190 Mev are allowed to strike a thin internal target, copious quantities of high energy neutrons are produced. These are found to be largely concentrated in a beam of about 10° half-width (total width at half maximum). The shape of this beam has been studied in some detail, using the activity induced in carbon disks by the reaction $C^{13}(n, 2n)C^{11}$ as a measure of the intensity; by this means a complete map of the beam is obtained with a single exposure, and the relatively high threshold of the reaction (20 Mev) automatically eliminates any background due to secondary or degraded neutrons below this energy. The targets used as neutron sources were of Be, Al, Cu, Mo, Sn, Ta, and Pb, all $\frac{1}{16}$ inch thick. The shape of the neutron beam is the same for all elements, being well represented by the function $I=(1+\alpha\theta^2)^{-1}$, where θ is the angle from the axis of the beam and α is a constant characteristic of the target. The half-widths, however, vary significantly from target to target, increasing roughly linearly with atomic number from 0.16 radian for Be to 0.21 radian for Pb. Both shape and half-widths are in good agreement with the theory of Serber (following abstract). This work was done with the support of the Atomic Energy Commission.

A11. Production of High Energy Neutrons by Stripping, I. Energy Distribution. R. Serber, *University of California at Berkeley.*—The narrow beams of high energy neutrons, described in the preceding abstract, which result from the bombardment of nuclei by high energy deuterons are for the most part produced by a process in which the deuteron passes near the edge of the nucleus, the proton strikes the nucleus and is stripped off, while the neutron misses the nucleus and continues with almost the velocity of the incident deuteron. The cross section for this process is $\sigma=\frac{1}{2}\pi RR_d$, where R is the nuclear radius, and $R_d=\frac{1}{2}/(M\epsilon_d)^{\frac{1}{2}}=2.1\times10^{-13}$ cm is the deuteron radius (M is the proton mass, ϵ_d the binding energy of the deuteron). Since for the high deuteron velocities involved the time required for the stripping is short compared to the period of the deuteron, the neutron emerges from the collision with its momentum unchanged. The momentum is, of course, the resultant of the momentum due to the center of mass motion, $P_0=(ME_d)^{\frac{1}{2}}$, and the momentum of its motion within the deuteron. Since the momenta of the neutron in the deuteron are for the most part smaller than $P_1=\sqrt{M\epsilon_d}$, one sees that the emergent neutrons will have energies mostly in the band $(P_0\pm P_1)^2/2M=\frac{1}{2}E_d\left[1\pm\left(\frac{\epsilon_d}{E_d}\right)^{\frac{1}{2}}\right]^2$, ($\frac{1}{2}E_d\pm20$ Mev).

B3. Nuclear and Molecular Information from Microwave Spectra. C. H. Townes, A. N. Holden, and F. R. Merritt, *Bell Telephone Laboratories.*—In addition to previously reported work[1] the spectra of $O^{16}C^{13}S^{34}$, $O^{16}C^{13}S^{32}$ and $Cl^{35}C^{13}N^{14}$ near 24,000 megacycles have been examined. Internuclear distances will be discussed. No quadrupole effects were observed for C^{13} or S^{34}. The quadrupole coupling ($eQ\partial^2V/\partial z^2$) of C^{13} in the above molecules cannot be greater than 0.5 mc, which further[2] supports a spin of $\frac{1}{2}$ for C^{13}. Coupling for S^{34} is less than 1 mc, indicating that zero spin is probable. An evaluation of $\partial^2V/\partial z^2$ may be obtained for heavy nuclei bonded in a molecule by one or two p bonds. In these cases the non-spherical p electron shell produces a very large $\partial^2V/\partial z^2$, other effects being negligible. Evaluation of $\partial^2V/\partial z^2$ and use of quadrupole coupling values[1] give the following quadrupole moments in units of 10^{-24} cm^2. $Cl^{35}=-0.067$, $Cl^{37}=-0.051$, $Br^{79}=0.21$, $Br^{81}=0.16$, $|S^{34}|\leq.001$. Quadrupole couplings can also be used with known

quadrupole moments to determine the importance of non-spherical p structures in molecular bonds.

[1] Townes, Holden, Bardeen, and Merritt, Phys. Rev. 71, 644 (1947).
[2] Jenkins, Washington Meeting Am. Phys. Soc., paper L12 (1947).

B4. Loading of Resonant Cavities by Electron Beams. WAYNE G. ABRAHAM, *Stanford University.*—The shunt impedance of a resonant cavity is changed when an electron beam is passed through it in the direction of the electric field, as for instance in resonators for velocity modulation tubes. In cavities with grids the reduction in shunt resistance is found to be greater than theory would predict on the basis of finite transit time, resulting in undesired losses. This anomalous "beam loading" has been shown experimentally to be due to two factors, each a result of secondary emission. The first is due to the absorption of energy by the secondaries before they leave the grid space. The second occurs under certain conditions because of multiplier action of electrons making successive transits of the grid space in a manner sometimes called "multipactor action." By the elimination of all secondary emission, the beam loading has been shown to agree with that predicted by transit time theory.

B5. Ultra-Short Duration Flash Radiographs. J. C. CLARK, *Los Alamos.*—The duration and nature of the bursts of x-rays produced by the high speed flash radiographic equipment described by Slack and Ehrke have been studied by radiographing a very thin strip of lead cemented to a piece of explosive of high detonation velocity as the detonation proceeds. Such radiographs show that bursts of x-rays varying in duration between 1 and 3 microseconds are produced and that they are, in general, multiple in character, indicating an interrupted or oscillatory type of discharge through the x-ray tube. For many purposes a single burst of x-rays of much shorter duration is desirable. By studying the method of initiation of a cold cathode, Slack type tube, a circuit has been assembled which operates satisfactorily at relatively low voltages (60–100 kv), producing a single x-ray burst of duration 10^{-7} second, as measured by the same timing method.

B6. Ultra-Fast Counters. S. H. NEDDERMEYER, *University of Washington.*—A device has been described[1] which is capable of measuring the time interval between two pulses to an accuracy of about 3×10^{-11} sec. Useful application of the existing instrument for the measurement of particle velocities could probably be made with a vacuum multiplier type counter having a multiplication factor in the vicinity of 5×10^{9} and an effective capacitance of 10 e.s.u. Variation in over-all transit time, possible delayed emission, and matching conditions for the line are important, apart from the multiplication factor itself. Some of the possibilities and difficulties will be discussed.

[1] Phys. Rev. 69, 702 (1946). Paper to be published in Rev. Sci. Inst. July (1947).

B7. The Measurement of Short Time Intervals. LUIS W. ALVAREZ, *University of California at Berkeley.*—Modern "spectrum analyzers" present on a cathode-ray tube the frequency spectrum of repeated video pulses. The same pattern could be shown for a single pulse if a number of tuned receivers were used with appropriate delay lines in their outputs. For the gaussian pulse from a 931 electron multiplier, the spectrum would be gaussian with large signal-noise ratio beyond 1000 mc.[1] Receiver gains could be adjusted to show an apparently flat spectrum from 0 to 1000 mc for a single pulse. Then if two pulses with amplitude ratio n occurred with time delay T, the spectrum would have the form $1+n\cos 2\pi fT$. (For $T=2\times10^{-9}$ sec., minima at 250 and 750 mc.) By observing this "interference pattern," one measures T. At frequency f, the phase shift of the pattern is $2\pi f\Delta T$, independent of T. (For $f=10^{9}$ c.p.s. and $\Delta T=10^{-10}$ sec., $\Delta\phi=36°$.) With receiver spacing Δf proportional to f, the minimum detectable ΔT is a constant fraction of T which can be 0.1 in practice. ($\Delta T=10^{-10}$ for $T=10^{-9}$.) Receiver bandwidth has no effect on ΔT, which is determined by f max. Measurement will be by analysis of photographs, but automatic methods could be devised. This work was done under the auspices of the Atomic Energy Commission.

[1] R. D. Sard, J. App. Phys. 17, 768 (1946).

B8. Corona from Water Drops. W. N. ENGLISH, *University of California at Berkeley.* (*Introduced by Leonard B. Loeb.*)—A capillary tube as used by Zeleny provides a liquid "point" in a point to plane corona gap and permits further investigation of the effects described by Macky for falling drops, by using positive and negative polarity. Photographic records of oscillograph pulses, and of the liquid point with and without argon flash lamp illumination make possible a study and interpretation of the effects in the light of recent corona theory.[1] In brief, the regular corona processes appear to be superimposed on effects due to the ejection of charged drops of liquid. With positive point and increasing voltage, three distinct regions are observed. In the first, streamer pulses are superimposed on "spray" pulses of about 1000 microseconds duration because of the ejection of very fine drops, as observed by Macky. At higher voltage, positive space charge due to streamers and burst corona so weakens the field at the point that ejection of liquid ceases and the drop becomes rounded and stable. At still higher voltage, the liquid surface is violently disrupted and large drops ejected which quickly wet the plane electrode. With a negative point, trichel pulses are observed, followed closely by "spray" pulses somewhat similar to those for positive point, with trichel pulses superimposed. These increase in frequency and, to some extent, in amplitude, just as for negative metal points, while the ejection of water and luminosity spreads over the end of the capillary. No stable region occurs.

[1] L. B. Loeb, Phys. Rev. 71, 712 (1947).

B9. Dust Electrostatics. JAMES W. HANSEN, *University of California at Berkeley.* (*Introduced by Leonard B. Loeb.*)—The apparatus used by Hopper and Laby to study the charge on oil drops has been redesigned to study the charge on dust particles in the size range of 50 to 1 micron in diameter. By this method photographs of a large number

of tracks can be obtained, allowing the use of statistical methods in determining relationships. Using sulfur dust in a sulfur coated tube and finely ground quartz in a quartz tube, it has been shown that a dust can become highly charged by frictional contact with a surface of the same material. Charges of both signs exist simultaneously in the same cloud and the charge per particle varies enormously over a wide range. A definite relation seems to exist between the size of the particle and the charge which it carries, large charges occurring on large particles. A tentative hypothesis is advanced, based on the formation of aggregates, to explain this relationship. The theoretical selectivity of measurement of the apparatus has been investigated mathematically and has indicated nothing to show that such a relationship between particle size and charge is instrumental and not real.

B10. On the Radiation of Sound from an Unflanged Circular Pipe. HAROLD LEVINE AND JULIAN SCHWINGER, *Harvard University.*—A rigorous and explicit solution has been obtained for the problem of wave propagation in a semi-infinite unflanged circular pipe, which is valid throughout the wave-length range of the dominant mode. In addition to the determination of the reflection coefficient within the pipe, the power gain function, embodying the characteristics of the radiation pattern, is calculated explicitly. A reciprocity theorem is derived which relates the absorption cross section of the pipe for a plane wave, incident from the external space, to the gain function for this direction. In particular, the absorption cross section for a wave incident normally on the mouth is simply the geometrical area. When the wave length of the sound vibrations is large compared to the diameter of the pipe, the dominant mode velocity potential is the same as if the pipe were lengthened by a certain fraction of the radius and the open end then behaved as a loop. The rigorous value of this end correction is found to be 0.6133, and supplants the experimental estimates of Rayleigh[1] (0.6), Boehm[2] (0.656) and Bate[3] (0.66).

[1] Lord Rayleigh, *Theory of Sound, II*, Chapter 16 and Appendix A.
[2] W. M. Boehm, Phys. Rev. 31, 341 (1910).
[3] A. E. Bate, Phil. Mag. 10, 617 (1930); 24, 453 (1937).

B11. A Variational Principle for Scattering Problems. JULIAN SCHWINGER, *Harvard University.*—A reformulation of the general scattering problem, in terms of a variational principle, has been devised. An explicit expression is obtained for the elements of the scattering matrix, which has the property of being stationary with respect to variations relative to the correct wave function. When combined with various techniques for obtaining approximate trial functions, and an iteration procedure for systematic improvement of the trial function, the use of the variational principle provides a powerful method for the solution of scattering problems. The author has applied the method extensively to wave guide problems-neutron diffusion questions have also been attacked in this manner. A discussion will be given of the variational treatment of proton-proton and neutron-proton scattering. By employing as a trial wave function that appropriate to some convenient fixed energy, approximate but accurate scattering formulae are obtained, which exhibit the energy dependence of the cross section without explicit specification of the radial dependence of the interaction. The analysis of scattering experiments is thereby simplified. The proton-proton scattering data, in particular, will be discussed.

D1. A Cloud-Chamber Study of the Ionization By High Energy Cosmic-Ray Electrons. EVANS CLEMENT, *University of California at Berkeley.*—The ionization produced by high energy cosmic-ray electrons has been measured in a cloud chamber in order to determine whether the ionization produced by a high velocity particle continues to rise with the energy or whether it takes on a constant value as has been predicted theoretically. A lateral clearing field was arranged so that the ionization could be measured in the upper half of the cloud chamber; lead plates were placed in the lower half so that the electron would produce a shower from which its energy could be estimated. The ionization produced by electrons was measured and compared to the minimum ionization as determined from the average ionization produced by mesotrons. According to the theoretical formula of Halpern and Hall the maximum ionization should be 1.4 $I_{\min}$. In most of the pictures taken the ionization was consistent with this value. There were several pictures, however, where the ionization was extremely high. These may either indicate that the theoretical formula is invalid, or they may result from the coincidence of two or more particles. If a high energy pair is produced just above the cloud chamber, the tracks may be superposed in the cloud chamber.

D2. Cosmic Ray Tracks in Photographic Emulsions Produced at High Altitudes.* HARRIET H. FORSTER, *University of California at Berkeley.* (*Introduced by Robert B. Brode.*)—Kodak "fine grain alpha-particle" plates and Ilford "Nuclear Research" plates with an emulsion thickness varying from 25μ–100μ have been exposed to cosmic radiation both at sea level and at high altitudes. High altitude exposures were made on a number of B-29 flights at Inyokern, California, at an average height of 35,000 feet. The exposures were made on a pile of plates consisting of from 1 to 6 pairs. In each pair the emulsion sides of the plates were facing each other. The pile was wrapped in black paper and sealed in a cardboard box. Exposure times were varied from 1 to 30 hours. Single particle trajectories and multiple branchings with up to 6 tracks have been observed and directional effects have been investigated. A large increase in the number of nuclear events with increasing altitude has been found, this effect being especially marked for higher energy processes, e.g., nuclear disintegrations.

* The research described in this abstract was supported in part by the Office of Naval Research.

D3. Further Measurements on the Mass of the Mesotron.* J. G. RETALLACK, *University of California.*—W. B. Fretter[1] has reported 26 measurements of the mass of the mesotron with probable errors of individual measurements about ± 30 electron masses. The experiment is being repeated with some improvements. To improve the meas-

urement of curvature in a magnetic field, the chamber is surrounded by a water cooled (±0.35°C) copper shield. A symmetrical arrangement of 3 exhaust ports has reduced spurious curvatures of 30 no-field tracks; 20 have radii of curvature greater than 35 meters, and 10 have radii about 20 meters. To improve the measurement of range, 15 lead plates ¼ inch thick have been placed in a chamber in the shape of a truncated pyramid. Thus, mesotrons stopped in the chamber will be readily identified by the increased ionization over the plate in which it stops. The illuminated region is 6 inches deep and 20 inches square. The Geiger counters define a cone requiring 4 inches depth.

* The research described in this abstract was supported in part by the Office of Naval Research.

[1] W. B. Fretter, Phys. Rev. 70, 625 (1946).

D4. Temperature Coefficients of Cosmic-Ray Components. D. H. LOUGHRIDGE AND F. M. MILLICAN, *University of Washington.*—Studies of data from a cosmic-ray telescope and atmospheric "mass temperatures" from Raob soundings have yielded temperature coefficients for hard (30-cm lead), medium (10-cm lead), and soft (½-cm lead) components. These coefficients increase with increasing fractions of the atmosphere for the hard and medium components. Preliminary results are: Hard, $-.19\pm.02$ percent/°C, $-.19\pm.02$, $-.24\pm.02$, and $-.29\pm.04$ for the fractions ½, 6/10, ¾, and 1, respectively: Medium, $-.20\pm.04$ percent/°C, $-.22\pm.03$, $-.26\pm.04$, and $-.35\pm.07$, respectively. The average correlations are $.85\pm.04$ and $.67\pm.08$, respectively. Correlations fall off as fractions less than ½ whose temperatures approach surface values are taken. The soft component correlations are so low results are not quoted. There is some indication that the coefficient is positive and that correlations improve as surface temperatures are approached. The hard and medium coefficients show good proportionality to the average value of $[\partial Z/\partial T]_J$ obtained by assuming that an increase in intensity is linearly proportional to a downward shift in air mass as suggested by Benedetto.[1] Preliminary analysis of data from a Millikan-Neher type meter with 12-cm lead shielding gives coefficients of the same order of magnitude varying similarly to the hard and medium telescope results for atmospheric fractions from ½–1.

[1] F. A. Benedetto *et al.*, Phys. Rev. 61, 266 (1942).

D5. Propagation of Cosmic Rays through Interstellar Space. JAMES W. FOLLIN, JR., *California Institute of Technology.*—An investigation has been made of the interaction of high energy particles with interstellar matter and radiation to determine the range of such particles. The most important such interaction is the loss of energy by energetic electrons through a Compton scattering process (this is easily seen in a coordinate system moving with the electron). The transverse acceleration in a stellar magnetic field causes radiation of energy* and this is important if the source is in or near a star. The origin of cosmic-ray particles is not known and several hypotheses have been examined. The results are strongly affected by the possibility of a general gallactic magnetic field; unfortunately the problem of its existence is completely unsolved. The conclusion reached is that there should be few primary electrons with energy greater than about 10^{12} ev, but until the origin is determined this result cannot be considered final.

* Pomeranchuk, J. Phys. Acad. Sci. U.S.S.R. 2, 65 (1940).

D6. Penetrating Showers Produced in Lead at Sea-Level.* W. B. FRETTER, *University of California at Berkeley.*—The penetrating showers produced by cosmic rays in lead at sea level have been observed in a counter-controlled cloud chamber containing eight one-half-inch lead plates. Several showers were observed that contained only penetrating particles, but in others electronic particles were simultaneously produced in varying amounts. Production of electrons appears to be characteristic of the higher energy events. It may be possible to explain the simultaneous production of penetrating particles and electrons by following the suggestion of Oppenheimer and postulating the production of very short-lived neutral mesons that decay to give the soft radiation. Absence of the electronic radiation in low energy events may then be explained by fluctuations and the inability of low energy soft radiation to penetrate the lead plate in which the event occurs. Large angular spread (usually about 30°) of the penetrating particles is characteristic of these events, in contrast to the highly collimated core of electronic showers. Primary particles penetrating the atmosphere may be responsible for the showers observed, since the frequency of observed events is not inconsistent with the expected number of primaries at sea level as estimated from the free path of primaries in the atmosphere.

* The research described in this abstract was supported in part by the Office of Naval Research.

D7. Stars in Photographic Emulsions Produced by Particles Accelerated by the Cyclotron. EUGENE GARDNER, *Radiation Laboratory, University of California at Berkeley.*—Alpha-particles and deuterons accelerated by the 184-inch Berkeley cyclotron are being studied with the aid of commercial photographic plates made especially for charged particle studies. The plates are exposed to the circulating beam inside the cyclotron tank. The particle trajectories do not, in general, lie in the emulsion for their entire range; however, it is possible to study sections of tracks which correspond to known energies by making observations near the edge where the beam enters the emulsion. Sections of tracks corresponding to various energies are obtained by exposing plates at various radii in the cyclotron. Some alpha-particle tracks are observed to branch into two or more tracks. This branching, or star formation, is attributed to a disintegration of some nucleus in the emulsion. For stars formed by alpha-particles, the track of the initiating particle can ordinarily be seen, and the track is particularly clear for energies of 200 Mev or lower. For stars formed by deuterons we are not able to see the track of the initiating particle. This paper is based on work performed with the support of the Atomic Energy Commission.

D8. Balanced Ionization Chamber for Differential Measurements of Gamma-Rays. CLYDE WIEGAND, *University of California at Berkeley.* (*Introduced by E. Segrè.*)—In

connection with an investigation[1] on the half-life of beryllium, it was important to have an apparatus that could measure small differences of strong gamma activities. Such an apparatus was constructed. It consists of two equal ionization chambers connected to a single electrometer. The arrangement of the circuit is such that ionization current produced in one chamber tends to cancel the ionization current produced in the second chamber. The electrometer uses a conventional circuit employing an FP-54 tube. As a test of its performance and as another application, the half-life of Be^7 (52 days) and of 106-day Y were determined by measuring the variation of their activity against that of a radium standard. In a time of the order of 1/100 of the half-life it was possible to measure the half-life to an accuracy of ± 4 percent by using a sample equivalent in gamma-activity to 50 μg radium. It was found that the fluctuations observed in the actual balancing of the chambers was that to be expected on a statistical basis due to the discontinuous nature of radioactive emission. This paper is based on work performed with the support of the Atomic Energy Commission.

[1] E. Segrè, Phys. Rev. 71, 274 (1947).

D9. A Vacuum X-Ray Spectrometer.* S. T. STEPHENSON AND F. D. MASON, *Washington State College.*—A vacuum x-ray spectrometer is described which is suitable for use as a single or double crystal instrument in the region out to 15A. Novel features in this vacuum instrument include: the flexibility of either single or double crystal techniques, Geiger counter detection of intensities with the counter driven by a synchronous motor, and automatic recording of the Geiger counter output. The double crystal arrangement is of the Ross[1] type which allows the x-ray tube and the mount for crystal B to be stationary. A slit system replaces crystal A for single crystal work. The Geiger counter design provides a very thin window supported on both sides so that it will not blow in when exposed to air nor out when in the spectrograph. Preliminary results on the performance of the instrument will be presented.

* This work has been carried out under a contract with the Office of Naval Research.
[1] P. A. Ross, Rev. Sci. Inst. 3, 253 (1932).

D10. Cosmic Rays as Products of Radioactivity. GERTRUDE SCHWARZMANN.—Interpreting particle waves as alternating currents with direct current components, decomposition of a light wave into two alternating currents with opposite direct current components as materialization, the reverse wave phenomenon as dematerialization, allows of interpreting formation and decay of compounded nuclei as follows: Two light waves, revolving in opposite senses about each other, decompose into component light waves, decomposing in turn each into a proton pair or electron pair. Formation of neutrons, consisting of negatron and satellite positron, prevents redematerialization of equal numbers of proton pairs and electron pairs, the more so because both constituents of stable neutrons are assumed to be in the corpuscle-state. The original nucleus consists of Z protons and Z neutrons. Electron-capture by individual protons somewhat upsets the equilibrium of the nucleus. Its alpha-decay originates in simultaneous positron-decay of n neutrons revolving clockwise and of n neutrons revolving counterclockwise, followed by simultaneous dematerialization of $2n$ proton pairs. Outside the parent nucleus production of two multi Bev cosmic rays, each resultant of the superposition of n light waves revolving in the same sense, competes with the formation of an alpha-particle of atomic number $2n$.

D11. A Non-Homogeneous Cosmological Model. GUY C. OMER, JR., *California Institute of Technology.*—The non-homogeneous cosmological models with spherical symmetry and zero pressure first used by Lemaitre[1] and Tolman[2] have been integrated exactly. The special solutions with a zero cosmological constant are applied to the cosmological problem. If we assume, as a first approximation, that the observer is near the center of the universe, the following three relations are readily evolved: (1) The observed red-shift for a source at a stated coordinate. (2) The total number of nebulae which are contained within a sphere of stated coordinate radius. (3) The observed magnitude for a source of known luminosity located at a stated coordinate. It is then shown that a M_1 model which is nearly homogeneous throughout the observable range agrees with the observations within the experimental error.

[1] G. Lemaitre, Ann. Soc. Scient. de Bruxelles, **A53**, 51 (1933).
[2] R. C. Tolman, Proc. Nat. Acad. Sci. **20**, 169 (1934).

D12. Electronic Energy Levels in Simple Crystal Models. DAVID S. SAXON* AND REINA A. HUTNER, *Philips Laboratories, Inc., Irvington, New York.*—The use of simple crystal models as an aid to the understanding of electronic processes in crystals has not been as extensive, perhaps, as might be expected in view of the difficulty of calculations for real crystals. As is well known, these processes depend only quantitatively on the detailed properties of the crystal; most of the characteristic features are retained even in the most highly simplified models.[1] An attempt has been made therefore to systematically examine these characteristic features by using one dimensional models of a crystal in which the lattice potential consists of a series of Dirac δ-functions. The problems which have been or are being studied include the following: The wave functions and energy levels in pure crystals—polyatomic as well as monatomic; the scattering, wave functions and energy levels associated with impurities in the crystal lattice; the interaction between impurity states; solid solutions; conductivity. In addition the problem of extending these results to more realistic potentials and to models of two and three dimensions is being studied.

* Now at University of California, Los Angeles.
[1] See for example, Kronig and Penney, Proc. Roy. Soc. 130, 499 (1931).

D13. Character of the Radiation Field and Shielding at the 184" Cyclotron. B. J. MOYER, R. HILDEBRAND, N. KNABLE, T. J. PARMLEY, AND H. YORK, *University of California at Berkeley.*—Absorption experiments with ionization chamber detection using various absorbing materials in the fast neutron beam (~100-Mev max.) have shown transition effects followed by approximately ex-

ponential reduction in ionization with increasing absorber thickness. Data will be presented on the transition effects with various arrangements of materials and on the exponential absorption coefficients. A brief summary of these data follows: (1) If the neutron beam first passes through an equilibrium thickness of some material and then enters a variable thickness of absorber of lower atomic number, the transition effect will be "positive," i.e., there is an increase in ionization due to a greater yield of recoil and exchange protons from the second medium than from the first. (2) The absorption cross section per atom increases, but its value per proton decreases with increasing Z. Data taken with carbon detectors using the $C^{12}(n, 2n)C^{11}$ reaction show similar absorption but without transition effects. Measurements will be reported on the effectiveness of the five-foot concrete shielding, and on the composition of the external radiation field with respect to its content of gamma-rays, neutrons, and secondary particles. Acknowledgment is due to Dr. F. Oppenheimer for information contributed from related experiments. This work was done under the auspices of the Atomic Energy Commission.

D14. Cu^{60} Radioactivity. C. E. LEITH, ALEC BRATENAHL, and B. J. MOYER, *University of California at Berkeley.*—A β^+, γ-activity of 24.5 minute half-life has been discovered and assigned to Cu^{60}. It has been produced by the reactions $Ni^{60}(p, n)$, $Ni^{60}(d, 2n)$, and $Ni^{58}(\alpha, pn)$. The target materials were isotopically enriched by the calutron process. Protons of energies up to 15 Mev produced in the 37-inch frequency modulated cyclotron were used for the first reaction, 18-Mev deuterons and 36-Mev alpha-particles produced by the 60-inch cyclotron for the others. The β^+ energy has been measured by absorption in Al as 1.8 Mev. The γ-energy has been measured by absorption in lead, using Co^{60} γ-absorption for calibration as 1.3 Mev. Chemical separation of Cu from the Ni target after proton bombardment assigned the activity to Cu, and separation of target isotopes in a calutron immediately after bombardment showed that this isotope must be 60. The proton threshold energy for the $Ni^{60}(p, n)Cu^{60}$ reaction lies between 4 and 5 Mev. Recognition is due to R. E. Butler who contributed to the early efforts in this study, and to Robert Lilly for the chemistry involved. This paper is based on work performed with the support of the Atomic Energy Commission.

E1. Sensitive d.c. Current-Amplifier Operated from a.c. SEVILLE CHAPMAN, *Stanford University.*—A simple three-stage amplifier made from ordinary parts except for an input resistor of 10^{13} ohms (or less) connected to the second (control) grid of a ($12.50) Victoreen VX-41 electrometer tube is described. Its grid current is less than 2×10^{-15} ampere. Other tubes are Raytheon CK505 and CK507. Input capacitance is about 8 micromicrofarads. The amplifier is a.c. operated, a total of 50 ma d.c. current including filament current is provided by a conventional 150-volt regulated supply. A 0–100 microammeter is in a bridge circuit in the CK507 plate circuit. The amount of negative feedback (usually about 10 db) from the CK507 plate to the first (space charge) grid of the VX-41 is controlled by a variable resistor in series with the meter, thus the zero reading is unaffected by adjustment of gain. A deflection of 100 microamperes requires $+0.0330$ or -0.0335 volt. Without voltage regulation, supply voltage variation of one volt deflects the meter less than 20 microamperes. Initial drift after a 20-minute warm-up is about 50 microampere/hour; 24 hours later, 5 microampere/hour. Random meter fluctuations correspond to a fluctuating input voltage of about 2×10^{-4} volt.

E2. The Sound Pressure in Water Resulting from a Point Source in Air.* E. GERJUOY, *University of Southern California.*—If a point source is placed in air above an infinite flat water surface, rays leaving the source within a cone of 13° are refracted at the surface, with increasing divergence as the angle of incidence approaches the critical angle, so that directly transmitted energy reaches every point in the liquid. Rays outside the 13° cone are totally reflected. The directly transmitted pressure can be calculated by ray acoustics, and varies as the inverse fourth power of the distance from the source, for points near the surface and far from the source. In the region of total reflection there is also a term decreasing exponentially with distance from the surface. Since the pressure at the surface varies as the inverse square of the distance from the source, a hydrophone within a wave-length of the surface, in the region of total reflection, should respond to the exponentially decreasing term, rather than to the directly transmitted pressure. This experiment would be a quantitative and less ambiguous demonstration of penetration of fields into the second medium in total reflection than the analogous optical experiments which are usually performed with beams of finite cross section. For such beams energy necessarily penetrates the second medium.

* This paper is based in part on work done for the Office of Scientific Research and Development.

E3. The Vertical Reflection of Supersonic Sound from the Sea Bottom. R. W. RAITT, *Marine Physical Laboratory,** *University of California.*—The manner in which supersonic sound is reflected from the sea bottom is being investigated by studying the echoes received with sound beams of 18 kc and 24 kc frequency directed vertically downwards. Although the theory is not clearly understood, preliminary results have served to decide between two hypotheses: (1) The bottom reflects sound like a flat mirror, so that the echo is a replica of the emitted pulse. (2) The bottom reflects the sound diffusely, so that the insonified area returns many echoes; these will return to the receiver at different times and the echo will be elongated and distorted; varying phase displacements between these component echoes, caused by the motion of the receiving ship, will be expected to produce fluctuation of the echo shape; the average shape of the echo will depend on the geometry of the sound beam and on the angular dependence of the bottom scattering coefficient. From many observations, covering a wide variety of bottoms off California, no echoes of the type expected on hypothesis (1) have been observed. All of them exhibit the properties expected on hypothesis (2).

* This work represents one of the results of research carried out under contract with the Bureau of Ships and Office of Naval Research, Navy Department.

E4. An Acoustic Interferometer for the Measurement of Sound Velocity in the Ocean. R. J. URICK, *Naval Research Laboratory.**—A fixed-path variable-frequency acoustic interferometer has been developed which is capable of recording small changes of sound velocity as the instrument is lowered from a surface vessel. Simultaneous measurements of velocity and water temperature have been made near the surface of the ocean. Good general agreement is observed between the velocity-depth plots obtained with the interferometer and those computed from bathythermograph and thermopile observations for sea states of 0 to 3 and for depths as great as 150 feet. A velocity microstructure is frequently recorded which deviates as much as $\frac{1}{10}$ percent from the velocity obtained from bathythermograph observations, but which is in good agreement with the temperature microstructure observed with a thermopile recorder.

* This work was performed while at the USN Electronics Laboraotry, San Diego, California.

E5. Electrostatic Analyzer for 1.5-Mev Protons. T. LAURITSEN, W. A. FOWLER, AND C. C. LAURITSEN, *California Institute of Technology.*—An electrostatic deflector has been constructed and used to analyze the proton beam of a 1.5-Mev statitron. The analyzer consists of two plates curved through 90° on a 1.1 meter radius and separated by 8.6 mm. Fields up to 30 kv per cm are maintained by a transformer-rectifier power supply electronically regulated to a few hundredths of one percent. The proton beam from the generator, defined by a 0.5-mm aperture, is first subjected to a coarse magnetic analysis to separate out mass 2 and heavier components and then passes into the electrostatic deflector through a 1-mm slit. After analysis the beam emerges through an 0.7-mm slit provided with insulated jaws which control an auxiliary corona load on the generator and automatically correct the voltage to keep the beam central in the slit. The system has been in operation for a number of months in the neighborhood of 1 Mev and has yielded resolution of better than 1 kev at currents of the order of 1 μa. This work was carried on under contract with the Office of Naval Research.

E6. Cobalt 61 Radioactivity. THOMAS J. PARMLEY AND BURTON J. MOYER, *Radiation Laboratory, University of California at Berkeley.*—Isotopes of Ni^{61} and Ni^{62} were subjected to fast neutron bombardment from the Crocker Laboratory 60-inch cyclotron. Among the activities produced was a 1.75±.05 hour half-life associated most strongly with the Ni^{61} sample. Chemical extractions showed this activity belonged to cobalt. The mass assignment was established as follows: (1) Electrolytic copper was activated with fast neutrons. The cobalt extraction yielded a 1.75-hour half-life activity. (2) Calutron analysis of neutron activated electrolytic copper placed this activity in 61-mass position. (3) Normal nickel was bombarded with 22-Mev deuterons followed successively by cobalt separation and calutron analysis. The 1.75-hour activity appeared in 61-mass position. Ni^{64} was bombarded with 14-Mev protons from the 37-inch cyclotron with the activity appearing in the cobalt extraction as a $Ni^{64}(p, \alpha)Co^{61}$ reaction. Absorption measurements in aluminum gave a maximum β-energy of about 1.1 Mev with no indication of a gamma-ray. This problem was carried out under the auspices of the Atomic Energy Commission.

E7. Some Excitation Functions of Alphas and Deuterons on Bi. ELMER L. KELLY AND E. SEGRÈ, *University of California at Berkeley.*—As a part of a systematic investigation of excitation functions the absolute cross sections for the reactions $(\alpha, 2n)$, $(\alpha, 3n)$, (d, p), $(d, 3n)$, (d, n) on Bi will be presented. The energy of the projectiles ranges up to 38 Mev for the α-particles and up to 19 Mev for the deuterons. The thresholds for $(\alpha, 2n)$, $(\alpha, 3n)$, and $(d, 3n)$ reactions are respectively 19 Mev, 29 Mev, and 12 Mev. The technique used is the usual one of bombarding stacked foils, but some improvements have been made on the definition of energy and measurement of current. Also the stopping power of Bi and other substances used has been redetermined with respect to Al. The relation of these curves to present theories on excitation functions and to other experimental data[1] on the subject will also be discussed. This paper is based on work performed under contract W-7405-Eng-48, with the Atomic Energy Commission, in connection with the Radiation Laboratory, University of California.

[1] Tatel and Cork, Phys. Rev. 71, 159 (1947).

E8. The γ-Instability of Mesons. R. J. FINKELSTEIN,* *University of California at Berkeley.*—The following examples of γ-instability are investigated: (a) $M_0 \rightarrow \gamma_1 + \gamma_2$, (b) $M_1 \rightarrow \gamma_1 + \gamma_2 + \gamma_3$, (c) $M_1 \rightarrow M_0 + \gamma$, (d) $M_1^{\pm} \rightarrow M_0^{\pm} + \gamma$, where M_0 and M_1 mean a pseudoscalar and a (heavier) vector meson, respectively, and the superscript $\pm$ indicates the charge, if there is one. If the coupling constant and meson masses appropriate to the Schwinger mixture are used, the lifetimes are found to be: $\tau_a = 1\times10^{-18}$ sec., $\tau_b = 2\times10^{-11}$ sec., $\tau_c = 1\times10^{-18}$ sec., and $\tau_d = 4\times10^{-18}$ sec. In all cases except (b) the calculation leads to logarithmically divergent integrals.

* On leave from Argonne National Laboratory, Chicago, Illinois.

E9. On the Scattering of Neutrons by O_2 Molecules. OTTO HALPERN, *Columbia University.*—The theoretical analysis of the scattering of monochromatic neutron beams by gaseous O_2 molecules allows separating the contributions arising from nuclear and magnetic forces. The nuclear part must be subdivided into elastic, unelastic and hyper-elastic collisions, each of which show a characteristic dependence on the wave-length of the incident neutrons and on the temperature of the scattering gas. The elastic part in particular is very small for neutron velocities down to the thermal range, but increases rapidly with the wave-length and exceeds twice the cross section of an O atom for wave-lengths near 5A. The magnetic scattering processes, though always incoherent, do not lead to any appreciable energy transfer by the neutrons; they become quantitatively very important with increasing neutron wave-lengths. A comparison of the theory with recent experimental data will be given.

E10. Specific Ionization of 25- to 300-Kv Electrons. ROBERT H. FROST, *University of California at Berkeley.*—Measurements of the specific probable ionization of 25- to 300-kv electrons have been made in hydrogen, helium, and argon, and in the water-alcohol vapor used in a Wilson cloud chamber. Following the method used by Carl E. Nielsen for air, the ionization was measured by counting the water droplets formed in the chamber under known conditions of condensation efficiency, and the momentum determined by measuring the diameter and pitch of the helical tracks in a magnetic field. Ionization in the vapor was determined by using different pressures of the same gas in the chamber, assuming that the ionization in the gas was proportional to its pressure. Pictures have been taken with hydrogen gas at pressures ranging from 12 cm to 70 cm of mercury. At the lower pressure the ionization in the vapor is twice the ionization in the hydrogen, so that the value obtained for the former was not too sensitive to uncertainties in the value for the latter. Corrections were made for the background, for the superposition of drop images, for the elongation of the track produced by the expansion of the chamber, and for the variable time of entry of electrons into the chamber.

E11. Stability of a Reciprocating Electron. F. W. WARBURTON, *University of Redlands.*—The reciprocal force of two electrical charges[1] which is independent of the observer, provides a magnetic force which can balance the electrostatic repulsion and describe a stable electron. This occurs for the simplified model, in which the two halves of the electron are separated a distance r, when they revolve about their centroid with speed $c/2$. Using the mass equivalent of their electrostatic and magnetic energy, one finds $r=1.4(10)^{-13}$ cm. This type of stable electron has the small magnetic moment of 1.7 nuclear magnetons, and has no intrinsic angular momentum since the net force on each half is zero and no mass is attributed to each part alone. When gyromagnetism and "spin" are described by using the magnetic potential energy[2] in the Lagrangian and Hamiltonian functions, no spin magnetic moment and momentum are needed in addition to orbital magnetic moment and momentum. The concept of mass as the external aspect of the internal electrical energy alone is strengthened when mechanical mass originates from the internal electrical energy of the non-massive electrical parts of an elementary particle.

[1] F. W. Warburton, Phys. Rev. **69**, 40 (1946); **70**, 86 (1946).
[2] F. W. Warburton, Phys. Rev. **63**, 460A (1943).

E12. Noise in Electrometer Tubes. A. THEODORE FORRESTER, *University of Southern California.*—In some recent papers expected noise in electrometer tubes has been calculated by using simple triode formulae. According to a theory developed by North[1] but applied only to screen grid tubes, the interposition of a positive grid between the cathode and plate causes the ratio of mean square plate current fluctuation to average plate current to be greater than in a negative grid triode. Since the electrometer tubes invariably contain a positive space charge grid which draws a current large compared to the plate current, it is necessary to apply the ideas of North to the calculation of the plate noise. Sufficient data were available[2] for the Western Electric D-96475 to make possible a calculation of the expected shot noise. This was found to be equivalent to an input resistor of 815,000 ohms, 11.4 times the value obtainable from the usual triode term $3/g_m$. An approximation to the noise in similar tubes may be obtained by supposing the plate current fluctuations to be temperature limited shot noise, i.e., $d\langle i^2\rangle_{Av}=2eI_p df$.

[1] D. O. North, RCA Rev. **5**, 244 (1940).
[2] D. B. Penick, Rev. Sci. Inst. **6**, 115 (1935).

E13. Rise Time of Pulses in Silver Chloride Crystal Counters. ROBERT HOFSTADTER, *Princeton University.*—The rise time of pulses[1] in silver chloride has been studied at the temperature of liquid nitrogen. The pulses are produced by high energy electrons released in the crystal by gamma-rays from radium. The first crystal studied was 2 mm thick. With applied voltage of 1000 volts, the rise time of the largest pulses, observed by eye on an oscilloscope screen, was the rise time of the amplifier. This amplifier, designed by W. C. Elmore, has a rise time of about 1.5×10^{-7} second. Thus the crystal pulse rises in about 1.5×10^{-7} second or less. If the rise time for the largest pulses is taken to be the time required for an electron, released by the high energy particle near the cathode, to drift through the crystal to the anode, an elementary calculation gives a rise time of 1.7×10^{-8} second, under the conditions specified. Results of the Frolich-Mott theory were used in this calculation.[2] For a rise time of 1.5×10^{-7} second, the mobility is calculated as 270 cm/sec. per volt/cm. Preliminary investigation of a second crystal, one centimeter thick, will be discussed.[3]

[1] P. J. Van Heerden, *The Crystal Counter*, Dissertation, Utrecht, 1945.
[2] H. Frohlich and N. F. Mott, Proc. Roy. Soc. **171A**, 496 (1939).
[3] This work was partially supported by the U. S. Navy.

SUPPLEMENTARY PROGRAMME

SP1. Production of High Energy Neutrons by Stripping, II. Angular Distribution. R. SERBER, *University of California at Berkeley.**—Continuing from abstract A11 one can see that similarly, most of the neutrons will come off at an angle to the direction of the deuteron beam less than $\theta = P_1/P_0 = (d/Ed)^{\frac{1}{2}} \sim 6°$. The angular spread of the neutron beam is expected to be somewhat wider for heavy nuclei than for light ones because of the deflection of the deuteron by the Coulomb field of the nucleus, and, to a lesser extent, because of multiple scattering in the target. A nearly linear increase in half-width with Z is predicted. The calculated curves of neutron intensity as a function of angle agree well with the measurements of Helmholz, McMillan, and Sewell in regard to shape, absolute width, and variation with atomic number. In addition to the stripping process, high energy neutrons will be produced by direct nuclear encounters, and, for more distant impacts, by the dissociation of the deuteron by the Coulomb field of the nucleus. The total number of high energy neutrons produced by the former process should be comparable to the number produced by stripping, but since a considerably wider angular distribution is to be expected, these give only a small contribution to the narrow forward peak. The cross section is proportional to Z^2. These papers are based on work performed with the support of the Atomic Energy Commission.

* To be called for after paper A11 if time permits.

Author Index to Abstracts of papers presented at the Stanford Meeting

Abraham, Wayne G.—No. B4
Alvarez, Luis W.—No. B7
Bergmann, Peter—No. C5
Bloch, Felix—No. A1
Brode, R. B.—No. B2
Chapman, Seville—No. E1
Clark, J. C.—No. B5
Clement, Evans—No. D1
Cohen, Richard E. and R. F. Christy—No. A3
Cunningham, B. B., H. H. Hopkins, M. Lindner, D. R. Miller, P. R. O'Connor, I. Perlman, G. T. Seaborg, and R. C. Thompson—No. A8
Eckart, Carl—No. C4
English, W. N.—No. B8
Eyring, Carl F.—No. C2
Finkelstein, R. J.—No. E8
Follin, James W., Jr.—No. D5
Forrester, A. Theodore—No. E12
Forster, Harriet H.—No. D2
Fowler, W. A., C. C. Lauritsen, and T. Lauritsen—No. A2
Fretter, W. B.—No. D6
Frost, Robert H.—No. E10
Gardner, Eugene—No. D7
Gerjuoy, E.—No. E2
Halpern, Otto—No. E9
Hansen, James W.—No. B9
Helmholz, A. C., Edwin M. McMillan, and Duane Sewell—No. A10
Hofstadter, Robert—No. E13
Kelly, Elmer L. and E. Segrè—No. E7
Knudsen, Vern O.—No. C1
Lauritsen, C. C., T. Lauritsen, and W. A. Fowler—No. A4
Lauritsen, T., W. A. Fowler, and C. C. Lauritsen—No. E5
Leith, C. E., Alec Bratenahl, and B. J. Moyer—No. D14
Levine, Harold and Julian Schwinger—No. B10
Loughridge, D. H. and F. M. Millican—No. D4
Moyer, B. J., R. Hildebrand, N. Knable, T. J. Parmley, and H. York—No. D13
Neddermeyer, S. H.—No. B6
Omer, Guy C., Jr. —No. D11
Parmley, Thomas J. and Burton J. Moyer—No. E6
Powell, Wilson M.—No. A7
Raitt, R. W.—No. E3
Retallack, J. G.—No. D3
Rubin, Sylvan—No. A5
Saxon, David S. and Reina A. Hunter—No. D12
Schwarzmann, Gertrude—No. D10
Schwinger, Julian—No. B11
Seaborg, G. T., B. B. Cunningham, H. H. Hopkins, M. Lindner, D. R. Miller, P. R. O'Connor, I. Perlman, and R. C. Thompson—No. A9
Serber, R.—No. A11, SP1
Sewell, D. C., L. Henrich, and J. Vale—No. A6
Slater, J. C.—No. B1
Stephenson, S. T. and F. D. Mason—No. D9
Townes, C. H., A. N. Holden, and F. R. Merritt—No. B3
Urick, R. J.—No. E4
Warburton, F. W.—No. E11
Wiegand, Clyde—No. D8
Young, R. W.—No. C3